UNIVERSITY OF SOUTHAMPTON

FACULTY OF ENGINEERING, SCIENCE & MATHEMATICS

School of Engineering Sciences

Analysis of an Alternative Topology for Steel-Concrete-Steel Sandwich Beams Incorporating Inclined Shear Connectors

by

Manit Leekitwattana

Thesis for the degree of Doctor of Philosophy

March 2011

Declaration of Authorship

I, Manit Leekitwattana, declare that the thesis entitled 'Analysis of an Alternative Topology for Steel-Concrete-Steel Sandwich Beams Incorporating Inclined Shear Connectors' and the work presented in the thesis are both my own, and have been generated by me as the result of my own original research. I confirm that:

- this work was done wholly or mainly while in candidature for a research degree at this University;
- where any part of this thesis has previously been submitted for a degree or any other qualification at this University or any other institution, this has been clearly stated;
- where I have consulted the published work of others, this is always clearly attributed;
- where I have quoted from the work of others, the source is always given. With the exception of such quotations, this thesis is entirely my own work;
- I have acknowledged all main sources of help;
- where the thesis is based on work done by myself jointly with others, I have made clear exactly what was done by others and what I have contributed myself;
- parts of this work have been published as listed in List of Publications.

Signed: _____

Date: _____

"You can't stay in your corner of the Forest waiting for others to come to you. You have to go to them sometimes."

Winnie the Pooh

UNIVERSITY OF SOUTHAMPTON

Abstract

Faculty of Engineering, Science & Mathematics
School of Engineering Sciences

Doctor of Philosophy

Analysis of an Alternative Topology for Steel-Concrete-Steel Sandwich Beams Incorporating Inclined Shear Connectors

by Manit Leekitwattana

This thesis presents a new concept in steel-concrete-steel sandwich construction in which a bi-directional corrugated-strip core is proposed as an alternative inclined shear connector. The focus is on the feasibility study of fabrication techniques and the theoretical study of the structural responses of both unfilled and concrete-filled steel-concrete-steel sandwich beams under static flexural loading using numerical and analytical methods. Two possible fabrication techniques to create the proposed bi-directional corrugated-strip core are presented. The unfilled sandwich beam is studied using a finite element method and three analytical methods referred to as the modified stiffness matrix, the braced frame analogy, and the discrete beam methods The finite element method is used to investigate the stiffness and strength behaviour of the unfilled sandwich beam. The modified stiffness matrix method provides good correlation with the finite element method. The other two analytical methods are less accurate. The assessment of the effect of geometrical parameters defining the bi-directional corrugated-strip core is carried out. The responses of the strength and stiffness, especially the transverse shear stiffness, are examined and discussed. The optimum configuration of the core is found at the angle of the inclined part of the corrugation is about 45°. The concrete-filled sandwich beam is studied using the finite element method. The finite element method is used to investigate the transverse shear strength and the crack development of a four-point loaded concrete-filled sandwich beam. The assessment of the effect of geometrical parameters defining the inclined shear connectors is carried out. The responses of the concrete-filled sandwich beam are examined and discussed. The optimum advantage of the transverse shear strength of the concrete-filled sandwich beam is also found when the inclined shear connectors align at an angle 45°. It is found that creating the proposed core with a 45° pattern provides a great advantage in transverse shear stiffness and strength in both the unfilled and concrete-filled sandwich beams.

Acknowledgements

First of all, I would like to thank my sponsor, the Energy Policy and Planning Office (EPPO), the Ministry of Energy, Royal Thai Government, Thailand, who has provided me the three-year PhD scholarship, from October 2006 to September 2009.

I also would like to thank the International Maritime College, Kasetsart University Si Racha Campus, Thailand, who has allowed me to do full-time PhD study for four years, from October 2006 to September 2010, and has provided working benefit continually.

I then would like to thank my supervisors, adviser, and internal and external examiners who have technically supported me through my whole PhD work.

I would especially like to thank my supervisors, Prof. R. A. Shenoi and Dr S. W. Boyd, for their kind supervision and instruction throughout my PhD work.

I would like to thank my adviser, Prof. S. S. J. Moy, from the School of Civil Engineering and the Environment for his kind advisory role at the beginning of my PhD work.

I am also very grateful to my internal examiner, Dr A. G. Bloodworth, from the School of Civil Engineering and the Environment and my external examiner, Prof. M. Robinson, from the School of Mechanical and Systems Engineering, Newcastle University for their kind suggestion and recommendation for my PhD thesis.

I wish to thank my colleagues in the Fluid Structure Interactions Research Group for their technical help in this research. I also wish to thank Ms E. Dagnall and my friends for their wonderful living support in Southampton.

Finally, I would especially like to thank my family in Thailand who have played the important role in mentally supporting me with their true love.

List of Publications

Paper 1: M. Leekitwattana, R. A. Shenoi, and S. W. Boyd. Transverse shear strength of a bi-directional corrugated-strip-core steel sandwich plate. In S. L. Chan, editor, *Proceedings of the Sixth International Conference on Advances in Steel Structures (ICASS'09)*, volume II, pages 959–968, Hong Kong, China, 16–18 December 2009. The Hong Kong Institute of Steel Construction.

Paper 2: M. Leekitwattana, S. W. Boyd, and R. A. Shenoi. An alternative design of steel-concrete-steel sandwich beam. In *9th International Conference on Sandwich Structures (ICSS-9)*, Pasadena, California, USA, 14–16 June 2010.

Paper 3: M. Leekitwattana, S. W. Boyd, and R. A. Shenoi. Transverse shear stiffness of steel sandwich beam with bi-directional corrugated-strip core. In *Pacific Structural Steel Conference 2010 (PSSC2010)*, Beijing, China, 19–22 October 2010.

Paper 4: M. Leekitwattana, S. W. Boyd, and R. A. Shenoi. Evaluation of the transverse shear stiffness of a steel bi-directional corrugated-strip-core sandwich beam. *Journal of Constructional Steel Research*, 67(2):248–254, 2011.

Contents

List of Figures

List of Tables

Abbreviations

2D	Two-Dimensional
3D	Three-Dimensional
BFA	Braced Frame Analogy Method
Bi-CSC	Bi-Directional Corrugated-Strip Core
Bi-Steel	Bi-Steel Sandwich Construction
CSC	Corrugated-Strip Core
DBM	Discrete Beam Method
DSC	Double-Skin Sandwich Construction
FBD	Free Body Diagram
FE	Finite Element
FEM	Finite Element Method
FE-TPB	Finite Element Method of Three-Point Loaded Beam
FE-UC	Finite Element Method of Unit Cell
FPB	Four-Point Loaded Beam
LNG	Liquefied Natural Gas
MSM	Modified Stiffness Matrix Method
PFM	Plane-Frame Model
RC	Reinforced Concrete
SCS	Steel-Concrete-Steel
SRM	Slide-Rotate Method
TDM	Top-Down Method
TPB	Three-Point Loaded Beam
UC	Unit Cell

Symbols

a	distance between a support and an applied load of four-point loaded beam
A	cross section area
b	width
c	direction cosine
C	compressive force
d	distance between the neutral axes of top and bottom face plates
D	flexural stiffness
D_o	flexural stiffness of face plates about the neutral axis of sandwich beam
D_Q	transverse shear stiffness
E	modulus of elasticity
f	stress
f_c	length of the flat leg of corrugated-strip plate, or compressive strength of concrete
f_{ct}	split-cylinder tensile strength of concrete
f_r	modulus of rupture of concrete
f_y	yielded stress of steel
f'_c	ultimate compressive strength of concrete
f'_t	direct tensile strength of concrete
f'_u	ultimate tensile stress of steel
F	force
g	distance
G	shear modulus

h	height
H	force
I	moment of inertia
k	constant, or linear rotational stiffness
k_b	elongation factor of inclined chord in flexural mechanism of braced frame analogy method
k_{cb}	width coefficient of corrugated-strip plate
k_{ch}	transverse shear stiffness contribution factor of the flat legs of corrugated-strip plate
k_{ci}	transverse shear stiffness contribution factor of the inclined parts of corrugated-strip plate
k_G	shear correction factor
k_i, k_j	linear rotational stiffness factors at nodes i and j
k_{sy}, k_{sz}	elongation factors of inclined chord in shear mechanism of braced frame analogy method
k_v	transverse shear strength index
l	length of diagonal shear crack line
l_d	effective length of the inclined part of corrugated-strip plate
L	length
M	moment
P	load
P_c	ultimate load of concrete-filled sandwich beam without shear connectors
P_v	ultimate load of concrete-filled sandwich beam with vertical shear connectors
Q	transverse shear force, or stiffness quantity
$\bar{Q}$	transformed stiffness quantity
r	reduction factor
s	direction sine

s_c	half pitch of the corrugation unit of corrugated-strip plate
s_x, s_y	equivalent horizontal length of the inclined part of corrugated-strip plate in the x- or y-direction
t	thickness
T	tensile force
V	shear force
V_{BS}	transverse shear strength of concrete-filled Bi-Steel sandwich beam
w_c	unit weight of concrete
z	distance between the neutral axes of sandwich beam and face plate
$\bar{z}$	distance between the neutral axes of sandwich beam and core
β	angle of diagonal shear crack line
β_t	shear transfer coefficient
δ	displacement
ϵ	normal strain
ϵ_{ck}	corresponding strain at tensile crack
ϵ_{cku}	corresponding strain at tensile failure
ϵ_{cu}	corresponding strain at compressive failure
ϵ_{st}	strain-hardening strain
ϵ_y	yield strain
ϵ'_c	corresponding strain at ultimate compressive stress
γ	shear strain
γ_i, γ_j	flexibility stiffness factors at nodes i and j
ν	Poisson's ratio
ϕ	angle
ψ	angle
σ	normal stress
τ	shear stress
θ	angle of the inclined part of corrugated-strip plate, or

	rotational angle at the end of a beam
ξ	angle
Δ	deflection
Δ_c	corresponding deflection at applied load P_c
$\{F\}$	force matrix
$\{F_c\}$	known effort force matrix
$\{F_f\}$	unknown effort force matrix
$[k]$	local stiffness matrix
$[K]$	global stiffness matrix
$[K_{cc}]$, $[K_{cf}]$, $[K_{fc}]$, $[K_{ff}]$	partitioned matrices of global stiffness matrix
$[K^I_{cc}]$, $[K^I_{cf}]$, $[K^I_{fc}]$, $[K^I_{ff}]$	partitioned matrices of global inverse stiffness matrix
$[T]$	transformation matrix
$\{\Delta\}$	displacement matrix
$\{\Delta_c\}$	compatibility constraint displacement matrix
$\{\Delta_f\}$	free displacement matrix

Subscripts

$\square_b$	of bottom face plate
$\square_c$	of concrete, or
	of core, or
	of corrugated-strip core, or
	of corrugated-strip plate
$\square_{c1}$	of corrugated-strip plate C1
$\square_{c2}$	of corrugated-strip plate C2
$\square_s$	of steel
$\square_t$	of top face plate
$\square_{tc}$	of transverse corrugated-strip plate
$\square_v$	of transverse shear reinforcements
$\square_{x,y,z}$	in the x-, y-, or z-axis, or
	in the x-, y-, or z-direction
$\square_{bx,by,bz}$	of bottom face plate in the x-, y-, or z-direction
$\square_{cx,cy,cz}$	of corrugated-strip plate in the x-, y-, or z-direction

$\square_{tx,ty,tz}$	of top face plate in the x-, y-, or z-direction
$\square_{xy,yz,zx}$	in the xy-, yz-, or zx-plane
$\square_{1,2,3}$	in the 1-, 2-, or 3-axis, or
	in the 1-, 2-, or 3-direction
$\square_{12,23,31}$	in the 12-, 23-, or 31-plane
$\square_{i}$	of any number of 1, 2, or 3
$\square_{j}$	of any number of 1, 2, or 3
$\square_{ij}$	of any number of $i = 1$, 2, or 3, and $j = 1$, 2, or 3

Superscripts

$\square^{b}$	of bottom face plate
$\square^{c}$	of core, or
	of corrugated-strip core
$\square^{f}$	of face plates
$\square^{t}$	of top face plate
$\square^{x,y,z}$	in the x-, y-, or z-axis, or
	in the x-, y-, or z-direction
$\square^{1,2,...}$	of nodes 1, 2, ...

Remark: If appropriate, some of the symbols mentioned above may have duplicate definitions and may also locally redefined in parts of the thesis. Other symbols not mentioned here may be locally defined in the thesis. Subscripts and superscripts are applied to any symbols with general definition defined here unless particular definition specified locally.

Dedicated to my family

Chapter 1

Introduction

1.1 Background

The need for large structures with higher specific strength and stiffness is increasing. This is especially true of recent engineering structures such as ship and building structures where there is an interest in increasing the payload to structure weight ratio. To deliver such structures, engineers can either find a new structural material or produce a new structural topology. The former method is however quite difficult to complete because a qualification for new materials is expensive and time consuming. The latter method is more realistically possible because engineers can select any combination of existing materials and arrange them into a desired structural topology such as a sandwich structure.

A sandwich structure represents a special form of plate structure where two relatively thin, strong, and stiff face plates are separated from each other by a relatively thick and lightweight core. The potential result is a special plate structure with high stiffness and strength to weight ratio. Another benefit of the sandwich structure is a variety of structural designs. While the face plates are usually made of metal- or composite-based materials and shaped in a conventional plate pattern, the core can be either made of any relatively lightweight solid material or shaped in any structural topology pattern. These two advantages have led to the wide usage of sandwich structures in engineering disciplines such as for aerospace, automotive, civil, and marine applications.

In civil engineering applications, a steel-concrete-steel (SCS) sandwich construction has been developed using the sandwich structure concept. It is another combination of steel and concrete materials that have played significant roles in the creation of a vast array of engineering structures. The SCS sandwich construction represents a special form of

sandwich structure. It consists of two steel face plates and concrete core that are connected together by mean of a series of shear connectors. The state-of-the-art construction forms of the SCS sandwich structures are (1) double-skin sandwich construction (DSC), (2) Bi-Steel sandwich construction (Bi-Steel), and (3) alternative SCS sandwich construction. They are different only due to the pattern of their shear connectors, as shown in Fig. 1.1.

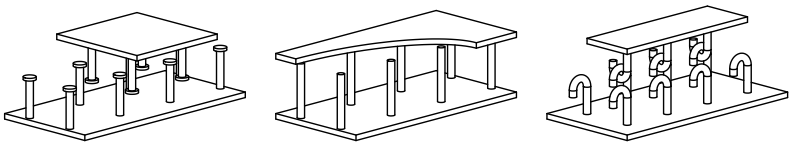

FIGURE 1.1: Sketches of (a) double-skin, (b) Bi-Steel, and (c) alternative steel-concrete-steel sandwich construction

Being an alternative construction technique, the DSC was introduced for the Conwy River submerged-tube-tunnel crossing project in the mid 1980s. Although the DSC is similar to steel-concrete composite construction, it was not qualified for this project due to the difficulties of on-site construction, especially the depth control of the sandwich core [1]. The Bi-Steel form overcame some of the existing on-site construction problems of the DSC. Having the innovative prefabrication technique developed by British Steel (later, Corus) [1], both ends of a shear connector can be simultaneously fixed to the steel face plates. The alternative SCS sandwich construction with the innovative J-J hook connectors has also been recently proposed as a competitive construction form [2–6]. It seems to be an advantageous solution as a simplified low-cost-construction technique because it just requires simplified construction tools that are now generally available at the construction site.

Although the SCS sandwich construction was originated in civil/structural engineering applications, it has been further researched and developed not only for civil applications but also for shipbuilding/offshore applications [2, 7–10]. With an increasing variety of concrete types, lightweight concrete has become a suitable alternative to standard civil construction concrete and therefore suitable for the highly weight critical marine industry [8]. The initial idea is to deliver a competitive solution against a conventional stiffened plate. Figure 1.2 shows the concept of using an SCS sandwich panel for a shipbuilding application presented by Dai and Liew [10]; it may be adapted, for example, for tanker ships, LNG ships, or large offshore structures.

The behaviour of the SCS structures has been widely researched, for example, in [6, 11, 12]. However, recent developments for shipbuilding may be divided into two fields: to introduce either a lightweight concrete core [2–8] or a new shear connector system [2–6].

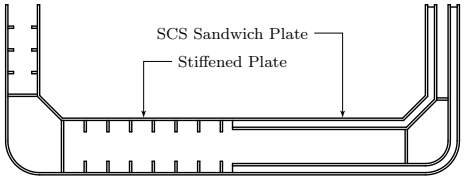

FIGURE 1.2: A concept of replacing the stiffened plate of a ship hull structure by a steel-concrete-steel sandwich plate presented by Dai and Liew [10]

This research deals with the latter in which a new concept design of shear connector is introduced.

Considering the existing construction forms of SCS structures, it may be seen that all of the current types of shear connector are similar in alignment pattern. They all align in the vertical direction – the axis of shear connector is normal to the face plates. However, it is known that a concrete-filled SCS sandwich beam under bending load suffers diagonal shear cracks [4, 11–15]. In the opinion of the author, this may be alleviated using inclined shear connectors. Therefore, it is proposed to further research this alternative engineering solution.

1.2 Aims and Objectives

This research presents a new alternative to the SCS sandwich construction in which a bi-directional corrugated-strip core (Bi-CSC) system is used as shear connectors, as conceptually illustrated in Fig. 1.3. The research aims to present the possibility to implement this novel SCS sandwich construction using available construction techniques and to present the potential advantages of this novel sandwich construction.

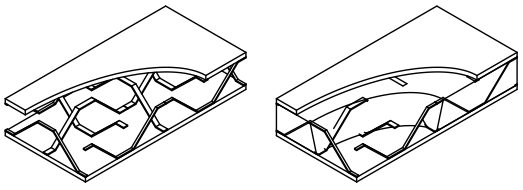

(a) (b)

FIGURE 1.3: Steel-concrete-steel sandwich construction with bi-directional corrugated-strip core (a) an unfilled sandwich structure, and (b) a concrete-filled sandwich structure

Having the inclined parts of each corrugation unit, it can be seen that the whole Bi-CSC system consists of a series of inclined members. The inclined members would therefore act as inclined shear connectors for a concrete-filled SCS sandwich beam and also as additional bracing members for an unfilled SCS sandwich beam. Therefore, the

research aims to study not only the concrete-filled SCS sandwich beam but also the unfilled beam. The objective is to address the advantage of stiffness and strength of this proposed sandwich beam using numerical and analytical methods. The main focus is on the effect of configuration of the Bi-CSC system, especially the angle of the inclined part of the corrugation unit, to the transverse shear stiffness and strength of both the unfilled and concrete-filled SCS sandwich beams. One of the barriers to understanding the response of the Bi-CSC system is an efficient method of analysing the structure. As this construction is truly three dimensional, a finite element analysis is likely to be computationally expensive. Therefore, one key objective is the development of simplified analytical methods for the assessment of the Bi-CSC response.

1.3 Novelties and Contributions

In order to propose the new alternative SCS sandwich construction with Bi-CSC, it is necessary to present the concept design and to understand its structural responses. Of such these requirements are the fabrication techniques to create the Bi-CSC topology and the understanding of the effect of the Bi-CSC configurations to the stiffness and strength of both the unfilled and concrete-filled SCS sandwich beams.

To the current knowledge of the author, it has been found that there are no existing SCS sandwich beam studies with inclined shear connectors used in SCS sandwich construction. Therefore, this research will contribute to the current engineering knowledge of the SCS sandwich construction. The novelties and the contributions of this research are listed as follows:

- The novel SCS sandwich construction with the Bi-CSC topology and the conceptual fabrication techniques.
- The understanding of the stiffness and strength responses of the unfilled SCS sandwich beam with Bi-CSC as a function of core configurations.
- The simplified analytical methods to obtain the flexural and transverse shear stiffnesses of the unfilled SCS sandwich beam with Bi-CSC and other similar cores.
- The understanding of the transverse shear strength response of the concrete-filled SCS sandwich beam with inclined shear connectors as a function of the angle of shear connectors.

The major novelty of this research is the novel SCS sandwich construction with the Bi-CSC topology. This proposed sandwich structure presents a new alternative form

of the SCS sandwich construction in which the alternative inclined shear connectors is represented in the form of the Bi-CSC topology. The literature has shown that there is no similar SCS sandwich construction with the proposed Bi-CSC topology or the proposed inclined shear connectors used in the SCS sandwich construction. Although similar sandwich structures with CSC can be found in Ray [16, 17], it is found that those cores are different from the proposed Bi-CSC topology. Besides the proposed Bi-CSC topology, two conceptual fabrication techniques referred to as the top-down method (TDM) and the slide-rotate method (SRM) are probably originally presented in this research.

The understanding of the stiffness and strength responses of the unfilled SCS sandwich beam with Bi-CSC as a function of core configuration is the knowledge contribution in the unfilled corrugated-like core sandwich construction. In addition to the experimental study of the similar sandwich structures with CSC by Ray [18], this research presents the other responses of the beam using the numerical and analytical methods. It is found that this research can contribute additional response of the beam with Bi-CSC to the existing experimental results of other similar sandwich structures with CSC [18]. While the results presented in Ray [18] are limited to some structural responses of the beam with uni-directional CSC topology, the results presented in this research can further represent the structural responses of the beam with the Bi-CSC topology.

The simplified analytical methods to obtain the flexural and transverse shear stiffnesses of the unfilled SCS sandwich beam with Bi-CSC and other similar cores presented in this research are the further contributions of the theoretical study of the unfilled corrugated-like core sandwich construction. In this research, three simplified analytical methods, referred to as the modified stiffness matrix method (MSM), the braced frame analogy method (BFA), and the discrete beam method (DBM), are presented as the alternative simplified methods to overcome an indeterminate core topology such as the proposed Bi-CSC topology. It is found that the MSM can extend the theoretical method to obtain the transverse shear stiffnesses of the unfilled truss core sandwich beam presented by Lok et al. [19, 20] which is limited to only a determinate core topology. The BFA and the DBM may also be the alternative methods to overcome the indeterminate core topology if they are later refined in their conceptually techniques.

The understanding of the transverse shear strength response of the concrete-filled SCS sandwich beam with inclined shear connectors as a function of the angle of shear connectors is also a new knowledge contribution in the concrete-filled SCS sandwich construction. To the current knowledge of the author, the research of the SCS sandwich construction with the proposed inclined shear connectors or other similar inclined shear

connectors has not been presented in any public publications of this subject. Therefore, any understanding of the responses of the concrete-filled SCS sandwich beam with the proposed inclined shear connectors should dominate the recent research of the SCS sandwich construction.

1.4 Structure of the Thesis

This thesis is divided into nine chapters and is described diagrammatically in Fig. 1.4.

First, Chapter 1 presented here introduces the motivations, aims, objectives, and novelties and contributions of this research. It also outlines the contents of this thesis.

Chapter 2 reviews the existing sandwich constructions, especially the state-of-the-art SCS sandwich constructions. The major gaps in the existing research and development of the SCS sandwich constructions are introduced.

Chapter 3 presents the possibility to implement the proposed SCS sandwich construction with the Bi-CSC system using available construction techniques. The methods to set corrugated-strip plates out in bi-directional format are conceptually proposed.

Then, the next four chapters present the numerical and analytical studies of the unfilled SCS sandwich beam with the Bi-CSC topology.

The numerical study of the unfilled type of the SCS sandwich beam with the Bi-CSC system using three dimensional (3D) finite element (FE) model is presented in Chapter 4. The main focus is on the stiffness and strength behaviour of the proposed unfilled SCS sandwich beam under static load condition. In addition, the deformation of the sandwich beam is also observed and discussed.

Rather than using the computational expensive 3D FE approach, three analytical methods are presented in the next three chapters as alternative simplified approaches to obtain the response of the unfilled sandwich beam with the Bi-CSC topology. The numerical solutions obtained from Chapter 4 are used as a reference for the validation of these three simplified analytical methods.

The adopted analytical method based on the force-distortion relationship of a repetitive unit cell and the stiffness matrix method is proposed in Chapter 5. This proposed method is named as the modified stiffness matrix method (MSM). It is used to derive the transverse shear stiffness of the proposed Bi-CSC topology. The MSM is proposed in this research to overcome the high indeterminacy of the proposed structural core topology. The validation of the MSM with existing analytical solutions [19, 20] and numerical

solutions (Chapter 4) is also presented in this chapter. This analytical method is then used to assess the effect of geometric parameters defining the Bi-CSC. The performance of the unfilled SCS sandwich beam with the Bi-CSC system compared with other unfilled corrugated-like core sandwich beams is then examined and discussed.

Next, Chapter 6 presents another alternative analytical method based on the force-distortion relationship and the braced frame analogy; this method is therefore named as the braced frame analogy method (BFA). It is used to decompose the stiffness of the unfilled SCS sandwich beam into two parts: sandwich face plates and sandwich core. Although the BFA seems to be valid with some assumptions and some specific configurations of the unfilled sandwich beam, it is introduced to be used as a simplified method to evaluate the stiffness contribution of the proposed core topology to the overall stiffness and strength of the unfilled SCS sandwich beam. The BFA can be further refined to achieve a solution that is more accurate.

Chapter 7 also presents one more alternative analytical method to study the stiffness behaviour of the unfilled SCS sandwich beam with the Bi-CSC system. This alternative method is based on the discrete beam approach; therefore, it is named as the discrete beam method (DBM). The DBM is proposed in the earlier stage of this research and used as a method to decompose the stiffness of the unfilled sandwich beam into the face plates and core components. The comparison between the DBM and BFA is also presented in this chapter. It seems that the DBM agrees with the BFA in some specific configurations of the unfilled sandwich beam. However, the DBM may need to be further refined with more accurate assumptions.

The numerical study of the concrete-filled SCS sandwich beam with an inclined shear connector system is then presented in Chapter 8. This chapter first introduces the fundamental behaviour of the diagonal shear crack failure along with the rational of transverse shear reinforcement system. The limitations of the state-of-the-art Bi-Steel sandwich beam are also reviewed. The concrete-filled SCS sandwich beam with the inclined shear connector system is then studied using the 3D FE approach. The potential advantage of the proposed sandwich beam compared in various core configurations is then examined and discussed. The main focus is on the transverse shear strength and the diagonal shear crack behaviour of the concrete-filled SCS sandwich beam.

Last, Chapter 9 concludes the major contents of the research. The suggestions for the future research of the SCS sandwich beam with the Bi-CSC or the inclined shear connector systems are also introduced.

In addition to the major contents presented from Chapter 1 to 9, some supplementary information is noted in appendix. Appendix A presents explanatory notes of derivation

of the neutral axis of the unfilled sandwich beam with the Bi-CSC topology and the constants k_b and k_s used for the BFA in Chapter 6.

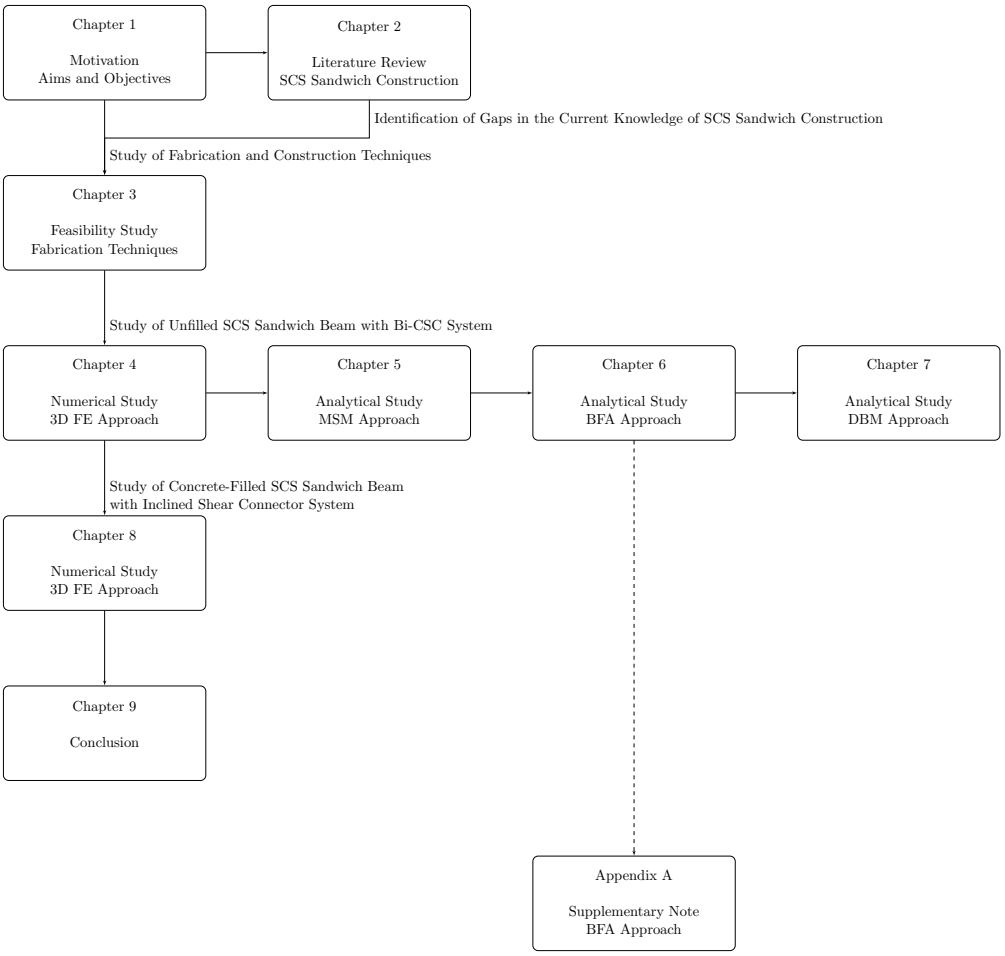

FIGURE 1.4: The diagrammatical structure of the thesis

Chapter 2

Literature Review of Sandwich Construction

2.1 Background

A sandwich structure represents a special form of plate structures where two relatively thin, strong and stiff face plates referred to as sandwich face plates are separated from each other by a relatively thick and lightweight core. They are connected to each other by a number of connecting methods, for example, adhesive bonding, riveting, and welding. Practically, the sandwich face plates are designed to withstand bending and axial stresses and the core is designed to withstand a transverse shear stress.

The potential advantages of sandwich structures are their high stiffness and strength to weight ratios and their variety of structural designs. The former is probably the most well-known and most advantageous characteristic often quoted in literature, for example, in [21, 22], and is the result of separating the sandwich face plates away from each other by the sandwich core. If both the sandwich face plates and the core can properly work together as a unique system without delaminating or disconnecting, the stiffness of the sandwich structures increases as they get thicker [21, 22]. The latter advantage, previously described, is also important. It allows engineers to select two or more desired materials and then to combine them together to perform the sandwich structures. For example, a steel plate may be used as the sandwich face plate on one side and an aluminium plate may be used as the other sandwich face plate on the other side. The sandwich core may be of another material such as polymeric foam. While the sandwich face plates can resist structural loads, the polymeric foam core can be a sound barrier and a thermal insulator. In addition, the sandwich core can be designed

in various forms of either a solid core or a structural core. Designers have the freedom to select any combinations of engineering materials that meet specific design requirements.

In terms of core topologies, the sandwich construction may be classified into two major groups: (1) solid core sandwich construction, and (2) structural core sandwich construction, as shown in Fig. 2.1.

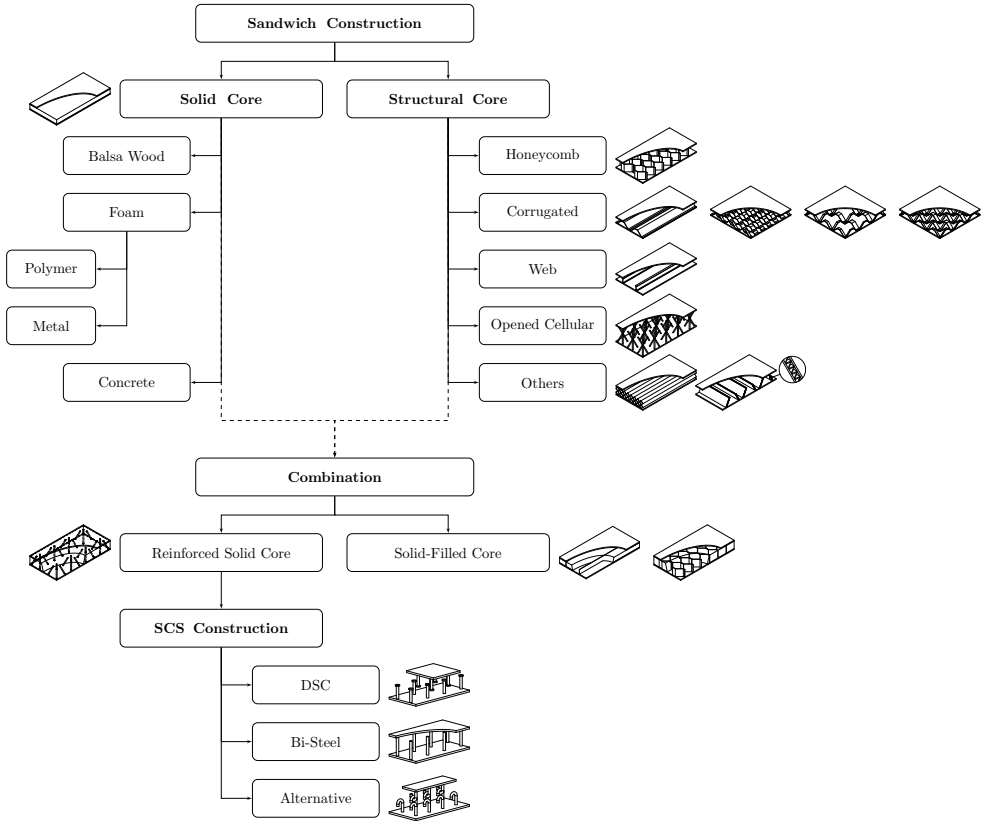

FIGURE 2.1: A classification of sandwich construction

The solid core sandwich construction is probably the earliest sandwich construction form. It was initially developed in the period of the World War I and II [22]. The core is typically made of lightweight materials such as balsa wood or polymeric foam and shaped in a rectangular block.

The balsa wood is probably the first material used as the sandwich core [22]. It is an anisotropic material which has high strength in the direction of fibre growth. Therefore, it is normally cut in a cubic block with its fibre direction perpendicular to the plane of the block; as a result, the fibre direction is also perpendicular to the sandwich face plates [22].

The polymeric foam, e.g., polyurethane (PUR), polystyrene (PS), and polyvinylchloride (PVC), is commonly used as the sandwich core. This is because of its relatively light weight; most polymeric foam has density lower than 500 kg/m^3 [22].

In addition to the polymeric-based material, foam can be made of a metallic-based material such as aluminium. It has recently been developed as the sandwich core [23, 24]. The metallic foam is considerably more advantageous than the polymeric foam in some mechanical behaviour, for example, being higher stiffness, being higher temperature resistance [23, 24], and being higher impact energy absorption [25][1].

Concrete – a popular engineering material used in civil/structural applications – is also the available material choice of the solid core sandwich construction. Although the weight of concrete is relatively heavy, the use of concrete in the solid core sandwich construction has been developed for shipbuilding applications for a few years [2, 7–10, 27]. It demonstrates some advantages of safety performance such as high energy impact absorption [8]. In addition, the lightweight concrete with dry density of below 1,000 kg/m^3 is now available [8].

Figure 2.2 shows the variety of the state-of-the-art concrete types. It can be seen that there is lightweight concrete such as autoclaved aerated concrete or foamed concrete available to select as an engineering material. Both the lightweight concrete types are the special concrete with plenty of air bubbles formed inside the mass of concrete. They are practically different only in their mixing methods. While the autoclaved aerated concrete is made by mixing normal concrete compounds, i.e., cement, sand, and water, with a bubble catalyst such as aluminium powder [28, 29], the foamed concrete is made by injecting stable pre-formed foam into ready-mixed slurry-state concrete [30]. The result of these methodologies is solid-state concrete with an amount of air bubbles; as a result, these concrete types are relatively light compared with standard construction concrete. The dry weight of, for example, foamed concrete ranges between 400 and 1,600 kg/m^3 [30]. Therefore, it is possibly a competitive sandwich core material.

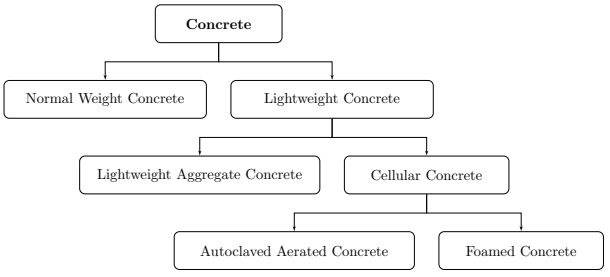

FIGURE 2.2: A classification of concrete

[1] cited by Sypeck and Wadley [26]

The structural core sandwich construction is the other major sandwich construction form. While the solid core is practically shaped in a rectangular solid block, the structural core can be designed in various structural forms. It is probably further subclassified into five minor groups: (1) honeycomb core, (2) corrugated core, (3) web core, (4) opened cellular core, and (5) other structural cores.

The honeycomb core is probably the first popular structural core [20]. It was developed in the aerospace industry in the late 1940s [22]. The structural shape of the core is initially designed to be similar to a natural honeycomb cell. It has been further developed in various shapes such as a square cell, an over-expanded hexagonal cell, and a deformed honeycomb cell [22, 31]. Although honeycomb core sandwich structures are quite expensive and difficult to produce, they are widely used in many engineering applications due to their high strength and stiffness to weight ratios. Moreover, the innovative folded-honeycomb production technology introduced by EconCore N.V. [32] is the successive method to combine the mechanical advantages of the honeycomb core sandwich structures with the automated production of corrugated cardboard. This concept provides the cost efficient continuous production of honeycomb core sandwich structures made using thermoplastic sheets.

The corrugated core is another type of the structural core sandwich construction. A corrugated core sandwich structure typically consists of two face plates and a corrugated sheet formed in various corrugation profiles such as trapezoidal shape, sinusoidal shape, and triangular shape. Instead of arranging the corrugated sheet in a one-way pattern, however, the corrugated sheet can be arranged in a two-way pattern [33]. In addition, the corrugated core can be designed in various advanced patterns such as an offset-corrugated core [34, 35], a bi-directionally corrugated core [16, 36], and a cross-corrugated core [17]. These corrugated cores consist of a series of corrugated-strip plates which are arranged in either uni- or bi-directional format.

The web core also represents another form of the structural core sandwich construction. The core is a series of strong stiffeners which have cross section in various shapes such as I-, C-, Z- and O-sections [37]. The sandwich face plates and the web core can be connected to each other by any mechanical means such as spot welding or riveting [38]. Moreover, they may be welded together from the outside of sandwich structures using laser-welding technology [39]. Therefore, it seems that there are no limitations to the possible web core topology. In current practice, the stiffeners are arranged in the longitudinal direction of the sandwich plates; as a result, it is strong in this longitudinal direction and relatively weak in the transverse direction.

The opened cellular core is now competitive with other structural cores [26]. It is considerably more advantageous than some of other structural cores, for example, allowing

fluids to pass through the core [40] and being stronger and stiffer than the metallic foam core for the same relative density [33]. The Kagome and the Pyramidal cores developed by Cellular Materials International Inc. [33] are the state-of-the-art examples of this sandwich construction. The advanced fabrication technique of these cores can be found in Wadley et al. [41].

Other structural cores such as a prismatic core [42] or a second-order core [43] are the examples of the structural core sandwich construction. Three-dimensional (3D) shell cores such as an egg-box core [41] or a dimpled shape core [21] are also the other examples of the structural core sandwich construction. These structural cores are being developed to achieve a higher performance sandwich structure. For example, the strength to weight ratio of a second-order corrugated core sandwich structure is more than that of an equivalent corrugated core sandwich structure for the same relative density [43]. The compressive strength of a second-order honeycomb core sandwich plate is also three to six times as much as that of an equivalent honeycomb sandwich plate [44, 45][2].

In addition to the stand-alone solid core or the structural core, the sandwich core can be any combinations of the solid and structural cores to form either a reinforced solid core or a solid-filled structural core. For the former, a simple solid block made of foam can be stitched with metallic rods to form a 3D pin reinforced solid core [46]. The transverse stiffness and the strength of this special sandwich construction is considerably more improved than those of an unreinforced solid core [47]. For the latter, the void of structural cores such as the web core or the honeycomb core may be filled by a solid core material such as balsa wood, polymeric foam, and concrete. It was found that, for a solid-filled web core sandwich panel, the shear stiffness in the perpendicular direction to the axis of stiffeners was increased [48][3]. For a solid-filled honeycomb core, the cell walls of the unfilled honeycomb core were also reinforced by solid foam [49].

2.2 Steel-Concrete-Steel (SCS) Sandwich Construction

Because of the variety of the design and construction of the existing sandwich structures, it may be concluded here that there are no limitations of further invention and development to achieve a higher performance sandwich structure. A steel-concrete-steel (SCS) sandwich construction is another example of the sandwich construction which has been proposed, researched, and developed since the mid 1980s [1]. The development trend is to introduce a new type of concrete and/or a new type of shear connectors [2–8]. It is

[2] cited by Kooistra et al. [43]

[3] see Paper B: H. Kolsters and D. Zenkert. Numerical and experimental validation of a stiffness model for laser-welded sandwich panels with vertical webs and a low-density core.

also further adapted from civil to shipbuilding engineering applications [2, 7–10]. This motivation challenges the author to present another novel construction form of the SCS sandwich construction, and to develop a means of assessing its performance.

The SCS sandwich construction represents another special form of sandwich construction which may be classified into the group of reinforced solid core sandwich construction. It consists of two steel face plates and a concrete core which are connected together by means of a series of shear connectors. It is another combination of steel and concrete which have played significant roles in the creation of steel-concrete composite structures. To perform fully composite action, the internal loads between the steel face plates and the concrete core are transferred from each other by the shear connectors.

2.2.1 Construction Forms

The state-of-the-art construction forms of the SCS sandwich structures are (1) double-skin sandwich construction (DSC), (2) Bi-Steel sandwich construction (Bi-Steel), and (3) alternative SCS sandwich construction. They are different in the pattern of their shear connectors, as shown in Figs. 1.1 and 2.3.

The DSC is probably the first form of the SCS sandwich construction. It consists of two steel plates, a concrete core, and a group of shear stud connectors. A shear stud connector is mechanically welded to either the top steel face or the bottom steel face plate using a stud welding gun. The length of the shear stud can be either shorter than or equal to the depth of the concrete core. Obviously, the DSC is similar to steel-concrete composite construction. The DSC was originally proposed as the alternative construction method for the Conwy River submerged-tube-tunnel crossing project in the UK by the Tomlinson brothers in the mid 1980s [1, 12]. By that time, however, it was not qualified and selected for the project due to the difficulty in on-site quality control, especially controlling the depth of the sandwich core in the unfilled stage [1]; moreover, there was no previous evidence to demonstrate the efficiency of this construction method. Nevertheless, the proposal of the DSC has challenged engineers to further invent another SCS sandwich construction.

The Bi-Steel is the second form of the SCS sandwich construction. It also consists of two steel plates, a concrete core, and a group of shear stud connectors. Unlike the DSC, however, both ends of the shear stud connector of the Bi-Steel are simultaneously welded to both the top and bottom steel face plates using the innovative prefabrication technique developed by British Steel plc. (later, Corus) [1]. As a result, the Bi-Steel can minimise some on-site construction problems of the DSC. The Bi-Steel is the commercially available product of Corus (formerly, British Steel plc.) [50]. It was initially proposed when

Mr H. G. Bowerman[4] realised that the problems of the DSC could be solved if both the two ends of the shear stud connector could be welded to the top and bottom steel face plates simultaneously. This objective was achieved [14] and the Bi-Steel product has been manufactured since 1997 [51].

In addition to the first two types of the SCS sandwich construction, the research group of the National University of Singapore has also proposed another alternative SCS sandwich construction. Instead of using the shear stud connectors, this alternative consists of two steel face plates, a concrete core, and a group of innovative J-hook connectors [2–6]. This alternative SCS sandwich construction is probably proposed for shipbuilding and offshore applications [2, 9, 10]. It seems to be the advantageous solution of a simplified low-cost-construction technique compared with the Bi-Steel [2, 3] because it just requires simplified construction tools which are now generally available at construction sites. Similar to the shear stud connector, the J-hook connector can also be welded to either the top steel face plate or the bottom steel face plate using a modified stud welding gun [4, 5]. The research and development of this alternative SCS sandwich construction is probably in progress.

Considering the existing SCS sandwich construction, it can be seen that the state-of-the-art shear connectors are a single-ended friction-welded stud connector, a both-ended friction-welded bar connector, and a single-ended friction-welded J-hook connector; they are used in the DSC, the Bi-Steel, and the alternative SCS sandwich construction, respectively. However, there are a few more alternative shear connectors conceptually presented by Liew and Wang [2], for example, a bolt-and-nut connector and a self-adhesive slot connector. All shear connector types mentioned here are graphically illustrated in Fig. 2.3.

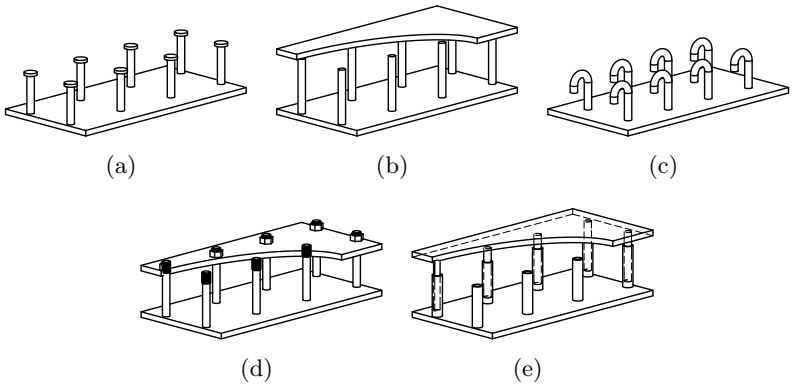

FIGURE 2.3: Sketches of shear connectors used in steel-concrete-steel sandwich construction (a) single-ended friction-welded stud connectors, (b) both-ended friction-welded bar connectors, (c) single-ended friction-welded J-hook connectors, (d) bolt-and-nut connectors, and (e) self-adhesive slot connectors

[4] Mr Hugh Gordon Bowerman – a former technical manager of Corus Bi-Steel [1]

2.2.2 Applications

Being the alternative construction technique of civil/structural engineering applications, the DSC was originally introduced in the UK in the mid 1980s [1]. Although it was not qualified for the proposal of the Conwy River submerged-tube-tunnel crossing project, the concept of the SCS sandwich construction has been further developed. The Bi-Steel is probably the well-known SCS sandwich construction form used in recently engineering applications, for example, blast protection structures, perimeter security walls, and shear walls of tall building structures [52].

The applications of the SCS sandwich construction have also been feasibly studied for nuclear power plants [53]. The idea is to deliver high performance solutions against a conventional construction form such as a reinforced concrete (RC) structure. Conceptually, it seems that an SCS sandwich beam is stronger and stiffer than an equivalent RC beam. At the same strength, the depth of the SCS sandwich beam is less than that of the RC beam because of the optimum positioning of the steel face plates. In addition, the constructability of the SCS sandwich structures seems to be better than that of the RC structures. Figure 2.4 demonstrates the construction process of the SCS sandwich construction compared with the RC construction; it can be seen that the overall construction time may be reduced by 50% [53].

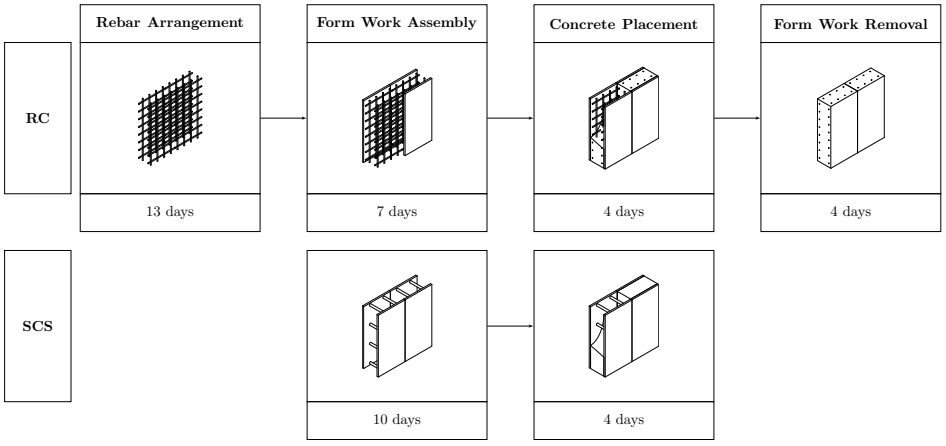

FIGURE 2.4: A comparison of construction process between a steel-concrete-steel sandwich structure and a reinforced concrete structure [modified from 53]

Although the SCS sandwich construction was originated in civil/structural engineering applications, it has been also further researched and developed for shipbuilding/offshore applications [2, 7–10]. The initial concept is to deliver competitive solutions against conventional stiffened plates, as previously compared in Fig. 1.2. The applications are possibly, for example, tanker ships, LNG ships, and large offshore structures. With the variety of concrete materials, the lightweight concrete with dry density of below

1,000 kg/m^3 is now available to be the alternative material for marine applications [8]. The potential advantages of steel-lightweight concrete-steel sandwich structures to shipbuilding applications have been noted by Kujala and Noury [54]. The advantages are, for example, an increase in plate buckling and hull torsion stiffnesses, an improvement in noise and vibration damping properties, and an increase in energy absorption (in case of collision or grounding). The past and on-going development projects of the SCS sandwich construction for shipbuilding applications may be found at Aker Yards [54] and Keppel offshore and marine Ltd. [2].

2.2.3 Research and Development

The SCS sandwich structures have been being researched and developed since it was proposed as the alternative construction form for the Conwy River submerged-tube-tunnel crossing project in the mid 1980s. The major timeframe of the research and development may be divided into three phases: (1) research of the DSC, from 1985 to 2002, (2) research of the Bi-Steel, from 1987 to present, and (3) research of the alternative SCS sandwich construction, from 2005 to present, as chronologically illustrated in Fig. 2.5. It should be noted that the years indicated here are approximate numbers according to the information of the research publications listed in Table 2.1.

Initially, the research of the DSC had been intensively studied at the University of Wales, UK. The experimental research to investigate the structural behaviour and the failure modes of the DSC structures for the proposal of the Conwy River submerged-tube-tunnel crossing project was conducted [1]. The fifty-three one-third scale specimens of the DSC structures were set up to investigate the effect of the thickness of a steel face plate, the length of a shear stud connector, the spacing between shear stud connectors, and the compressive strength of concrete. The specimens were divided into eighteen DSC beams [11], twenty-three DSC columns, and twelve DSC beam-column structures [55]. In addition, the full scale specimens of six wide DSC beams, two DSC columns and three DSC beam-columns were also studied [56]. The fundamental failure modes of the DSC beams subjected to a static load condition were found and reported as, for example, yielding of the tension plate, horizontal slipping at the interface between the steel face plate and the concrete core, and vertical shear failing of the concrete core. The structural behaviour was explained by Oduyemi and Wright [11]. The design criteria were developed based on the experimental data [56]. The closed-form solutions were later presented by Wright and Oduyemi [57]. The study of six four-point loaded beams with relatively low span to depth ratios was later presented by Roberts et al. [58]. The series of fatigue tests of the DSC beams were also carried out by Roberts and Dogan [59].

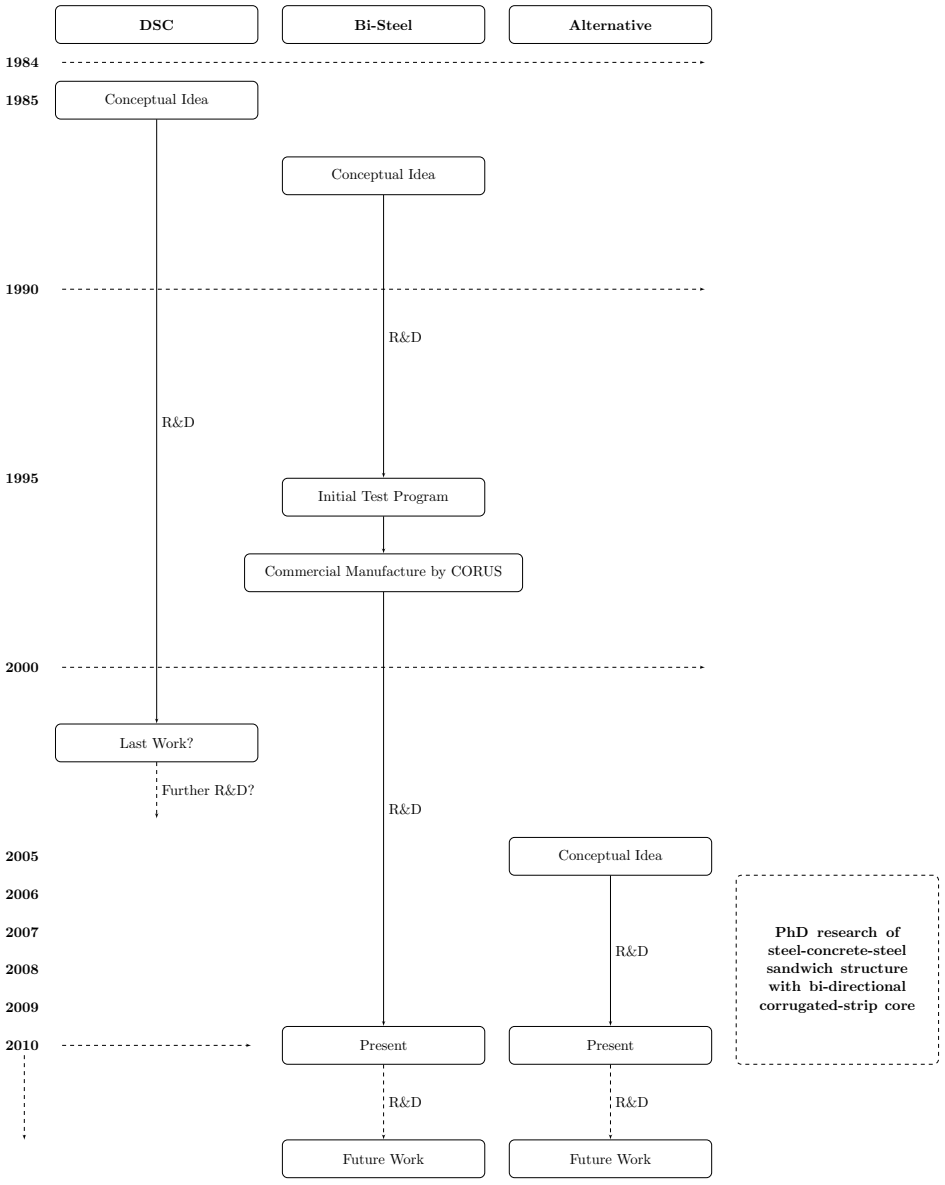

FIGURE 2.5: A timeframe of the research and development of steel-concrete-steel sandwich construction

The research to improve the composite strength of the DSC beams by increasing surface roughness of the steel face plates was conducted by Subedi and Coyle [13]. It was found that the buckling problem of the compression steel face plate caused by debonding at the steel-concrete interface could be improved using the surfaced steel face plates such as the Expamet surfaced steel plate[5] or the Wavy wire surfaced steel plate[6] [13].

The research of the Bi-Steel had also been mainly conducted in the UK universities. Most research was carried out by PhD research students, for example, McKinley [60]

[5] Expamet surfaced steel plate – a steel plate with 2.16 *mm* thick expanded metal mesh welded on to the steel plate [13]

[6] Wavy wire surfaced steel plate – a steel plate with sinusoidal bent 6 *mm* diameter wire laid flat and welded on to the steel plate [13]

at City University, Clubley [61] at the University of Southampton, Coyle [62] at the University of Dundee, and Foundoukos [63] at Imperial College of Science, Technology and Medicine, the University of London.

The series of sixteen full-scale SCS sandwich beams – included the DSC and the Bi-Steel beams – were experimentally studied and reported by McKinley and Boswell [64]. The objective was to investigate the elastic and plastic behaviour of simply supported beams subjected to a three-point loading condition. It was found that both the DSC and the Bi-Steel beams yielded the same behaviour of elastic and early plastic deformations and load characteristics. However, the failure modes of the DSC beams were different from those of the Bi-Steel beams. Typically, the Bi-Steel beams failed due to local buckling of the compression face plates whereas the DSC beams failed by pulling the shear studs out of the concrete core. McKinley and Boswell [64] also further developed analytical solutions to express the elastic behaviour of the SCS sandwich beam.

In 2007, the experimental study to obtain the static behaviour of eighteen Bi-Steel beams was reported by Xie et al. [12]. The beams were 400 mm wide with two rows of both-ended friction-welded bar connectors in the transverse direction and the concrete core was the ready-mix concrete of grade C40/50. The failure modes of beams subjected to the static load were observed and reported as a tension plate failure, a bar tension failure, a bar shear failure, and a concrete shear failure, as graphically shown in Fig. 2.6. In addition to the static test of Bi-Steel beams, the fatigue tests of eighteen Bi-Steel beams was also carried out and reported by Foundoukos et al. [65]. It was found that the beams could also fail in the tension plate failure and in the bar shear failure.

The diagonal shear crack of the concrete core of the Bi-Steel beam under the static load initially developed from the tensile crack at a bar connector. The behaviour of the Bi-Steel beam such as the deflection or the tension in the bar connector did not affected from this initial crack. The diagonal shear crack continually occurred as the applied load increased. It was found that this following diagonal shear crack was independent from the initial tension crack and appeared in the tension region of the concrete core at about 45° to the axis of the beam [12].

Numerical and analytical studies were later presented by Foundoukos and Chapman [15]. It was found that the existing analytical solutions based on a truss model and an equivalent steel beam model yielded the good prediction of the behaviour of the tension face plate of the Bi-Steel beams subjected to a three-point loading condition compared with a numerical study using the ABAQUS/Explicit FE package. However, for the compression face plate, the truss model was more accurate than the equivalent steel beam model. Further development of the truss model was carried out to overcome the Bi-Steel beams subjected to a uniform load case. In this case, the truss model was less

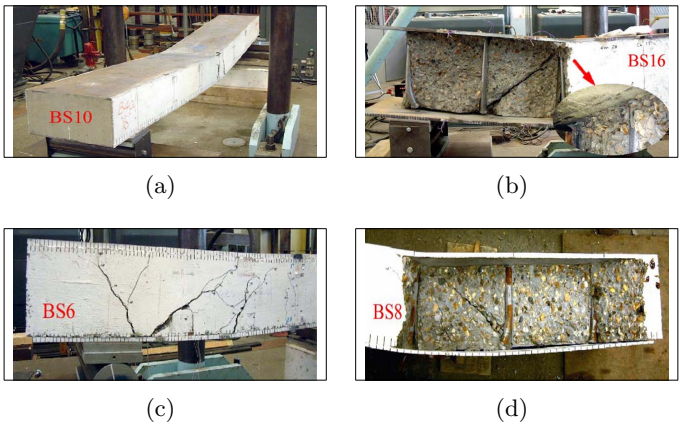

FIGURE 2.6: Typical failure modes of Bi-Steel sandwich beams subjected to static load conditions (a) a tension plate failure, (b) a bar tension failure, (c) a concrete shear failure, and (d) a bar shear failure [12, see the original photographs in Fig. 6, Page 741]

accurate in the force of the compression face plate than the equivalent steel beam model. However, Foundoukos and Chapman [15] noted that the truss model may be used as an analytical method because it was conservative. Further investigation of the transverse shear capacity of the Bi-Steel beams was also carried out using the FE method.

Moving from the UK to Singapore, the research of the alternative SCS sandwich beams has been carried out mainly at the National University of Singapore. Most research was of the alternative SCS sandwich beams with the novel J-hook connectors and the lightweight concrete core [2–6, 9, 10]. The research objective was to investigate the structural behaviour of these innovative SCS sandwich beams, especially their fatigue performance [6, 9] and their structural behaviour under impact loading [3, 5].

To the current knowledge of the author, the previous research may be summarised in tabular form as presented in Table 2.1.

2.3 Identification of Gaps in the Current Knowledge

The need for high performance sandwich structures, especially of stiffness and strength, is increasing. This specific requirement leads to the improvement of design and construction of the sandwich structures. To deliver such sandwich structures, engineers can either adapt an existing or introduce a new production/construction method.

In the structural core sandwich construction, the corrugated core sandwich structures are the obvious examples of the variety of designs; the cores of these sandwich structures can be designed in various patterns, as shown in Fig. 2.7. The conventional corrugated core sandwich structure as shown in Fig. 2.7(a) is theoretically strong in the x-direction,

TABLE 2.1: Summary of research on steel-concrete-steel sandwich construction

Year	Reference	SCS [a]			Shear Connector [b]					Mode [c]			Specimen [d]						Load [e]							Studied Parameter [f]										
		DSC	BS	ASC	SC	BFWC	JHC	ABC	BC/PBC	ES	NS	TS	B	C	BC	S	W	SC-P	SC-T	SL	FL	IEL	PL	UL	AL	SL-W	t_f	h_c	s_c/n	s_c/h_c	l_c	L/h_c	f'_c	FCE	d_c	s_c	ρ_c	CT	θ_c
1989	Oduyemi and Wright [11]	X			X					X		X	X					X		X			X				X	X			X		X					—No Available Information—
1991	Wright and Oduyemi [57]	X			X							X	X							X			X	X			X				—Not Varied—							
	Wright et al. [56]	X			X					X				X	X					X			X		X		X	X			X		X					
	Wright et al. [55]	X			X					X		X	X	X	X					X			X		X				X									
1996	Roberts et al. [58]	X			X					X		X	X					X		X			X								—Not Varied—							
1998	Burgan and Naji [66]	X			X					X		X			—N/A—								—N/A—								—N/A—							
	Hoff [67]	X			X					X					—N/A—								—N/A—								—N/A—							
	Roberts and Dogan [59]	X			X					X		X	X					X			X										—Not Varied—							
	Sun and Johnson [68]	X			X							X			—N/A—								—N/A—								—N/A—							
	Takeuchi et al. [69]	X			X					X							X								X	X												
1999	McKinley [60] [g]	X	X		X	X																																
2001	Clubley [61] [g]		X			X																																
	Coyle [62] [g]	X			X				X																													
2002	Bowerman and Chapman [70]		X			X					—N/A—					—N/A—							—N/A—								—N/A—							
	Bowerman et al. [1]		X			X					—N/A—					—N/A—							—N/A—								—N/A—							
	McKinley and Boswell [64]	X	X		X	X				X		X	X							X			X								—Not Varied—							
	Shanmugam et al. [71]	X			X						X					X				X			X				X		X									
	Subedi and Coyle [13]	X			X					X			X					X		X			X				X				X	X						
2003	Clubley et al. [72]		X			X				X	X							X		X							X											
	Clubley et al. [73]		X			X					X							X		X							X											
	Dixon and Bowerman [51]		X			X					—N/A—					—N/A—							—N/A—								—N/A—							

TABLE 2.1: Continued

Year	Reference	SCS [a]			Shear Connector [b]					Mode [c]			Specimen [d]					Load [e]						Studied Parameter [f]									
		DSC	BS	ASC	SC	BFWC	JHC	ABC	BC/PBC	ES	NS	TS	B	C	BC	S	W	SC-P	SC-T	SL	FL	IEL	PL	UL	AL	SL-W	t_f	h_c	s_c/n	s_c/h_c	l_c	L/h_c	f'_c	FCE	d_c	s_c	ρ_c	CT	θ_c
2005	Foundoukos [63] [g]		X		X					X	X								X	X	X						X											X	
	Xie and Chapman [74]		X		X					X	X									X							X											X	
	Xie et al. [75]		X		X					X	X								X	X							X											X	
2006	Dai and Liew [9]			X				X		X	—N/A—				—N/A—							—N/A—										—N/A—							
	Dai and Liew [10]			X			—N/A—			X	—N/A—				—N/A—							—N/A—										—N/A—							
	Xie and Chapman [14]			X		X				X	X	X	—Research Summary—									—Research Summary—									—Research Summary—							
2007	Foundoukos et al. [65]			X		X				X	X	X						X	X		X																		
	Liew and Wang [2]			X		X	X	X		X	X							X														—N/A—						
	Liew et al. [3]			X		X				X	X											X																	
	Xie et al. [12]			X		X				X	X												X																
2008	Foundoukos and Chapman [15]			X		X				X	X	X											X																
	Liew [27]			X		X					—N/A—				—N/A—								—N/A—																
	Sohel [76] [g]			X		X											X																						
2009	Liew and Sohel [4]			X		X					X	X				X					X			X				X			X				X			X	
	Liew et al. [5]			X		X					X	X									X			X				X							X			X	
	Xuexin [77] [g]			X		X																						X								X	X	X	
2010	Dai and Liew [6]			X		X					X	X									X							X				—N/A—							

—No Available Information—

[a] DSC – Double-skin Sandwich Construction, BS – Bi-steel Sandwich Construction, ASC – Alternative SCS Sandwich Construction

[b] SC – Stud Connector, BFWC – Both-end Fiction Welded Connector, JHC – J-J Hook Connector, ABC – Proposed Adhesive Bonded Connector, BC/PBC – Bolted Connector/Proposed Bolted Connector

[c] ES – Experimental Study, NS – Numerical Study, TS – Theoretical Study

[d] B – Beam, C – Column, BC – Beam-Column, S – Slab, W – Wall, SC-P – Shear Connector – Push-out/Pull-out Test, SC-T – Shear Connector – Tension Test

[e] SL – Static Load, FL – Fatigue Load, IEL – Impact/Explosive Load, PL – Point Load (Beam Specimen), UL – Uniformly Distributed Load (Beam Specimen), AL – Axial Load (Column Specimen), SL-W – Shear Load (Wall Specimen)

[f] t_f – Thickness of steel faceplate, h_c – Depth of sandwich core, s_c/n – Ratio of connector spacing over amount of shear connector, s_c/h_c – Ratio of connector spacing over depth of sandwich core, l_c – Length of shear connector, L/h_c – Ratio of beam span over depth of sandwich core, f'_c – Concrete strength, FCE – Flash Collar Effect, d_c – Diameter of shear connector, s_c – Spacing of shear connector, ρ_c – Concrete density, CT – Concrete Type, θ_c – Alignment angle of shear connector

[g] see further detail in original thesis or related paper presented in this table

but less strong in the y-direction [31]. However, the weak point of this simple arrangement can be improved by arranging the corrugated core in both the x- and y-directions [33], as shown in Fig. 2.7(b). Moreover, the corrugated core can also be constructed with corrugated-strip plates such as the offset-corrugated core [35], the bi-directionally corrugated core [16], and the cross-corrugated core [17], as shown in Figs. 2.7(c), 2.7(d), and 2.7(e), respectively. These cores consist of a series of corrugated-strip plates which are arranged in either uni- or bi-directional format. The stiffness of these alternative corrugated sandwich plates can be controlled in both the x- and y-directions. It was found by Ray [18] that the transverse shear stiffness per unit weight density of the offset-corrugated core was 96% higher than that of the conventional corrugated core. The cross-corrugated core was also more efficient in transverse shear stiffness than the conventional corrugated core; its shear stiffness was 173% higher [18].

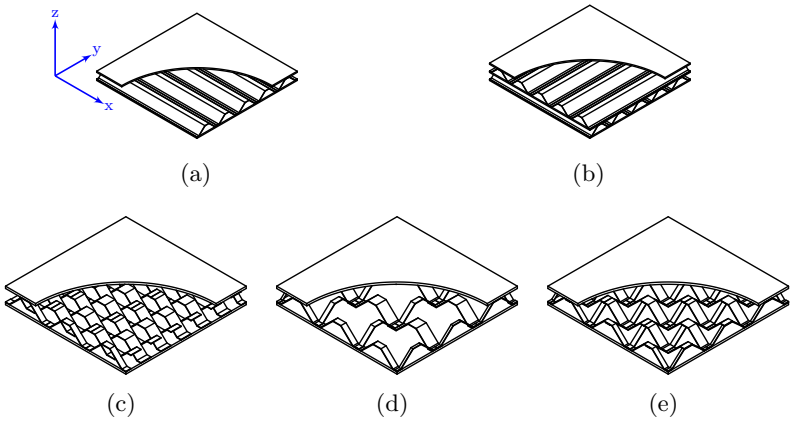

FIGURE 2.7: Sketches of (a) conventional one-way, (b) two-way [33], (c) offset- [35], (d) bi-directional [16], and (e) cross- [17] corrugated core sandwich construction

The innovative design and construction is also found in the SCS sandwich construction. The major innovation is to introduce a new shear connector type. However, it may be seen that all the current shear connector types are similar in an alignment pattern. They all align in the vertical direction – the axis of the shear connector is normal to the face plates. Although the consequential improvement is probably a better produce ability or constructability, the stiffness and strength of the recent SCS sandwich structures may probably not reach the optimum performance, especially of the transverse shear stiffness and strength.

In the SCS sandwich construction, it is well known that the shear connector has to act as a mechanical part to maintain the composite action between the steel face plates and the concrete core; it has to prevent the horizontal slip and the vertical separation of the concrete core from the steel face plates [1]. These major functions are similar to those of the shear connector of steel-concrete composite construction [78, 79].

In the steel-concrete composite construction, however, it is known that the type of the shear connector depends on the type of load. Therefore, there are various shear connector types used in this composite construction, for example, as shown in Figs. 2.8(a) to 2.8(e). A single-ended friction-welded stud connector is very popular for general load conditions due to its economy and product ability [1, 80]. This shear connector with typical size of 19 to 22 *mm* diameter has been widely used in most steel-concrete composite bridges for over 40 years [81]. In the case of greater shear stress requirements, however, another suitable type of the shear connector may be a larger stud connector, a bar connector, or a perforated plate connector. The use of large stud connector with extra size of 30 *mm* diameter may be found in Shim et al. [82] and Lee et al. [83]. In the case of high tensile stress requirements, a long stud or a hoop connector may be used [78].

The special design of the shear connector is also found in another similar composite construction. In timber wood-lightweight concrete composite construction, a 45°-angle screw connector, as shown in Fig. 2.8(f), was found as an effective shear connector [84]. This is because the inclined screw will be primarily loaded in tension instead of shear.

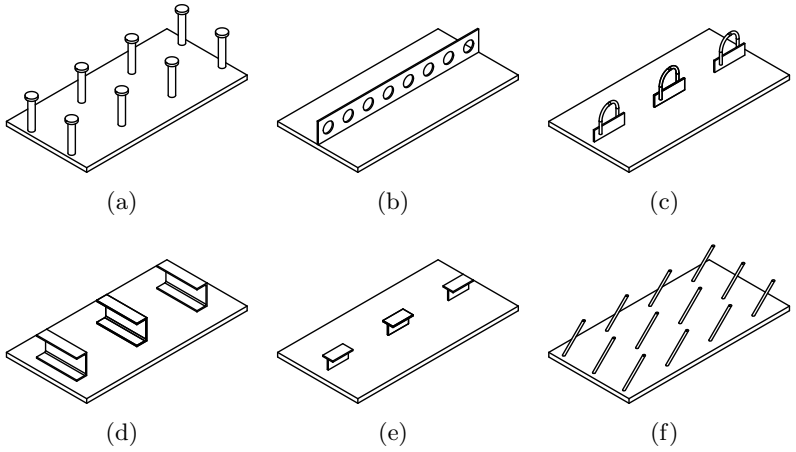

FIGURE 2.8: Sketches of (a) single-ended friction-welded stud, (b) Perfobond, (c) bar with hoop, (d) channel, (e) T-shaped shear connectors used in steel-concrete composite construction [78, 85], and (f) inclined screw shear connectors used in timber-concrete composite construction [84]

Moving back to the SCS sandwich construction, it is also known that a concrete-filled SCS sandwich beam under bending load suffers diagonal shear cracks [4, 11–15]. The diagonal shear crack is one of the typical failure modes of the SCS sandwich beams, as previously shown in Fig 2.6. Although the concrete shear failure is not the primary mode of failure, it typically occurs in combination with another failure mode. Xie et al. [12] recommended that it should be prevented so that the SCS sandwich beam primarily fails due to the tension plate failure to ensure that the ductility behaviour of the SCS sandwich beam can be achieved.

Providing some kind of transverse shear reinforcements is the way to overcome the diagonal shear crack failure. This method is able to prevent crack propagation and to increase the strength and the ductility of beams. The concept of providing transverse shear reinforcements is generally found in conventional RC beams [86, 87]; it is also found in the SCS sandwich beams [50]. In addition to maintaining the composite action between the steel face plates and the concrete core, the shear connectors within the SCS sandwich beam also act as transverse shear reinforcements.

In the conventional RC beams, there is much evidence and research supporting the concept of using the transverse shear reinforcements to increase the shear strength of the beams. The transverse shear reinforcements such as a vertical stirrup[7], an inclined stirrup, a 45° bent-up bar and a steel plate have been used for many years. Recently, a carbon-fibre reinforced plastic (CFRP) sheet can also be found as the transverse shear reinforcements. These mentioned systems can be designed in either a vertical alignment pattern or an inclined alignment pattern.

The vertical stirrup is very popular in the RC construction because of the ease of use. The inclined stirrup and the bent-up bar are occasionally used due to the difficulty in construction process. However, all of them are practically found as the solutions for shear design of RC beams [87]. For the steel plate system, the experimental study by Adhikary and Mutsuyoshi [88] showed that the brittle diagonal shear failure mode of the RC beams was effectively prevented by the transverse shear reinforcements. The failure mode of the beams also changed from the brittle diagonal shear crack to the ductile flexural failure mode. The shear strength of the beams with the epoxy bonded steel plates was increased by 72% compared with the beam without the transverse shear reinforcements. The experimental study of the CFRP-strip shear reinforcements aligned in 45° angle to the neutral axis of the concrete beams also showed that the shear strength was increased by approximately 300% [89].

By comparison, the inclined shear reinforcements are considerably more advantageous than the vertical shear reinforcements. In RC design practices, the inclined stirrup and the bent-up bar are considerably more efficient than the vertical one [87]. The experimental studies of the CFRP and other similar materials also showed that the inclined strip shear reinforcements were more advantageous in the transverse shear strength of the beam than the vertical one [90–93]. Based on the experimental investigation of the CFRP-strip shear reinforcements, Taljsten [94] recommended that the direction of the shear reinforcement strips should be perpendicularly aligned to the diagonal shear crack line to achieve the most effective performance of the shear reinforcements.

[7] Stirrup – a close loop or an opened loop of bent rod in, for example, circular shape, rectangular shape, U shape and W shape for supporting longitudinal reinforcing bars in reinforced concrete structures

It may be seen from some engineering practices and research of the RC beams, for example in [93–108], that the shear strength contributed by the transverse shear reinforcements significantly depends on the alignment angle of the shear reinforcements. Most of the formulae provided by these references approximately yield the optimum point of the shear strength capacity of the shear reinforcements when they are perpendicularly aligned to the diagonal shear crack line. In the opinion of the author, this may also be alleviated using the inclined shear connectors in the SCS sandwich construction.

Although the SCS sandwich beam and the RC beam are similar in their structural components, as comparably illustrated in Fig. 2.9, it can be seen that the current design of the shear connectors of the SCS sandwich beam is limited to the vertical alignment pattern only, as compared in Table 2.2. Therefore, it may imply that the applications of the inclined shear connectors – the inclined transverse shear reinforcements – may not be now clearly understood. In the author's opinion, it should be further researched and developed to achieve the possible advantage of this alternative engineering solution.

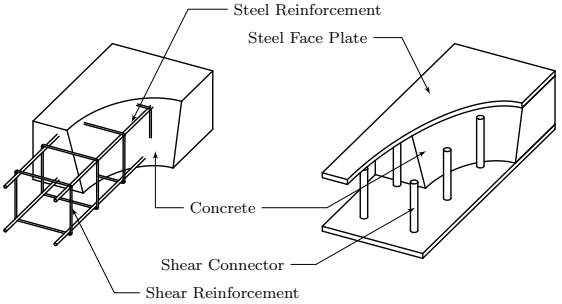

FIGURE 2.9: A comparison between a steel-concrete-steel sandwich beam and a reinforced concrete beam

TABLE 2.2: A comparison in alignment patterns of transverse shear reinforcement systems between reinforced concrete (RC) beams and steel-concrete-steel (SCS) sandwich beams

Alignment Pattern	Transverse Shear Reinforcement System					
	RC Beam			SCS Beam		
	S [a]	BB [b]	SP [c]	SC [d]	BFWC [e]	AC [f]
Vertical	109, 110		88, 90–92, 108, 111–113	11, 13, 55–60, 62, 64, 66, 67, 69, 71	1, 12, 14, 15, 51, 60, 61, 63–65, 70, 72–75	2, 3, 62
Inclined		110	88–92, 112–114	*There is no current engineering application using inclined shear connectors.*		

[a] S – Stirrup
[b] BB – Bent-up Bar
[c] SP – Strip Plate (made of steel or fibre-reinforced polymer (FRP) material)
[d] SC – Stud Connector
[e] BFWC – Both-end Fiction Welded Connector
[f] AC – Alternative Connector

However, it can be clearly seen from column θ_c of Table 2.1 that the study of the effect of the inclined shear connectors to the structural behaviour of the SCS sandwich beam

is missing. This is due to only the vertical shear connectors being used in the state-of-the-art SCS sandwich construction. The innovative SCS sandwich structure with the inclined shear connectors and the understanding of its structural behaviour should dominate and contribute to the current engineering knowledge of the SCS sandwich construction, both of the unfilled and concrete-filled types.

2.4 Concluding Remark

The literature demonstrates the variety of the design and construction of the sandwich structures and presents the possibility to invent a new type of sandwich construction. In the SCS sandwich construction, the major development is to introduce the new shear connector type; the development trend is from the single-ended friction-welded shear stud connector to the both-ended friction-welded shear stud connector to the innovative J hook connector. It can be seen from the existing forms of the SCS sandwich construction that, however, all shear connector types recently used are aligned in the same pattern, i.e., in the perpendicular direction to the steel face plates.

According to the literature, it is known that the concrete-filled SCS sandwich beams may suffer the diagonal shear crack of the concrete core. Although the existing shear connectors can be incorporated to overcome this problem, they may probably not provide the optimum strength capacity. In similar construction such as the RC beams, there is evidence to support the theory that the inclined shear reinforcements are more effective in terms of strength capacity than the vertical shear reinforcements. Some evidence in the steel-concrete and timber-wood composite construction also mention the use of the shear connector corresponding to load conditions.

Therefore, in the SCS sandwich beams, aligning the shear connector in the angular direction could be an advantage. However, there is no current design and construction of the SCS sandwich beams with the inclined shear connectors. This may imply that the understanding of the structural behaviour due to the inclined shear connector is missing from the current knowledge of the SCS sandwich construction, both in the unfilled and concrete-filled types.

Chapter 3

Design and Construction of a Steel-Concrete-Steel Sandwich Beam with Bi-Directional Corrugated-Strip Core

3.1 Construction Process

Practically, the construction process of steel-concrete-steel (SCS) sandwich structure is as diagrammatically illustrated in Fig. 3.1. The process starts from connecting prefabricated steel plates and shear connectors by, for example, a welding method [4, 5, 50]. This process can be either off- or on-site; it can also be done using either portable man-operated tools [4, 5] or large computer-operated machines [50]. An unfilled SCS sandwich panel is created and will function as concrete formwork. At this stage, additional temporary supports may be needed to control distance between the top and bottom face plates. After firmly placed, the slurry-state concrete will be poured into the void of the unfilled SCS sandwich panel, and then be cured until the concrete sets to a solid state.

Since a concrete pouring technique may follow a qualified procedure of concrete constructions or other existing SCS sandwich constructions, for example in [50], this research therefore aims to develop the construction process of the unfilled SCS sandwich structure only.

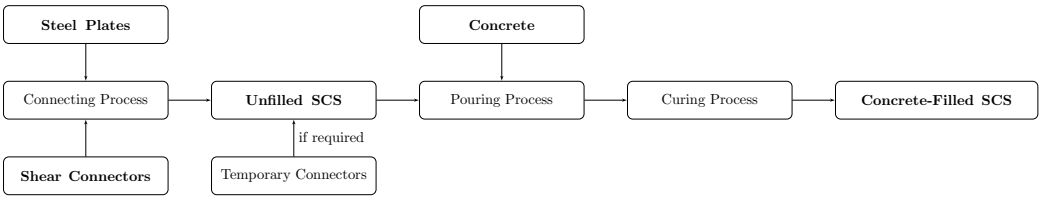

FIGURE 3.1: Construction process of steel-concrete-steel sandwich construction

3.2 Configuration of an Unfilled Sandwich Beam

Figure 3.2 shows the unfilled stage of an SCS sandwich beam with bi-directional corrugated-strip core (Bi-CSC) system. The main components of this proposed sandwich structure are the steel face plates and the corrugated-strip plate. The corrugated-strip plate may be either a single-unit or a continuous-multi-unit of corrugation. The Bi-CSC system consists of a group of corrugated-strip plates which are aligned in both the x- and y-directions. The Bi-CSC system then functions as the structural sandwich core for the unfilled stage and later as the shear connector for the concrete-filled stage.

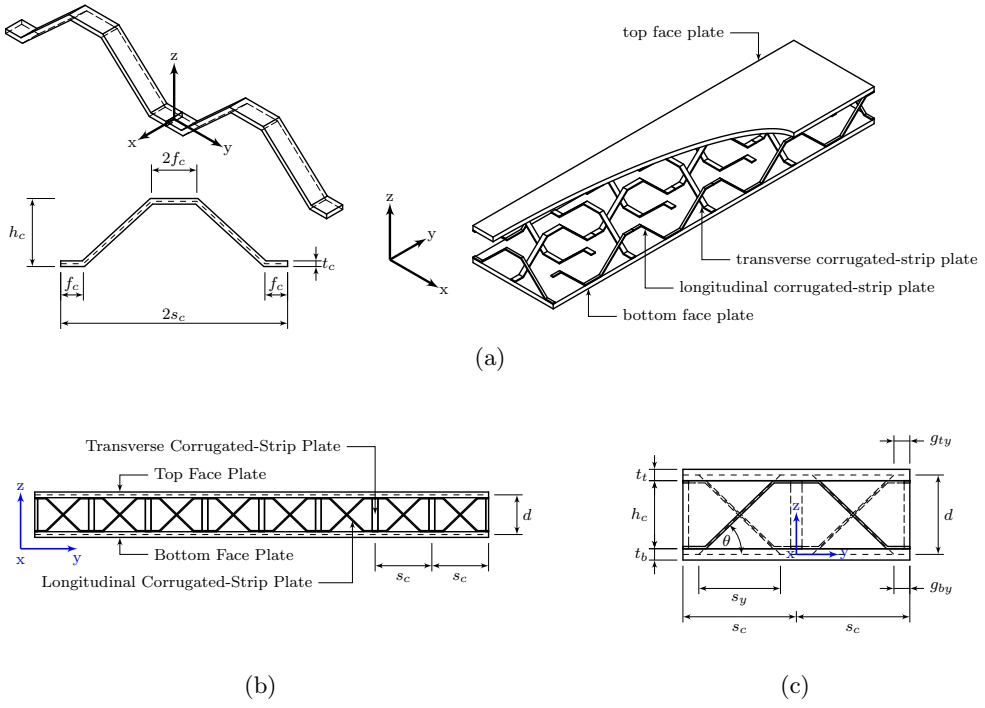

FIGURE 3.2: Configurations of unfilled steel-concrete-steel sandwich beam with bi-directional corrugated-strip core (a) an isometric view, (b) a longitudinal view, and (c) a repetitive unit cell

The dimensional geometry of the sandwich beam is defined by five conventional parameters: thickness of the top face plate, t_t, thickness of the bottom face plate, t_b, depth of the sandwich core, h_c, width of the beam, b, and length of the beam, L. The geometry

of a repetitive unit of corrugated-strip plate is defined by five parameters: width of the strip plate, b_c, thickness of the plate, t_c, horizontal length of the corrugation unit, s_c, length of the flat leg, f_c, and height of the corrugation, h_c. The corrugated-strip plates are preferably arranged with equal spacing s_c in both the x- and y-directions. However, it is not necessary to use the same configuration in both directions, as shown in Fig. 3.3. If applicable, the subscript tc is used to denote any geometric parameter of transverse corrugated-strip plate, i.e., in the x-direction.

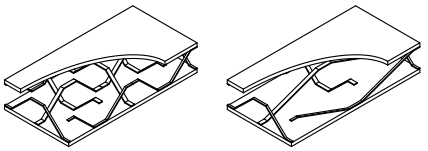

(a) (b)

FIGURE 3.3: A comparison of the configuration of an unfilled steel-concrete-steel sandwich beam with bi-directional corrugated-strip core between the x- and y-directions (a) the same configuration in both the x- and y-directions, and (b) the different configuration between the x- and y-directions

The width of the corrugated-strip plate can be expressed in terms of the width of the sandwich beam as $b_c = k_{cb}b$ where k_{cb} is defined as a coefficient of width of the corrugated-strip plate. Practically, the coefficient k_{cb} can vary in the range of 0.0 to 0.50. Figure 3.4 demonstrates four configurations of corrugated-strip core depended on the coefficient k_{cb}. The possible configurations should probably lie between Fig. 3.4(b) and 3.4(c).

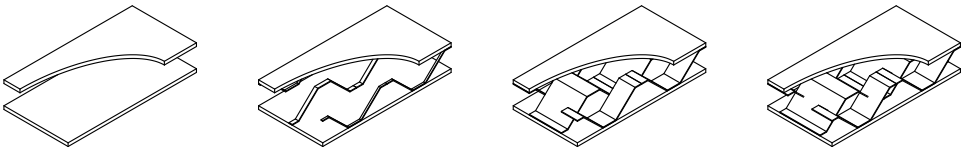

$k_{cb} = 0$ (a) $0 < k_{cb} < 0.50$ (b) $k_{cb} = 0.50$ (c) $k_{cb} > 0.50$ (d)

FIGURE 3.4: Configurations of corrugated-strip plate in terms of the width coefficient, k_{cb}

Each corrugation unit of the corrugated-strip plate consists of two inclined parts. These parts align at angle θ with the y-axis – the longitudinal axis of sandwich beam. The parameter θ can be expressed in terms of previously defined parameters as Eq. 3.1

$$\frac{1}{\tan\theta} = \frac{s_c - 2f_c}{h_c - t_c} = \frac{s_y}{d} \tag{3.1}$$

Instead of the parameter θ, the angle of the inclined part of the corrugation unit can be indirectly expressed in terms of parameter s_y/d. Here, s_y is the horizontal projection

of the extended local neutral axis of the inclined part of the corrugated-strip plate (see Fig. 3.2(c)); it is equal to $s_c - (g_{ty} + g_{by})$. The parameter g_{ty} is the horizontal distance between the intersection point of the local neutral axis of the top face plate and the extended local neutral axis of the transverse corrugated-strip plate and the intersection point of the local neutral axis of the top face plate and the extended local neutral axis of the longitudinal corrugated-strip plate. Similarly, g_{by} is defined in the same manner where the local neutral axis of the top face plate is replaced by the local neutral axis of the bottom face plate. The parameters g_{ty} and g_{by} can be expressed in terms of previously defined parameters as Eq. 3.2. In practice, g_{ty} and g_{by} do not need to be equal to each other except the case of a symmetrically geometric section, i.e., $t_t = t_b$.

$$g_{ty} = f_c - \frac{t_t + t_c}{2\tan\theta} \tag{3.2a}$$

$$g_{by} = f_c - \frac{t_b + t_c}{2\tan\theta} \tag{3.2b}$$

It should be noted that the value of g_{ty} or g_{by} may be less than zero if $f_c < \frac{t_t+t_c}{2\tan\theta}$ or $f_c < \frac{t_b+t_c}{2\tan\theta}$, respectively. In this research, however, the value of g_{ty} and g_{by} are limited to being not less than zero; therefore, the core should be designed so that the following condition is satisfied.

$$f_c \geq \begin{cases} \frac{s_c}{2}\left(\frac{t_t+t_c}{t_t+h_c}\right) & \text{for } g_{ty} \\ \frac{s_c}{2}\left(\frac{t_b+t_c}{t_b+h_c}\right) & \text{for } g_{by} \end{cases} \tag{3.3}$$

Figure 3.5 demonstrates four major configurations of corrugated-strip core which depend on the parameter s_y/d. Creating a configuration where the inclined part is normal to the face plates can be achieved by setting s_y/d to zero (Fig. 3.5(a)). An angled inclined part can be achieved by three possible values of s_y/d. If s_y/d is less than 1.0, the angle will be greater than 45° (Fig. 3.5(b)). The specific inclined angle at 45° can be achieved by setting s_y/d to 1.0 (Fig. 3.5(c)). If s_y/d is greater than 1.0, the angle will be less than 45° (Fig. 3.5(d)).

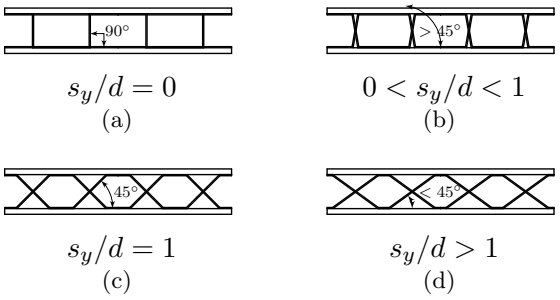

$s_y/d = 0$ (a) $\quad 0 < s_y/d < 1$ (b)

$s_y/d = 1$ (c) $\quad s_y/d > 1$ (d)

FIGURE 3.5: Configurations of corrugated-strip plate in terms of the ratio s_y/d

3.3 Fabrication Techniques

Conceptually, the novel unfilled SCS sandwich structure with the Bi-CSC system proposed in this research can be fabricated and assembled. This is because the components of the unfilled stage, i.e., the steel face plate and the corrugated-strip plate, are similar to existing engineering applications. In addition, the similar techniques to arrange the corrugated-strip plates in the bi-directional format, i.e., in both the x- and y-directions and to assembly them with the steel face plates have been found in the existing corrugated-core sandwich construction [16, 17] as earlier shown in Figs. 2.7(d) and 2.7(e).

Figure 3.6 illustrates the conceptual fabrication process proposed by the author. First, the longitudinal CSCs may be placed on the bottom face plate and firmly fixed to the plate (Fig. 3.6(a)). Second, the transverse CSCs, if required, may be moved downward and slid into the holes of the longitudinal CSCs (Fig. 3.6(b)). It may also be firmly fixed to the plate. Then, the top face plate may be placed on and fixed to both the longitudinal and transverse CSCs (Fig. 3.6(c)). In the author's opinion, there is a possibility to bond the bottom and top face plates to the flat legs of corrugated-strip plates as instructed by Ray [16, 17]. Moreover, the face plates and the flat legs of the core may be mechanical connected using spot welds, rivets, or self-tapping screws [38]. They may also be welded from outside the sandwich face plates using laser-welding technology [39]. As a result, the top and bottom face plates should be fixed to the core. An SCS sandwich plate may be later assembled from sandwich beam modules. Then, concrete can be poured into the unfilled core (Fig. 3.6(d)).

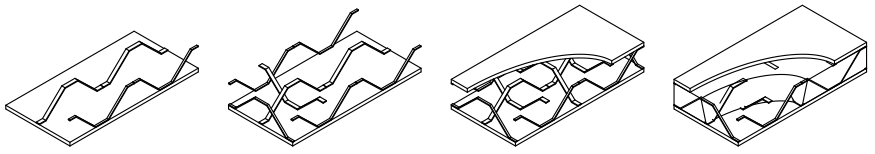

FIGURE 3.6: Conceptual construction process of a steel-concrete-steel sandwich structure with bi-directional corrugated-strip core

In detail, there are two possible methods to set a group of corrugated-strip plates out in the bi-directional format: the top-down method (TDM) and the slide-rotate method (SRM).

First, the overview of the TDM is illustrated in Fig. 3.7. After firmly placing the longitudinal corrugated-strip plates, the first transverse corrugated-strip plate should be moved downward from the top of the bottom plate (Fig. 3.7(a)). When the lower

leg of such part is below the top of the longitudinal corrugated-strip plate, as marked (1), the whole part of this corrugated-strip plate should be rotated and slid leftward to the hole, as marked (2) (Fig. 3.7(b)). Then, it should be slowly moved downward and rotated until the other leg of this part is below the top of the other longitudinal corrugated-strip plate, as marked (3). Afterward, this part should be moved downward and slid rightward to the other hole, as marked (4) (Fig. 3.7(c)). Then, it should be moved downward, placed on the bottom plate, and firmly fixed to the bottom plate. The next transverse corrugated-strip plate should be placed on, one by one, in the same process (Fig. 3.7(d)).

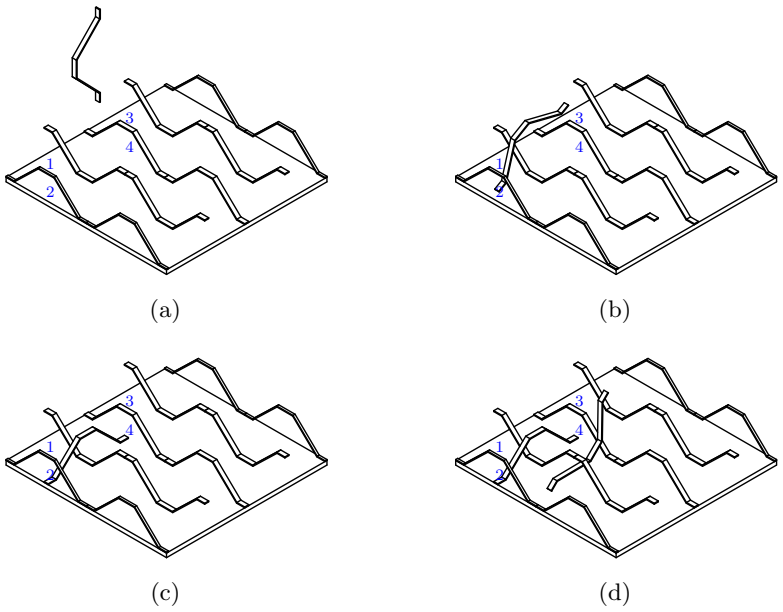

FIGURE 3.7: The top-down method

Second, the overview of the SRM is illustrated in Fig. 3.8. After firmly placing the longitudinal corrugated-strip plates, the first transverse corrugated-strip plate should be slid throughout the hexagonal holes of the longitudinal corrugated-strip plates from one side of the bottom plate to the other (Fig. 3.8(a)). Before sliding, the transverse corrugated-strip plate should be aligned so that its longitudinal axis, i.e., the y-axis, and the straight line which passes through all centre points of the holes are coincident. The transverse corrugated-strip plate should be slowly rotated after it reaches position (Fig. 3.8(b)), and then placed on and firmly fixed to the bottom plate (Fig. 3.8(c)). The next transverse corrugated-strip plate should be placed on, one by one, in the same process (Fig. 3.8(d)).

In the SRM, there are two possible planes to insert and slide the transverse corrugated-strip plate throughout the hexagonal holes of the longitudinal corrugated-strip plates without collision; they are clearly illustrated in Fig. 3.9. According to the clear distance

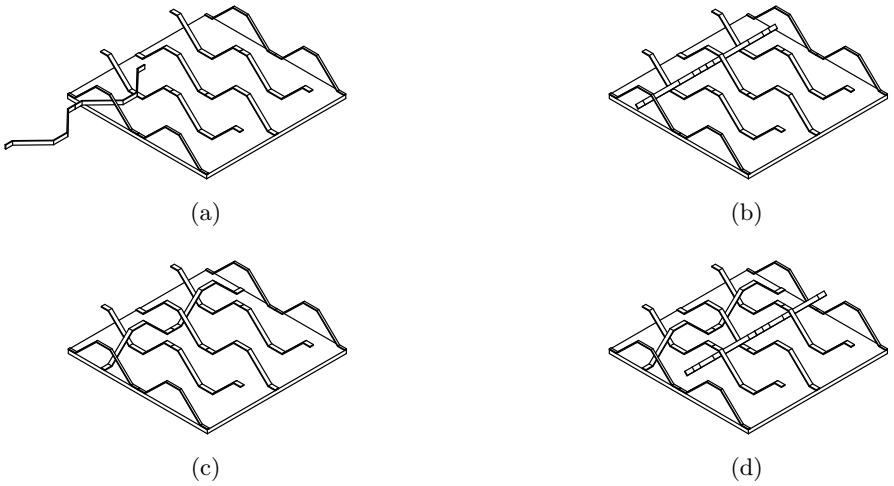

(a) (b) (c) (d)

FIGURE 3.8: The slide-rotate method

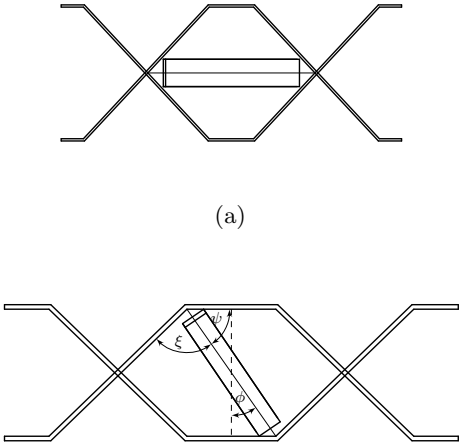

(a)

(b)

FIGURE 3.9: Possible planes to insert and slide a transverse corrugated-strip plate through a hexagonal hole (a) the alternative A, and (b) the alternative B

of the hexagonal hole on these inserting planes, the width of corrugated-strip plate b_c is limited to not greater than the minimum value of Eq. 3.4a or 3.4b, for alternative inserting plane A or B, respectively.

$$b_c \leq \begin{cases} \left(s_c - h_c - \frac{t_c}{\sin\theta}\right)\tan\theta \\ h_c - 2t_c \end{cases} \tag{3.4a}$$

$$b_c \leq \begin{cases} (2l_d - h_c)\tan\psi \\ (2l_d - h_c)\tan\xi \end{cases} \tag{3.4b}$$

where

$$
\begin{aligned}
l_d &= \sqrt{\left(\frac{h_c}{2} - t_c\right)^2 + \left(f_c - \frac{t_c}{2}\tan\frac{\theta}{2}\right)^2} \\
\psi &= 90 - \phi \\
\xi &= 90 - (\theta - \phi) \\
\phi &= \arctan\left(\frac{f_c - \frac{t_c}{2}\tan\frac{\theta}{2}}{\frac{h_c}{2} - t_c}\right)
\end{aligned}
$$

It should be noted that any limitation presented in this thesis is limited to conceptually designing proposes only. In industrial practice, further investigation of technical limitations and production cost should be carried out.

3.4 Applications

The potential use of the innovative unfilled SCS sandwich structure is possibly to substitute any conventional orthotropic stiffened steel panel which has less transverse shear strength in the y-direction. This innovative structural topology may be used as any sandwich deck panel/plate for ship building, offshore, and railway applications. Moreover, it may be used as any two-way floor slab for building applications.

In addition to the innovative unfilled SCS sandwich structure, the innovative concrete-filled SCS sandwich structure could also possibly substitute any current applications of Bi-Steel sandwich structures in which a relatively high transverse shear strength is required, for example, a relatively deep and short beam, or a beam subjected to relatively high concentrated load.

These potentials are presented in Chapters 4 and 5 in which an equivalent unfilled web-core topology is conceptually compared to the innovative unfilled SCS topology representing a comparison with more traditional stiffened structure. In Chapter 8, the equivalent concrete filled Bi-Steel, i.e., 90° inclined shear connectors, is compared to the innovative concrete-filled SCS topology.

3.5 Concluding Remark

The novel SCS sandwich structure with Bi-CSC system is proposed. The configuration of unfilled stage is the major innovative part of this proposed sandwich structure. It consists of two conventional steel face plates and a group of corrugated-strip plates. The

innovative CSC core acts as an additional bracing member of the unfilled stage and later as an inclined shear connector of the concrete-filled stage of this proposed SCS sandwich structure.

The novel design and development is to set a group of corrugated-strip plates out in a bi-directional format and to connect the sandwich face plate and core together. It was seen that there is a possibility to fabricate and construct this proposed sandwich structure. The existing construction technique of special corrugated core sandwich plate [16, 17] may be adapted to this proposed structure. In addition, there are two possible methods to creat Bi-CSC system, i.e., the TDM and the SRM, originally presented in this research.

Chapter 4

Numerical Study of the Stiffness and Strength of an Unfilled Sandwich Beam

4.1 Background

In the absence of experimental data to assess the performance of the new design concept of the steel-concrete-steel (SCS) sandwich construction, a finite element (FE) approach can be used. Provided appropriate steps are taken to provide confidence in the results obtained. The literature can show that an appropriate FE approach can provide reliable results compared with experimental testing [37, 115]. Due to the cost of manufacture of experimental test specimens, an FE approach can often be considered a cost effective alternative provided validation of the model's accuracy is assessed.

A few numerical studies using the FE modelling approach have been carried out as an alternative method to investigate the stiffness and strength of the sandwich beam, for example, Romanoff et al. [37, 115] used an FE approach to understand the stiffness and strength behaviour of unfilled web core sandwich beams. Cheng et al. [116] and Zangani et al. [117] also used the FE approach to deduce the stiffness of corrugated-like core sandwich beams. Other FE studies of truss-like core sandwich beams can be found, for example, in [20, 118].

To evaluate the stiffness and strength of the proposed bi-directional corrugated-strip core (Bi-CSC) sandwich beam, a numerical study based on the FE approach is used here along with the force-distortion relationship approach of a three-point loaded beam [117, 119] and of a repetitive unit cell [19, 20, 120]. While the FE approach itself can

represent the stress and deformation of a sandwich beam, the stiffness of the beam needs to be calculated from the relationship of applied force and distortion of a beam and of a unit cell.

For a three-point loaded beam, the stiffness of a sandwich beam can be deduced from a relationship between applied load and corresponding displacement at the midspan of the beam, as shown in Fig. 4.1(a). The relationship between the applied force, P, and the total deflection at midspan of beam, Δ_z, – the combination of the bending and shear deflections – can be expressed as Eq. 4.1a. This expression provides the basis for determination of the flexural stiffness D_y from plotting Δ_z/PL^3 and $1/L^2$, where L is the length of the beam, from a series of required data P, Δ_z and L in which D_y can be yielded from the approximate interception point on the Δ_z/PL^3 axis [119] (see Eq. 4.1b and Fig. 4.1(b)). Similarly, this expression also provides the basis for determination of the shear stiffness D_{Qy} from plotting Δ_z/PL and L^2 in which D_{Qy} can be yielded from the approximate interception point on the Δ_z/PL axis [119] (see Eq. 4.1c and Fig. 4.1(c)).

$$\Delta_z = \frac{PL^3}{48D_y} + \frac{PL}{4D_{Qy}} \tag{4.1a}$$

$$\frac{\Delta_z}{PL^3} = \frac{1}{48D_y} + \frac{1}{4D_{Qy}L^2} \tag{4.1b}$$

$$\frac{\Delta_z}{PL} = \frac{L^2}{48D_y} + \frac{1}{4D_{Qy}} \tag{4.1c}$$

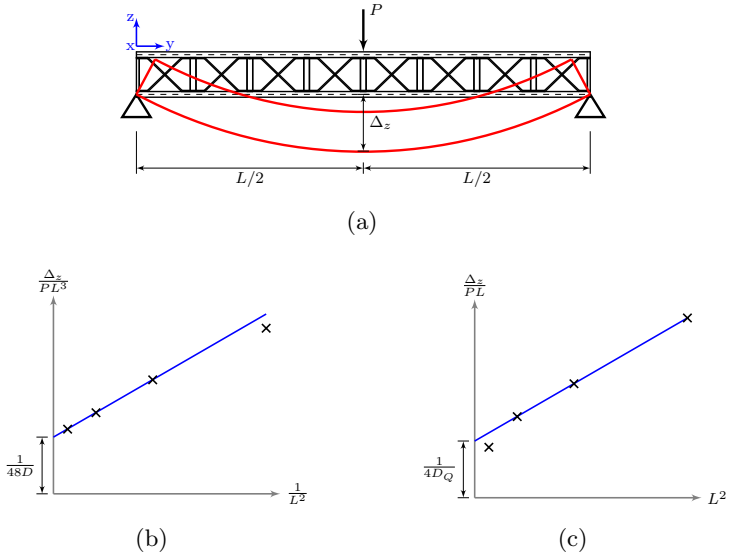

FIGURE 4.1: Formulation of the stiffness of a sandwich beam using the three-point loaded beam approach (a) a three-point loaded beam, (b) plot for evaluation of flexural stiffness, D_y, and (c) plot for evaluation of transverse shear stiffness, D_{Qy}

The transverse shear stiffness of a sandwich beam can also be calculated from its repetitive unit cell if the relationship between an effort shear force and a corresponding displacement is known. The unit cell approach has been used as a simplified tool to deduce the transverse shear stiffness, D_{Qy}, of a corrugated-like core sandwich beam (in the y-direction), for example, in [19, 20]. This unit cell approach can be used to reduce the complexity of the FE model of a sandwich beam; it can also reduce computation time.

Figure 4.2(a) shows a two-dimensional (2D) simplified repetitive unit cell cut from a sandwich beam. The unit cell is subjected to a transverse shear force, Q_y, and a couple of horizontal force, $H = Q_y s_c/d$, where s_c is the half pitch of the corrugation unit of corrugated-strip plate or the length of the unit cell, and d is the distance between the neutral axes of top and bottom face plates, to maintain the static equilibrium [120]. Under this configuration, it can be seen that the unit cell is a symmetrical structure subjected to anti-symmetrical loading. Therefore, the unit cell can be further reduced into one-half of the structure with the supplementary boundary conditions at the plane of symmetry [121, 122]. Applying the symmetrical technique, the one-half unit cell, as shown in Fig. 4.2(b), is fixed at point 1 to eliminate the rigid-body movement of the unit cell and point 5 is not able to move in the z-direction. The relative displacements, e.g., δ_y^4, δ_y^8 and δ_z^4 of this structure, as shown in Fig. 4.2(c), can be calculated using an FE method.

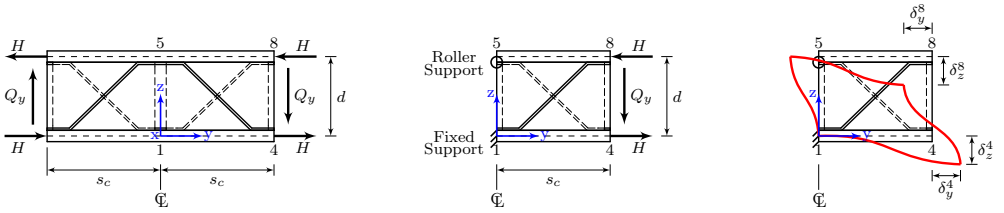

FIGURE 4.2: Formulation of the transverse shear stiffness of a sandwich beam using the unit cell approach (a) a unit cell subjected to transverse shear force, (b) a one-half unit cell, and (c) the deformed shape of a one-half unit cell

Introducing the force-distortion relationship technique and the assumption that the core is so sufficiently stiff in the vertical direction that the depth of the core is always constant [20, 120], the transverse shear stiffness, D_{Qy}, of the unit cell can be expressed as follows [19, 20, 120]:

$$D_{Qy} = \frac{Q_y}{\frac{\delta_y^4+\delta_y^8}{d} + \frac{\delta_z^4}{s_c}} \tag{4.2}$$

The assumption that the depth of the core is always constant means that the displacements in the z-direction of both the top and bottom face plates at the same position in the y-direction are equal. This assumption had been applied in combination with the small displacement assumption in the derivation of the transverse shear stiffness, D_{Qy}, of a corrugated core sandwich beam [120] and of a truss core sandwich beam [20]. It is also applied in this research because of the current study is also limited to the small displacement response of the beams.

4.2 Finite Element Modelling Approach

4.2.1 General Criteria

The numerical study of the stiffness and strength of an unfilled sandwich beam was carried out using the FE software ANSYS Release 11.0 [123]. The ANSYS software was run under the operating software Microsoft Windows XP Professional Version 2002. The hardware condition was a desktop computer with Intel® Core™2 CPU 6600 @ 2.40 GHz and 1.98 GB of RAM.

The analysis method was static mode with a simplified bi-linear stress-strain behaviour of steel (see Sec. 4.2.2). The unfilled sandwich beam was modelled in 3D geometry along with the solid elements (see Sec. 4.2.3). Two major models: 3D FE models of an unfilled sandwich beam (see Sec. 4.2.4) and of an unfilled unit cell (see Sec. 4.2.5) were studied. The former was studied to understand its stiffness and strength behaviour. The latter was analysed to deduce the transverse shear stiffness, D_{Qy}. The topologies of the core varied from truss-like core to bi-directional CSC topologies. The reliability of the FE results was achieved by checking the convergence of the FE solution with varying mesh size from 1 mm to 4 mm. It was found that the typical 2 mm mesh size may be used in this chapter to obtain a possible accurate result with optimum computation time. It can be seen from Fig. 4.3, which presents the transverse shear stiffness, D_{Qy}, of the unfilled truss core unit cell, that the percentage difference between the 1 mm mesh size and the 2 mm mesh size is about 1%. The FE results obtained from the model with the typical 2 mm mesh size were also later validated with the existing solution of the web and truss core sandwich beams provided by Romanoff et al. [37, 115] and Lok et al. [19, 20], respectively (see Sec. 4.3). It was found that the presented FE models with the typical 2 mm mesh size provided good correlation with these references.

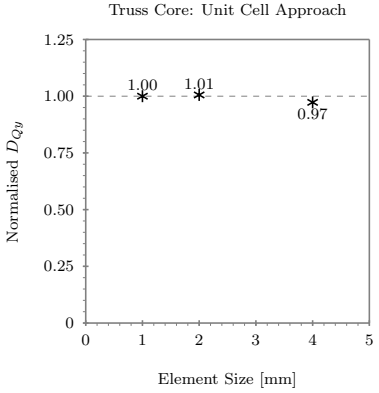

FIGURE 4.3: A convergence study of finite element model: an example of unfilled unit cells

4.2.2 Material Properties of Steel

The components of the unfilled sandwich beam are made of steel. Although the stress-strain relationship of steel is not truly linear as shown in Fig. 4.4(a), the simplified stress-strain relationship curve may be used for modelling the property of steel. In addition, its compression behaviour can also be reliably the same as the tension behaviour [71, 124, 125].

The simplified curve may be constructed from a tri-linear line [15, 125] or from a bi-linear line [71, 124, 125]. In this chapter, the bi-linear stress-strain relationship, as shown in Fig. 4.4(b), was used to present the perfectly elastic-plastic material property model of the steel [71, 124]. The compression behaviour was assumed to be the same as the tension behaviour. The first linear line is used to present the linear elastic behaviour, as expressed by Eq. 4.3a, from zero up to the yield stress, f_y, of the steel. The second linear line, as expressed by Eq. 4.3b, is used to present the perfectly plastic behaviour of the steel beyond its yield stress, f_y. Beyond the proportional elastic limit, the strain, ϵ, continually increases without any increase in the stress, σ, from the proportional strain, ϵ_y, to the strain-hardening strain, ϵ_{st}. This phenomenon is known as the plasticity behaviour of the steel. The strain ϵ_{st} may be approximately ten to fifteen times the strain ϵ_y [126].

Here, the modulus of elasticity, E_s, and the yield stress, f_y, were defined as of 206,000 N/mm^2 and of 355 N/mm^2, respectively, as presented in Table 4.1. As a result, the strain at yield stress, ϵ_y, was equal to 0.0017. The modulus of elasticity, E_s, of 206,000 N/mm^2 was equal to that used in the FE analysis of web core sandwich beams by Romanoff et al. [37, 115]; therefore, the FE result of this research can be validated with

Romanoff et al.'s solutions [37, 115].

$$f_s = E_s \epsilon_s \tag{4.3a}$$

$$f_s = f_y \tag{4.3b}$$

Table 4.1 summaries the physical properties of steel material used in this chapter.

TABLE 4.1: Physical properties of the steel

Property	Notation	Value	Unit	Remark
Yield Stress	f_y	355	N/mm^2	BS EN10025 1993 Grade S355J2G3 Material for general applications [50]
Modulus of Elasticity	E_s	206,000	N/mm^2	[115]
Poisson's Ratio	ν_s	0.30	-	[15, 50]

In the ANSYS software, three material properties of the steel are required for definition. The first two fundamental properties, i.e., the modulus of elasticity, E_s, and Poisson's ratio, ν_s, are defined using the MP command [123]. The last property is the tensile uniaxial stress-strain relationship of the steel. It is defined using the TB command with the BISO option. The BISO option is used to specify the steel material model as bi-linear isotropic hardening. The steel material behaviour is illustrated by the bi-linear stress-strain curve starting at the origin with positive stress and strain values. The initial slope of the curve is taken as the modulus of elastic, E_s, of the steel. Beyond the yield stress, f_y, the curve continues along the second slope defined by the other tangent modulus, E_{st}, [123]. In this chapter, the tangent modulus E_{st} is set to zero. The stress-strain data at each key point is then defined using the TBDATA command.

4.2.3 Element Type

To create a realistic 3D geometry, solid elements were used to model both the face plates and the core. The SOLID45 element type in the ANSYS element library was used for any part made of the steel. This element type was used to model the steel face plates by Clubley et al. [72] in their numerical study of the shear strength behaviour of Bi-Steel sandwich panels. Figure 4.5 shows the geometry of the SOLID45 element. The SOLID45 is a general purposed element for the 3D modelling of solid structures. The element is an eight-node element having three degrees of freedom, i.e., translations in the nodal x-, y-, and z-directions, at each node. The material property of the SOLID45 element is defined in the isotropic condition. The element has plasticity, large deflection, and large strain capabilities.

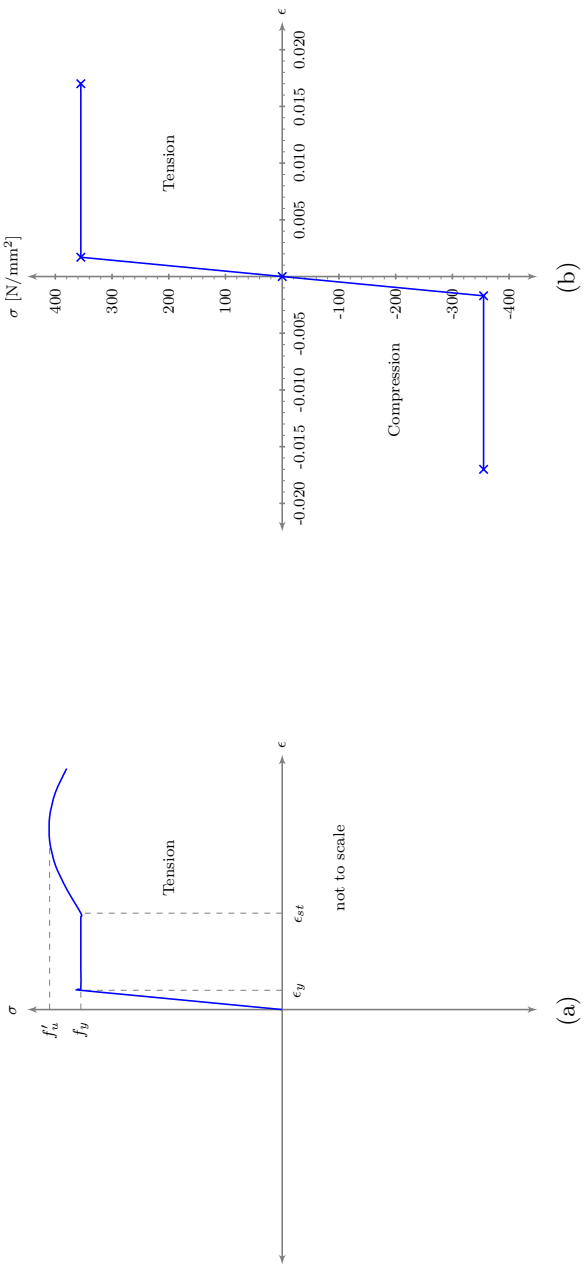

FIGURE 4.4: Stress-strain relationship curve of the steel (a) the idealised tensile stress-strain relationship curve, and (b) the simplified bi-linear stress-strain relationship curve

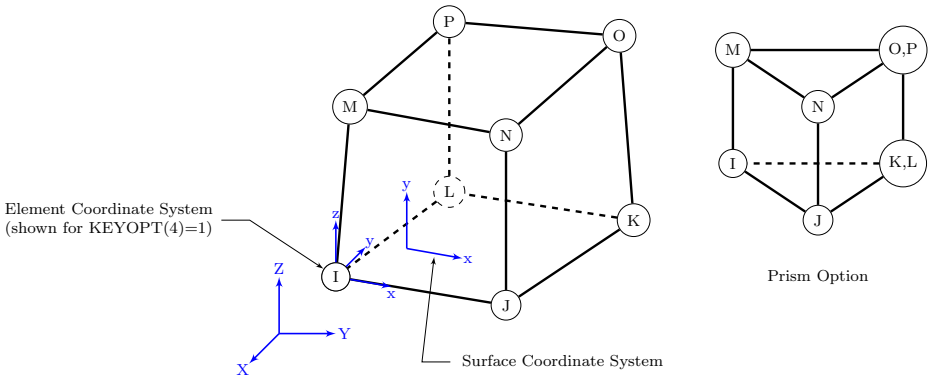

FIGURE 4.5: Geometry of the SOLID45 element [modified from 123]

4.2.4 Modelling an Unfilled Sandwich Beam

4.2.4.1 Geometry

Although a 2D FE model may be used to reduce the complexity for modelling and the computation time required for analysing, a 3D FE model was decided upon and analysed in this chapter because of the out-of-plane arrangement of the corrugated-strip plates in the proposed core topology. Due to a lack of experimental results for validation of the model's accuracy, a realistic 3D geometry would present more reliable results than a simplified/equivalent 2D geometry.

A 3D FE model of an unfilled sandwich beam, as shown in Fig. 4.6(a), was modelled and analysed to study the stiffness and strength behaviour of the sandwich beam. The unfilled sandwich beam model consists of the top and bottom steel face plates and a series of corrugated-strip plates. The connections between the face plates and core elements are defined as fully rigid.

Although the sandwich beam can consist of infinite repetitive unit cells, the unfilled sandwich beam studied in this chapter was limited to consist of two to eighteen unit cells. This decision was made to ensure that the beam model can be run with the computer hardware specified in Sec. 4.2.1. The length of beam was maintained to consist of n corrugations of CSC, i.e., $L = 2ns_c$.

Due to the symmetry of the structure, only a quarter of the complete unfilled sandwich beam model, as shown in Fig. 4.6(b), is required for analysis. This is a substructure of the complete symmetrical unfilled sandwich beam subjected to symmetrical load; it was used to reduce the computation time.

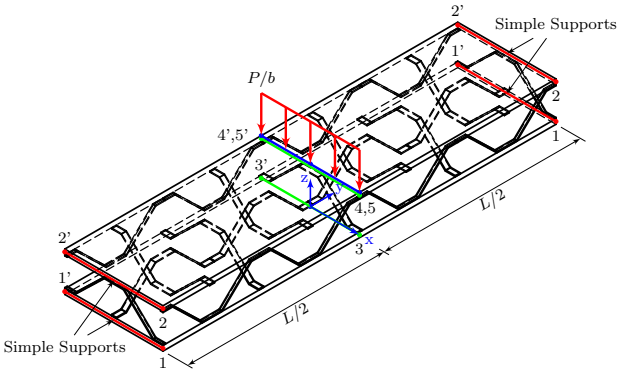

(a)

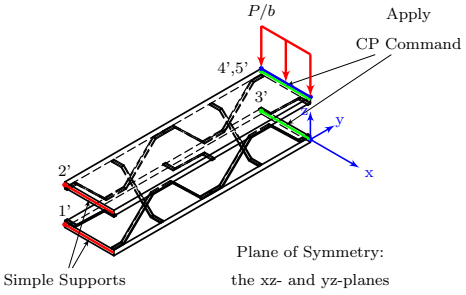

(b)

FIGURE 4.6: Geometry of (a) a three-point loaded unfilled sandwich beam with bi-directional corrugated-strip core, and (b) its sub-structure

4.2.4.2 Boundary and Constraint Conditions

The conventional boundary conditions of the simply supported beam were set up at all nodes along the lines 1-1' and 2-2'. These nodes were not free to move in any directions, i.e., $\delta_x = \delta_y = \delta_z = 0$, to simulate the simple support at the end of the bottom and top face plates. To satisfy the reduced symmetrical structure condition [121, 122], the nodes on the xz-plane were free to move in the z-direction only, i.e. $\delta_x = \delta_y = 0$.

In order to reduce the local deformation effect beneath the loading line 5-5', an additional constraint boundary condition was set up. This restrained all nodes along the lines 3-3' and 4-4' so that they all equally displace in the z-direction; it was used to perform virtual stiffener beneath the loading line. Therefore, the depth of the sandwich core on the xz-plane after deformation remained the same as that of the sandwich core before deformation. Similar constant-depth conditions can be found in the support location in which the displacements in the z-direction were restrained at both the top and bottom face plates.

It should be noted here that the conventional boundary conditions defined in this chapter may be an idealised case. As a result, the validity of the numerical study in this chapter is limited to the presented boundary conditions. In laboratory practice, the real supports may locate below the bottom face plate only. Therefore, the numerical model may need to re-modify to demonstrate the realised case so that the comparison between the numerical and experimental studies can be carried out. Nevertheless, the support condition used in this chapter is similar to one of the support conditions for the unfilled Bi-Steel sandwich beam noted in Bi-Steel: Design & Construction Guide [50, Sec. 9.2.5 Effect of boundary conditions] and for the unfilled web core sandwich beams studied by Romanoff et al. [37, 115]. It was used here to ensure that the core depth is always maintained as constant at the support edges and it corresponded with Romanoff et al.'s FE model [37, 115] which will be used to provide some validation of the present models accuracy.

4.2.4.3 Loading Condition

To simulate a three-point loaded beam, a transverse force per unit width of sandwich beam, P/b, was imposed along the line 5-5' on the top face plate. According to the reduced symmetrical structure condition, however, this load was divided by two. The uniform load P/b was then proportionally distributed to the element nodes on the line 5-5'. For derivation of stiffness, a total unit load was applied.

4.2.4.4 Formulation of Flexural and Transverse Shear Stiffnesses

To deduce the flexural and transverse shear stiffnesses from the three-point loaded beam, a series of required data (P, Δ_z and L) were recorded from the FE beam model in which the length of beam varied in terms of the number of corrugations, i.e., $L = 2ns_c$ where $2 \leq n \leq 18$. The vertical displacement of node 4 was recorded as Δ_z and then used to plot with corresponding length L using the technique presented in Sec. 4.1.

4.2.5 Modelling an Unfilled Unit Cell

4.2.5.1 Geometry

Similar to the unfilled sandwich beam, a 3D model of the unfilled unit cell was created. The 3D FE model of a repetitive unfilled unit cell, as shown in Fig. 4.7(a), was modelled and analysed to deduce the transverse shear stiffness, D_{Qy}. The unfilled unit cell model

also consisted of the steel face plates and steel core. The connections between the face and core elements were also defined as fully rigid.

Due to the symmetry of the structure, only a quarter of the complete unfilled unit cell, as shown in Fig. 4.7(b), is required for analysis. This is a substructure of a complete unfilled unit cell subjected to anti-symmetrical load; it was also used to reduce the computation time.

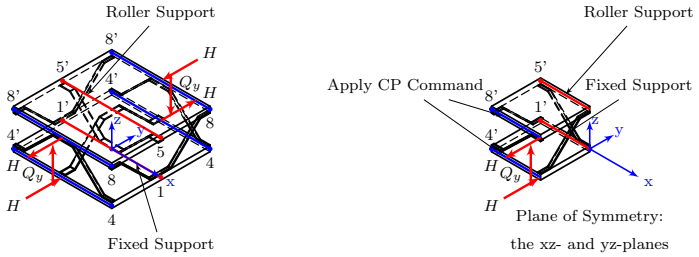

(a) (b)

FIGURE 4.7: Geometry of (a) an unfilled unit cell with bi-directional corrugated-strip core, and (b) its sub-structure

4.2.5.2 Boundary and Constraint Conditions

To satisfy the conditions as mentioned in Sec. 4.1, two conventional boundary conditions were set up. First, any nodes of the bottom face plate in the xz-plane was fixed in any degree of freedom, i.e., $\delta_x = \delta_y = \delta_z = 0$, to prevent space movement of the model. Second, the remaining nodes on the xz-plane were free to move in the y-direction only to satisfy the reduced anti-symmetrical structure condition [121, 122].

In order to maintain the constant-core-depth assumption, an additional constraint boundary condition was applied. This restrained all nodes along the lines 4-4' and 8-8' so that they all equally displace in the z-direction.

4.2.5.3 Loading Condition

A total unit transverse shear force per unit width of sandwich beam, Q_y/b, was imposed on the left plane of the unit cell. A distribution of this force between the top and bottom face plates had been first randomly studied. According to this preliminary study, any distribution ratios between the top and bottom face plates yielded the same output value. Therefore, this study applied the total unit transverse shear force on line 8-8', i.e., on the top face plate, only. To maintain the static equilibrium, the unit cell also needs to be

subjected to a horizontal force couple, $Q_y s_c/d$, at both the top and bottom face plates [120], i.e., along the lines 8-8' and 4-4', respectively. The uniform unit transverse shear force was proportionally distributed to the element nodes. This routine procedure was also applied for the horizontal force couple.

4.2.5.4 Formulation of Transverse Shear Stiffness

To deduce the transverse shear stiffness, D_{Qy}, from the unit cell, the horizontal and vertical displacements of nodes 4 and 8 were recorded as δ_y^4, δ_y^8 and δ_z^4, respectively. These displacements were then used to calculate the stiffness D_{Qy} from Eq. 4.2 using the technique presented in Sec. 4.1.

4.3 Validation of the Finite Element Models

To evaluate the reliability of the FE model presented by the author, the validation was carried out against existing results. It was divided into two validation stages: (1) the validation of the deflection and stress of the beam against the solution of the unfilled web core sandwich beam provided by Romanoff and Varsta [37], and (2) the validation of the transverse shear stiffness, D_{Qy}, of the beam model and of the unit cell model against the solution of the unfilled truss core sandwich beam provided by Lok et al. [19, 20].

For the first validation, four 3D FE models of web core sandwich beams were set up in the same configuration as those of Romanoff and Varsta [37]; they were defined as case A, B, C, and D[1]. However, the element types were different; rather than using the 3D solid element, Romanoff and Varsta [37] used shell element type. The comparisons of the maximum deflection at midspan, deformation shape of the beam, and the flexural stress at the surface of the top face plate were carried out. These comparable values were set according to the existing available data in the publication of Romanoff and Varsta [37]. Table 4.2 presents the comparison of the maximum deflection obtained from the presented FE model and from Romanoff and Varsta [37]. It can be seen that the FE model presented by the author yields close results to the reference in most cases; the percentage differences are less than 6%. The significant difference between both models may be found only in case A where the percentage difference is about 9%. The differences in each case may arise from the difference in element type. However, another validation of the deformation shape of the beam, as shown in Fig. 4.8(a), shows that the presented FE model is the same in development trend as Romanoff and Varsta [37]. The

[1] see detail of the configurations A, B, C, and D in Romanoff and Varsta [37], Table 1, Page 484

similar behaviour can also be found in comparison of the surface flexural stress of the top face plate, as presented in Fig. 4.8(b); it can be seen that there are few differences in numerical value from those of Romanoff and Varsta [37], Fig. 7, Page 485 and Fig. 9, Page 486.

TABLE 4.2: Comparison of the maximum deflection of the unfilled web-core sandwich beams obtained from the presented finite element method and the Romanoff and Varsta's solution [37]

Configuration [a]	*A* I1/4 × 80/80	*B* I4/4 × 20/80	*C* I3/4 × 40/120	*D* I5/1 × 150/50
Romanoff and Varsta [37]	−4.7030	−0.2325	−0.8985	−1.2890
Presented FE Method	−4.3012	−0.2384	−0.9387	−1.3633
Percentage Difference	−8.54%	2.52%	4.47%	5.76%

[a] see detail of the configurations A, B, C, and D in Romanoff and Varsta [37], Table 1, Page 484 – the general notation used to identify the beams is Case ID I$[t_f]/[t_w] \times [h_c]/[s_c]$, in *mm* unit

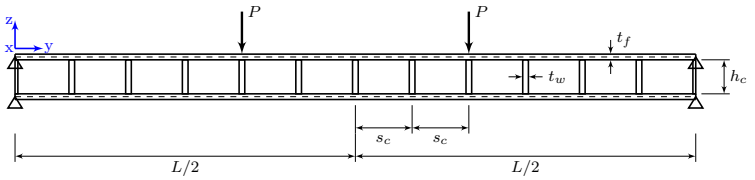

For the second validation, the FE models of the unfilled sandwich beam and of the unfilled unit cell with a compatible truss core to that of Lok et al. [19, 20] were set up. The sandwich cross section was symmetrical, i.e., both the top and bottom face plates were identical in material and section properties. This section was selected due to the analytical solution provided by Lok et al. [19, 20] was valid for only symmetrical section. The material property of the steel was linear elastic. Poisson's ratio effect was not included. The configuration of the truss core was designed with non-dimensional parameters. All configuration parameters were kept constant except for the s_y/d ratio.

The transverse shear stiffness, D_{Qy}, obtained from the FE three-point loaded sandwich beam model referred to as FE-TPB and from the FE unit cell model referred to as FE-UC presented by the author were then compared with the solutions obtained from the analytical method of Lok et al. [19, 20]. Figure 4.9 shows the comparison of the transverse shear stiffness, D_{Qy}, obtained from the FE-TPB, the FE-UC, and Lok et al. [19, 20]. It can be seen that the solutions obtained from the FE-UC are very close to those of Lok et al. [19, 20] without any significant percentage differences. The percentage differences of FE-UC solution compared with Lok et al.'s solution [19, 20] are less than 2% for most values of s_y/d in the range of $0 \leq s_y/d \leq 5.0$. The value greater than 3% can be found only at $s_y/d = 0.25$ (see Table 4.3).

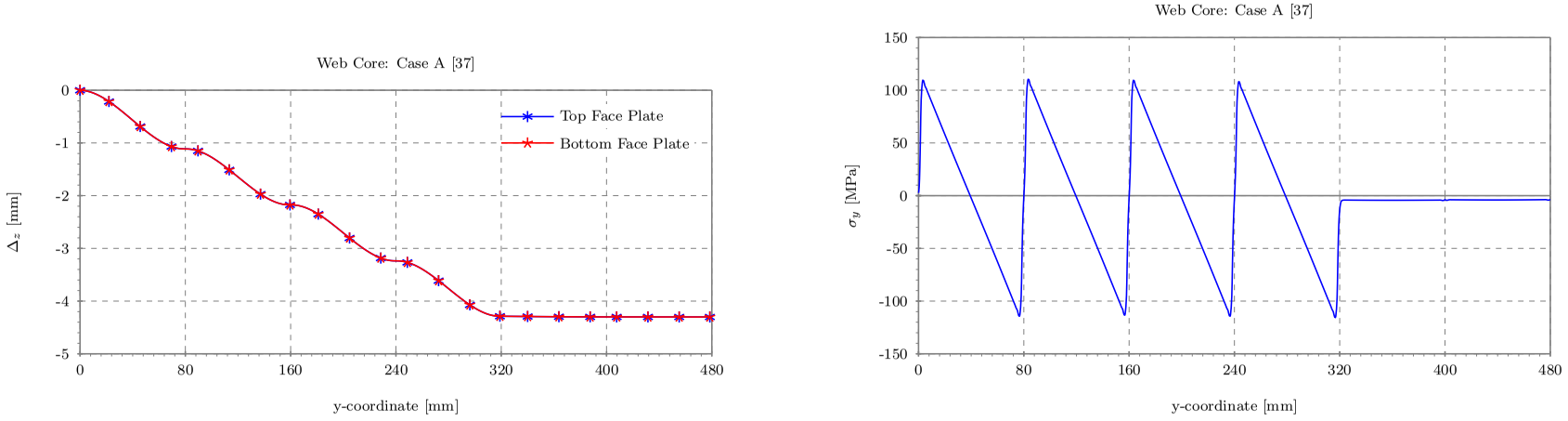

FIGURE 4.8: (a) deformation shape, and (b) surface stress at the top face plate of the unfilled web core sandwich beam (case A) obtained from the presented finite element method of three-point loaded beam

For the validation of the FE-TPB, it can also be seen from Fig. 4.9 that the FE-TPB gives the similar trend of the stiffness D_{Qy} to Lok et al. [19, 20]. Although the results appear to diverge when $s_y/d > 1.0$, both the curve lines seem to be continuingly parallel with approximately 8% of difference (see Table 4.3).

It should be noted that the evaluation of the FE-TPB was limited in the range of $0 \leq s_y/d \leq 2.0$. This is because of the limitation of the computational processing unit used in this chapter. Beyond the point of $s_y/d > 2.0$, the FE-TPB needs to solve a huge number of the FE equations. However, the range of $0 \leq s_y/d \leq 2.0$ is reasonable since it covers the effective range of s_y/d as previously found in the unit cell model using the method of Lok et al. [19, 20] and the FE-UC method.

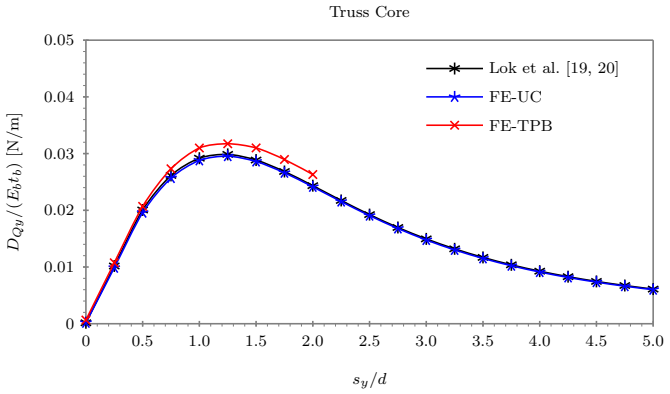

FIGURE 4.9: Comparison of the transverse shear stiffness, D_{Qy}, of the unfilled truss core sandwich beam obtained from the presented finite element methods (the FE-TPB and the FE-UC) and Lok et al.'s method [19, 20]

TABLE 4.3: Comparison of the transverse shear stiffness, D_{Qy}, of unfilled truss core sandwich beams obtained from the presented finite element methods (the FE-TPB and the FE-UC) and the Lok et al.'s method [19, 20]

	D_{Qy}					
s_y/d	Lok et al. [19, 20]	FE-TPB	PD-L [a]	FE-UC	PD-L [a]	PD-T [b]
0.00	0.0002	N/A	N/A	0.0002	-2.35%	N/A
0.25	0.0102	0.0107	5.60%	0.0099	-3.07%	-8.21%
0.50	0.0201	0.0207	3.16%	0.0196	-2.37%	-5.36%
0.75	0.0261	0.0273	4.49%	0.0257	-1.77%	-5.99%
1.00	0.0292	0.0310	6.17%	0.0288	-1.33%	-7.06%
1.25	0.0299	0.0317	6.26%	0.0295	-1.05%	-6.88%
1.50	0.0289	0.0310	7.41%	0.0286	-0.90%	-7.73%
1.75	0.0268	0.0290	7.90%	0.0266	-0.84%	-8.10%
2.00	0.0243	0.0263	8.07%	0.0241	-0.86%	-8.26%
3.00	0.0150	N/A	N/A	0.0148	-1.29%	N/A
4.00	0.0093	N/A	N/A	0.0091	-1.62%	N/A
5.00	0.0061	N/A	N/A	0.0060	-1.82%	N/A

[a] PD-L – Percentage Difference, compared with Lok et al. [19, 20]
[b] PD-T – Percentage Difference, compared with the FE-TPB

According to the validation of the unfilled web and truss core sandwich beams, it can be seen that the FE models presented by the author provides correlation with the existing

solutions provided by Romanoff and Varsta [37] and by Lok et al. [19, 20], respectively. Therefore, it is reasonable to conclude that these FE models give accurate results and can be further used in this research.

4.4 Evaluation of the Performance of the Proposed Core Topology

In this section, the performance of the presented Bi-CSC topology was evaluated and also compared with two similar core topologies, i.e., the truss core [19, 20] and the X-truss core (previously referred to as the offset-corrugated core [18, 35]) with some values of the width coefficient of the corrugated-strip plate, k_{cb}. The configurations of these selected core topologies were similar, as shown in Fig. 4.10. They were set to verify the contribution of each pattern of the core topology to the stiffness and strength behaviour of the unfilled sandwich beam. All geometric parameters were kept constant except the ratio of s_y/d. This parameter indirectly represents the angle of the inclined part of the corrugation which can vary from 0° to 90°. Here, s_y/d varies from 0 to 2.0; therefore, the angle varies from 26.6° to 76.0°. Table 4.4 summarise the value of geometric parameters used in this section.

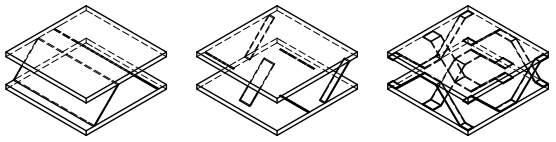

(a) (b) (c)

FIGURE 4.10: Configurations of the unfilled sandwich beam case studies with (a) truss core, (b) X-truss core, and (c) Bi-CSC

TABLE 4.4: Configuration of the case studies

Parameter	Case Study			Note
	truss core	X-truss core	Bi-CSC	
b	100			
t_t	12			$t_t/t_b = 1$
t_b	12			
k_{cb}	1.00	0.50, 0.25, and 0.10	0.30, 0.25, and 0.20	
t_c	2			$t_c/t_b = 1/6$
s_c	vary in terms of s_y/d where $0 \leq s_y/d \leq 2.0$			
f_c	20			$f_c/t_b = 10/6$
h_c	120			$h_c/t_b = 10$

Conceptually, the presented configurations of the Bi-CSC topology studied in this chapter (also the next two chapters) may possibly be produced using either the top-down method (TDM) or the slide-rotate method (SRM) presented in Section 3.3, Chapter 3.

As previously mentioned in Section 3.3, there are limitations to the SRM fabrication technique. Figure 4.11 demonstrates the limitation if applying the SRM for the presented configurations of the Bi-CSC topology. In this figure, the star-marked and the cross-marked lines present the maximum limitation of k_{cb} ($k_{cb} = b/b_c$) which can be defined so that the width of corrugated-strip core, b_c, is not greater than the limitation of the alternative inserting plane A and B, i.e., the limitation of b_c obtained from Eq. 3.4a and 3.4b, respectively. It can be seen that the studied configurations of the Bi-CSC topology with selected k_{cb} of 0.30, 0.25 and 0.20 can be fabricated using the SRM (only the alternative inserting plane A) if $s_y/d \geq 1.0$; otherwise, the TDM should be used.

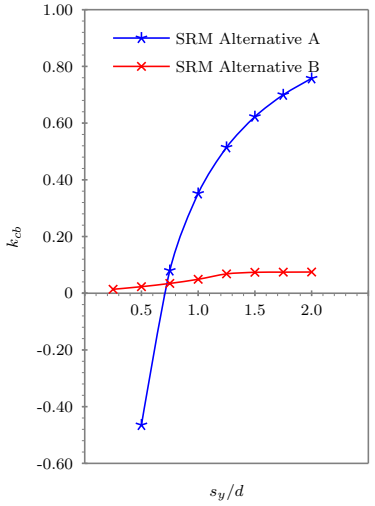

FIGURE 4.11: Possible maximum value of k_{cb} obtained from the slide-rotate method to make the unfilled Bi-CSC topology studied in this chapter

4.4.1 Flexural Stiffness

Based on the formulation technique presented in Sec. 4.1, the flexural stiffness, D_y, of the unfilled sandwich beam with three different core topologies, i.e., the truss core, the X-truss core, and the Bi-CSC, were obtained. The flexural stiffness, D_y, was first normalized by the flexural stiffness, D_o, where D_o is the contribution of the face plates to the flexural stiffness of the sandwich beam; here, the stiffness D_o equals to $E_b t_b d^2/2$ [21, 22]. The normalized flexural stiffness D_y was then plotted against s_y/d in the range of $0.25 \leq s_y/d \leq 2.0$.

It can be seen in the results presented in Fig. 4.12 that the normalised flexural stiffness, D_y, of the configurations of the unfilled sandwich beam studied in this section are about 1.0. Therefore, it may be concluded that the flexural stiffness, D_y, contributed by the presented core topology can be neglected. This is a similar result found for another unfilled sandwich beam with very weak core [21, 22].

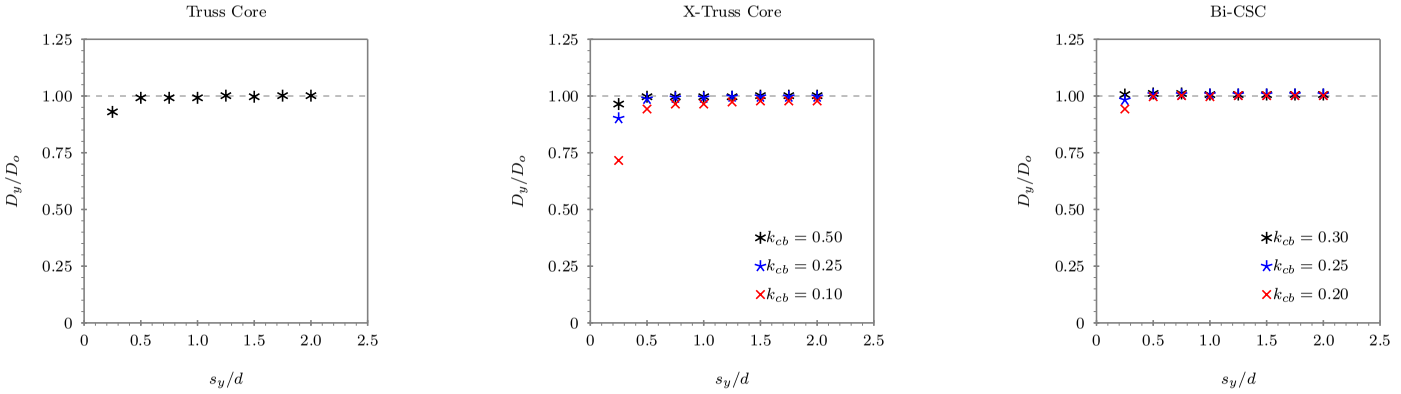

FIGURE 4.12: Plot of the flexural stiffness, D_y, of unfilled sandwich beams with various core topologies obtained from the presented finite element method of three-point loaded beam (FE-TPB) (a) truss core, (b) X-truss core, and (c) Bi-CSC

4.4.2 Transverse Shear Stiffness

In addition to the flexural stiffness, D_y, the transverse shear stiffness, D_{Qy}, of the unfilled sandwich beam with these three different core topologies were also analysed. The transverse shear stiffness, D_{Qy}, was obtained from both the unfilled sandwich beam model and the unfilled unit cell model using the formulation techniques presented in Sec. 4.1. The transverse shear stiffness, D_{Qy}, was first factorised by $E_b t_b$. Then, it was plotted against s_y/d in the range of $0.0 \leq s_y/d \leq 5.0$ for the truss core unit cell model. However, the evaluation of the transverse shear stiffness, D_{Qy}, of the sandwich beam and unit cell with the X-truss and the Bi-CSCs were limited in the range of $0.25 \leq s_y/d \leq 2.0$. The evaluation was not carried out at $s_y/d = 0.0$ because the core did not perform as an X-like core. In addition, the evaluation was not carried out beyond $s_y/d > 2.0$ because these points seem to be out of the effective range of s_y/d, as initially seen from the study of the truss core sandwich beam and the truss core unit cell (see Fig. 4.9).

Unlike the behaviour of the flexural stiffness, D_y, the transverse shear stiffness, D_{Qy}, significantly depends on s_y/d; it is also not able to be neglected. For the truss core sandwich beam, it can be seen from Fig. 4.9 that increasing s_y/d from 0.0 to 1.25 yields an increase in value of D_{Qy}. As s_y/d continues to 5.0, D_{Qy} then gradually reduces. This trend infers that the alignment angle of the inclined part of the truss core significantly affects to the transverse shear stiffness, D_{Qy}, of the unfilled sandwich beam. The optimum point of the stiffness, D_{Qy}, of the truss core occurs at $s_y/d = 1.25$ (at $\theta = 38.7°$). At this configuration, the stiffness D_{Qy} is approximately 200% greater than that of $s_y/d = 0.25$.

The similar behaviour of transverse shear stiffness, D_{Qy}, can also be found in the other core topologies. For the X-truss core sandwich beam, for example, it can be seen from Fig. 4.13. that increasing s_y/d from 0.25 to 1.0 yields an increasing value of D_{Qy} from 0.0169 to 0.0453. Then, the stiffness D_{Qy} gradually reduces to 0.0302 as s_y/d continues to 2.0 (see Table 4.5(a)). The optimum point of the stiffness D_{Qy} of the X-truss core occurs at $s_y/d = 1.0$ or $\theta = 45°$. At this configuration, the stiffness D_{Qy} is approximately 2.7 times the stiffness D_{Qy} at $s_y/d = 0.25$. The similar behaviour can be found at all values of k_{cb}, i.e., 0.50, 0.25, and 0.10, studied in this section.

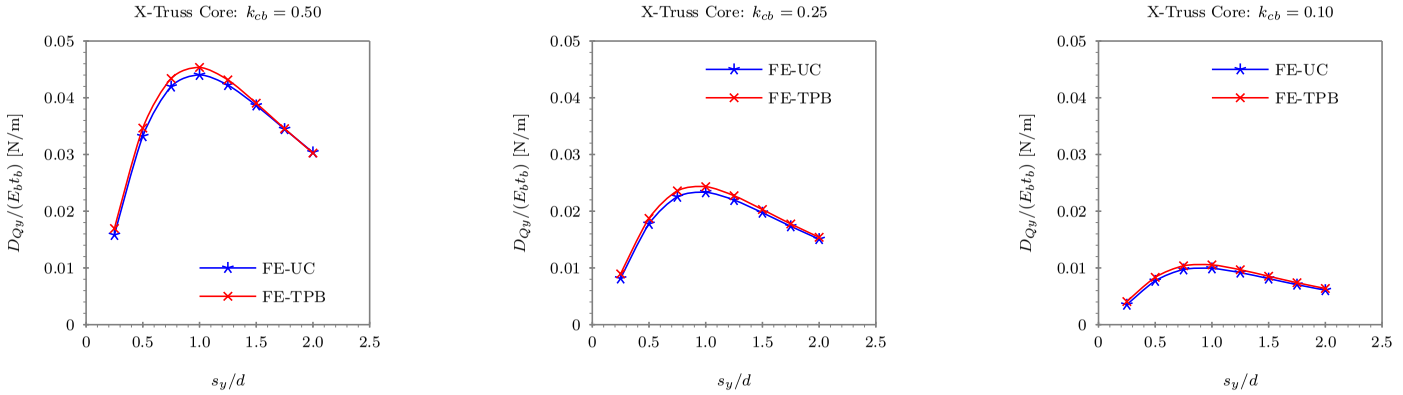

(a) $k_{cb} = 0.50$ (b) $k_{cb} = 0.25$ (c) $k_{cb} = 0.10$

FIGURE 4.13: Plot of the transverse shear stiffness, D_{Qy}, of unfilled sandwich beams with X-truss core obtained from the presented finite element methods (the FE-TPB and the FE-UC)

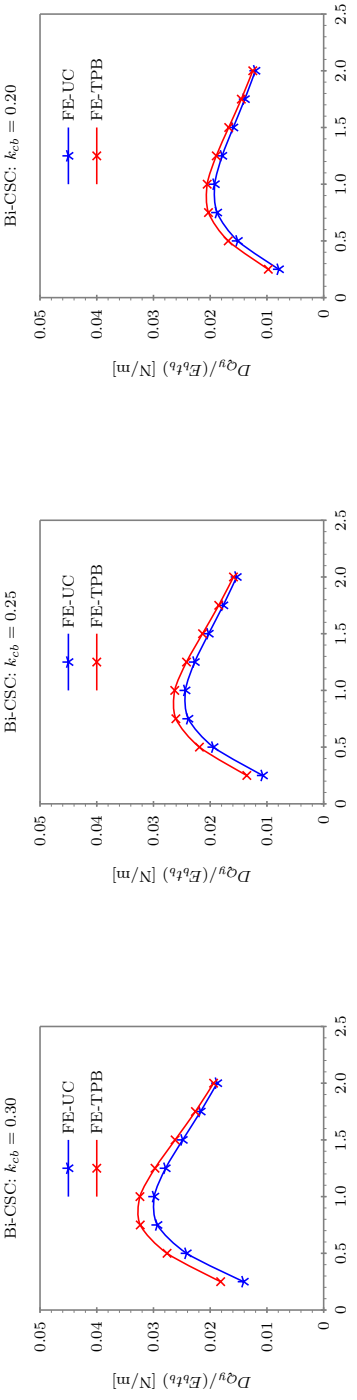

(a) $k_{cb} = 0.30$ (b) $k_{cb} = 0.25$ (c) $k_{cb} = 0.20$

FIGURE 4.14: Plot of the transverse shear stiffness, D_{Qy}, of unfilled sandwich beams with bi-directional corrugated-strip core obtained from the presented finite element methods (the FE-TPB and the FE-UC)

TABLE 4.5: Transverse shear stiffness, D_{Qy}, of unfilled sandwich beams with various core topologies obtained from the presented finite element methods (the FE-TPB and the FE-UC)

(a) unfilled X-truss core sandwich beams

s_y/d	0.25	0.50	0.75	1.00	1.25	1.50	1.75	2.00
	$k_{cb} = 0.50$							
FE-TPB	0.0169	0.0347	0.0434	0.0453	0.0432	0.0390	0.0346	0.0302
FE-UC	0.0158	0.0332	0.0420	0.0440	0.0422	0.0386	0.0345	0.0304
PD-T [a]	−6.69%	−4.13%	−3.28%	−2.91%	−2.13%	−1.02%	−0.24%	0.39%
	$k_{cb} = 0.25$							
FE-TPB	0.0089	0.0187	0.0236	0.0243	0.0227	0.0203	0.0178	0.0154
FE-UC	0.0081	0.0178	0.0225	0.0233	0.0220	0.0197	0.0173	0.0151
PD-T	−9.06%	−5.22%	−4.44%	−4.08%	−3.36%	−2.79%	−2.36%	−2.06%
	$k_{cb} = 0.10$							
FE-TPB	0.0041	0.0083	0.0104	0.0105	0.0097	0.0085	0.0074	0.0064
FE-UC	0.0035	0.0077	0.0097	0.0099	0.0092	0.0081	0.0070	0.0061
PD-T	−13.70%	−7.46%	−6.22%	−5.90%	−5.23%	−4.85%	−4.66%	−4.66%

(b) unfilled bi-directional corrugated-strip core sandwich beams

s_y/d	0.25	0.50	0.75	1.00	1.25	1.50	1.75	2.00
	$k_{cb} = 0.30$							
FE-TPB	0.0182	0.0276	0.0323	0.0324	0.0297	0.0262	0.0226	0.0194
FE-UC	0.0141	0.0242	0.0293	0.0299	0.0279	0.0249	0.0217	0.0188
PD-T	−22.37%	−12.51%	−9.34%	−7.78%	−6.30%	−5.10%	−4.04%	−3.21%
	$k_{cb} = 0.25$							
FE-TPB	0.0135	0.0219	0.0261	0.0263	0.0242	0.0214	0.0185	0.0159
FE-UC	0.0107	0.0194	0.0239	0.0244	0.0227	0.0203	0.0177	0.0153
PD-T	−20.87%	−11.28%	−8.43%	−7.33%	−5.99%	−5.05%	−4.29%	−3.56%
	$k_{cb} = 0.20$							
FE-TPB	0.0098	0.0168	0.0203	0.0205	0.0189	0.0167	0.0145	0.0125
FE-UC	0.0079	0.0151	0.0188	0.0192	0.0179	0.0159	0.0139	0.0120
PD-T	−19.11%	−9.98%	−7.49%	−6.48%	−5.50%	−4.79%	−4.22%	−3.66%

[a] PD-T – Percentage Difference, compared with the FE-TPB

Figure 4.14 presents the similar behaviour of the transverse shear stiffness, D_{Qy}, as a function of s_y/d for the unfilled bi-direction CSC sandwich beam. For this core topology, it can also be seen that the optimum point of the transverse shear stiffness, D_{Qy}, for all coefficient k_{cb} occur at s_y/d between 0.75 and 1.0 or θ between 53° and 45°.

In comparison, arranging the corrugated-strip plates in a bi-directional format yields a few more advantages in transverse shear stiffness than the X-truss. Figure 4.15 presents the comparison in transverse shear stiffness obtained from the FE-TPB method between these two core topologies. These cores are, for example, compared at the same k_{cb} of 0.25. It can be seen that arranging the corrugated-strip plates in a bi-directional format can provide about 51% more transverse shear stiffness than the X-truss format compared at $s_y/d = 0.25$. This advantage still occurs at any s_y/d greater than 0.25. However, the trend of percentage advantage seems to decrease. At $s_y/d = 1.00$, the Bi-CSC yields about 8% more transverse shear stiffness than the X-truss core. At $s_y/d = 2.00$, the Bi-CSC yields about 3% more transverse shear stiffness than the X-truss core.

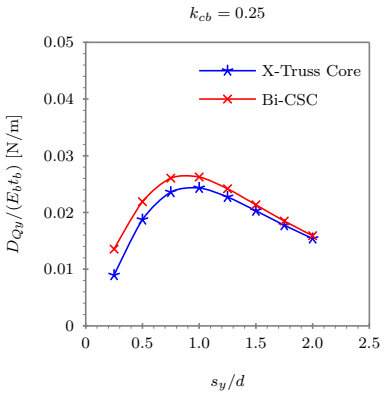

FIGURE 4.15: Comparison in transverse shear stiffness obtained from the presented finite element method (FE-TPB) between the X-truss core and the bi-directional corrugated-strip core (compared at $k_{cb} = 0.25$)

4.4.3 Stress in the Sandwich Beam

Figure 4.16 presents the development of normal stress, σ_y, obtained at the outer surface of the top face plate of the unfilled sandwich beam. The unfilled sandwich beam consisted of ten repetitive unit cells of the truss core, the X-truss core with $k_{cb} = 0.50$, the X-truss core with $k_{cb} = 0.25$, and the Bi-CSC with $k_{cb} = 0.25$. All cores were set up in the same dimensional configuration. The parameter s_y/d was set to 1.00; as a result, the length of the beam was 3200 mm.

For the truss core sandwich beam, it can be seen from Fig. 4.16(a) that the normal stress, σ_y, at the surface of the top face plate develops as a repetitive zigzag pattern. The stress σ_y starts from 0.0 MPa at $x = 0.0$ mm and linearly increases to 0.32 MPa at $x \approx 140$ mm; it then suddenly drops to -0.43 MPa at $x \approx 180$ mm. Beyond this minimum point, the stress rebounds to reach the second maximum point of stress located in the next unit cell. The same zigzag pattern is again found in the next unit cell. The development of stress σ_y in the zigzag pattern may imply that the top face plate is deformed in double-curvature pattern in each unit cell, as can be seen, for example, from Fig. 4.17.

For the X-truss core sandwich beam with $k_{cb} = 0.50$, it can be seen from Fig. 4.16(b) that the normal stress, σ_y, at the surface of the top face plate also develops in the repetitive zigzag pattern. However, the difference of stress between the upper and lower peaks of the zigzag line of each unit cell is seen to decrease. In comparison with the truss core sandwich beam, the stress σ_y at the upper peak of, for example, the first unit cell is about half that of the truss core. The stress σ_y at the lower peak is also about half that of the truss core. This may imply that arranging the core in the X-truss pattern is better than the conventional truss core pattern; the normal stress, σ_y, is significantly

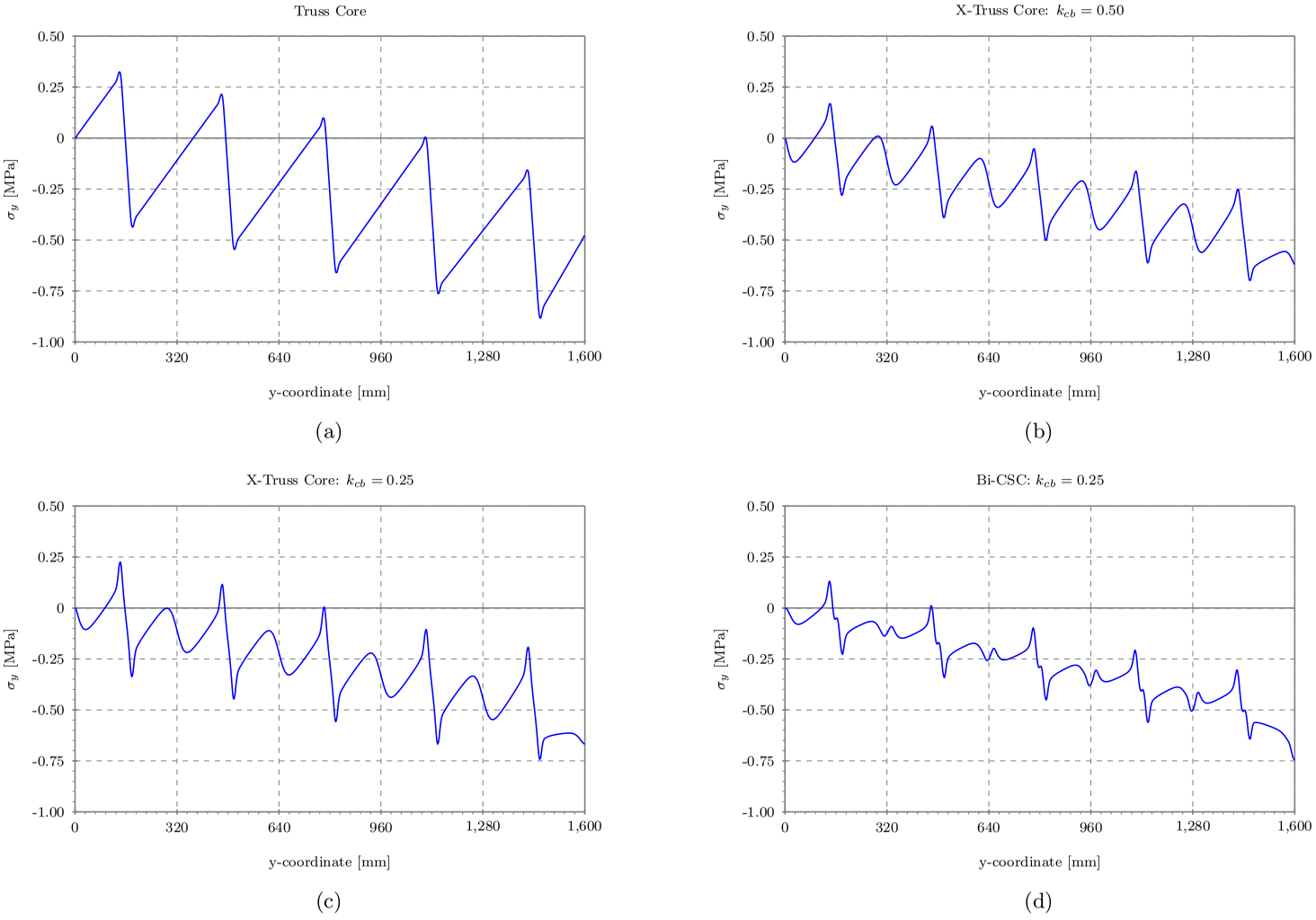

FIGURE 4.16: Normal stress at the surface of the top face plate of unfilled sandwich beams with (a) truss core, (b) X-truss core ($k_{cb} = 0.50$), (c) X-truss core ($k_{cb} = 0.25$), and (d) Bi-CSC ($k_{cb} = 0.25$)

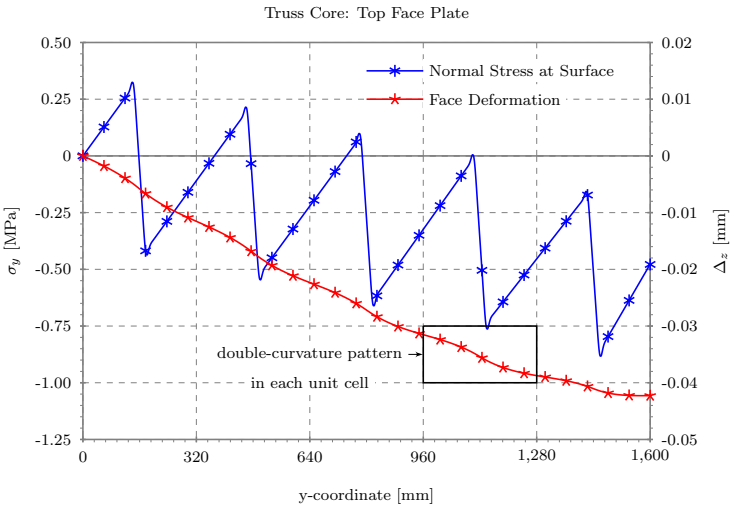

FIGURE 4.17: Deformation of the face plates in double curvature pattern: an example of unfilled truss core sandwich beams

reduced. The similar zigzag line is also found in the X-truss core sandwich beam with $k_{cb} = 0.25$ (see Fig. 4.16(c)).

The Bi-CSC sandwich beam with $k_{cb} = 0.25$ was also investigated. It is found that the normal stress, σ_y, also distributes in the zigzag pattern along the top face plate. However, it can be seen from Fig. 4.16(d) that the stress σ_y at the upper peak is significantly reduced. Compared with the X-truss core sandwich beam with $k_{cb} = 0.50$, the stress at this point is about 10% less. This may imply that introducing the X-truss core in the bi-directional format, i.e., the Bi-CSC, can more evenly distribute the normal stress, σ_y, along the outer surface of the top face plate without creating significantly high stress concentration. Therefore, the Bi-CSC seems to be a better arrangement of core topology compared with the truss core and the X-truss core with $k_{cb} = 0.50$.

Considering the normal stress, σ_y, at the local neutral axis of the top face plate, i.e., at the mid-height of the top face plate, it can be seen from Fig. 4.18 that the stress distribution along the length of the beam is improved. The stress distribution changes from a step function for the truss-core sandwich beam (Fig. 4.18(a)) to an approximately linear function for the X-truss core sandwich beam and the Bi-CSC sandwich beam (Figs. 4.18(b) to 4.18(d), respectively). This may imply that arranging the core in the X core or the Bi-CSC topology provides a uniform distribution of the normal stress at the neutral axis of the face plate and consequent reduces the stress concentration at the connection point of the core.

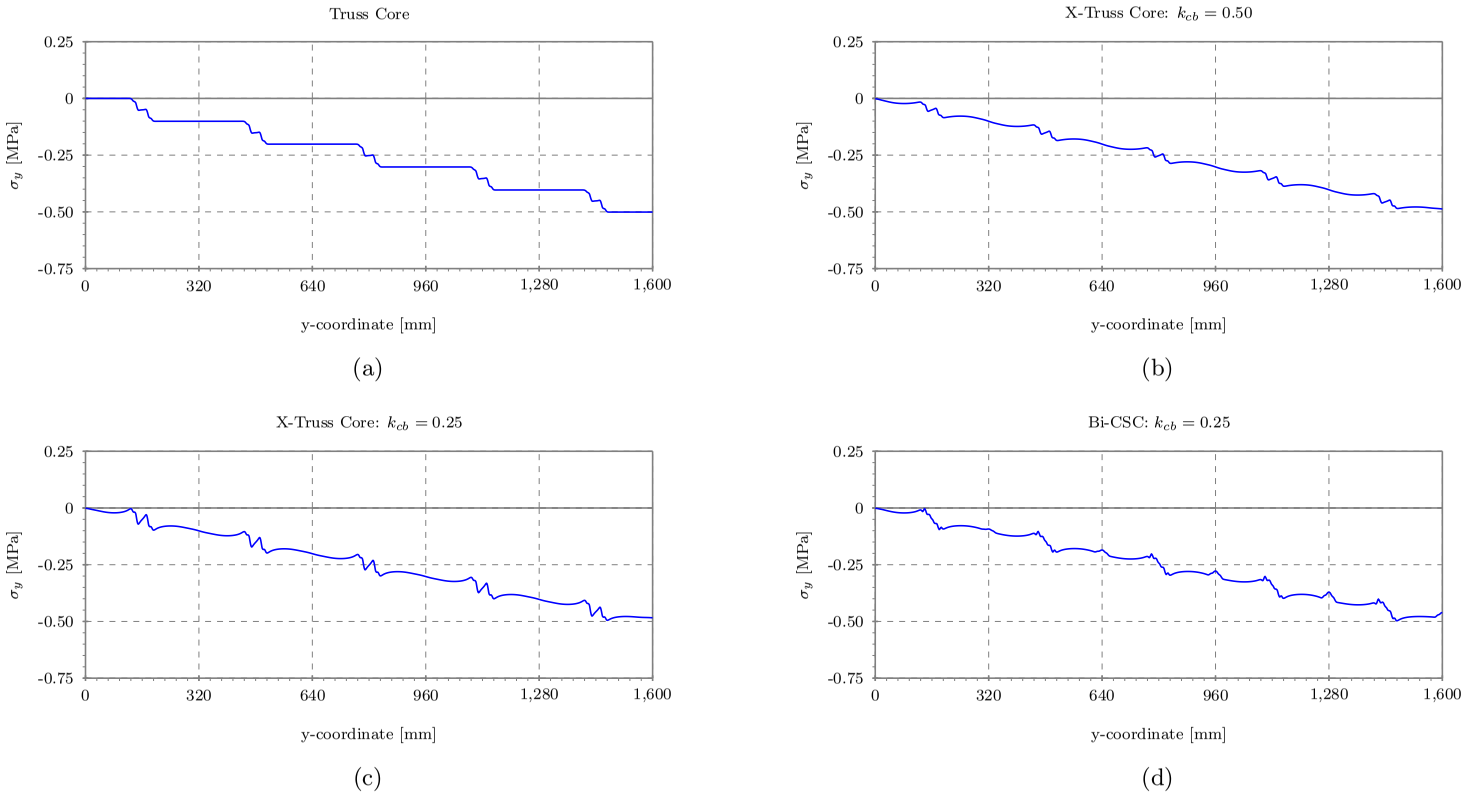

FIGURE 4.18: Normal stress at the neutral axis of the top face plate of unfilled sandwich beams with (a) truss core, (b) X-truss core ($k_{cb} = 0.50$), (c) X-truss core ($k_{cb} = 0.25$), and (d) Bi-CSC ($k_{cb} = 0.25$)

4.5 Concluding Remark

The numerical study of the unfilled sandwich beam with various core topologies was carried out using the 3D FE models. Both the unfilled sandwich beam and the repetitive unit cell were modelled and analysed using the FE software ANSYS Release 11.0 [123]. While the stress of the beam was obtained from the FE model itself, the flexural stiffness, D_y, and the transverse shear stiffness, D_{Qy}, were obtained from the FE result along with the force and distortion relationship of the three-point loaded beam and the unit cell approaches.

The FE beam model was validated with the existing FE solution of the unfilled web core sandwich beam provided by Romanoff and Varsta [37]. In addition, the transverse shear stiffness, D_{Qy}, obtained from both the FE beam and the unit cell models were validated with the existing analytical solution of the unfilled truss core sandwich beam provided by Lok et al. [19, 20]. The validation showed that the presented FE models agreed well with the references. To deduce the transverse shear stiffness, D_{Qy}, a unit cell approach could be used to reduce the complexity and computation time of the FE beam model.

The presented FE models were then used to evaluate the performance of the proposed core topology and also compared with the truss core and X-truss core topologies. It was found that the flexural stiffness, D_y, of all cores studied in this chapter can be neglected. However, it was found that the transverse shear stiffness performance of the core varies with the ratio of s_y/d and may not be neglected. The optimum point of the transverse shear stiffness, D_{Qy}, of the presented core topology was found at s_y/d about 1.0; this phenomenon was similar to the truss and the X-truss core topologies. It was found that the proposed Bi-CSC topology yields a few more advantages in transverse shear stiffness compared to the X-truss core topology. The study of the stress at the face plate of the sandwich beam showed that introducing the Bi-CSC topology could yield a more uniform distribution of the normal stress and also reduced the peak stress at the connection point of the web.

The next chapter presents a simplified analytical method referred to as the modified stiffness matrix method (MSM). The MSM is one of three simplified analytical methods to obtain the stiffness of the unfilled sandwich beam with the Bi-CSC topology presented in this research. Rather than using the computational expensive FE method presented in this chapter, the MSM is presented as an alternative approach to overcome a high degree of indeterminacy of the proposed Bi-CSC topology.

Chapter 5

Modelling the Transverse Shear Stiffness of an Unfilled Sandwich Beam using a Modified Stiffness Matrix Method

5.1 Background

To derive the transverse shear stiffness of an unfilled corrugated-like core sandwich beam, a simplified analytical approach of a unit cell based on the force-distortion relationship technique may be used. This technique relies on the estimation of the sandwich property into an equivalent property. The force-distortion relationship technique assumes that the stiffness of the sandwich structure could be found if the deformation of the unit cell could be known. Consequently, the relationship between effort forces and responding displacements, i.e., the stiffness, could be known.

The force-distortion relationship technique had been used to derive the equivalent elastic constants of corrugated core sandwich plates. Libove and Hubka [120] presented the well-known formulas for evaluating the elastic constants of the corrugated core sandwich plate in which the core was a curve-straight shape. Ko [127] derived the effective elastic constants for a super-plastically formed/diffusion-bonded unidirectional corrugated core sandwich structure in which the thickness of the corrugated sheet is not uniform due to the production technique. Nordstrand et al. [128] proposed the theoretical solutions for a curved, corrugated core based on the ordinary curved beam theory. Various corrugation patterns were studied and compared in their effective transverse shear modulus. Ray

[18] further adapted the concept of Libove and Hubka [120] to determine the transverse shear stiffness of his innovative offset-corrugated core sandwich beam.

For web-like core sandwich structure, the force-distortion relationship technique had also been used to derive the equivalent elastic constants of a C-core sandwich beam [129] and a Z-core sandwich beam [130]. Further theoretical analysis to include the contraction force between the C- or Z-core and the sandwich face plates was also developed by Fung et al. [38, 131]. For the Z-core sandwich beam, it was found that the arrangement of the Z-core and the direction of applied shear force affect the transverse shear stiffness in two manners: namely, weak or strong arrangement. The equivalent stiffness parameters of an extruded truss-core sandwich beam were also studied based on the force-distortion relationship technique by Lok et al. [19, 20].

In practice, the deformation of a unit cell can be calculated using any plane-frame structural analysis method such as the unit load method [19, 20]. Nevertheless, the force-distortion relationship technique would be too complicated for an indeterminate structural core topology such as the proposed bi-directional corrugated-strip core (Bi-CSC) topology because it needs to perform complex equilibrium, constitutive and compatibility equations. Therefore, another simplified analytical method named the modified stiffness matrix method (MSM) is presented in this research to overcome a high degree of indeterminacy of the proposed core topology.

5.2 Modified Stiffness Matrix Method

5.2.1 Assumptions

In this chapter, some assumptions have been set as follows:

- The stress-strain relationship of the steel material is limited to only the linear elastic region. The compression behaviour is also the same as the tension behaviour.
- The deformation of the unit cell is assumed small.
- The Bi-CSC is assumed to be sufficiently stiff in the z-direction so that the depth of the sandwich core after deformation remains the same as before deformation. If applicable, this assumption also applies to other similar core topologies. This assumption is set in accordance with the deformed behaviour of the FE sandwich beam model (Chapter 4) in which there is slightly different deformation in the z-direction between the top and bottom face plates. It can be seen from Fig. 5.2 and Table 5.1 that the percentage difference obtained from the FE sandwich beam

model between the top and bottom face plates are less than 0.30% for all case studies presented in Table 5.1.

TABLE 5.1: Comparison of the vertical distortion of the top and bottom face plates of unfilled sandwich beams with various core topologies obtained from the finite element method of three-point loaded beam (FE-TPB)

(a) an unfilled truss core sandwich beam

y-coordinate	0	320	640	960	1280
Top Face Plate	0	−0.0115	−0.0223	−0.0315	−0.0387
Bottom Face Plate	0	−0.0115	−0.0223	−0.0316	−0.0386
PD [a]	*N/A*	−0.03%	0.05%	−0.15%	0.28%

(b) unfilled X-truss core sandwich beams

y-coordinate	0	320	640	960	1280
	$k_{cb} = 0.50$				
Top Face Plate	0	−0.0115	−0.0223	−0.0315	−0.0387
Bottom Face Plate	0	−0.0108	−0.0209	−0.0294	−0.0357
PD	*N/A*	0.00%	0.00%	0.00%	0.00%
	$k_{cb} = 0.25$				
Top Face Plate	0	−0.0115	−0.0223	−0.0315	−0.0387
Bottom Face Plate	0	−0.0121	−0.0235	−0.0333	−0.0409
PD	*N/A*	0.00%	0.00%	0.00%	0.00%

(c) an unfilled Bi-CSC sandwich beam

y-coordinate	0	320	640	960	1280
	$k_{cb} = 0.25$				
Top Face Plate	0	−0.0115	−0.0223	−0.0315	−0.0387
Bottom Face Plate	0	−0.0119	−0.0229	−0.0325	−0.0398
PD	*N/A*	0.00%	0.01%	0.01%	0.01%

[a] PD – Percentage Difference, compared with the top face plate

- The Bi-CSC is also assumed to be equally displaced in the y-direction for each unit cell so that the displacement in the y-direction may be represented by the point at the mid-width of the sandwich beam. This assumption is also set in accordance with the deformed behaviour of the FE sandwich beam model in which there is slightly different displacement in the y-direction between any point of both the top and bottom face plates of each unit cell. It can be seen from Fig. 5.2 that the percentage difference obtained from the FE sandwich beam model between the mid-width and the edge of the sandwich beam are less than 1.0% for the X-truss core with $k_{cb} = 0.50$ and 0.25 as well as for the Bi-CSC with $k_{cb} = 0.25$.

- If applicable, the Bi-CSC is assumed to be connected to the face plates through rigid-link elements. This assumption also applies to other similar core topologies.

5.2.2 Equivalent Two-Dimensional Plane-Frame Model

Figure 5.3 shows an unfilled sandwich beam cut from a sandwich plate with Bi-CSC by two parallel planes. The configuration of this unfilled sandwich beam is defined by

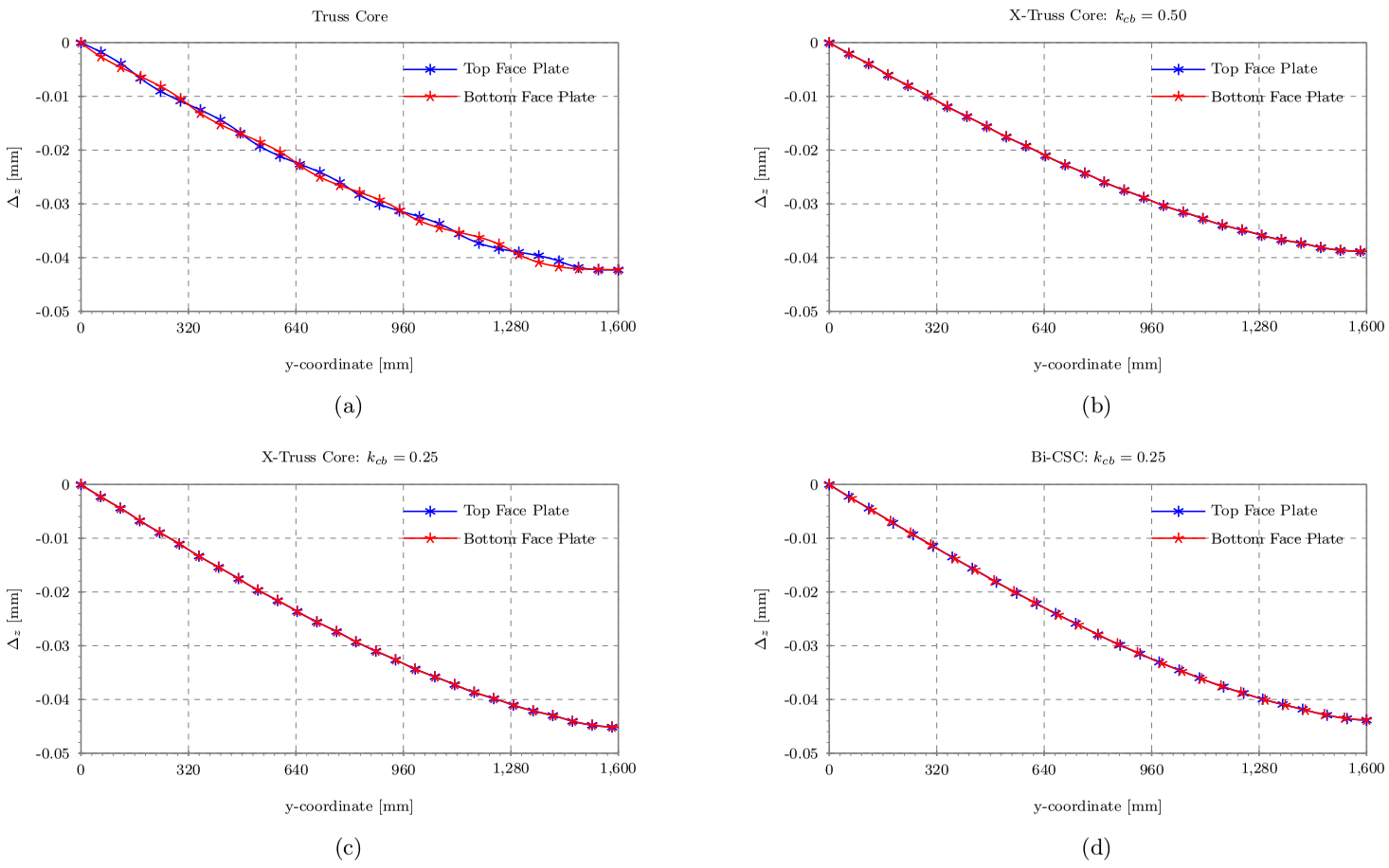

FIGURE 5.1: Vertical distortion of the top and bottom face plates of unfilled sandwich beams obtained from the finite element method of three-point loaded beam (FE-TPB) with (a) truss core, (b) X-truss core with $k_{cb} = 0.50$, (c) X-truss core with $k_{cb} = 0.25$, and (d) Bi-CSC with $k_{cb} = 0.25$

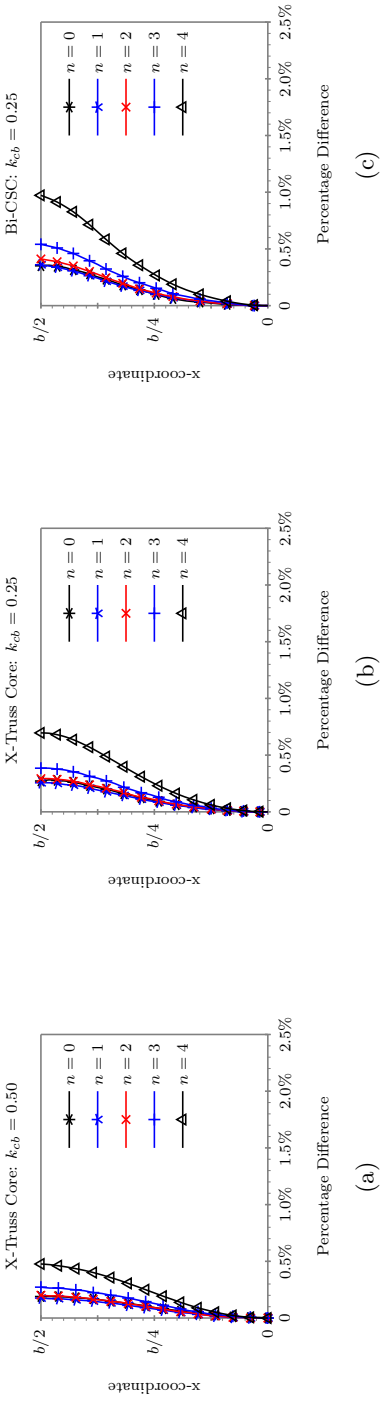

FIGURE 5.2: Horizontal distortion of unfilled sandwich beams obtained from the finite element method of three-point loaded beam (FE-TPB) with (a) X-truss core with $k_{cb} = 0.50$, (b) X-truss core with $k_{cb} = 0.25$, and (c) Bi-CSC with $k_{cb} = 0.25$

the parameters previously mentioned in Fig. 3.2. Although there may be two different configurations of the sandwich beam, they are considered equivalent to each other. This is because their material properties and geometric dimensions are identical. Moreover, the longitudinal section, i.e., the section cut in the y-direction, of these two configurations are equivalent to each other.

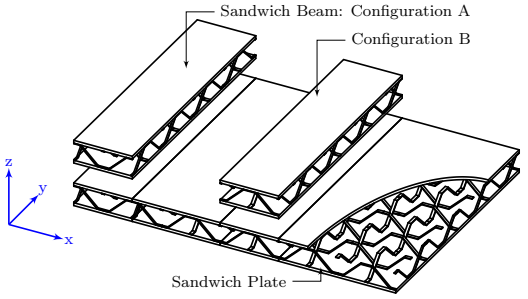

FIGURE 5.3: Unfilled sandwich beams with bi-directional corrugated-strip core cut from an unfilled sandwich plate

The equivalent two-dimensional (2D) plane-frame model (PFM), as shown in Fig. 5.4(b), is used in this research to represent a real unfilled sandwich beam (Fig. 5.4(a)). Any part of the unfilled sandwich beam is represented by a single straight line which passes through the local neutral axis of such a part. The 2D PFM consists of five basic element types. The first four element types are the top chord, the bottom chord, the inclined chord, and the vertical chord. They are compatible in material properties and geometric dimensions with the top face plate, the bottom face plate, the longitudinal corrugated-strip core (CSC), and the transverse CSC, respectively, as shown in Table 5.2. If applicable, the fifth element type is used to connect the top or bottom chord with the inclined or vertical chord. In the 2D PFM, this element type is modelled as a rigid-link element; it is much stiffer than the previously mentioned four basic element types. The rigid-link element is used based on the assumption that the connections between the face and the core are fully bonded so that there are no relative displacements. A similar concept of using rigid-link element can be found in Libove and Hubka [120] where the corrugated core was assumed to be connected with the face plates through this element type.

Instead of cutting the unfilled sandwich plate to model the unfilled sandwich beam as demonstrated in Fig. 5.3, another alternative configuration of the unfilled sandwich beam may be presented with alternative two parallel cutting planes. Figure 5.5 illustrates two alternatives of the unfilled sandwich beams with full width, $b = 2 \times s_c$, (Fig. 5.5(a)) and half width, $b = s_c$, (Fig. 5.5(b)). Although these two unfilled sandwich beams seem to be different, it may be seen that they are compatible with each other especially their longitudinal section. Neglecting torsional effects, both alternatives can be used in this chapter.

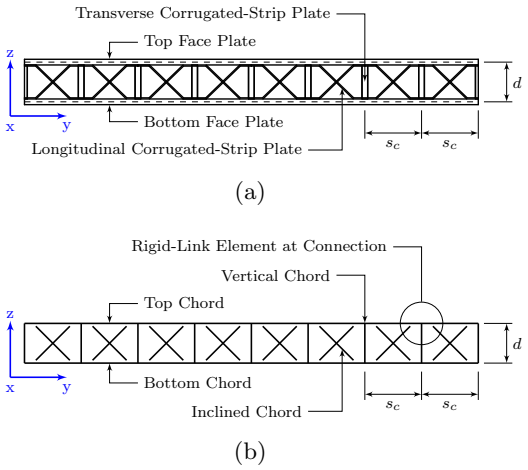

FIGURE 5.4: (a) a real unfilled sandwich beam, and (b) an equivalent two-dimension plane-frame model

TABLE 5.2: Structural models and mechanical properties of the elements of the equivalent two-dimension plane-frame model (2D PFM)

Unfilled Sandwich Beam	Equivalent Two-Dimension Plane-Frame Model		
	Element	Structural Model	Mechanical Property
Top Face Plate	Top Chord	Beam	$E_t = E_t$ $A_t = bt_t$ $I_t = \frac{1}{12}bt_t^3$
Bottom Face Plate	Bottom Chord	Beam	$E_b = E_b$ $A_b = bt_b$ $I_b = \frac{1}{12}bt_b^3$
Longitudinal CSC	Inclined Chord	Beam	$E_c = E_c$ $A_c = b_c t_c$ $I_c = \frac{1}{12}b_c t_c^3$
Transverse CSC	Vertical Chord	Beam	$E_{tc} = E_c$ $A_{tc} = b_c \frac{t_c}{\sin\theta_{tc}}$ $I_{tc} = 2\left[\frac{1}{12}\left(\frac{b_c}{2}\right)^3 t_c\right]$
–	Rigid Link	Beam	very stiff

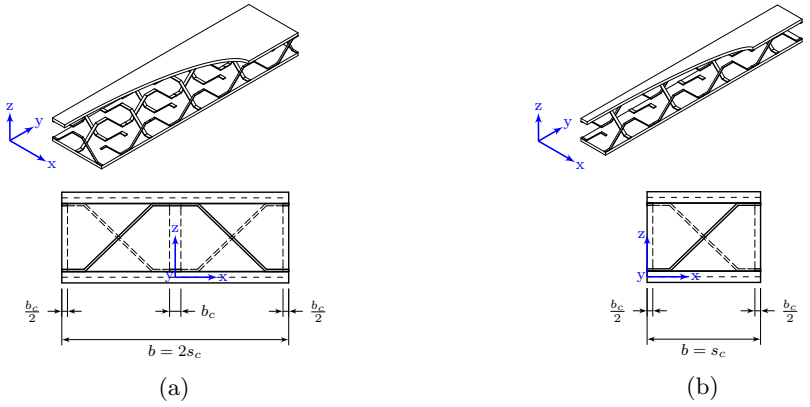

FIGURE 5.5: Two alternative configurations of an unfilled sandwich beam cut from an unfilled sandwich plate (a) a beam with full width (b) a beam with half width

5.2.3 Formulation of Transverse Shear Stiffness

The transverse shear stiffness, D_{Qy}, of the unit cell of the PFM can be formulated using the technique and Eq. 4.2 mentioned in the previous chapter. This is because the unit cell of the PFM is equivalent to the unit cell presented in the FE methods.

5.2.4 Formulation of the Stiffness Matrix Equation of a Unit Cell

Based on the stiffness matrix analysis of a plane-frame structure, the relationship between effort forces and displacements can be expressed as follows:

$$\{F\} \quad = \quad [K]\{\Delta\} \quad = \quad [T]^T[k][T]\{\Delta\} \tag{5.1}$$

where $[K]$ is the global stiffness matrix of a unit cell defined in terms of the local stiffness matrix, $[k]$, of each element and the coordinate transformation matrix, $[T]$.

Because of the constant core depth assumption, the displacements δ_z^4 and δ_z^8 of the one-half unit cell (Fig. 4.2(c)) should be identical. To account for such a compatibility constraint condition, therefore, the stiffness equations must be partitioned to separate the degrees of freedom, $\{\Delta\}$, into two parts: (1) the compatibility constraint displacements, $\{\Delta_c\}$, and (2) the free displacements, $\{\Delta_f\}$, as follows:

$$\begin{Bmatrix} F_f \\ \dots \\ F_c \end{Bmatrix} = \begin{bmatrix} K_{cc} & \vdots & K_{cf} \\ \dots & & \dots \\ K_{fc} & \vdots & K_{ff} \end{bmatrix} \begin{Bmatrix} \Delta_c \\ \dots \\ \Delta_f \end{Bmatrix} \tag{5.2}$$

Here, $\{F_c\}$ are the known forces applied to each point of the unit cell and $\{F_f\}$ are the unknown effort forces applied to the constraint points so that the compatibility constraint condition at these points is achieved. After inversion of Eq. 5.2, as shown by Eq. 5.3a, the inverted stiffness matrix, $[K]^{-1}$, is partitioned to give Eq. 5.3b.

$$\begin{Bmatrix} \Delta_c \\ \dots \\ \Delta_f \end{Bmatrix} = \begin{bmatrix} K_{cc} & \vdots & K_{cf} \\ \dots & & \dots \\ K_{fc} & \vdots & K_{ff} \end{bmatrix}^{-1} \begin{Bmatrix} F_f \\ \dots \\ F_c \end{Bmatrix} \tag{5.3a}$$

$$\begin{Bmatrix} \Delta_c \\ \dots \\ \Delta_f \end{Bmatrix} = \begin{bmatrix} K^I_{cc} & \vdots & K^I_{cf} \\ \dots & & \dots \\ K^I_{fc} & \vdots & K^I_{ff} \end{bmatrix} \begin{Bmatrix} F_f \\ \dots \\ F_c \end{Bmatrix} \tag{5.3b}$$

Therefore, $\{\Delta_c\}$ can be expressed as follows:

$$\{\Delta_c\} = \left[K_{cc}^I\right]\{F_f\} + \left[K_{cf}^I\right]\{F_c\} \tag{5.4}$$

Thus,

$$\left[K_{cc}^I\right]\{F_f\} = \{\Delta_c\} - \left[K_{cf}^I\right]\{F_c\} \tag{5.5}$$

Equation 5.5 will be used to achieve the unknown effort forces at points 4 and 8 of the one-half unit cell (Fig. 4.2(b)), i.e., the transverse shear forces at the top and bottom face plates, which correspond to the compatibility constraint condition at these points. A summation of these two forces should be equal to the effort transverse shear force, Q_y. Introducing the compatibility constraint condition, i.e., $\delta_z^4 = \delta_z^8 = \delta_z$, and letting Q_y^b equals the transverse shear force acting on the bottom face plate, one can yield that

$$\left[K_{cc}^I\right]\begin{Bmatrix} -Q_y^b \\ -(Q_y - Q_y^b) \end{Bmatrix} = \begin{Bmatrix} \delta_z \\ \delta_z \end{Bmatrix} - \left[K_{cf}^I\right]\{F_c\} \tag{5.6a}$$

or

$$\left[K_{cc}^I\right]\begin{Bmatrix} -Q_y^b \\ Q_y^b \end{Bmatrix} = \begin{Bmatrix} \delta_z \\ \delta_z \end{Bmatrix} - \left[K_{cf}^I\right]\{F_c\} - \left[K_{cc}^I\right]\begin{Bmatrix} 0 \\ -Q_y \end{Bmatrix} \tag{5.6b}$$

Having the solution for Q_y^b from Eq. 5.6b, then, one can solve for the free displacements, $\{\Delta_f\}$, from the other partitioned matrix of Eq. 5.3b, as follows:

$$\{\Delta_f\} = \left[K_{fc}^I\right]\{F_f\} + \left[K_{ff}^I\right]\{F_c\} \tag{5.7}$$

Finally, the transverse shear stiffness of the unit cell can be calculated from Eq. 4.2.

5.2.5 Formulation of the Local Stiffness Matrix of an Element

In this research, the local stiffness matrix, $[k]$, is formulated from a beam element with a linear rotational spring model at both ends of the beam element. The linear rotational spring model represents the linear relationship between the moment, M, and rotational angle, θ, at each end of the beam; this relationship is defined as $M = k\theta$ where k is the linear rotational stiffness [132–134].

The stiffness k is used to represent the flexibility condition at the end of the beam; it can vary in the range of $0 \leq k \leq \infty$. The stiffness k is set to zero to account for an

ideally pinned joint condition at the end of the beam element while it is set to infinity to account for an ideally rigid end condition.

Having the linear rotational spring model at both ends of the beam element, the local stiffness matrix, $[k]$, of the beam element can be expressed as Eq. 5.8 [132].

$$[k] = \begin{bmatrix} \frac{EA}{L} & 0 & 0 & -\frac{EA}{L} & 0 & 0 \\ & 12\frac{EI}{L^3}\frac{\gamma_i+\gamma_j+\gamma_i\gamma_j}{4-\gamma_i\gamma_j} & 6\frac{EI}{L^2}\frac{2\gamma_i+\gamma_j}{4-\gamma_i\gamma_j} & 0 & -12\frac{EI}{L^3}\frac{\gamma_i+\gamma_j+\gamma_i\gamma_j}{4-\gamma_i\gamma_j} & 6\frac{EI}{L^2}\frac{\gamma_i+2\gamma_j}{4-\gamma_i\gamma_j} \\ & & 4\frac{EI}{L}\frac{3\gamma_i}{4-\gamma_i\gamma_j} & 0 & -6\frac{EI}{L^2}\frac{2\gamma_i+\gamma_j}{4-\gamma_i\gamma_j} & 2\frac{EI}{L}\frac{3\gamma_i\gamma_j}{4-\gamma_i\gamma_j} \\ & & & \frac{EA}{L} & 0 & 0 \\ & & sym & & 12\frac{EI}{L^3}\frac{\gamma_i+\gamma_j+\gamma_i\gamma_j}{4-\gamma_i\gamma_j} & -6\frac{EI}{L^2}\frac{\gamma_i+2\gamma_j}{4-\gamma_i\gamma_j} \\ & & & & & 4\frac{EI}{L}\frac{3\gamma_j}{4-\gamma_i\gamma_j} \end{bmatrix} \tag{5.8}$$

Here, γ_i and γ_j are the flexibility stiffness factors at the end nodes i and j, respectively, of the beam element; they are expressed as follows:

$$\gamma_i = \frac{L}{L + \frac{3EI}{k_i}} \tag{5.9a}$$

$$\gamma_j = \frac{L}{L + \frac{3EI}{k_j}} \tag{5.9b}$$

Equation 5.8 can express the local stiffness matrix, $[k]$, of the beam element with any flexibility condition at the end of the beam. In the case of setting $k_i = k_j = \infty$, the flexibility stiffness factors γ_i and γ_j will equal one. As a result, the local stiffness matrix, $[k]$, of a conventional beam element is presented. Conversely, setting $k_i = k_j = 0$ leads to nil flexibility stiffness factors γ_i and γ_j. Consequently, the local stiffness matrix, $[k]$, is of a conventional truss element.

It should be noted here that the local stiffness matrix, $[k]$, of the beam element with the linear rotational spring model at both ends of the beam element is used instead of a conventional local stiffness matrix, $[k]$, of the beam element in this research as the basis for further evaluation of the truss model in the next chapter.

5.3 Validation of the Transverse Shear Stiffness

To evaluate the reliability of the presented MSM, the validation was carried out. It was divided into two validation stages: (1) the validation of the transverse shear stiffness, D_{Qy}, against the analytical solution of the unfilled truss core sandwich beam provided by Lok et al. [19, 20], and (2) the validation of the transverse shear stiffness, D_{Qy},

against the FE solution of the unfilled sandwich beams with various core topologies obtained from the finite element method of three-point load beam (FE-TPB) presented in Chapter 4. At the second stage, Lok et al.'s solution [19, 20] is no longer available for validation because it does not overcome an indeterminate truss-like core topology. Figure 5.6 shows the configurations of 2D PFM used for validation.

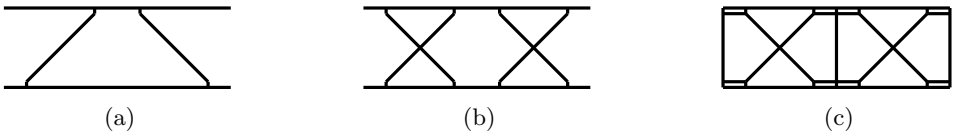

FIGURE 5.6: Configurations of the equivalent two-dimension plane-frame model of unit cells with (a) truss core, (b) X-truss core, and (c) Bi-CSC

At the first stage of validation, the selected configuration of the truss core unit cell was modelled using the 2D PFM. Here, the connections between the face plates and the core were rigid-link elements (see Fig. 5.6(a)). The rigid-link elements were much stiffer than other elements, i.e., their axial and bending stiffnesses were set to $10^6 \times E_c A_c$ and $10^6 \times E_c I_c$, respectively. Having the linear elastic property without Poisson effect, it can be seen from Fig. 5.7 and Table 5.3 that the MSM agrees very well with Lok et al.'s solution without any percentage difference. Therefore, the MSM is a reasonably reliable analytical method and can be used for further study of the unfilled truss core sandwich beam.

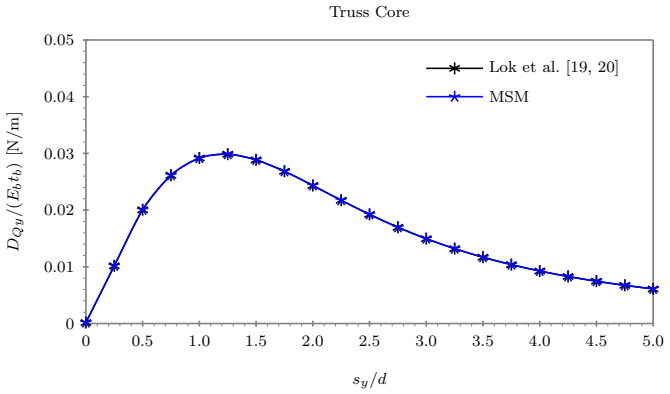

FIGURE 5.7: Comparison of the transverse shear stiffness, D_{Qy}, of unfilled truss core sandwich beams obtained from the presented modified stiffness matrix method (MSM) and Lok et al.'s method [19, 20]

At the second stage of validation, the unit cell with two core topologies, i.e., the X-truss core and the Bi-CSC topologies, were selected to analyse and compare with the FE solution obtained from the FE-TPB. Neglecting the production process, the face plates and the core were assumed to be homogeneous. The 2D PFM of these unit cells were

TABLE 5.3: Comparison of the transverse shear stiffness, D_{Qy}, of unfilled truss core sandwich beams obtained from the presented modified stiffness matrix method (MSM) and Lok et al.'s method [19, 20]

s_y/d	0.25	0.50	0.75	1.00	1.25	1.50	1.75	2.00
Lok et al. [19, 20]	0.0102	0.0201	0.0261	0.0292	0.0299	0.0289	0.0268	0.0243
MSM	0.0102	0.0201	0.0261	0.0292	0.0299	0.0289	0.0268	0.0243
PD-L [a]	0.00%	0.00%	0.00%	0.00%	0.00%	0.00%	0.00%	0.00%

[a] PD-L – Percentage Difference, compared with Lok et al. [19, 20]

modelled in a similar manner as of the truss core unit cell, as illustrated in Figs. 5.6(b) and 5.6(c).

For the X-truss core topology, it can be seen from Fig. 5.8 that both the MSM and the FE-TPB solutions are very similar to each other. All configurations with variable k_{cb} studied in this section show a similar relationship between D_{Qy} and s_y/d which have an effective range of s_y/d between 0.75 and 1.25. Although the percentage differences between both methods are quite large at some values of s_y/d, it can be seen that such differences are less than 4.50% when considering the effective range of s_y/d (see Table 5.4(a)). For $k_{cb} = 0.50$, the percentage difference at $s_y/d = 1.00$ is about 2.50%. The percentage difference of $k_{cb} = 0.25$ at $s_y/d = 1.00$ is only about 0.40%.

Figure 5.9 and Table 5.4(b) present the comparison of the transverse shear stiffness, D_{Qy}, of the unfilled sandwich beam with the Bi-CSC topology obtained from the MSM and the FE-TPB. It can be seen that both methods also yield close solution when s_y/d is in the ranges of 0.50 and 2.00. In this range, the maximum percentage difference is not greater than 4.30%. A few higher percentage differences can be found at s_y/d equal to 0.25 where the maximum percentage difference may be, for example, about 16.0% at $k_{cb} = 0.30$.

According to the validations of transverse shear stiffness, D_{Qy}, it can be seen that the analytical solutions obtained from the presented MSM are well consistent with the existing analytical solution [19, 20] and the FE solution obtained from the presented FE-TPB. Therefore, it is reasonable to conclude that the presented MSM is accurate enough and can be used for further study of the transverse shear stiffness, D_{Qy}, of the unfilled sandwich beam with at least three core topologies presented and validated in this chapter.

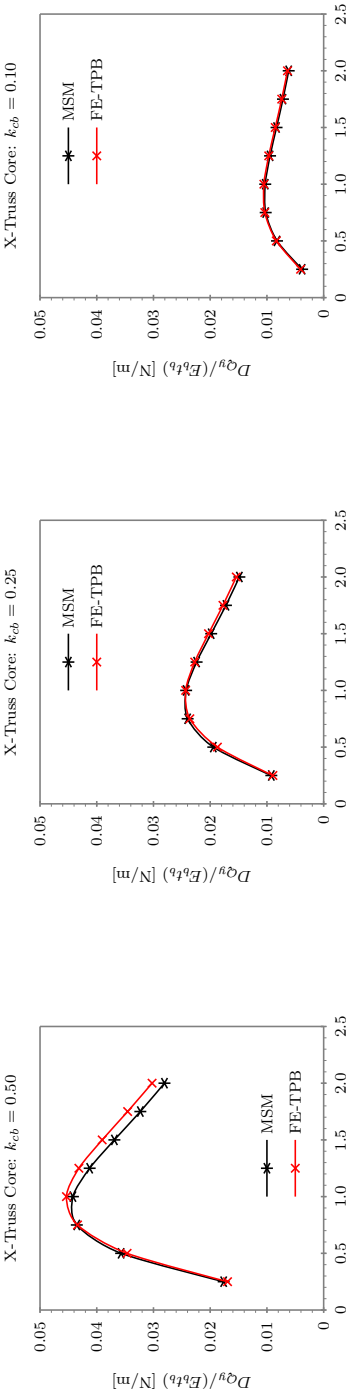

(a) $k_{cb} = 0.50$ (b) $k_{cb} = 0.25$ (c) $k_{cb} = 0.10$

FIGURE 5.8: Comparison of the transverse shear stiffness, D_{Qy}, of unfilled X-truss core sandwich beams obtained from the presented modified stiffness matrix method (MSM) and the finite element method of three-point loaded beam (FE-TPB)

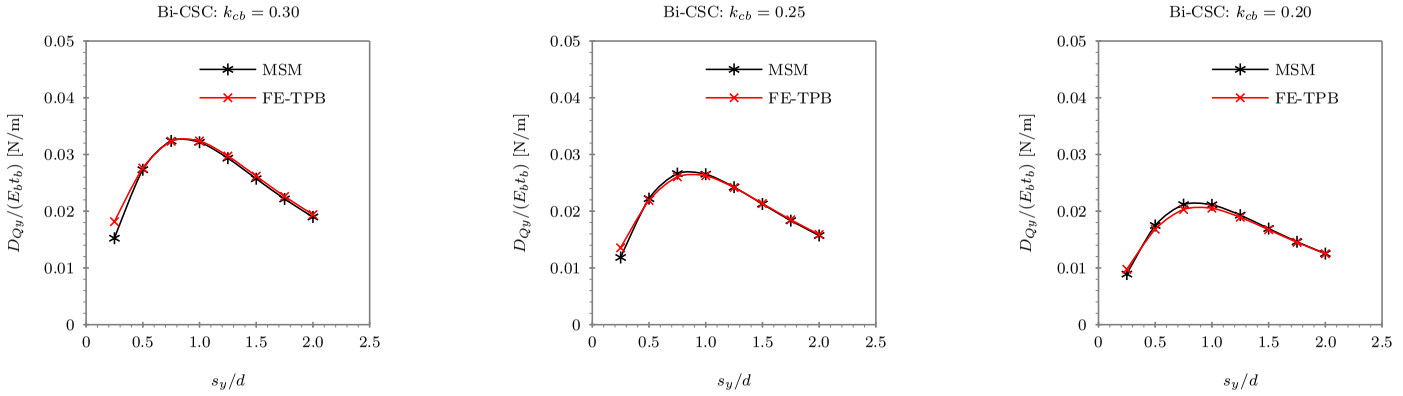

(a) $k_{cb} = 0.30$ (b) $k_{cb} = 0.25$ (c) $k_{cb} = 0.20$

FIGURE 5.9: Comparison of the transverse shear stiffness, D_{Qy}, of unfilled bi-directional corrugated-strip core sandwich beams obtained from the presented modified stiffness matrix method (MSM) and the finite element method of three-point loaded beam (FE-TPB)

TABLE 5.4: Comparison of the transverse shear stiffness, D_{Qy}, of unfilled sandwich beams with various core topologies obtained from the presented modified stiffness matrix method (MSM) and the finite element method of three-point loaded beam (FE-TPB)

(a) unfilled X-truss core sandwich beams

s_y/d	0.25	0.50	0.75	1.00	1.25	1.50	1.75	2.00
	$k_{cb} = 0.50$							
FE-TPB	0.0169	0.0347	0.0434	0.0453	0.0432	0.0390	0.0346	0.0302
MSM	0.0176	0.0357	0.0435	0.0442	0.0412	0.0369	0.0323	0.0281
PD-T [a]	4.03%	3.03%	0.29%	−2.52%	−4.41%	−5.50%	−6.47%	−7.22%
	$k_{cb} = 0.25$							
FE-TPB	0.0089	0.0187	0.0236	0.0243	0.0227	0.0203	0.0178	0.0154
MSM	0.0092	0.0195	0.0240	0.0242	0.0224	0.0198	0.0172	0.0149
PD-T	3.11%	3.85%	1.66%	−0.34%	−1.46%	−2.31%	−2.98%	−3.53%
	$k_{cb} = 0.10$							
FE-TPB	0.0041	0.0083	0.0104	0.0105	0.0097	0.0085	0.0074	0.0064
MSM	0.0038	0.0082	0.0102	0.0103	0.0094	0.0083	0.0072	0.0062
PD-T	−6.68%	−1.44%	−1.51%	−2.27%	−2.41%	−2.67%	−2.99%	−3.37%

(b) unfilled Bi-CSC sandwich beams

s_y/d	0.25	0.50	0.75	1.00	1.25	1.50	1.75	2.00
	$k_{cb} = 0.30$							
FE-TPB	0.0182	0.0276	0.0323	0.0324	0.0297	0.0262	0.0226	0.0194
MSM	0.0152	0.0273	0.0324	0.0322	0.0293	0.0257	0.0222	0.0190
PD-T	−16.09%	−1.04%	0.18%	−0.72%	−1.30%	−1.76%	−1.98%	−2.19%
	$k_{cb} = 0.25$							
FE-TPB	0.0135	0.0219	0.0261	0.0263	0.0242	0.0214	0.0185	0.0159
MSM	0.0118	0.0222	0.0266	0.0265	0.0242	0.0213	0.0183	0.0157
PD-T	−12.58%	1.48%	2.22%	1.03%	0.25%	−0.39%	−0.85%	−1.12%
	$k_{cb} = 0.20$							
FE-TPB	0.0098	0.0168	0.0203	0.0205	0.0189	0.0167	0.0145	0.0125
MSM	0.0089	0.0175	0.0212	0.0211	0.0193	0.0169	0.0146	0.0125
PD-T	−8.57%	3.93%	4.21%	2.89%	2.00%	1.22%	0.63%	0.24%

[a] PD-T – Percentage Difference, compared with the FE-TPB

5.4 Evaluation of the Performance of the Proposed Core Topology

In this section, the performance of the presented Bi-CSC topology was evaluated and compared with two similar core topologies, i.e., the truss core and the X-truss core with $k_{cb} = 0.50$ and $k_{cb} = 0.25$. The configurations of these selected core topologies were set to have the same configuration. All geometric parameters were kept constant except the ratios s_y/d and f_c/s_c. These two ratio parameters indirectly present the angle of inclined part of corrugation that can vary from 0° to 90°. Here, s_y/d varied from 0 to 2.0; therefore, the angle varied from 26.6° to 76.0°. The ratio f_c/s_c varied from 0 to 0.5. It should be noted that the angle depends on not only the ratio f_c/s_c but also the height of core, h_c; therefore, the range of angle varied with the ratio f_c/s_c should be later presented in detail in discussion of each specific case study. The width of the sandwich beam, b, also varied in different three values. Table 5.5 summarise the value of geometric parameters used in this section.

In the details of modelling using the MSM, the assumption is that the connections

TABLE 5.5: Configurations of the case studies

Parameter	Case Study		Note
	s_y/d	f_c/s_c	
b	100, 200, 400		
t_t	12		$t_t/t_b = 1$
t_b	12		
k_{cb}	1.00 for truss core 0.50 and 0.25 for X-truss core 0.25 for Bi-CSC		
t_c	2		$t_c/t_b = 1/6$
s_c	vary in terms of s_y/d where $0 \leq s_y/d \leq 5.0$	100	
f_c	$f_c = 20$	vary in terms of f_c/s_c where $0 \leq f_c/s_c \leq 0.5$	
h_c	120		$h_c/t_b = 10$

between the face plates and the core are represented using rigid-link elements. Here, the truss core and the X-truss core were modelled using only one rigid-link element and the Bi-CSC was modelled using two rigid-link elements at each connection. The use of two rigid-link elements in the latter core topology is to ensure that the assumption that the face plates and the core are fully bonded can be achieved.

The evaluations of the transverse shear stiffness, D_{Qy}, affected by the ratios s_y/d and f_c/s_c are presented in Figs. 5.10 and 5.11, respectively. In each figure, the transverse shear stiffness, D_{Qy}, factorised by $E_b t_b$ is presented on the top, and the factorised transverse shear stiffness, $D_{Qy}/E_b t_b$, per unit weight of core is presented on the bottom. The transverse shear stiffness $D_{Qy}/E_b t_b$ per unit weight of core is also normalised by the value of the truss core sandwich beam at $s_y/d = 1.00$ and $f_c/s_c = 0.25$ for each case study of variables s_y/d and f_c/s_c.

Considering the performance of the transverse shear stiffness, D_{Qy}, of the proposed core as a function of s_y/d, it can be seen from Fig. 5.10 that the transverse shear stiffness of the truss core sandwich beam is significantly improved when introducing core arrangement in the X-truss topology pattern. Of the two values of k_{cb} studied in this section, the X-truss core with $k_{cb} = 0.25$ is the most effective arrangement which yields the maximum transverse shear stiffness over unit weight of core material. Compared with the truss core at $s_y/d = 0.75$ at the same weight of the core, the X-truss core with $k_{cb} = 0.25$ is 83% stiffer than the truss core. This improvement is similar to the study of the offset-corrugated core by Ray [18] in which the transverse shear stiffness per unit weight density of the offset-corrugated core is 96% higher than that of the conventional corrugated core. The same behaviour is exhibited for every value of the sandwich beam width for both the truss core sandwich beam and the X-truss core sandwich beam studied in this section.

However, it may be clearly seen from Fig. 5.10 that introducing the CSC in a bi-directional format does not provide any advantage in the transverse shear stiffness, D_{Qy}, per unit weight of core material over the truss core topology, especially when the

ratio s_y/d is greater than 1.00 (the angle of the inclined part of the CSC is 45°). A few benefits of arranging the CSC in the bi-directional format can be found if s_y/d is less than 1.00. At $b = 400$, for example, this core is about 25.0% when $s_y/d = 0.50$ and 5.0% when $s_y/d = 0.75$ stiffer than the truss core compared at the same unit weight of the core material. This may infer that introducing the arrangement of the CSC into the bi-directional format may not yield the most optimum performance of the transverse shear stiffness, D_{Qy}, of the unfilled sandwich beam if considering the weight of the core.

Nevertheless, the transverse shear stiffness, D_{Qy}, of the Bi-CSC itself is obviously higher than that of the X-truss core with $k_{cb} = 0.25$ if not considering the weight of the core. This may support the advantage of the arrangement of the CSC into the bi-directional format. In addition, it should be noted that the transverse CSC needs to be presented in the proposed Bi-CSC topology so that the transverse shear stiffness, D_Q, of the unfilled sandwich plate can be controlled in both the x- and y-directions. As previously mentioned in Sec. 2.3, the advantage of another similar core topology, i.e., the cross-corrugated core, was also noted by Ray [18]. Therefore, further investigation should be carried out to evaluate the possible performance of the unfilled sandwich plate with the proposed core topology.

Considering the effect of the ratio f_c/s_c to the performance of the transverse shear stiffness, D_{Qy}, of the proposed core, it can be seen from Fig. 5.11 that the transverse shear stiffness of the truss core sandwich beam is also significantly improved when introducing core arrangement in the X-truss topology pattern. The X-truss core with $k_{cb} = 0.50$ and $k_{cb} = 0.25$ yield a similar trend of the transverse shear stiffness per the unit weight of the core material. The advantage of the X-truss core over the truss core is clearly found in the range of f_c/s_c between 0.15 and 0.35. In this range, the transverse shear stiffness, D_{Qy}, of the X-truss core can be 200.0% higher than that of the truss core compared at the same unit weight of the core at the f_c/s_c of 0.30.

It can be seen from Fig. 5.11 that introducing the Bi-CSC topology also provides the advantage of the transverse shear stiffness, D_{Qy}, per the unit weight of the core material over the truss core topology. However, the advantage depends not only on the ratio f_c/s_c but also on the width of the sandwich beam, b. Of the studied cases in this section, a great advantage can be found for both $b = 200$ and $b = 400$ at f_c/s_c approximately greater than 0.20 (the angle of the inclined part of the CSC is about 63.0°). At f_c/s_c greater than 0.40 ($\theta = 80.4°$), the Bi-CSC is also more advantageous in the transverse shear stiffness, D_{Qy}, than the X-truss core. It seems that the advantage increases as f_c/s_c also increases. Compared with the X-truss core with $b = 400$ and $k_{cb} = 0.25$ at the same weight of the core, the stiffness D_{Qy} of the Bi-CSC at $f_c/s_c = 0.40$ is about 60.0% higher than that of the X-truss core.

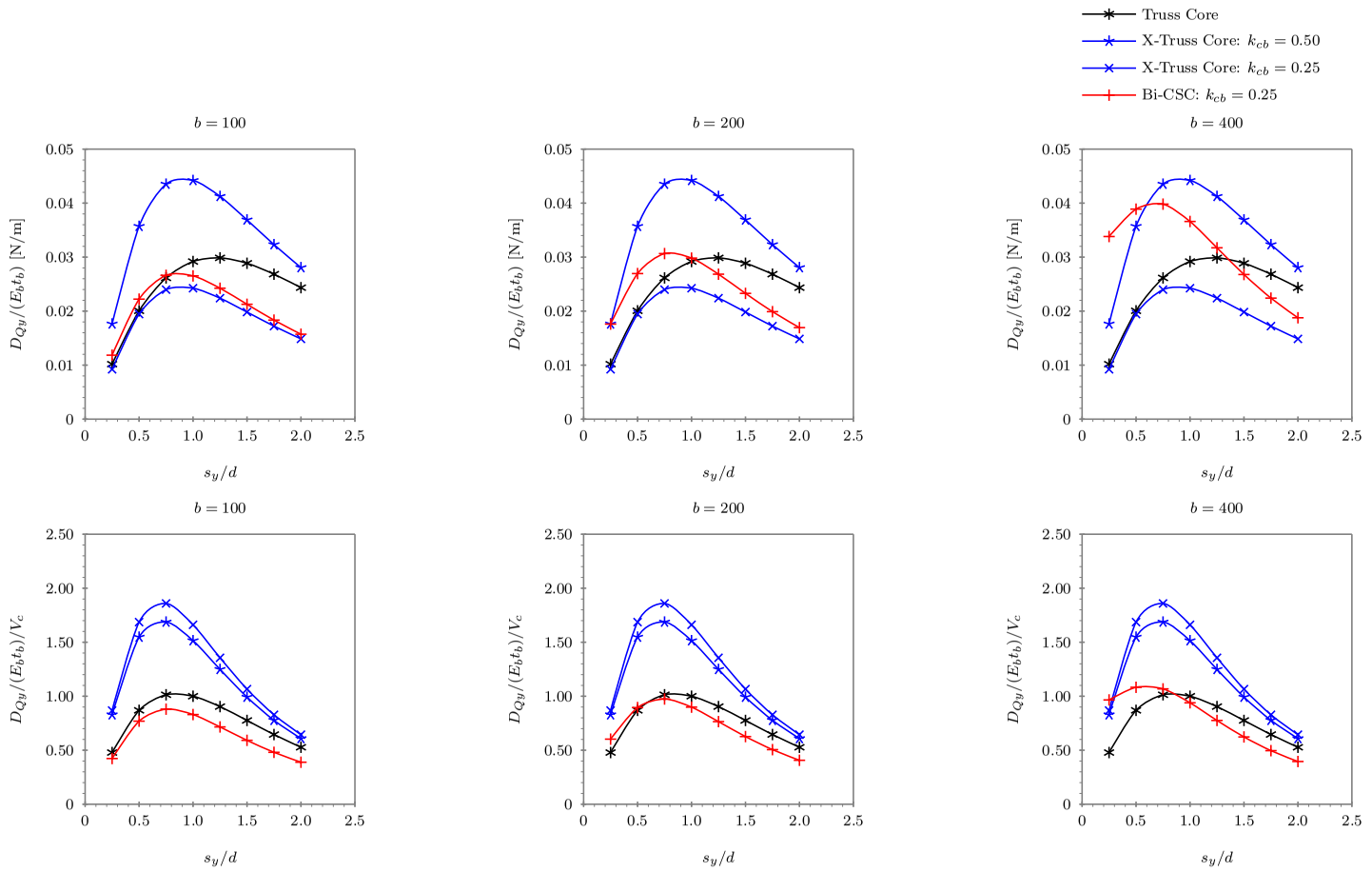

(a) $b = 100$ (b) $b = 200$ (c) $b = 400$

FIGURE 5.10: Comparison of the transverse shear stiffness (top) and the transverse shear stiffness per unit weight of the core (bottom) of various core topologies as a function of s_y/d

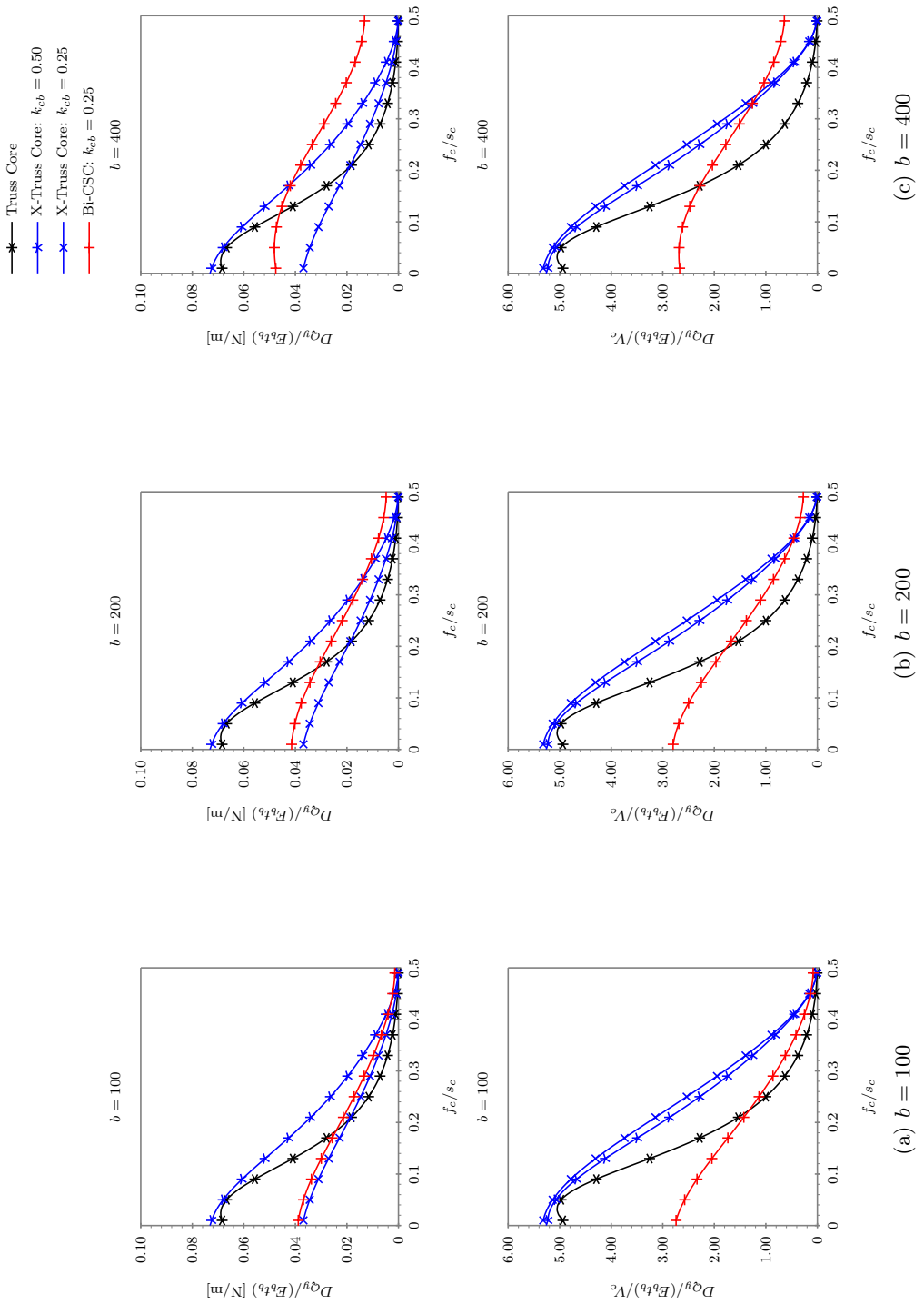

(a) $b = 100$ (b) $b = 200$ (c) $b = 400$

FIGURE 5.11: Comparison of the transverse shear stiffness (top) and the transverse shear stiffness per unit weight of the core (bottom) of various core topologies as a function of f_c/s_c

This may infer that introducing the arrangement of the CSC into the bi-directional format can provide a better performance in the transverse shear stiffness, D_{Qy}, when the angle of the inclined part of the corrugation approaches 90°. The advantage is possibly provided by the presence of the transverse CSC in the x-direction. When the inclined part of the longitudinal CSC approaches 90°, the core will nearly perform as the conventional web core. As a result, the inclined part of each corrugation will lose its diagonal bracing action and consequent transverse shear resisting capacity presented from its internal axial force. Contrary to the longitudinal CSC, the transverse CSC may still provide the same transverse shear resistance due to the plate still remaining in the same configuration in its transverse direction, i.e., in the local x-direction, which does not vary with the ratio f_c/s_c. Figure 5.11 demonstrates three configurations of the sandwich beam with Bi-CSC. It can be obviously seen that the configurations of transverse CSC remain the same whereas the configurations of longitudinal CSC significantly changes in accordance with changing the ratio f_c/s_c.

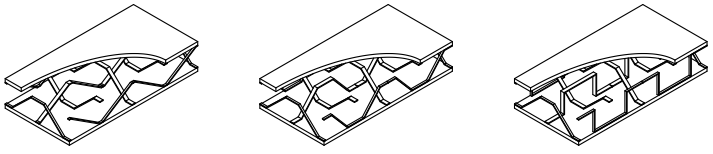

$f_c/s_c = 0.05$ (a) $f_c/s_c = 0.25$ (b) $f_c/s_c = 0.50$ (c)

FIGURE 5.12: Configurations of the corrugated-strip plate in terms of the ratio f_c/s_c

5.5 Concluding Remark

The simplified analytical method named the modified stiffness matrix method (MSM) was presented. The method was based on the force-distortion relationship of the repetitive unit cell of the unfilled sandwich beam and the conventional stiffness matrix method. The modified stiffness matrix method was proposed to overcome the high degree of indeterminacy of the presented bi-directional corrugated-strip core (Bi-CSC) topology. The 3D configurations of the unfilled sandwich beam with the presented core topology and other similar truss-like core topologies were simplified as 2D plane-frame structures with beam elements. The connections between the sandwich face plates and the core were modelled using rigid-link elements.

The formulation of the transverse shear stiffness, D_{Qy}, was presented. The local stiffness matrix of each element was performed using the model of beam with linear rotational springs at both ends of the beam element. This specific model of local stiffness matrix was presented to overcome any flexibility condition at the end of the beam element.

The presented MSM was validated using other similar core topologies, i.e., the truss core and the X-truss core. The validations were carried out against the existing analytical solution of the truss core sandwich beam provided by Lok et al. [19, 20] and against the FE result based on the 3D FE model of a three-point loaded beam presented in Chapter 4. The validation showed that the MSM agreed well with other approaches.

The presented MSM was then used to evaluate the performance of the proposed core topology. The performance of the Bi-CSC topology was then compared with the performance of the truss core topology and the X-truss core topology at the same weight of the core material. It was found that the transverse shear stiffness performance of the core varied with the ratios s_y/d and f_c/s_c. It also depended on the width of the sandwich beam, b. By comparison with the ratio s_y/d, the Bi-CSC was less advantageous than the X-truss core. However, it was possibly more advantageous than the truss core if s_y/d was less than 1.00 (the angle of the inclined part of the CSC is 45°). By comparison with the ratio f_c/s_c, the Bi-CSC was also more advantageous than the truss core if f_c/s_c was greater than 0.20. It was also more advantageous than the X-truss core in a few specific ranges of f_c/s_c. The great benefit occurred when f_c/s_c approaches 0.50 – the inclined part of corrugation approaches vertical web core configuration, i.e., $\theta = 90°$. It seems that the presented benefit in the transverse shear stiffness, D_{Qy}, of the Bi-CSC topology was provided by the presented transverse CSC in the x-direction.

The next chapter presents another simplified analytical method referred to as the braced frame analogy method (BFA). The BFA is the second simplified analytical method to obtain the stiffness of the unfilled sandwich beam with the Bi-CSC topology presented in this research. The BFA is also proposed to overcome a high degree of indeterminacy of the proposed Bi-CSC topology, and to separate the stiffness contribution of the core from the overall stiffness of the unfilled sandwich beam.

Chapter 6

Modelling the Stiffness of an Unfilled Sandwich Beam using a Braced Frame Analogy

6.1 Background

In addition to the modified stiffness matrix method (MSM) presented in Chapter 5, another simplified analytical approach of a unit cell based on the force-distortion relationship technique named the braced frame analogy method (BFA) is presented in this chapter. This technique also relies on the estimation of the sandwich property into an equivalent property. This technique also assumes that the stiffness of the sandwich structure could be found if the deformation of the unit cell could be known. Consequently, the relationship between effort forces and corresponding displacements, i.e., the stiffness, could be known.

In detail, the BFA assumes that the flexural and transverse shear stiffnesses are obtained from separate flexural and transverse shear load mechanisms. This assumption is based on the fact that the deformation of the unfilled sandwich beam with some structural core topologies, e.g., a web core, may be separated into two deformation modes: (1) bending deformation, and (2) shear deformation [37, 50].

Although the deformation of a unit cell can be calculated using any plane-frame structural analysis method such as the unit load method [19, 20] or the MSM presented in Chapter 5, the simplified analytical method along with the braced frame model with a truss assumption is proposed in this chapter. This simplified method is used to overcome the high degree of indeterminacy in the core topology. It is also used to analyse the

stiffness from each component of the sandwich beam separately so that the contribution of the proposed core topology can be deduced.

6.2 Braced Frame Analogy Method

6.2.1 Assumptions

In addition to the assumptions set in Chapter 5, some additional assumptions have been set in this chapter as follows:

- The deformation of a sandwich beam is assumed to be deformed into two separate modes: (1) a bending deformation mode, and (2) a shear deformation mode, as illustrated in Fig. 6.1. The former is caused by the elongation of the sandwich face plates in which its response may be calculated using a bending theory. The latter is caused by the transverse shear load in which its response may be assumed as the deformation of a shear panel. Similar assumptions have been found in the study of an unfilled web-core sandwich beam [37] and of an unfilled Bi-Steel sandwich beam [50].

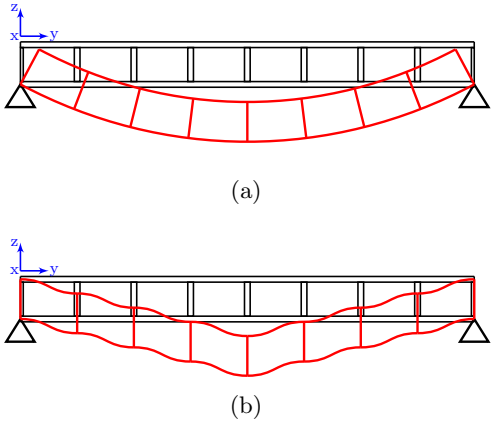

FIGURE 6.1: Two deformed shapes of an unfilled sandwich beam (a) a bending deformation mode, and (b) a shear deformation mode

- During bending deformation, the straight plane of the sandwich beam cross section which is normal to the neutral axis of the undeformed beam remains straight after deformation. Also, the plane is still normal to the deformed neutral axis.

- During shear deformation, the shear panel is deformed into two separate deformation directions: (1) the shear deformation in the z-direction, and (2) the shear deformation in the y-direction.

6.2.2 Equivalent Two-Dimensional Braced Frame Model

In this chapter, the plane-frame model (PFM) used in Chapter 5 is further adapted to be the equivalent two-dimensional (2D) braced frame model (BFM). The BFM is similar to the PFM in which all parts of the model are represented by a single straight line which pass through the local neutral axis of each part and consisted of the top chord, the bottom chord, the inclined chord, the vertical chord, and if applicable the rigid-link element. They are compatible in material properties and geometric dimensions with the top face plate, the bottom face plate, the longitudinal corrugated-strip core (CSC), and the transverse CSC, respectively, as shown in Table 6.1.

TABLE 6.1: Structural models and mechanical properties of the elements of the braced frame analogy method

Unfilled Sandwich Beam	Two-Dimension Braced Frame Model		
	Element	Structural Model	Mechanical Property
Top Face Plate	Top Chord	Beam	$E_t = E_t$ $A_t = bt_t$ $I_t = \frac{1}{12}bt_t^3$
Bottom Face Plate	Bottom Chord	Beam	$E_b = E_b$ $A_b = bt_b$ $I_b = \frac{1}{12}bt_b^3$
Longitudinal CSC	Inclined Chord	Truss [a]	$E_c = E_c$ $A_c = b_c t_c$
Transverse CSC	Vertical Chord	Beam	$E_{tc} = E_c$ $A_{tc} = b_c \frac{t_c}{\sin\theta_{tc}}$ $I_{tc} = 2\left[\frac{1}{12}\left(\frac{b_c}{2}\right)^3 t_c\right]$

[a] in the MSM, the inclined chord is modelled as a beam

However, it should be noted that the ends of the inclined chord connected to other elements are assumed as a hinge. The inclined chord in this chapter is therefore performed as a truss element and can be subjected to only an axial force. This is the only aspect of the BFM which is different from the PFM.

The truss element assumption of the inclined chord is set in accordance with the analytical result of the unfilled sandwich beam with various truss-like core using the MSM presented in Chapter 5. For the specific case study presented here, it can be seen from Table 6.2 that there is no significant difference between modelling the inclined chord as the beam element or as the truss element. Therefore, the truss element assumption may be used to model the inclined chord of the BFM. This decision is made to reduce the number of equations needed to be solved in the proposed BFA so that the analytical technique and solution may be simplified and calculation time may also be reduced. This assumption has also been conceptually noted in Allen [31] in which the core of truss-like core sandwich beams may be modelled as the truss element so that the stiffness is contributed from only the contraction or the extension of the core.

TABLE 6.2: Evaluation of the transverse shear stiffness, D_{Qy}, of unfilled sandwich beams with various core topologies obtained from the presented modified stiffness matrix method (MSM) with and without the truss assumption

(a) unfilled truss core sandwich beams

s_y/d	0.25	0.50	0.75	1.00	1.25	1.50	1.75	2.00
without truss assumption	0.0102	0.0201	0.0261	0.0292	0.0299	0.0289	0.0268	0.0243
with truss assumption	0.0100	0.0199	0.0260	0.0291	0.0298	0.0288	0.0268	0.0243
PD [a]	−1.32%	−0.74%	−0.58%	−0.46%	−0.35%	−0.25%	−0.17%	−0.11%

(b) unfilled X-truss core sandwich beams

s_y/d	0.25	0.50	0.75	1.00	1.25	1.50	1.75	2.00
	$k_{cb} = 0.50$							
without truss assumption	0.0176	0.0357	0.0435	0.0442	0.0412	0.0369	0.0323	0.0281
with truss assumption	0.0175	0.0357	0.0435	0.0442	0.0412	0.0369	0.0323	0.0281
PD	−0.44%	−0.13%	−0.07%	−0.05%	−0.03%	−0.02%	−0.01%	−0.01%
	$k_{cb} = 0.25$							
without truss assumption	0.0092	0.0195	0.0240	0.0242	0.0224	0.0198	0.0172	0.0149
with truss assumption	0.0092	0.0194	0.0240	0.0242	0.0224	0.0198	0.0172	0.0149
PD	−0.44%	−0.11%	−0.05%	−0.03%	−0.02%	−0.01%	−0.01%	0.00%
	$k_{cb} = 0.10$							
without truss assumption	0.0038	0.0082	0.0102	0.0103	0.0094	0.0083	0.0072	0.0062
with truss assumption	0.0038	0.0082	0.0102	0.0103	0.0094	0.0083	0.0072	0.0062
PD	−0.43%	−0.10%	−0.04%	−0.02%	−0.01%	−0.01%	0.00%	0.00%

(c) unfilled Bi-CSC core sandwich beams

s_y/d	0.25	0.50	0.75	1.00	1.25	1.50	1.75	2.00
	$k_{cb} = 0.30$							
without truss assumption	0.0152	0.0273	0.0324	0.0322	0.0293	0.0257	0.0222	0.0190
with truss assumption	0.0152	0.0273	0.0324	0.0321	0.0293	0.0257	0.0222	0.0190
PD	−0.34%	−0.10%	−0.05%	−0.02%	−0.01%	−0.01%	0.00%	0.00%
	$k_{cb} = 0.25$							
without truss assumption	0.0118	0.0222	0.0266	0.0265	0.0242	0.0213	0.0183	0.0157
with truss assumption	0.0118	0.0222	0.0266	0.0265	0.0242	0.0213	0.0183	0.0157
PD	−0.36%	−0.10%	−0.05%	−0.02%	−0.01%	−0.01%	0.00%	0.00%
	$k_{cb} = 0.20$							
without truss assumption	0.0089	0.0175	0.0212	0.0211	0.0193	0.0169	0.0146	0.0125
with truss assumption	0.0089	0.0175	0.0212	0.0211	0.0193	0.0169	0.0146	0.0125
PD	−0.39%	−0.10%	−0.04%	−0.02%	−0.01%	−0.01%	0.00%	0.00%

[a] PD – Percentage Difference, compared with the model without truss assumption

Figure 6.2(b) shows the repetitive part of the BFM which illustrates some differences from the PFM.

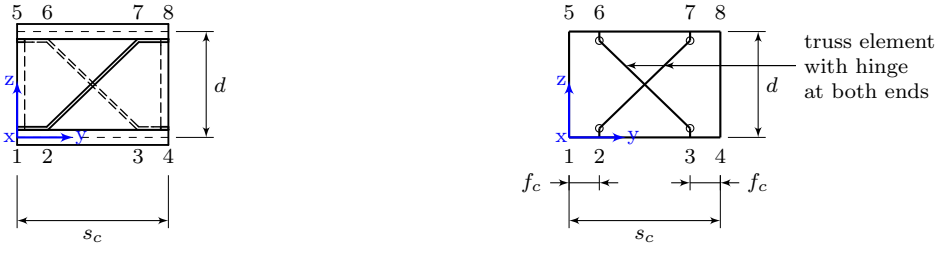

FIGURE 6.2: The repetitive part of (a) an unfilled sandwich beam, and (b) the equivalent two-dimensional braced frame model

6.3 Flexural Load Transfer Mechanism

6.3.1 Equilibrium of Force of a Unit Cell

Considering the unit cell of the BFM subjected to pure bending moment, M, as shown in Fig. 6.3(a), it can be expressed that the inclined chords should be extended if the neutral axis of the sandwich beam with an unsymmetrical section about the y-axis is located near the top face plate, i.e., $z_t < z_b$; as a result, the inclined chords are subjected to tensile force. Therefore, the equilibrium of force in the z-direction of the free body diagram (FBD) of the right part of the unit cell (Fig. 6.3(b)) yields that $F_{c1} = F_{c2} = F_c$. Consequently, the equilibrium of moment about the x-axis is as follows:

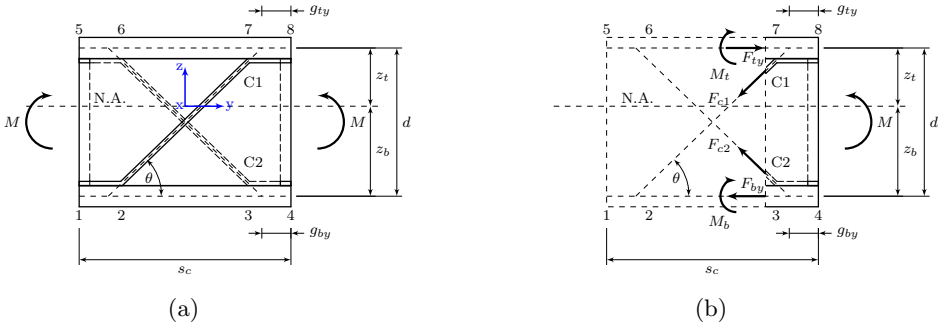

FIGURE 6.3: (a) the unit cell of the braced frame model subjected to pure bending moment, and (b) the free body diagram of the right part of the unit cell

$$M = M_t + M_b + F_{ty} z_t + F_{by} z_b + F_c (z_b - z_t) \cos\theta + F_c (g_{by} - g_{ty}) \sin\theta \quad (6.1)$$

6.3.2 Displacement Compatibility of a Deformed Unit Cell

According to the small displacement assumption, the deformed shape of the unit cell subjected to pure bending moment can be approximately represented using the straight line shape, as shown in Fig. 6.4. Considering this deformed shape, the elongation length at each layer of the face plate can be expressed in terms of δ_{ty}, for example, $\delta_{by} = \frac{z_b}{z_t}\delta_{ty}$.

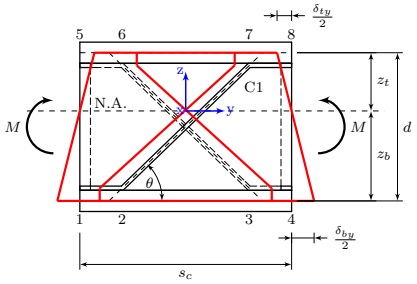

FIGURE 6.4: Deformed shape of the unit cell of the equivalent two-dimension braced frame model subjected to pure bending moment

The extended length of the inclined chords can be also expressed in terms of δ_{ty} as follows:

$$\begin{aligned} \delta_c &= \sqrt{L_z^2 + \left[L_y - \frac{1}{2}\left(\delta_{ty} - \delta_{by}\right)\right]^2} - L_c \\ &= \sqrt{L_z^2 + \left[L_y - \frac{1}{2}\left(1 - \frac{z_b}{z_t}\right)\delta_{ty}\right]^2} - L_c \\ &= k_b \delta_{ty} \end{aligned} \tag{6.2}$$

where k_b is elongation factor of the inclined chord expressed as follows[1]:

$$k_b = \begin{cases} -\dfrac{s_y}{d}\left(1 - \dfrac{z_b}{z_t}\right)\displaystyle\sum_{n=0}^{\infty} \frac{(-1)^n (2n)!}{(1-2n)\, n!^2 4^n} n \left(\frac{s_y^2}{d^2}\right)^{n-1} & \text{if } s_y \le d \\ -\left(1 - \dfrac{z_b}{z_t}\right)\displaystyle\sum_{n=0}^{\infty} \frac{(-1)^n (2n)!}{(1-2n)\, n!^2 4^n} n \left(\frac{d^2}{s_y^2}\right)^{n-1} & \text{if } s_y \ge d \end{cases} \tag{6.3}$$

and L_c is the initial length of the inclined chord expressed as $L_c = \sqrt{L_z^2 + L_y^2}$ where $L_z = h_c - t_c$ and $L_y = s_c - 2f_c$.

It should be noted that the small length between nodes 1 and 2 is assumed to not elongate. This means that the distance f_c before deformation remains the same as after deformation. This assumption is also applied to the small length between nodes 3 and 4, 5 and 6, and 7 and 8.

6.3.3 Governing Equation

Knowing the extended length of each member, the internal resultant force occurs in the top face plate, F_{ty}, the bottom face plate, F_{by}, and the inclined chords, F_c, can be

[1] see the derivation of the elongation factor k_b in Appendix A

expressed as follows:

$$F_{ty} = \frac{E_t A_t}{s_c}\delta_{ty} \tag{6.4a}$$

$$F_{by} = \frac{E_b A_b}{s_c}\delta_{by} \tag{6.4b}$$

$$F_c = \frac{E_c A_c}{L_c}\delta_c \tag{6.4c}$$

Similarly, the internal bending moment at the top face plate, M_t, and at the bottom face plate, M_b, – as a result of the internal forces F_{ty} and F_{by}, respectively – can be expressed as follows:

$$M_t = \frac{1}{12}\frac{E_t A_t t_t^2}{s_c z_t}\delta_{ty} \tag{6.5a}$$

$$M_b = \frac{1}{12}\frac{E_b A_b t_b^2}{s_c z_b}\delta_{by} \tag{6.5b}$$

Substitute Eqs. 6.4 and 6.5 into Eq. 6.1, thus

$$\begin{aligned} M = & \left\{\frac{1}{12}\frac{E_t A_t t_t^2}{s_c z_t} + \frac{E_t A_t z_t}{s_c} + \frac{1}{12}\frac{E_b A_b t_b^2}{s_c z_t} + \frac{E_b A_b z_b}{s_c}\frac{z_b}{z_t} + \right. \\ & \left. \frac{E_c A_c}{L_c} k_b \left[(z_b - z_t)\cos\theta + (g_{by} - g_{ty})\sin\theta\right]\right\}\delta_{ty} \end{aligned} \tag{6.6}$$

Equation 6.6 can be further expressed in terms of the bending curvature, $\frac{d^2 z}{dy^2}$, by introducing $\delta_{ty} = -s_c z_t \frac{d^2 z}{dy^2}$ [135], thus

$$\begin{aligned} M = & -\left\{\frac{1}{12}E_t A_t t_t^2 + E_t A_t z_t^2 + \frac{1}{12}E_b A_b t_b^2 + E_b A_b z_b^2 + \right. \\ & \left. \frac{E_c A_c}{L_c} k_b s_c z_t \left[(z_b - z_t)\cos\theta + (g_{by} - g_{ty})\sin\theta\right]\right\}\frac{d^2 z}{dy^2} \end{aligned} \tag{6.7}$$

Therefore, the governing equation of the sandwich beam subjected to pure bending moment is

$$\frac{d^2 z}{dy^2} = -\frac{M}{D_y} \tag{6.8}$$

where the flexural stiffness, D_y, is

$$\begin{aligned} D_y &= \frac{1}{12}E_t A_t t_t^2 + E_t A_t z_t^2 + \frac{1}{12}E_b A_b t_b^2 + E_b A_b z_b^2 + \\ &\quad \frac{E_c A_c}{L_c} k_b s_c z_t \left[(z_b - z_t)\cos\theta + (g_{by} - g_{ty})\sin\theta\right] \\ &= \frac{1}{12}E_t A_t t_t^2 + E_t A_t z_t^2 + \frac{1}{12}E_b A_b t_b^2 + E_b A_b z_b^2 + \\ &\quad \frac{E_c A_c}{L_c^2} k_b s_c z_t d \left(\frac{s_c - 2f_c}{h_c - t_c}\right)\left[(z_b - z_t) + \frac{1}{2}(t_t - t_b)\right] \end{aligned} \tag{6.9}$$

6.3.4 Summary of Calculation Procedure

Figure 6.5 illustrates the procedure to calculate the flexural stiffness, D_y, using the BFA.

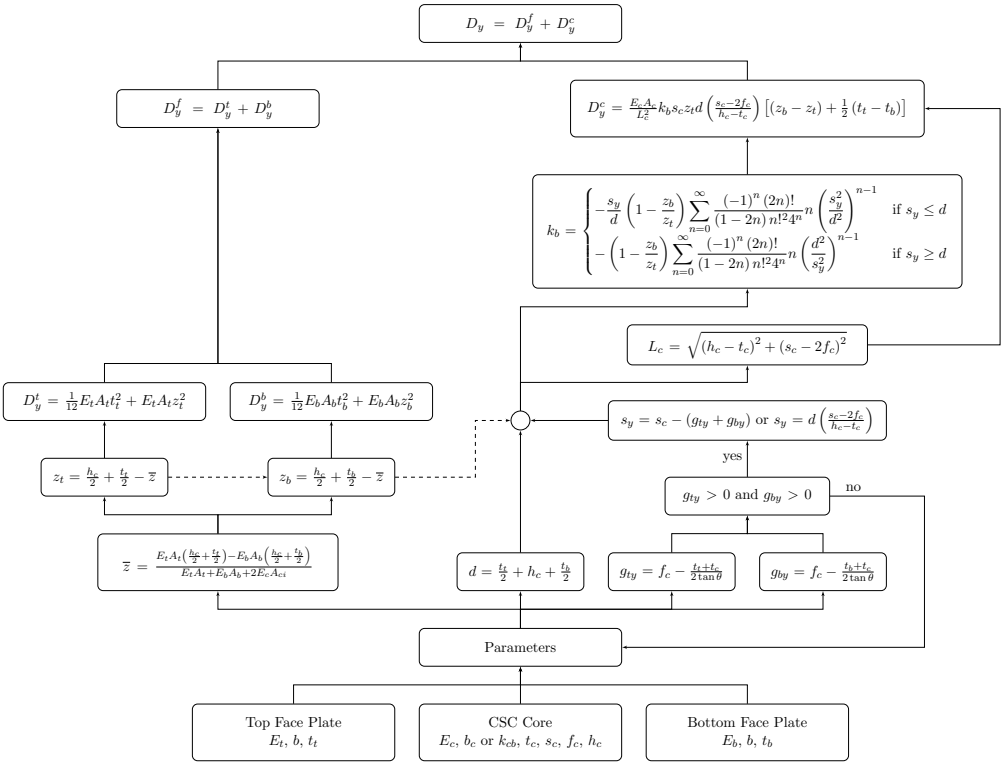

FIGURE 6.5: The Calculation procedure of the flexural stiffness, D_y

6.4 Transverse Shear Load Transfer Mechanism

6.4.1 Equilibrium of Force of a Unit Cell

Considering the FBD of the right-hand part of a unit cell subjected to the transverse shear force, Q_y, as shown in Fig. 6.6(b), the expression of the equilibrium of force in the y-direction yields that $F_{c1} = F_{c2} = F_c$. Therefore, the equilibrium of force in the z-direction can be expressed as follows:

$$F_{tz} + F_{bz} + 2F_c \sin\theta \quad = \quad Q_y \tag{6.10}$$

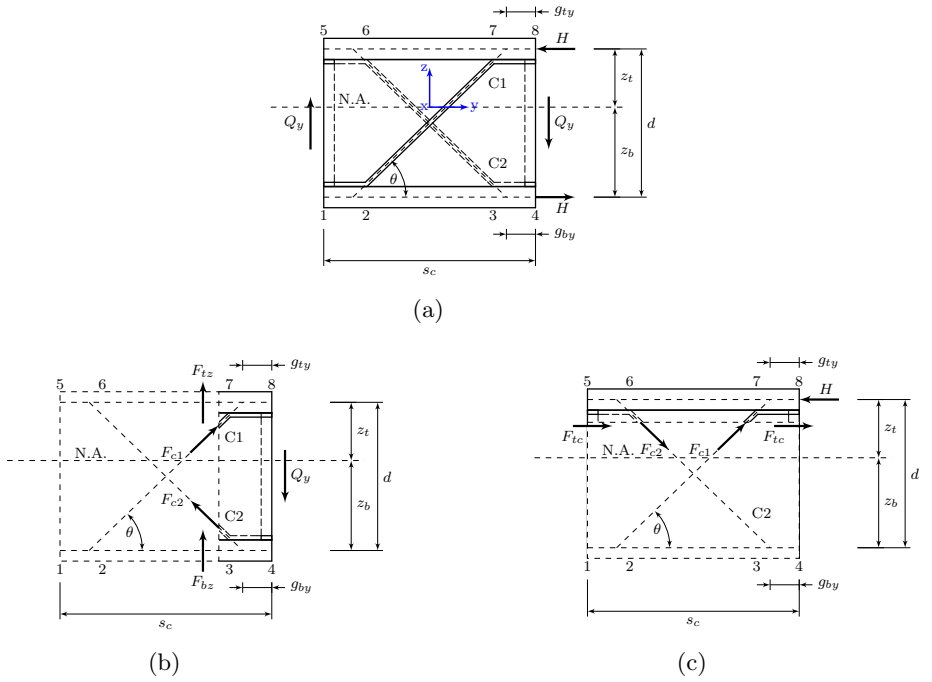

FIGURE 6.6: (a) the unit cell of the equivalent two-dimension braced frame model subjected to transverse shear force, (b) the free body diagram of the right part of the unit cell subjected to the transverse shear force, Q_y, and (c) the free body diagram of the top part of the unit cell subjected to a couple of horizontal force, H

6.4.2 Displacement Compatibility of a Deformed Unit Cell

In the BFA, the unit cell subjected to the transverse shear force, Q_y, is assumed to deform into two separate modes: (1) the deformation in the z-direction due to the transverse shear force, Q_y, itself (Fig. 6.7(a)), and (2) the deformation in the y-direction due to a couple of horizontal force, H, (Fig. 6.7(b)). A couple of horizontal force, H, is also applied to the unit cell to maintain the static equilibrium as earlier mentioned in detail in Sec. 4.1, Page 40.

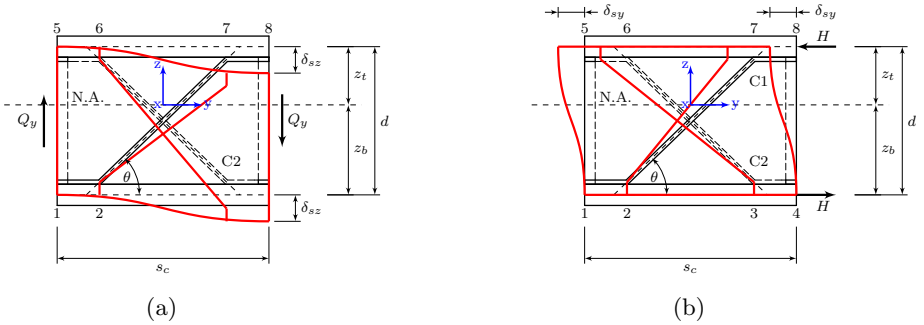

FIGURE 6.7: Deformed shape of the unit cell of the equivalent two-dimension braced frame model subjected to (a) transverse shear force, Q_y, and (b) a couple of horizontal force, H

Considering the first deformed configuration as illustrated in Fig. 6.7(a), any displacement in the z-direction of the top or bottom face plate may be found if the deformed shape of the unit cell can be approximately assumed in advance. Here, the whole unit cell subjected to only the transverse shear force, Q_y, is assumed to deform like a fixed-end beam. Thus, the face plate is considered to deform in a reverse curvature.

Because of the constant core depth assumption, the relative end displacement in the z-direction of the top face plate, δ_{tz}, and the bottom face plate, δ_{bz}, are identical; thus $\delta_{tz} = \delta_{bz} = \delta_{sz}$. The elongation length of the inclined chords C1 and C2 can be also expressed in terms of δ_{sz}, as δ_{c1} and δ_{c2} respectively, as follows:

$$\delta_{c1} = \sqrt{\left[L_z - \frac{L_y}{s_c}\delta_{sz}\right]^2 + L_y^2} - L_c \tag{6.11a}$$

$$\delta_{c2} = \sqrt{\left[L_z + \frac{L_y}{s_c}\delta_{sz}\right]^2 + L_y^2} - L_c \tag{6.11b}$$

Equation 6.11 can be further expressed in terms of the elongation factor k_{sz} as follows[2]:

$$-\delta_{c1} = \delta_{c2} = \delta_c = k_{sz}\delta_{sz} \tag{6.12}$$

where

$$k_{sz} = \begin{cases} 2\dfrac{s_c - 2f_c}{s_c}\displaystyle\sum_{n=0}^{\infty}\frac{(-1)^n\,(2n)!}{(1-2n)\,n!^2 4^n} n\left(\frac{s_y^2}{d^2}\right)^{n-1} & \text{if } s_y \le d \\ 2\dfrac{h_c - t_c}{s_c}\displaystyle\sum_{n=0}^{\infty}\frac{(-1)^n\,(2n)!}{(1-2n)\,n!^2 4^n} n\left(\frac{d^2}{s_y^2}\right)^{n-1} & \text{if } s_y \ge d \end{cases} \tag{6.13}$$

Here, the absolute value of the displacement lengths δ_{c1} and δ_{c2} are assumed to be equal in accordance with the FE results (Chapter 4). According to the study of the unfilled sandwich beam with the Bi-CSC of example configuration as presented in Table 6.3, it is found that the difference between the displacements δ_{c1} and δ_{c2} of each repetitive unit cell is less than 2.70%. Further derivation in Appendix A also shows that the displacements δ_{c1} and δ_{c2} are equal in absolute value. Therefore, it may be reasonable to introduce this assumption in the BFA to simplify the analytical method.

Because of the fixed-end beam behaviour assumption, the displacements δ_{tz} and δ_{bz} may be expressed in terms of the applied force as Eqs. 6.14a and 6.14b. Meanwhile, the

[2] see the derivation of the elongation factor k_{sz} in Appendix A

TABLE 6.3: Displacement of the inclined parts of unfilled sandwich beams with bi-directional corrugated-strip core obtained from the finite element method of three-point loaded beam (FE-TPB)

Unit Cell no.	1		2		3		4		5	
	1L	1R	2L	2R	3L	3R	4L	4R	5L	5R
δ_{c1} [$\times 10^{-4}$]	−6.4862	6.1946	−6.2054	6.2267	−6.1995	6.2299	−6.1904	6.2279	−6.2582	5.4402
δ_{c2} [$\times 10^{-4}$]	6.3154	−6.0356	6.0518	−6.0631	6.0385	−6.0738	6.0292	−6.0720	6.0836	−5.3200
PD [a]	2.70%	2.63%	2.54%	2.70%	2.67%	2.57%	2.67%	2.57%	2.87%	2.26%

[a] PD – Percentage Difference, compared in absolute value of δ_{c1} and δ_{c2}

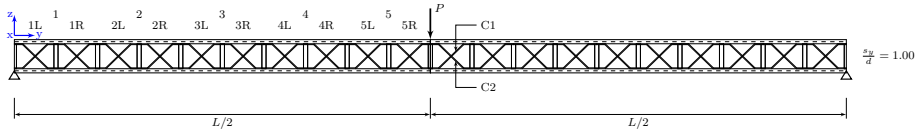

displacement δ_c can be expressed as Eq. 6.14c.

$$\delta_{tz} = \frac{1}{12}\frac{s_c^3}{E_t I_t} F_{tz} \tag{6.14a}$$

$$\delta_{bz} = \frac{1}{12}\frac{s_c^3}{E_b I_b} F_{bz} \tag{6.14b}$$

$$\delta_c = \frac{L_c}{E_c A_c} F_c \tag{6.14c}$$

Substitute Eq. 6.14 into Eq. 6.10, thus

$$Q_y = \left(12\frac{E_t I_t}{s_c^3} + 12\frac{E_b I_b}{s_c^3} + 2\frac{E_c A_c}{L_c} k_{sz} \sin\theta\right) \delta_{sz} \tag{6.15}$$

Similarly, the relationship between a couple horizontal force, H, and the displacement in the y-direction δ_{sy} of the second deformed configuration may be expressed as follows:

$$H = \left(24\frac{E_c I_{tc}}{(h_c - t_c)^3} + 2\frac{E_c A_c}{L_c} k_{sy} \cos\theta\right) \delta_{sy} \tag{6.16}$$

where k_{sy} is the elongation factor of the inclined chord expressed as follows[3]:

$$k_{sy} = \begin{cases} 2\dfrac{s_y}{d}\displaystyle\sum_{n=0}^{\infty} \frac{(-1)^n (2n)!}{(1-2n)\, n!^2 4^n} n \left(\frac{s_y^2}{d^2}\right)^{n-1} & \text{if } s_y \le d \\ 2\displaystyle\sum_{n=0}^{\infty} \frac{(-1)^n (2n)!}{(1-2n)\, n!^2 4^n} n \left(\frac{d^2}{s_y^2}\right)^{n-1} & \text{if } s_y \ge d \end{cases} \tag{6.17}$$

[3] see the derivation of the elongation factor k_{sy} in Appendix A

6.4.3 Formulation of Transverse Shear Stiffness

Having the deformed shape of a unit cell subjected to the transverse shear force, Q_y, as illustrated in Fig. 6.7, the transverse shear stiffness, D_{Qy}, of the unit cell may be expressed as follows:

$$\begin{aligned} D_{Qy} &= \frac{Q_y}{\frac{\delta_{sy}}{d} + \frac{\delta_{sz}}{s_c}} \\ &= \frac{Q_y}{\frac{H}{dD^y_{Qy}} + \frac{Q_y}{s_c D^z_{Qy}}} \\ &= \frac{1}{\frac{s_c}{d^2 D^y_{Qy}} + \frac{1}{s_c D^z_{Qy}}} \end{aligned} \tag{6.18}$$

where

$$D^z_{Qy} = 12\frac{E_t I_t}{s_c^3} + 12\frac{E_b I_b}{s_c^3} + 2\frac{E_c A_c}{L_c} k_{sz} \sin\theta \tag{6.19a}$$

$$D^y_{Qy} = 24\frac{E_c I_{tc}}{(h_c - t_c)^3} + 2\frac{E_c A_c}{L_c} k_{sy} \cos\theta \tag{6.19b}$$

6.4.4 Summary of Calculation Procedure

Figure 6.8 illustrates the procedure to calculate the transverse shear stiffness, D_{Qy}, using the BFA.

6.5 Verification of the Stiffness Equations

6.5.1 Flexural Stiffness Equation

In general, the contribution of the core to the flexural stiffness may be expressed into two possible cases as follows:

Unsymmetrical Section: If the top face plate is thicker and/or stronger than the bottom face plate so that $E_t t_t > E_b t_b$, the neutral axis of this cross section should be near the top face plate. This means that $z_t < z_b$. Thus, z_b/z_t is greater than one and then the term $-\frac{1}{2}\left(1 - \frac{z_b}{z_t}\right)$ of Eq. 6.2 is a positive value. As a result, the deformed inclined chords are lengthened and provide internal axial tensile forces to resist the applied moment, i.e., the core obviously provides some contribution to the flexural stiffness. Similar behaviour can be found in the case of the top face plate being thinner and/or weaker

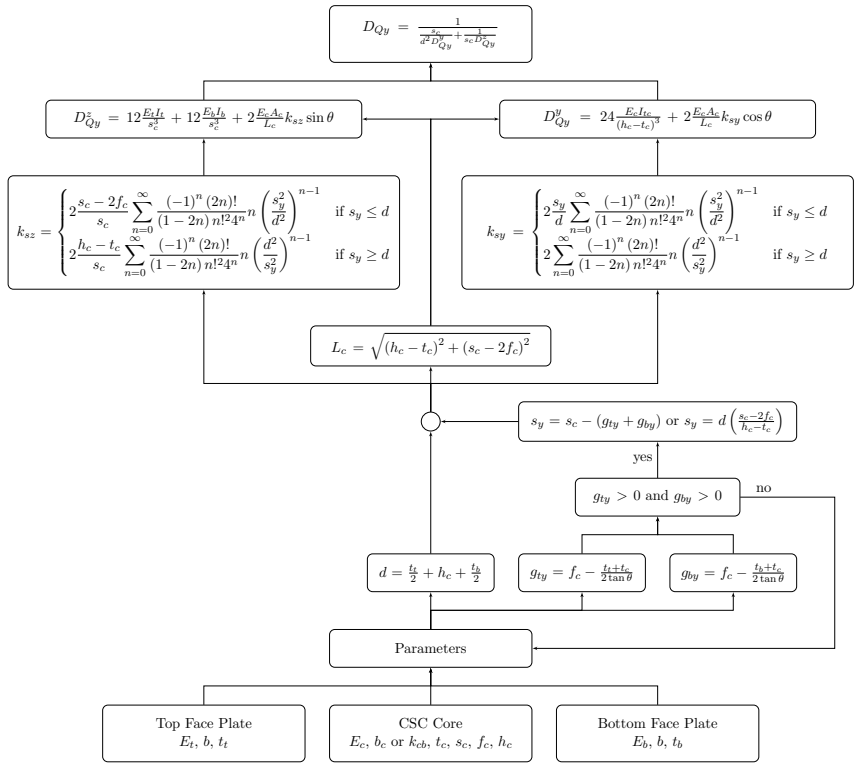

FIGURE 6.8: The calculation procedure of the transverse shear stiffness, D_{Qy}

that the bottom face plate so that $E_t t_t < E_b t_b$ in which the inclined chords are shortened and provide internal axial compressive forces.

Symmetrical Section: If the geometric cross section is symmetric, i.e., $t_t = t_b$, and the material properties of the top and bottom face plates are the same, i.e., $E_t = E_b$, the neutral axis of this cross section will be at the mid height of the cross section, i.e., $z_t = z_b$. Consequently, the inclined chords should be not axially deformed. This means that there are no internal axial forces occuring in these inclined chords. As a result, the flexural stiffness contribution of the core disappears as the terms $(z_b - z_t)$ and $(t_t - t_b)$ of Eq. 6.9 are null.

According to the two possible cases mentioned above, it may mean that the core will contribute to the flexural stiffness only if the sandwich beam has an unsymmetrical cross section.

In the case of symmetrical cross section, the flexural stiffness of sandwich beam with bi-directional CSC is therefore approximately equal to only the contribution of the face plates as found in the previous study of the FE sandwich beam model (see Sec. 4.4.1). Similar behaviour has been noted by Allen [31] in which the equivalent flexural stiffness of an unfilled truss core sandwich beam may be approximately equal to only the summation of the stiffness of the top and bottom face plates.

Having the assumption that the core is not presented, i.e., $E_c A_c = 0$, the flexural stiffness, D_y, will be reduced to the flexural stiffness of the sandwich beam with a weak core assumption [22] as follows:

$$D_y = \frac{1}{12} E_t A_t t_t^2 + E_t A_t z_t^2 + \frac{1}{12} E_b A_b t_b^2 + E_b A_b z_b^2 \tag{6.20}$$

6.5.2 Transverse Shear Stiffness Equation

To evaluate the reliability of the presented BFA, the analytical solutions of the transverse shear stiffness, D_{Qy}, of the unfilled Bi-CSC sandwich beam are verified by comparison with the numerical solutions obtained from the FE solution of three-point loaded beam presented in Chapter 4.

Figure 6.9 presents the comparison of the transverse shear stiffness, D_{Qy}, of the unfilled sandwich beam with Bi-CSC topology obtained from the BFA and the FE-TPB. It can be seen that the BFA does not correlate well with the FE-TPB. The BFA seems to give less stiffness than the FE-TPB method. This phenomenon may arise from assuming that the unit cell deforms like a fixed-end beam rather than a true deformation. Similar phenomenon can also be found in a truss core sandwich beam, especially when s_y/d is greater than one, as demonstrated in Fig. 6.10.

The analysis shows that the BFA correlates well in the development of trends with the FE method but the BFA results in differences in magnitude compared with the FE solution. Therefore, it may be noted here that the presented BFA may be used as a quick solving simplified analytical solution to study the stiffness response of the presented core topology in the feasibility study stage before a more refined computationally expensive analysis is later performed. However, although trends in response will be highlighted with the BFA method, the magnitudes will be incorrect.

6.6 Evaluation of the Stiffness Contribution of the Proposed Core Topology

In this section, the stiffness contribution of the presented Bi-CSC topology to overall stiffness of the unfilled sandwich beam was evaluated using the BFA. The contribution of the sandwich core may be extracted from the overall stiffness of the sandwich beam due to the flexural and transverse shear stiffness equations, as expressed in Eqs. 6.9 and 6.18, consisting of the separate contribution of the face plates and the core.

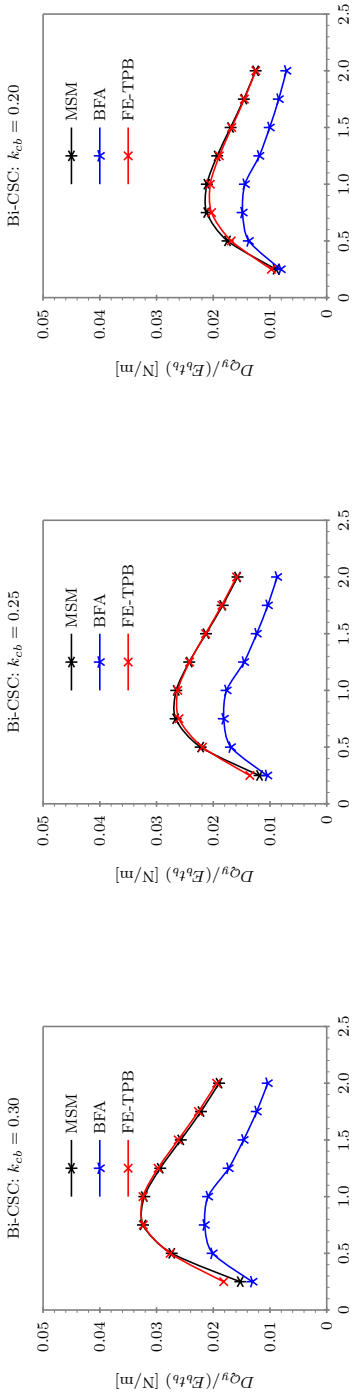

(a) $k_{cb} = 0.30$ (b) $k_{cb} = 0.25$ (c) $k_{cb} = 0.20$

FIGURE 6.9: Comparison of the transverse shear stiffness, D_{Qy}, of unfilled bi-directional corrugated-strip core sandwich beams obtained from the presented braced frame analogy method (BFA), the modified stiffness matrix method (MSM), and the finite element method of three-point loaded beam (FE-TPB)

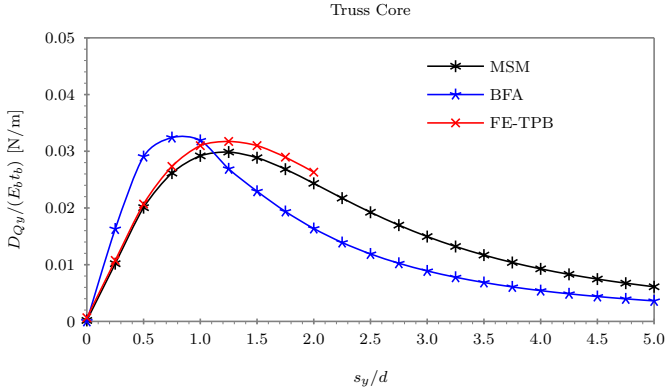

FIGURE 6.10: Comparison of the transverse shear stiffness, D_{Qy}, of unfilled truss core sandwich beams obtained from the presented braced frame analogy method (BFA), the modified stiffness matrix method (MSM), and the finite element method of three-point loaded beam (FE-TPB)

The configuration of the unfilled sandwich beam was set in both symmetrical and unsymmetrical configurations. All geometric parameters were kept constant except the ratios t_t/t_b and s_y/d. Table 6.4 summarise the values of the geometric parameters used in this section.

TABLE 6.4: Configuration of the case studies

Parameter	b	t_t	t_b	k_{cb}	t_c	s_c	f_c	h_c
Value	100, 200	3, 6, 12, 24	12	0.25	2	s_c	20	120
Note		$\frac{t_t}{t_b} = \frac{1}{4}, \frac{1}{2}, 1, 2$				vary in terms of s_y/d where $0 \leq s_y/d \leq 5.0$		

6.6.1 Flexural Stiffness

As earlier mentioned in Sec. 6.5.1, the flexural stiffness contribution of the core occurs only if the sandwich section is not symmetric. Therefore, the configuration of the unfilled sandwich beam studied in this section is limited to unsymmetrical cross sections only.

Although the core may contribute to the overall flexural stiffness if the cross section is unsymmetrical, it was found that the stiffness contribution of the presented Bi-CSC topology to the overall flexural stiffness of the unfilled sandwich beam can be neglected. This is because the contributions of all core configurations studied here are less than 3.20%, as can be seen from Fig. 6.11.

However, it should be noted that the corrugated-strip plate studied in this section is quite thin. In another core configuration with quite a thick plate, the flexural stiffness contribution of the core might be greater. Thus, it should be further studied in detail.

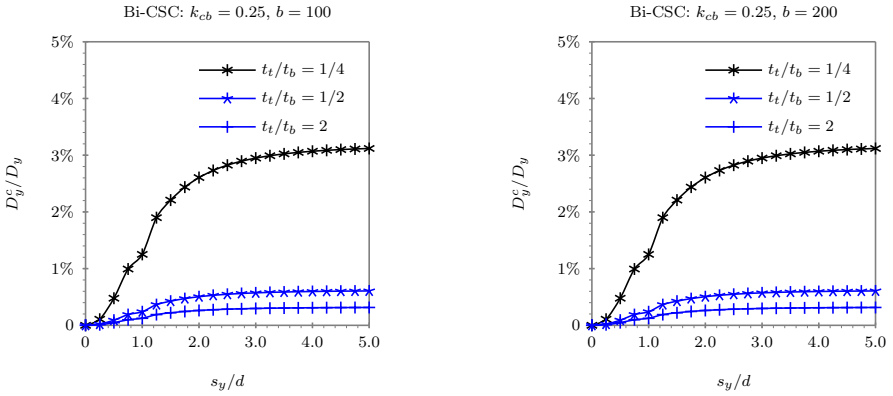

(a) $b = 100$ (b) $b = 200$

FIGURE 6.11: Flexural stiffness contribution of the bi-directional corrugated-strip core to the overall flexural stiffness of unfilled sandwich beams obtained from the presented braced frame analogy method (BFA)

6.6.2 Transverse Shear Stiffness

Unlike the flexural stiffness contribution of the core, the overall transverse shear stiffness, D_{Qy}, is significantly contributed to the core. As can be seen from Fig. 6.12, the transverse shear stiffness contribution of the core rapidly increases at lower values of s_y/d. In the range of $0 \leq s_y/d \leq 0.25$, the stiffness contribution seems to be the same for all cores, i.e., not dependent upon the value of t_t/t_b. At s_y/d equals 0.25, the contribution of the core is about 50% of overall stiffness. Then, the stiffness contribution of the core depends upon the value of t_t/t_b. It gradually increases and reaches a maximum at s_y/d about 1.50. For unsymmetrical cores with $t_t/t_b = 1/4$ and $t_t/t_b = 1/2$, the maximum stiffness contribution of the core is about 90%. The contribution of the core of about 70% is also found with the core having $t_t/t_b = 2$.

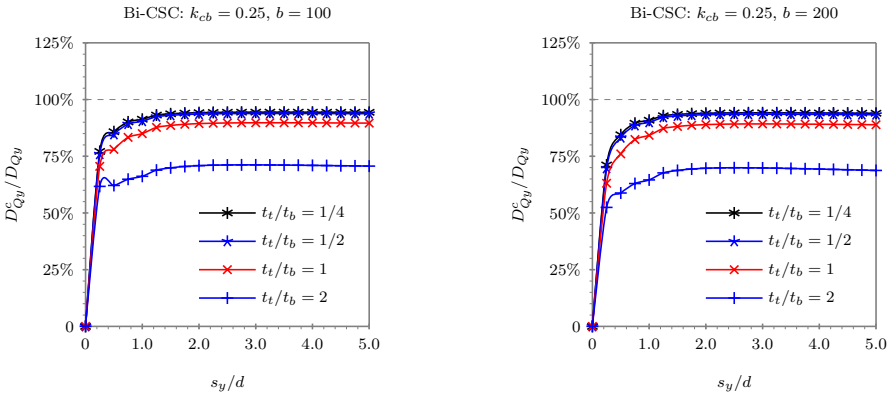

(a) $b = 100$ (b) $b = 200$

FIGURE 6.12: Transverse shear stiffness contribution of the bi-directional corrugated-strip core to the overall flexural stiffness of unfilled sandwich beams obtained from the presented braced frame analogy method (BFA)

Considering the transverse shear stiffness contributed by the core itself, it was found that the stiffness varies with the ratio of s_y/d. As can be seen from Fig. 6.13, the stiffness sharply increases from $s_y/d = 0$ to its peak at s_y/d about 0.75. Then, the stiffness gradually decreases. A similar trend of the stiffness can be found in all core configuration studied here. According to this phenomenon, it may mean that the optimum core configuration of the Bi-CSC is at s_y/d about 0.75 ($\theta \approx 53.0°$).

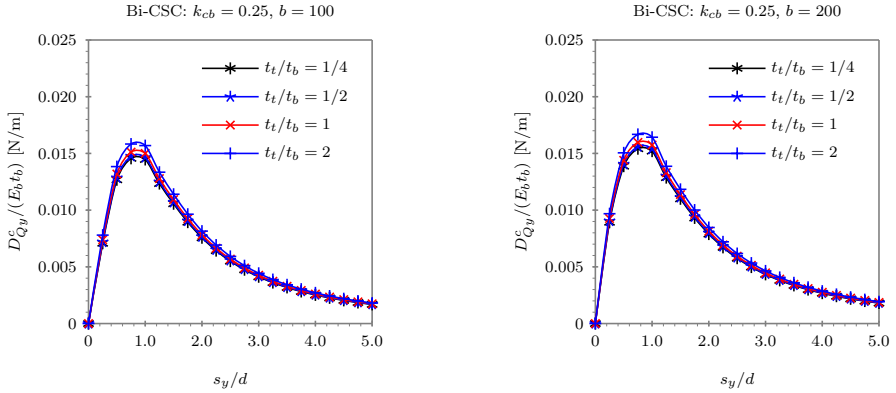

(a) $b = 100$ (b) $b = 200$

FIGURE 6.13: Transverse shear stiffness contribution of the bi-directional corrugated-strip core obtained from the presented braced frame analogy method (BFA)

6.7 Concluding Remark

The simplified analytical method named the braced frame analogy method (BFA) was presented. The method was also based on the force and distortion relationship of repetitive part of an unfilled sandwich beam. The BFA was also proposed as a simplified analytical method to overcome the high degree of indeterminacy of the presented bi-directional corrugated-strip core (Bi-CSC) topology. The 3D configuration of the unfilled sandwich beam with the presented core topology was also simplified as a 2D braced frame structure. The model was further adapted from the two-dimensional (2D) plane-frame model (PFM) presented in Chapter 5 in which only the inclined chords were adapted and modelled as truss elements.

The formulation of the flexural stiffness, D_y, was presented. It was performed using the flexural load mechanism of a repetitive part of a sandwich beam, i.e., the equilibrium of force and the displacement compatibility, in which the elongation of the inclined chord was in terms of an elongation factor k_b.

The formulation of the transverse shear stiffness, D_{Qy}, was also presented. It was also performed in a similar manner as the flexural stiffness in which the transverse shear

load mechanism of a repetitive part of the sandwich beam was used. The displacement compatibility of a repetitive part subjected to the transverse shear load was assumed to deform into two separate modes: (1) the deformation in the z-direction due to the transverse shear force, Q_y, and (2) the deformation in the y-direction due to a couple of horizontal force, H. The elongation of the inclined chord was also in terms of the elongation factors k_{sz} and k_{sy}.

The flexural and transverse shear stiffness equations obtained from the presented BFA were verified. It was found that the flexural stiffness reduces to the flexural stiffness equation of a sandwich beam assumed to have a very weak core. It was found that the transverse shear stiffness magnitude was not a good correlation with the FE solution obtained from an unfilled sandwich beam model.

The presented BFA was then used to evaluate the stiffness contribution of the proposed core topology. It was found that the flexural stiffness contribution of the core can be neglected. However, the overall transverse shear stiffness was significantly contributed by the core and can not be ignored. The maximum transverse shear stiffness contributed by the core can be about 90% of the overall stiffness. The contribution of the core varies with the cross section geometry. In addition, it was found that the optimum configuration of the core itself may be at s_y/d about 0.75 ($\theta \approx 53.0°$).

The next chapter presents the last simplified analytical method referred to as the discrete beam method (DBM). The DBM is the third simplified analytical method to obtain the transverse shear stiffness of the unfilled sandwich beam with the Bi-CSC topology presented in this research. The DBM is also proposed to overcome a high degree of indeterminacy of the proposed Bi-CSC topology, and to separate the stiffness contribution of the core from the overall stiffness of the unfilled sandwich beam. Rather than using the force-distortion relationship concept, as the basis concept of the MSM and the BFA, the transformation of stress and strain from the local coordinate system to the global coordinate system is introduced for the DBM.

Chapter 7

Modelling the Transverse Shear Stiffness of an Unfilled Sandwich Beam using a Discrete Beam Method

7.1 Background

In addition to deducing the transverse shear stiffness, D_Q, from the simplified analytical methods based on the force-distortion relationship technique as previously presented in Chapters 5 and 6, another simplified method based on the estimation of sandwich cross section properties into either a single- or multi-layer equivalent property may be used [136, 137]. This approach may be achieved by transforming the stress and strain of each part of the sandwich cross section from its own local coordinate system into the unique global coordinate system. In practice, the average transformed stiffness is then carried out and used as an equivalent stiffness property of the sandwich cross section.

A number of literature sources based on this approach have been found. In 2004, for example, Aboura et al. [136] presented the analytical solutions for a sinusoidal-corrugated cardboard sandwich panel. The elastic moduli of corrugation in the local system were first transformed to the global system and the average in-plane stiffness was then approximated over the depth of the sandwich section and the unit cell. Talbi et al. [137] also presented a similar work to obtain the equivalent stiffness of an unfilled corrugated core sandwich beam using a transformation stress and strain technique in which some methodologies to obtain equivalent stiffness properties were improved.

In the author's opinion, the estimation of stiffness properties using a transformation of stress and strain technique may be a much more simplified technique than the force-distortion technique because there is no need to perform complex constitutive and compatibility equations. It is arguable that therefore this technique may be presented as an alternative simplified analytical approach to understand the stiffness response of a sandwich cross section in preliminary stage. Since the flexural stiffness contribution of the presented core topology and other similar core topologies previously studied in Chapters 4, 5, and 6 can be neglected, only the transverse shear stiffness, D_Q, of sandwich cross section is derived in this chapter using the transformation of stress and strain technique and then compared with other previously presented methods.

7.2 Discrete Beam Method

7.2.1 Assumptions

In this chapter, all assumptions but the shear deformation shape assumed in the BFA are also applied to the discrete beam method (DBM). The shear deformation shape, however, is assumed to deform in a different shape as later detailed in Sec. 7.3.1.

7.2.2 Transformational Constitutive Law

In this chapter, a repetitive part of an unfilled sandwich beam is defined as shown in Fig. 7.1. Here, the local and global coordinate systems are defined as the 123-axis and xyz-axis systems, respectively.

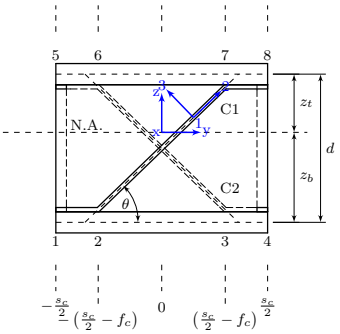

FIGURE 7.1: The repetitive part of an unfilled sandwich beam used in the discrete beam method

Since the engineering properties of the corrugated-strip core (CSC) are defined in its inclined plane, which is aligned in angle to the y-axis of the global coordinate system, the stress and strain of the core need to be transformed from its local coordinate system

to the global coordinate system of the sandwich beam. In general 2D stress at a point, the transformed tensor stress and strain equations are [138]

$$\begin{Bmatrix} \sigma_2 \\ \sigma_3 \\ \tau_{23} \end{Bmatrix} = \begin{bmatrix} m_2^2 & n_2^2 & 2m_2n_2 \\ m_3^2 & n_3^2 & 2m_3n_3 \\ m_2m_3 & n_2n_3 & m_2n_3 + m_3n_2 \end{bmatrix} \begin{Bmatrix} \sigma_y \\ \sigma_z \\ \tau_{yz} \end{Bmatrix} \tag{7.1a}$$

$$\begin{Bmatrix} \epsilon_2 \\ \epsilon_3 \\ \frac{1}{2}\gamma_{23} \end{Bmatrix} = \begin{bmatrix} m_2^2 & n_2^2 & 2m_2n_2 \\ m_3^2 & n_3^2 & 2m_3n_3 \\ m_2m_3 & n_2n_3 & m_2n_3 + m_3n_2 \end{bmatrix} \begin{Bmatrix} \epsilon_y \\ \epsilon_z \\ \frac{1}{2}\gamma_{yz} \end{Bmatrix} \tag{7.1b}$$

and the governing equation of engineering stress and strain relationship in the local coordinate system is [138]

$$\begin{Bmatrix} \sigma_2 \\ \sigma_3 \\ \tau_{23} \end{Bmatrix} = \begin{bmatrix} Q_{22} & Q_{23} & 0 \\ Q_{23} & Q_{33} & 0 \\ 0 & 0 & 2Q_{55} \end{bmatrix} \begin{Bmatrix} \epsilon_2 \\ \epsilon_3 \\ \frac{1}{2}\gamma_{23} \end{Bmatrix} \tag{7.2}$$

Utilising Eqs. 7.1 and 7.2, the governing equation of engineering stress and strain relationship in the global coordinate system is

$$\begin{Bmatrix} \sigma_y \\ \sigma_z \\ \tau_{yz} \end{Bmatrix} = \begin{bmatrix} \bar{Q}_{22} & \bar{Q}_{23} & \bar{Q}_{25} \\ \bar{Q}_{23} & \bar{Q}_{33} & \bar{Q}_{35} \\ \bar{Q}_{25} & \bar{Q}_{35} & \bar{Q}_{55} \end{bmatrix} \begin{Bmatrix} \epsilon_y \\ \epsilon_z \\ \gamma_{yz} \end{Bmatrix} \tag{7.3a}$$

or

$$\{\sigma_i\} = \left[\bar{Q}_{ij}\right] \{\epsilon_j\} \tag{7.3b}$$

where $i = 1, 2, 3$ and $j = 1, 2, 3$.

The $\bar{Q}_{ij}$ quantities are the transformed stiffness quantities obtained directly from [138] as follows:

$$\begin{Bmatrix} \bar{Q}_{22} \\ \bar{Q}_{23} \\ \bar{Q}_{25} \\ \bar{Q}_{33} \\ \bar{Q}_{35} \\ \bar{Q}_{55} \end{Bmatrix} = \begin{bmatrix} c^4 & 2c^2s^2 & s^4 & 4c^2s^2 \\ c^2s^2 & c^4 + s^4 & c^2s^2 & -4c^2s^2 \\ c^3s & -cs\left(c^2 - s^2\right) & -cs^3 & -2cs\left(c^2 - s^2\right) \\ s^4 & 2c^2s^2 & c^4 & 4c^2s^2 \\ cs^3 & cs\left(c^2 - s^2\right) & -c^3s & 2cs\left(c^2 - s^2\right) \\ c^2s^2 & -2c^2s^2 & c^2s^2 & \left(c^2 - s^2\right)^2 \end{bmatrix} \begin{Bmatrix} Q_{22} \\ Q_{23} \\ Q_{33} \\ Q_{55} \end{Bmatrix} \tag{7.4}$$

where c and s are the direction cosine and the direction sine of the angle between the 2- and y-axis respectively.

The Q_{ij} quantities are the stiffness quantities obtained from the local coordinate system, modified to incorporate isotropic materials without Poisson's effect in any direction of the local coordinate system, defined as follows:

$$\begin{bmatrix} Q_{22} & Q_{23} & 0 \\ Q_{23} & Q_{33} & 0 \\ 0 & 0 & Q_{55} \end{bmatrix} = \begin{bmatrix} E & 0 & 0 \\ 0 & E & 0 \\ 0 & 0 & G \end{bmatrix} \tag{7.5}$$

Constitutive Law of a Sandwich Face Plate: Since the local coordinates of the top and bottom face plates are identical with the global coordinate, there is no need to transform the stiffness quantities. Therefore, the simplified Eq. 7.6 can be applied directly to the transformed stiffness quantities, $\bar{Q}_{ij}$, of the top face plate and the same equation with subscript b indicates for the bottom face plate.

$$\begin{Bmatrix} \bar{Q}_{22} \\ \bar{Q}_{23} \\ \bar{Q}_{25} \\ \bar{Q}_{33} \\ \bar{Q}_{35} \\ \bar{Q}_{55} \end{Bmatrix}_t = \begin{Bmatrix} Q_{22} \\ Q_{23} \\ 0 \\ Q_{33} \\ 0 \\ Q_{55} \end{Bmatrix}_t \tag{7.6}$$

Constitutive Law of a Corrugated-Strip Core: Since the pattern of the corrugation of the CSC is divided into three repetitive parts along the y-direction, the constitutive law of the core needs to be divided into three parts. As can be seen in Fig. 7.1, the first two parts are related to the flat parts of the CSC located in the ranges of $-\frac{s_c}{2} \leq y \leq -\left(\frac{s_c}{2} - f_c\right)$ and of $\left(\frac{s_c}{2} - f_c\right) \leq y \leq \frac{s_c}{2}$. Since the local coordinates of these parts are identical with the global coordinate, there is no need to transform the stiffness quantities. Therefore, the same equation as Eq. 7.6 with new subscripts $c1$ and $c2$ can be also applied to these parts. On the other hand, the local corrugation plane in the range of $-\left(\frac{s_c}{2} - f_c\right) \leq y \leq \left(\frac{s_c}{2} - f_c\right)$ is aligned at an angle to the y-axis. Therefore, it is necessary to transform the local stress and strain to the global coordinate system. The transformed stiffness quantities, $\bar{Q}_{ij}$, of the inclined part C1 can be expressed as Eq. 7.7

and the same equation with subscript $c2$ indicates for the inclined part C2.

$$\begin{Bmatrix} \bar{Q}_{22} \\ \bar{Q}_{23} \\ \bar{Q}_{25} \\ \bar{Q}_{33} \\ \bar{Q}_{35} \\ \bar{Q}_{55} \end{Bmatrix}_{c1} = \begin{bmatrix} c^4 & 2c^2s^2 & s^4 & 4c^2s^2 \\ c^2s^2 & c^4+s^4 & c^2s^2 & -4c^2s^2 \\ c^3s & -cs\left(c^2-s^2\right) & -cs^3 & -2cs\left(c^2-s^2\right) \\ s^4 & 2c^2s^2 & c^4 & 4c^2s^2 \\ cs^3 & cs\left(c^2-s^2\right) & -c^3s & 2cs\left(c^2-s^2\right) \\ c^2s^2 & -2c^2s^2 & c^2s^2 & \left(c^2-s^2\right)^2 \end{bmatrix} \begin{Bmatrix} Q_{22} \\ Q_{23} \\ Q_{33} \\ Q_{55} \end{Bmatrix}_c \tag{7.7}$$

7.3 Transverse Shear Load Transfer Mechanism

7.3.1 Shear Deformation Shape of a Unit Cell

Similar to the BFA, the unit cell is subjected to a transverse shear force, Q_y, in the DBM and is also assumed to deform into two separate modes: (1) the deformation in the z-direction due to the transverse shear force, Q_y, itself, and (2) the deformation in the y-direction due to a couple of horizontal force, H, as illustrated in Fig. 7.2(a) and 7.2(b), respectively. Instead of assuming the shear panel deforms as a fixed-end beam, the simple shear deformation shape of the shear panel as shown in Fig. 7.2 is assumed for the DBM.

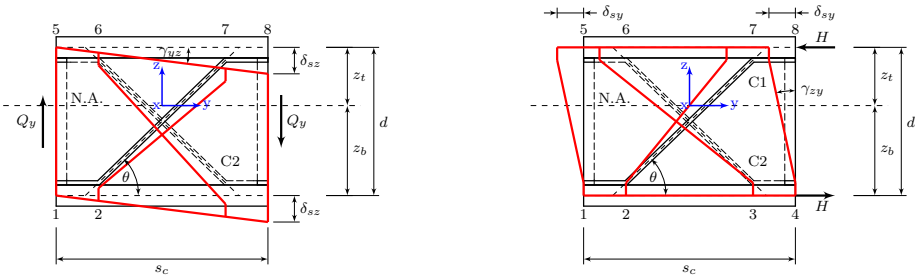

FIGURE 7.2: Shear deformation shapes of the unit cell subjected to (a) transverse shear force, Q_y, and (b) a couple of horizontal force, H

7.3.2 Average Shear Stiffness of a Unit Cell

Considering the first deformed configuration as illustrated in Fig. 7.2(a) and assuming that shear strain is constant through the depth of the sandwich cross section, the internal transverse shear force, Q_y, of the sandwich cross section at any cross section along the

y-axis may be calculated as follows [137]:

$$\begin{aligned} Q_y &= \int_{-z_b-\frac{t_b}{2}}^{z_t+\frac{t_t}{2}} \tau_{yz} b dz \\ &= \int_{-z_b-\frac{t_b}{2}}^{z_t+\frac{t_t}{2}} \left[\bar{Q}_{3j}\right] \{\epsilon_j\} b dz \end{aligned} \tag{7.8}$$

In the case of the sandwich beam subjected to only the transverse shear force, Q_y, Eq. 7.8 may be simplified as follows:

$$Q_y = \int_{-z_b-\frac{t_b}{2}}^{z_t+\frac{t_t}{2}} \bar{Q}_{55}\gamma_{yz} b dz \tag{7.9}$$

Thus, the shear stiffness of the sandwich cross section in the z-direction, D^z_{Qy}, at any distance along the y-direction is as follows:

$$\begin{aligned} D^z_{Qy} &= \int_{-z_b-\frac{t_b}{2}}^{z_t+\frac{t_t}{2}} \bar{Q}_{55} b dz \\ &= \left(D^z_{Qy,t} + D^z_{Qy,b}\right) + \left(D^z_{Qy,c1} + D^z_{Qy,c2}\right) \end{aligned} \tag{7.10}$$

where $D^z_{Qy,t}$ and $D^z_{Qy,b}$ are the shear stiffness of the top and bottom face plates respectively and $D^z_{Qy,c1}$ and $D^z_{Qy,c2}$ are the shear stiffness of CSCs C1 and C2 respectively.

Since the top and bottom face plates are aligned in the xy-plane of the global coordinate system, the shear stiffness of these face plates can be expressed as follows:

$$D^z_{Qy,t} = bG_t t_t \tag{7.11a}$$

$$D^z_{Qy,b} = bG_b t_b \tag{7.11b}$$

Since an inclined part of the CSC is aligned at an angle to the y-axis of the global coordinate system, the shear stiffness of CSCs C1 and C2 at any distance along the y-direction is function of y and can be expressed as follows:

$$D^z_{Qy,c1} = k_{cb} b \bar{Q}_{55,c1} t_{cz} \tag{7.12a}$$

$$D^z_{Qy,c2} = k_{cb} b \bar{Q}_{55,c2} t_{cz} \tag{7.12b}$$

where t_{cz} is the cross section of the CSC defined in terms of y as follows:

$$t_{cz} = \begin{cases} t_c & \text{if } -\frac{s_c}{2} \le y \le -\left(\frac{s_c}{2} - f_c\right) \\ \frac{t_c}{\cos\theta} & \text{if } -\left(\frac{s_c}{2} - f_c\right) \le y \le \left(\frac{s_c}{2} - f_c\right) \\ t_c & \text{if } \left(\frac{s_c}{2} - f_c\right) \le y \le \frac{s_c}{2} \end{cases} \tag{7.13}$$

Since the transformed stiffness quantities $\bar{Q}_{55,c1}$ and $\bar{Q}_{55,c2}$ in this case are identical, thus

$$\begin{aligned} D^z_{Qy,c} &= D^z_{Qy,c1} + D^z_{Qy,c2} \\ &= 2k_{cb} b \bar{Q}_{55,c} t_{cz} \end{aligned} \tag{7.14}$$

where $\bar{Q}_{55,c}$ is the stiffness quantity modified to incorporate isotropic materials without Poisson's effect in any direction of the local coordinate system, defined in terms of y as follows:

$$\bar{Q}_{55,c} = \begin{cases} G_c & \text{if } -\frac{s_c}{2} \le y \le -\left(\frac{s_c}{2} - f_c\right) \\ \left[c^4 + 2\left(1 + 2\nu_c\right) c^2 s^2 + s^4\right] G_c & \text{if } -\left(\frac{s_c}{2} - f_c\right) \le y \le \left(\frac{s_c}{2} - f_c\right) \\ G_c & \text{if } \left(\frac{s_c}{2} - f_c\right) \le y \le \frac{s_c}{2} \end{cases} \tag{7.15}$$

Since the shear stiffness $D^z_{Qy,c}$ of the CSC varies along the y-direction, the shear stiffness of the unit cell needs to average [137] as defined as follows:

$$\begin{aligned} \bar{D}^z_{Qy} &= \frac{1}{s_c} \int_{-\frac{s_c}{2}}^{\frac{s_c}{2}} D^z_{Qy} dy \\ &= D^z_{Qy,t} + D^z_{Qy,b} + \bar{D}^z_{Qy,c} \end{aligned} \tag{7.16}$$

In this case, only the stiffness of the corrugated-strip core needs to average as $\bar{D}^z_{Qy,c}$ expressed as follows:

$$\begin{aligned} \bar{D}^z_{Qy,c} &= \frac{1}{s_c} \int_{-\frac{s_c}{2}}^{\frac{s_c}{2}} D^z_{Qy,c} dy \\ &= \frac{1}{s_c} \int_{-\frac{s_c}{2}}^{\frac{s_c}{2}} 2k_{cb} b \bar{Q}_{55,c} t_{cz} dy \\ &= 2\frac{k_{cb} b}{s_c} G_c \left(k^z_{ch} + k^z_{ci}\right) \end{aligned} \tag{7.17}$$

where k^z_{ch} and k^z_{ci} are the contribution factors of the horizontal flat parts and the inclined parts of the CSC, respectively, expressed as follows:

$$k^z_{ch} = 2t_c f_c \tag{7.18a}$$

$$k^z_{ci} = \left[c^4 + 2\left(1 + 2\nu_c\right) c^2 s^2 + s^4\right] \frac{t_c}{\cos\theta} \left(s_c - 2f_c\right) \tag{7.18b}$$

In the case of neglecting the small horizontal flat parts of the CSC and assuming the inclined parts as a truss element, thus

$$k^z_{ch} = 0 \tag{7.19a}$$

$$k^z_{ci} = 2\left(1 + \nu_c\right) c^2 s^2 \frac{t_c}{\cos\theta} \left(s_c - 2f_c\right) \tag{7.19b}$$

It should be noted that there is no contribution of the transverse CSCs in this case.

Similarly, the relationship between a couple horizontal force, H, and the shear deformation in the y-direction of the second deformed configuration as illustrated in Fig. 7.2(b) may be derived as follows:

$$\begin{aligned} H &= \int_{-\frac{s_c}{2}}^{\frac{s_c}{2}} \tau_{zy} b dy \\ &= \int_{-\frac{s_c}{2}}^{\frac{s_c}{2}} \left[\bar{Q}_{3j}\right] \{\epsilon_j\} b dy \\ &= \int_{-\frac{s_c}{2}}^{\frac{s_c}{2}} \bar{Q}_{55} \gamma_{zy} b dy \end{aligned} \tag{7.20}$$

Thus, the shear stiffness of the sandwich cross section in the y-direction, D^y_{Qy}, at any distance along the z-direction is as follows:

$$\begin{aligned} D^y_{Qy} &= \int_{-\frac{s_c}{2}}^{\frac{s_c}{2}} \bar{Q}_{55} b dy \\ &= \left(D^y_{Qy,c1} + D^y_{Qy,c2}\right) + D^y_{Qy,tc} \end{aligned} \tag{7.21}$$

where $D^y_{Qy,c1}$ and $D^y_{Qy,c2}$ are the shear stiffness of the longitudinal CSCs C1 and C2 respectively and $D^y_{Qy,tc}$ is the shear stiffness of the transverse CSCs. In this case, there is no contribution by the top and bottom face plates as well as of the small horizontal flat parts of the CSC.

Since the inclined part of the CSC is aligned in angle to the y-axis of the global coordinate system, the shear stiffness of CSCs C1 and C2 at any distance along the z-direction can be expressed as follows:

$$D^y_{Qy,c1} = k_{cb} b \bar{Q}_{55,c1} t_{cy} \tag{7.22a}$$

$$D^y_{Qy,c2} = k_{cb} b \bar{Q}_{55,c2} t_{cy} \tag{7.22b}$$

where t_{cy} is the cross section of the CSC defined as follows:

$$t_{cy} = \frac{t_c}{\sin\theta} \tag{7.23}$$

Due to the transformed stiffness quantities $\bar{Q}_{55,c1}$ and $\bar{Q}_{55,c2}$ are identical, thus

$$\begin{aligned} D^y_{Qy,c} &= D^y_{Qy,c1} + D^y_{Qy,c2} \\ &= 2 k_{cb} b \bar{Q}_{55,c} t_{cy} \\ &= 2 k_{cb} b \bar{Q}_{55,c} \frac{t_c}{\sin\theta} \end{aligned} \tag{7.24}$$

where $\bar{Q}_{55,c}$ is the stiffness quantity modified to incorporate isotropic materials without Poisson's effect in any direction of local coordinate system, defined as follows

$$\bar{Q}_{55,c} = \left[c^4 + 2\left(1+2\nu_c\right)c^2s^2 + s^4\right]G_c \tag{7.25}$$

In case of assuming the inclined parts of longitudinal CSC as truss element, the stiffness quantity $\bar{Q}_{55,c}$ of Eq. 7.25 is further simplified so that

$$\bar{Q}_{55,c} = 2\left(1+\nu_c\right)c^2s^2G_c \tag{7.26}$$

Here, $D^y_{Qy,tc}$ is defined as follows

$$\begin{aligned} D^y_{Qy,tc} &= \int_{-\frac{s_c}{2}}^{\frac{s_c}{2}} \bar{Q}_{55,tc}\frac{t_c}{\sin\theta_{tc}}dy \\ &= 2\times 2\times \bar{Q}_{55,tc}\frac{t_c}{\sin\theta_{tc}}\frac{k_{cb}b}{2} \\ &= 2k_{cb}b\bar{Q}_{55,tc}\frac{t_c}{\sin\theta_{tc}} \end{aligned} \tag{7.27}$$

where $\bar{Q}_{55,tc}$ is the stiffness quantity of transverse CSC modified to incorporate isotropic materials without Poisson's effect in any direction of local coordinate system, defined as follows

$$\bar{Q}_{55,tc} = G_c \tag{7.28}$$

In this case, there is no need to average the shear stiffness of the CSCs due to it does not vary along the z-direction. Thus,

$$D^y_{Qy} = D^y_{Qy,c} + D^y_{Qy,tc} \tag{7.29}$$

7.3.3 Formulation of a Transverse Shear Stiffness

Having the deformed shape of the unit cell subjected to transverse shear force, Q_y, as illustrated in Fig. 7.2, the transverse shear stiffness, D_{Qy}, of the unit cell may be expressed as follows:

$$\begin{aligned} D_{Qy} &= \frac{Q_y}{\gamma_{zy}+\gamma_{yz}} \\ &= \frac{Q_y}{\frac{H}{D^y_{Qy}}+\frac{Q_y}{D^z_{Qy}}} \\ &= \frac{1}{\frac{s_c}{dD^y_{Qy}}+\frac{1}{D^z_{Qy}}} \end{aligned} \tag{7.30}$$

where $\bar{D}^z_{Qy}$ and D^y_{Qy} are previouly defined as Eqs. 7.16 and 7.29, respectively.

7.3.4 Shear Correction Factor

The shear stiffness $\bar{D}_{Qy}$ needs to be multiplied by the shear correction factor, k_G, to overcome the error caused by assuming a constant shear strain through the depth of the beam cross section [139]. For a solid rectangular cross section, the well-known shear correction factor $k_G = (5+5\nu)/(6+5\nu)$ [140] or 5/6 when the Poisson's ratio approaches zero has been introduced. Throughout this chapter, the Poissons ratio is assumed to be zero and therefore a shear correction factor of 5/6 is applied unless otherwise stated.

7.3.5 Summary of Calculation Procedure

Figure 7.3 illustrates the procedure to calculate the transverse shear stiffness, D_{Qy}, using the discrete beam method.

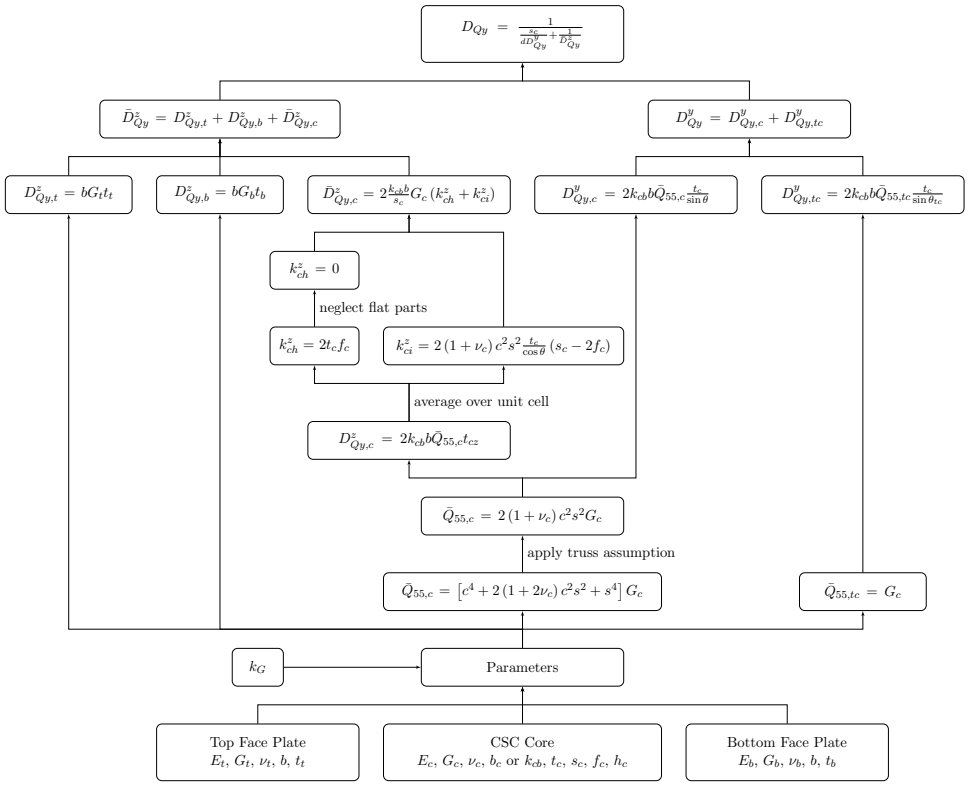

FIGURE 7.3: The calculation procedure of the transverse shear stiffness, D_{Qy}

7.4 Verification of the Transverse Shear Stiffness Equation

To evaluate the reliability of the presented DBM, the analytical solutions of the transverse shear stiffness, D_{Qy}, of the unfilled Bi-CSC topology are verified by comparison with the numerical solutions obtained from the FE-TPB presented in Chapter 4.

The transverse shear stiffness, D_{Qy}, obtained from the DBM and the FE-TPB methods are presented in Fig. 7.4. It can be seen that the DBM seems to provide a different trend with the FE-TPB. Good correlation in trend can be found only if s_y/d is greater than 1.00. When s_y/d is less than 1.00, the DBM solutions diverge from the FE-TPB solutions. This phenomenon indicates that the DBM is unsuitable for obtaining the transverse shear stiffness of an unfilled sandwich beam with Bi-CSC topology.

However, further investigation has been carried out to understand a possible cause of this problem. According to the assumption that the unit cell panel subjected to a transverse shear force, Q_y, deforms either as a fixed-end beam in the BFA or as a simple shear block in the DBM, it is therefore assumed that this assumption may cause the divergence of the transverse shear stiffness, D_{Qy}. The different deformation shape of the face plates between both methods are assured to be the major cause rather than the deformation of the core, as seen later in comparison of assumptions in Table 7.1. Extracting the contribution of the face plates from the transverse shear stiffness equations (Eq. 6.18 for the BFA and Eq. 7.30 for the DBM), it can be seen from Fig. 7.5 that both the BFA and the DBM yield a consistent trend of the transverse shear stiffness, D_{Qy}, with each other.

Consequently, the comparison of the transverse shear stiffness obtained from the DBM without the stiffness contribution of the face plates and from the FE-TPB was carried out. It was found that the DBM yields good correlation solution trend with the FE-TPB as presented in Fig. 7.6. However, there are still some differences in magnitude. This phenomenon is similar to the behaviour of the BFA; therefore, the possibility of using the DBM to obtain the transverse shear stiffness, D_{Qy}, of the unfilled sandwich beam with Bi-CSC topology should be limited due to the assumptions assumed in this chapter unless a further refined solution is obtained.

7.5 Comparison with the Braced Frame Analogy Method

In this section, the methodologies used in the BFA and the DBM are compared to each other in analytical concept, approach, assumptions, and techniques, as presented in tabular form as Table 7.1.

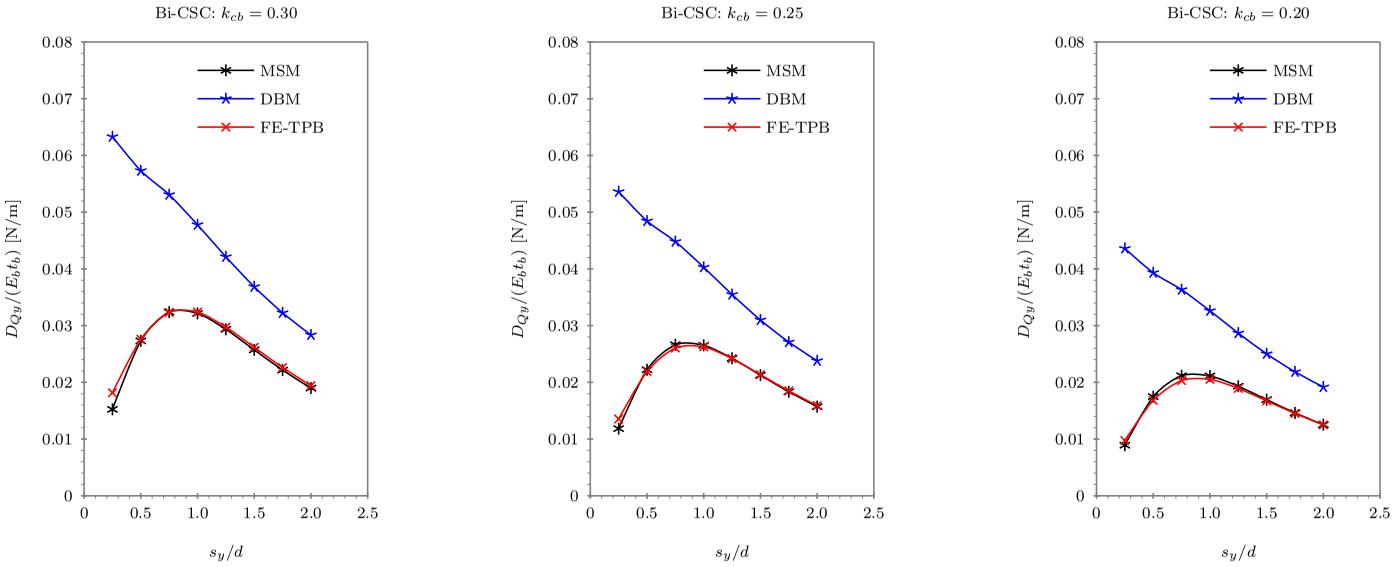

(a) $k_{cb} = 0.30$ (b) $k_{cb} = 0.25$ (c) $k_{cb} = 0.20$

FIGURE 7.4: Comparisons of the transverse shear stiffness, D_{Qy}, of unfilled bi-directional corrugated-strip core sandwich beams obtained from the presented discrete beam method (DBM), the modified stiffness matrix method (MSM), and the finite element method of three-point loaded beam (FE-TPB)

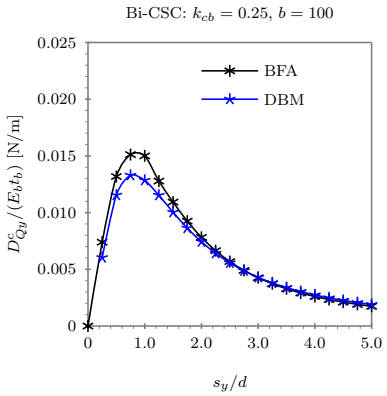

FIGURE 7.5: Comparison of the transverse shear stiffness contribution of the bi-directional corrugated-strip core obtained from the presented discrete beam method (DBM) and the braced frame analogy method (BFA) (configuration of sandwich beam: $b = 100$, $k_{cb} = 0.25$)

In general, both the BFA and the DBM are simplified analytical approaches possibly used to overcome the complexity of the topology in closed form analytical solutions, if they existed. For unfilled sandwich beam, a simplified approach usually relies on the estimation of sandwich properties into either a single- or multi-layer equivalent properties; this is the fundamental assumption of both the BFA and the DBM.

Although both methods are similar in fundamental concept since the complex shape of the structural core sandwich beam is modelled as an equivalent property, they are different in some methodologies.

By comparison in analytical concept and approach, the BFA is based on the displacement compatibility concept and the force-distortion relationship approach. This technique assumes that the stiffness of a sandwich structure could be found if the deformation shape of such a structure could be possibly known in advance. Consequently, the relationship between an effort force and a corresponding displacement, i.e., the stiffness, would be known. The DBM, on the other hand, is based on the transformation of the stress and strain of each element of the sandwich structure from the local to the global coordinate system. Then, an equivalent stiffness property may be achieved by averaging the elastic property over a unit cell.

By comparison in analytical assumptions, both the BFA and the DBM mostly have the same assumptions except the shear deformation shape of unit cell panel. While the unit cell panel is assumed to deform like a fixed-end beam in the BFA, the unit cell panel is assumed to deform as simple shear block in the DBM. This is the major difference in assumptions between the BFA and the DBM which may lead to the difference in analytical solutions and may need to be further investigated.

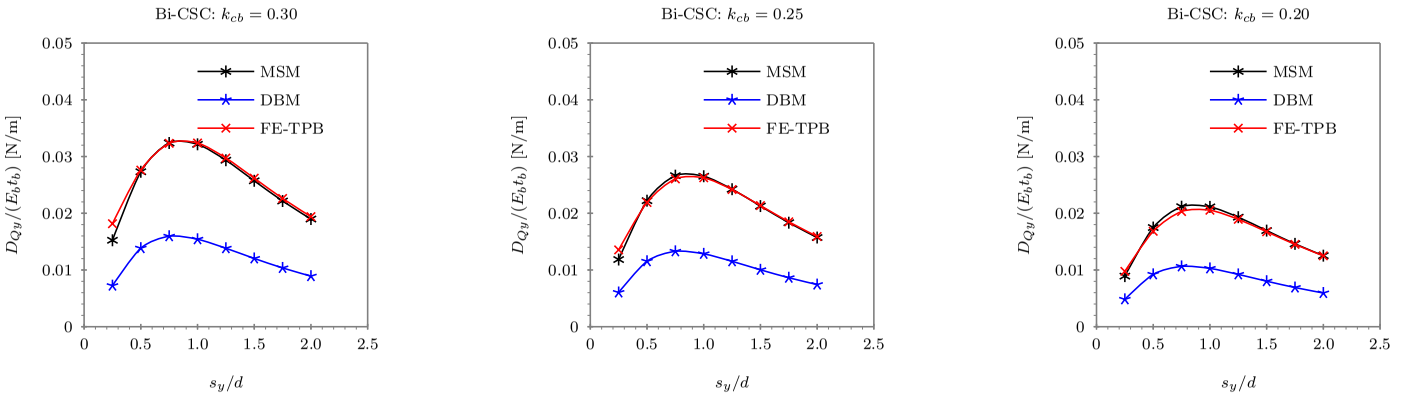

(a) $k_{cb} = 0.30$ (b) $k_{cb} = 0.25$ (c) $k_{cb} = 0.20$

FIGURE 7.6: Comparisons of the transverse shear stiffness, D_{Qy}, of unfilled bi-directional corrugated-strip core sandwich beams obtained from the presented discrete beam method (DBM) (extracting the contribution of the face plates), the modified stiffness matrix method (MSM), and the finite element method of three-point loaded beam (FE-TPB)

TABLE 7.1: Comparison in methodology and result between the braced frame analogy method (BFA) and the discrete beam method (DBM)

Description	Method	
	Braced Frame Analogy Method	Discrete Beam Method
Analytical Concept	Displacement compatibility concept	Average equivalent elastic property concept
Analytical Approach	Force-distortion relationship approach	Transformation of stress and strain approach
Assumptions	The stress-strain relationship of the steel material is limited to linear elastic. The compression behaviour is the same as the tension behaviour.	
	The deformation of the sandwich beam and its unit cell is assumed small.	
	The corrugated-strip core is assumed to be sufficiently stiff in the z-direction so that the depth of sandwich core after deformation remains the same as before deformation.	
	The corrugated-strip core is assumed to be equally displaced in the y-direction for each unit cell so that the displacement in the y-direction may be represented by the point at mid-width of sandwich beam.	
	The shear panel is deformed into two separate shear deformation directions: (1) shear deformation in the z-direction, and (2) shear deformation in the y-direction.	
	A unit cell panel is assumed to deform as a fixed-end beam. 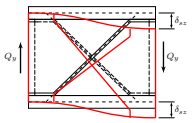	A unit cell panel is assumed to deform as a simple shear block. 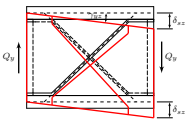
Analytical Techniques	Model unfilled sandwich beam as a 2D braced frame model with rigid-link elements if applicable	
	Perform inclined part of corrugated-strip core as a truss element with hinge ends	Apply only mechanical elastic properties of material in the 1-direction of the local coordinate system to the inclined part of the corrugated-strip core to perform truss element
	Perform equilibrium of forces and displacement compatibility equations of a repetitive unit cell with approximate elongation length of inclined elements	Transform stress and strain of each part of the unit cell from the local to global coordinate system and then perform the constitutive equation of unit cell
	Perform the transverse shear stiffness, D_Q, using the unit cell approach	Average stiffness in each direction over unit cell and then perform the transverse shear stiffness, D_Q, using the unit cell approach
Analytical Results	Yield good correlation in trend with the finite element solution (the FE-TPB) but difference in magnitude (see Fig. 6.9)	Yield poor correlation in trend with the finite element solution (the FE-TPB), the divergent trend can be found if $s_y/d < 1.00$ (see Fig. 7.4)
	Yield good correlation with each other if extracting the stiffness contribution of face plates from the transverse shear stiffness equation (see Fig. 7.5)	
	N/A	Yield good correlation in trend with the finite element solution (the FE-TPB) if extracting the stiffness contribution of face plates but difference in magnitude (see Fig. 7.6)

In analytical techniques, the 2D braced frame model is initially modelled in both the BFA and the DBM. To apply the truss element assumption to the inclined parts of the corrugated-strip core, however, the truss element with hinge ends is performed in the BFA whereas only the mechanical elastic properties of material in the 1-direction of the local coordinate system are applied.

The analytical procedures are then carried out in different techniques. In the BFA, the equations of the equilibrium of forces and the displacement compatibility of the deformed unit cell are performed along with the approximation of the elongation length of the inclined elements. The transverse shear stiffness, D_{Qy}, is directly derived from the displacements δ_{sy} and δ_{sz}. In the DBM, only the constitutive equations of the unit cell

are performed along with the transformation of the stress and strain of each part of the unit cell from the local to the global coordinate system. Before deriving the transverse shear stiffness, D_{Qy}, from γ_{zy} and γ_{yz}, however, the average equivalent elastic property over the unit cell is obtained.

Comparison of the analytical results shows that the BFA yields good correlation in trend with the FE-TPB but difference in magnitude. The DBM yields a divergent trend from the FE-TPB if $s_y/d < 1.00$ and a difference in magnitude. Extracting the stiffness contribution of the face plates from the transverse shear stiffness equation, it is found that both methods are consistent in the transverse shear stiffness contributed by the presented core topology. The transverse shear stiffness, D_{Qy}, obtained from the DBM without the contribution of the face plates has a similar trend but a shear stiffness is lower than that obtained from the FE-TPB. This is similar to the results found for the BFA in Chapter 6. Both of these methods could be considered less appropriate than the MSM presented in Chapter 5 where good correlation with the FE-TPB solution was found.

7.6 Concluding Remark

The simplified analytical method named the discrete beam method was presented. Unlike the BFA, this method was based on the transformation of the local stress and strain of each part of the repetitive unit cell of the unfilled sandwich beam to the global coordinate system. This method was proposed as an alternative simplified analytical method to overcome the high degree of indeterminacy of the presented bi-directional corrugated-strip core topology. The 3D configuration of an unfilled sandwich beam with the presented core topology was also simplified as a 2D braced frame structure with assumption that the inclined chords perform as truss elements.

The formulation of the transverse shear stiffness, D_{Qy}, was presented. The transformational constitutive law of stress and strain was first introduced and applied to the face plates and the core of the unfilled sandwich beam. The deformation of a repetitive part subjected to the transverse shear load was also assumed to deform in two separate modes. The constitutive equation of each deformation mode was then performed to deduce the average shear stiffness over the unit cell. Consequently, the transverse shear stiffness, D_{Qy}, was derived using the unit cell approach.

The transverse shear stiffness equation obtained from the presented DBM was verified. It was found that the transverse shear stiffness obtained from the DBM diverges from the finite element method if $s_y/d < 1.00$. This problem seems to be due to the assumed

deformation shape of the unit cell panel, especially of the face plates. Extracting the contribution of the face plates from the transverse shear stiffness equation, it can be seen that the DBM yields a good correlation with the finite element method but a difference in magnitude. Therefore, the use of the DBM to obtain the transverse shear stiffness of the unfilled sandwich beam with the presented core topology should be limited according to the assumptions presented in this chapter.

7.7 Concluding Remark of the Analysis of the Unfilled Sandwich Beam

The analysis of unfilled Bi-CSC sandwich beams were carried out using the numerical and analytical approaches. The numerical approach based on the 3D FE method was first presented in Chapter 4. Then, three simplified analytical methods were presented in Chapters 5, 6, and 7 referred to as the modified stiffness matrix method (MSM), the braced frame analogy method (BFA), and the discrete beam method (DBM), respectively. The MSM and the BFA are based on the force-distortion relationship technique while the DBM is based on the transformation of the stress and strain technique.

The objective of the analysis of the unfilled sandwich beam with Bi-CSC topology is to address the advantage of stiffness and strength of the proposed sandwich beam. The main focus is on the effect of the configuration of the Bi-CSC topology.

According to the numerical and analytical solutions presented in Chapter 4 to 7, it was found that the stiffness and strength of the unfilled sandwich beam significantly improved and varied with the configuration of the proposed core. Of such these possible advantages, the transverse shear stiffness, D_{Qy}, was the most interesting advantage. In terms of the transverse shear stiffness, D_{Qy}, the optimum configuration of the Bi-CSC topology can be found at s_y/d about 1.0 (the angle of the inclined part of the CSC is about 45°). It was found that the proposed Bi-CSC topology yields a few more advantages in transverse shear stiffness compared to the X-truss core topology.

In addition to the evaluation of the advantage of the proposed core topology, providing a simplified analytical method to obtain the stiffness of the proposed sandwich beam is also another aim in this unfilled beam section. It was found that the MSM provided good correlation with the FE method. Rather than using the computational expensive FE method, the MSM can be used to obtain the transverse shear stiffness, D_{Qy}, of the unfilled sandwich beam with the proposed Bi-CSC and other similar core such as the truss and the X-truss cores. It was also found that the MSM provided very good

correlation with the Lok et al.'s method [19, 20] when it was applied to the unfilled truss core sandwich beam.

The BFA and the DBM are the other two simplified analytical methods that can probably be used to obtain the transverse shear stiffness, D_{Qy}, of the proposed core. However, it was found that these two methods were less accurate than the MSM. They may provide a good structural response in trend but not in magnitude. Therefore, these two proposed methods should only be used in accordance with their assumptions presented in this thesis.

Besides the analysis of the unfilled sandwich beam, the next chapter presents the numerical study of the concrete-filled SCS sandwich beam with inclined shear connectors. The objective of the next chapter is also to investigate the possible advantage of the proposed SCS sandwich beam that may overcome the limitation of the current forms of SCS sandwich beams. The transverse shear strength and the development of the concrete crack are demonstrated using the 3D FE method.

Chapter 8

Numerical Study of the Transverse Shear Strength of a Concrete-Filled Sandwich Beam

8.1 Background

As previously mentioned in Chapter 2, the failure modes of a steel-concrete-steel (SCS) sandwich beam subjected to static load were experimentally observed and reported by, for example, [11, 12, 15]. These failure modes are technically referred to as described in Fig. 8.1(a). Remarkably, the failure modes of an SCS sandwich beam are similar to those of a reinforced concrete (RC) beam, as graphically compared between Fig. 8.1(a) and Fig. 8.1(b).

The diagonal shear crack failure is a failure mode found in both the SCS and RC beams. Technically, this failure may occur when the beam is subjected to a relatively high ratio of shear to normal. In addition, the beam made of relatively low tensile strength material may tend to crack easily. The latter may be the major cause of the diagonal shear crack failure in the RC and SCS beams because the tensile strength of concrete is remarkably low [87].

To demonstrate the diagonal shear crack in the SCS sandwich beam, a simplified approach based on the transformation of stress of a small element may be used. According to the fundamental mechanics of solids [126], the principal tensile stress of a plane stress element cut from a point of the concrete core subjected to stress in the local y- and

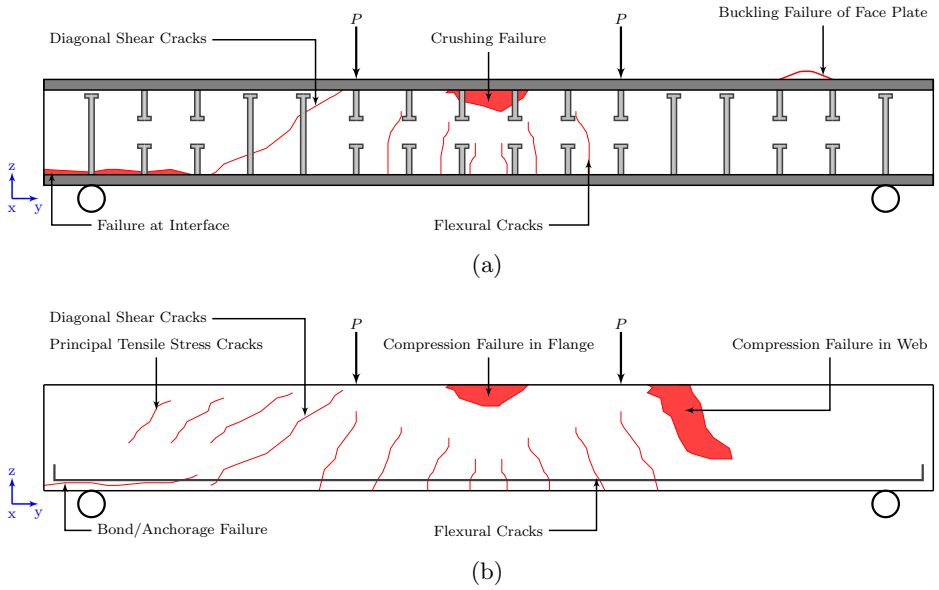

FIGURE 8.1: Possible failure modes of (a) a steel-concrete-steel sandwich beam [modified from 11], and (b) a reinforced concrete beam [modified from 94]

z-directions can be expressed as follows:

$$\sigma_1 = \frac{\sigma_y + \sigma_z}{2} + \sqrt{\left(\frac{\sigma_y - \sigma_z}{2}\right)^2 + \tau_{yz}^2} \tag{8.1}$$

Here, the normal stress, σ_z, in the concrete core is neglected and the normal stress, σ_y, and the shear stress, τ_{yz}, are expressed as follows:

$$\sigma_y = \frac{M_y E_c z}{D_y} \tag{8.2a}$$

$$\tau_{yz} = \frac{V_{yz}}{D_y}\left\{E_t t_t \bar{z} + \frac{1}{2}E_c\left[\left(\bar{z} - \frac{t_t}{2}\right)^2 - z^2\right]\right\} \tag{8.2b}$$

The location of the neutral axis, $\bar{z}$, and the flexural stiffness, D_y, of the cross section of the SCS sanwich beam may be calculated from the strain compatibility and the equilibrium of forces of the cross section. In a particular linear elastic case, the strain compatibility of the cross section is as shown in Fig. 8.2.

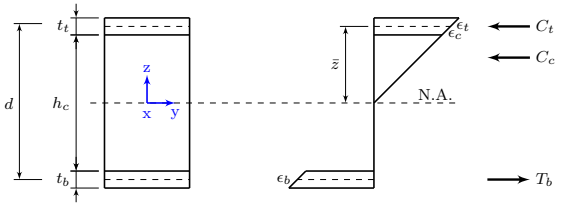

FIGURE 8.2: Strain compatibility of the cross section of a steel-concrete-steel sandwich beam

Assuming that the tensile strength of the concrete is neglected, the equilibrium of forces of the cross section is

$$C_t + C_c = T_b \tag{8.3}$$

where the compression force in top face plate, C_t, the compression force in concrete core, C_c, and the tension force in bottom face plate, T_b, are expressed in terms of the concrete strain, ϵ_c, as follows:

$$C_t = bE_t t_t \frac{\bar{z}}{\left(\bar{z} - \frac{t_t}{2}\right)} \epsilon_c \tag{8.4a}$$

$$C_c = \frac{1}{2} bE_c \left(\bar{z} - \frac{t_t}{2}\right) \epsilon_c \tag{8.4b}$$

$$T_b = bE_b t_b \frac{(d - \bar{z})}{\left(\bar{z} - \frac{t_t}{2}\right)} \epsilon_c \tag{8.4c}$$

Thus, the location of the neutral axis, $\bar{z}$, can be obtained from Eq. 8.3. Knowing the location of the neutral axis, $\bar{z}$, consequently, the flexural stiffness, D_y, of the cross section can be calculated as follows:

$$D_y = D_y^t + D_y^b + D_y^c \tag{8.5}$$

where

$$D_y^t = bE_t \left(\frac{1}{12} t_t^3 + \bar{z}^2 t_t\right) \tag{8.6a}$$

$$D_y^b = bE_b \left(\frac{1}{12} t_b^3 + (d - \bar{z})^2 t_b\right) \tag{8.6b}$$

$$D_y^c = \frac{1}{3} bE_c \left(\bar{z} - \frac{t_t}{2}\right)^3 \tag{8.6c}$$

Knowing the principal tensile stress, the direction of the principal tensile stress of each small concrete element can also be obtained [126]. Figure 8.3 demonstrates the directions of the principal tensile stresses in the concrete core of an SCS sandwich beam. It may be seen that most of the principal tensile stress directions in the concrete core align at an angle to the neutral axis of the SCS sandwich beam. The concrete core, therefore, tends to crack in a diagonal direction to the neutral axis of the SCS sandwich beam.

In addition to preventing the RC and SCS beams from failing in other failure modes, the diagonal shear crack failure also needs to be prevented to ensure that the structure is safe. Providing some kind of transverse shear reinforcements is a way to overcome this failure in the RC beam. This concept is also found in the SCS sandwich beam in which the shear connectors act as transverse shear reinforcements.

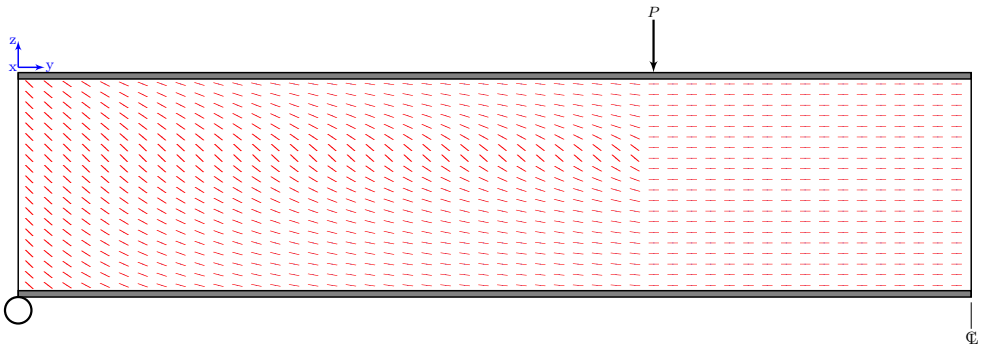

FIGURE 8.3: Principal tensile stress directions in the concrete core of a steel-concrete-steel sandwich beam

In the Bi-Steel sandwich beam – a particular case of the SCS sandwich beam, the total transverse shear strength of the cross section is the summation of the strength resistance of the concrete core and the bar connectors [50]. In addition to the resistance of the concrete, which is relatively low, the transverse shear strength of the cross section can be dramatically increased when the bar connectors are present, as may be seen in the strength resistance of each part in Table 8.1. As recommended in the Bi-Steel: Design & Construction Guide [50, Chapter 6, Page 14], the presence of an increasing number of bar connectors is probably the most effective method of improving the transverse resistance of the Bi-Steel sandwich compared to increasing the section depth or increasing the strength of concrete.

TABLE 8.1: Transverse shear strength capacity of the cross section of a concrete-filled Bi-Steel sandwich beam [50]

Strength	Formula	Remark
V_{wd} [a]	$0.9k_T \frac{A_{sw}}{s_y} \frac{h_c f_{yb}}{\gamma_{Ma}}$	$k_T = 2.5 \frac{f_y}{f_{yb}} \left(\frac{t}{d}\right)^{1.25} - \frac{\gamma_{Ma}}{f_{yb}} \left(\sigma_{tbc} + \sigma_{tbp} + \sigma_{tba}\right)$ $A_{sw} = \frac{b\pi d^2}{4 s_x}$ $\frac{t}{d} \leq 0.48$ $t = \min(t_t, t_b)$ $f_y \leq 355\ N/mm^2$
V_{Rd1} [b]	$\left[\frac{0.0525}{\gamma_{Mc}} f_{ck}^{2/3} k \left(1.2 + 40\rho_1\right) + 0.15\sigma_{cp}\right] b h_c$	$k = 1.6 - \frac{h_c}{1000}$ and $k \geq 1.0$ $\rho_1 = \frac{t_b}{h_c}$ and $\rho_1 \leq 0.2$
V_{Rd2} [c]	$0.45v \frac{f_{ck} b D}{\gamma_{Mc}}$	$v = 0.7 - \frac{f_{ck}}{200}$ and $v \geq 0.5$ $D = t_t + h_c + t_b$

[a] the resistance of friction welded bar connectors (as reinforcement)
[b] the resistance of concrete (acting with reinforcement)
[c] the limiting resistance strength of section
see the definition of the symbols mentioned in this table in [50]

However, it is found that the spacing between the bar connectors are technically limited to not less than 200 mm or $8 \times (t_t + t_b)$ [50] (see Fig. 8.4). This means that the number of bar connectors per unit length is also limited. As a result, the transverse shear strength resistance of the Bi-Steel cross section is limited unless the section depth and/or the strength of concrete are increased.

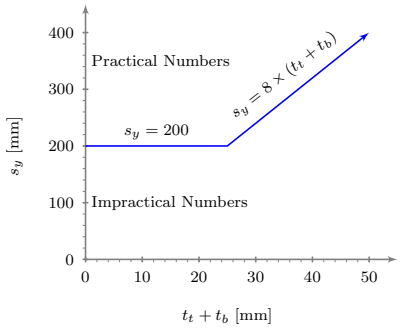

FIGURE 8.4: Limitation of the spacing of bar connectors of a Bi-Steel sandwich beam

To demonstrate the limitation of the transverse shear strength of the Bi-Steel cross section due to the spacing between the bar connectors, s_y, the Bi-Steel sandwich beams as shown in Fig. 8.5(b) are investigated. The concrete core depth, h_c, the thickness of top face plate, t_t, and the spacing between bar connectors, s_y, are variable parameters. Other parameters appearing in Table 8.1 are constant, as presented in Table 8.2.

TABLE 8.2: Value of the parameters used for evaluation of the transverse shear strength of a concrete-filled Bi-Steel sandwich beam [50]

Parameter [a]	Value	Unit	Remark
Steel Face Plates			
γ_{Ma}	1.1		fundamental case
Concrete Core			
f_{ck}	35	N/mm^2	selected value
σ_{cp}	0	N/mm^2	for no axial load case
γ_{Mc}	1.5		fundamental case
Bar Connectors			
d	25	mm	normal diameter of a bar connector
f_y	355	N/mm^2	selected value
f_{yb}	355	N/mm^2	normal yield strength of a friction welded bar connector
σ_{tbc}	0	N/mm^2	for a flat panel
σ_{tbp}	0	N/mm^2	for no internal pressure
σ_{tba}	0	N/mm^2	for no attachment

[a] see definition in [50]

Figure 8.5(a) presents the relationship between the transverse shear strength, V_{BS}^F, and the spacing of the bar connectors, s_y, of the Bi-Steel sandwich beam. The transverse shear strength, V_{BS}^F, is the strength value normalised by the strength value at $s_y = 200\ mm$, $h_c = 200\ mm$, and $t_t = 6\ mm$. The solid lines represent the transverse shear strength in the range of practical numbers of s_y and the dash lines represent the strength in the range of impractical numbers of s_y. The limitations of s_y are marked by the cross-marking points.

It can be seen from Fig. 8.5(a) that reducing the spacing s_y from 500 mm to 100 mm remarkably increases the transverse shear strength, V_{BS}^F, if the limitation of s_y is not introduced. This tendency can be found in both $h_c = 200$ and 600 mm and also in all values of t_t studied here. For the Bi-Steel cross section with $h_c = 200\ mm$, the strength

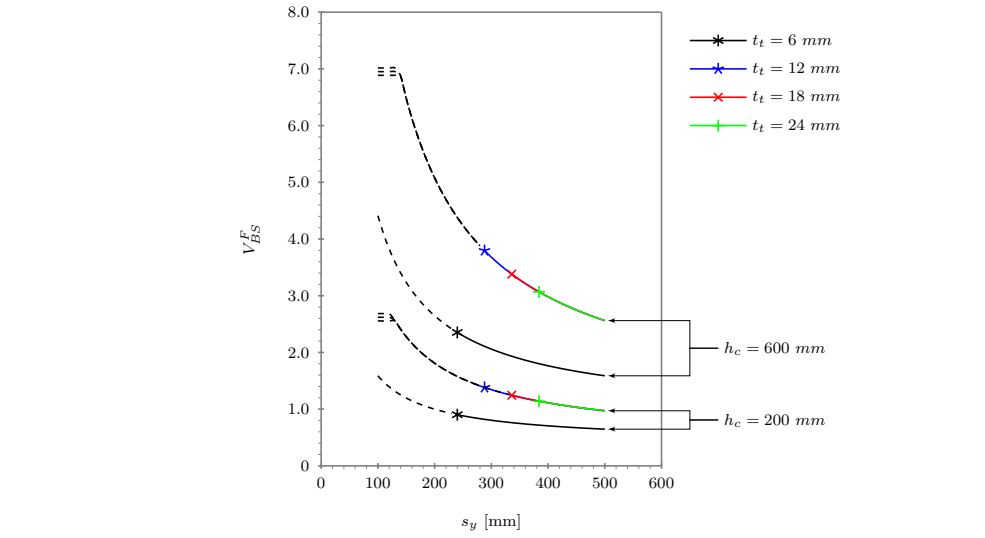

(a)

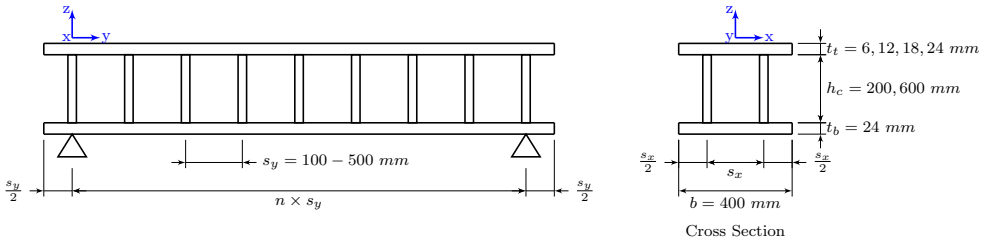

(b)

FIGURE 8.5: (a) relationship between the factored transverse shear strength, V_{BS}^F, and the spacing of bar connectors, s_y, and (b) configuration of the Bi-Steel case study

V_{BS}^F increases from 0.6 to 1.6 for $t_t = 6\ mm$ and from 1.0 to 2.7 for $t_t \geq 12\ mm$. For $h_c = 600\ mm$, the strength V_{BS}^F remarkably increases from 1.6 to 4.4 for $t_t = 6\ mm$ and from 2.6 to 7.0 for $t_t \geq 12\ mm$. The strength V_{BS}^F of all case studies increases about 270% when decreases the spacing s_y from 500 mm to 100 mm.

Because of the limitation of the spacing s_y, however, reducing s_y slightly affects to the strength V_{BS}^F. For the Bi-Steel cross section with $h_c = 200\ mm$, the strength V_{BS}^F increases from 0.6 to 0.9 (about 150%) for $t_t = 6\ mm$ and from 1.0 to 1.4 (about 140%) for $t_t = 12\ mm$ when s_y reduces from 500 mm to their limitation values 240 mm and 288 mm, respectively. A small percentage increase of the strength V_{BS}^F, about 110%, was found for $t_t = 24\ mm$ when s_y reduces from 500 mm to 384 mm. The similar behaviour can also be found for $h_c = 600\ mm$. It may imply, therefore, that reducing the spacing s_y between the bar connectors may not be the most effective method to increase the transverse shear strength of the Bi-Steel sandwich beam as recommended in the Bi-Steel: Design & Construction Guide [50].

However, there is another method to overcome the diagonal shear crack failure, for example, rearranging the position of supports, increasing the thickness of the beam, changing the structural material, or providing some kind of transverse shear reinforcements. In the author's opinion, changing the physical geometry of the beam may not be a suitable solution because it may affect architectural criteria and service requirements. Increasing the thickness of the beam may also increase the weight of structure. Introducing new structural materials such as high strength concrete may increase cost prohibitively. Providing transverse shear reinforcements is probably the best method since it should not affect the architectural and construction criteria. This is because the transverse shear reinforcements usually substitute concrete mass and perform their function inside the structure.

Instead of aligning the transverse shear reinforcements in vertical direction, an inclined alignment of transverse shear reinforcements can be introduced. This concept has been discussed in great detail in Chapters 4 to 5 for unfilled sandwich beams. This concept has also been found and technically proved of its advantage in the RC beam. The transverse shear strength resistance provided by the inclined shear reinforcement is more than the resistance provided by the vertical shear reinforcement, as previously mentioned in Chapter 2.

To demonstrate the advantage of the inclined shear reinforcement, a simplified mechanism of the RC beam with inclined shear reinforcements may be introduced. Considering the beam with the inclined transverse shear reinforcements, as shown in Fig. 8.6, the equilibrium of forces in the z-direction at the diagonal crack section can be expressed as follows:

$$A_v f_v \sin\theta \quad = \quad \sigma_1 b l \cos\beta \tag{8.7}$$

Here, A_v is the cross section area of the transverse shear reinforcement, f_v is the allowable tensile stress of the transverse shear reinforcement, and σ_1 is the average principal tensile stress at the diagonal crack section. The transverse shear reinforcements are aligned at an angle θ and the crack line is aligned at an angle β to the y-axis. b and l are the width of beam and the length of diagonal crack line, respectively.

Assuming that the diagonal crack section crosses only one inclined transverse shear reinforcement, the length of diagonal crack line, l, can be expressed in terms of the horizontal spacing, s_y, of the transverse shear reinforcement and the angles θ and β as follows:

$$l \quad = \quad s_y \frac{\sin\theta}{\sin\left(180 - \theta - \beta\right)} \tag{8.8}$$

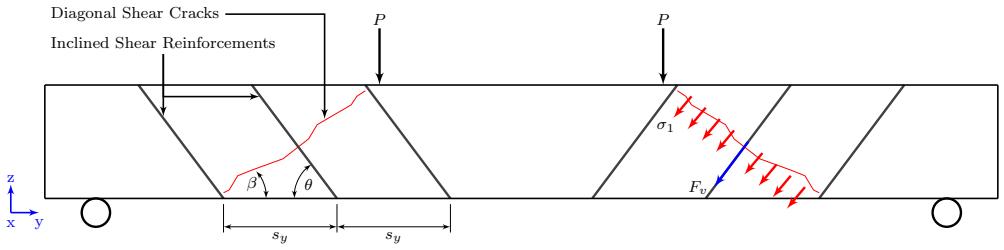

FIGURE 8.6: A concrete beam with inclined shear reinforcements and its equilibrium of force condition

Therefore, Eq. 8.7 can be expressed in another form as follows:

$$A_v f_v = k_v \sigma_1 b s_y \tag{8.9}$$

where

$$k_v = \frac{\cos\beta}{\sin(180 - \theta - \beta)} \tag{8.10}$$

Here, k_v is the strength index of the transverse shear reinforcement related to the angle of the transverse shear reinforcement, θ, and the angle of diagonal crack line, β. Knowing the angle β of the diagonal crack line, therefore, the strength index k_v depends on the angle θ only.

In the particular case where the angle β of the diagonal crack line equals 45° [107, 114], the relationship between the strength index k_v and the angle θ is as shown in Fig. 8.7. It can seen that the minimum point of the strength index k_v is at the angle θ equals 45°. This means that aligning the transverse shear reinforcements at 45° to the y-axis – in other words, aligning the transverse shear reinforcement at a perpendicular angle to the diagonal crack line – provides the minimum tensile stress in the reinforcement. Therefore, the strength at the position of the diagonal crack can be considerably increased if the transverse shear reinforcement is fully stressed to its maximum capacity.

As previously mentioned in Chapter 2, the advantage of aligning the transverse shear reinforcement in the inclined pattern has been found in many applications of the RC beam [87, 90–93]. However, it was found that there is no current application of the SCS sandwich beam with inclined shear connectors. Although the applications of the proposed Bi-CSC topology may be found in the unfilled corrugated core or truss-like core sandwich structures, it was found that those applications had never been adapted for the concrete-filled SCS sandwich structure. Therefore, the applications of the proposed Bi-CSC, i.e., the inclined shear connectors, should be studied to investigate the possible advantage of this alternative solution in the concrete-filled SCS sandwich beam.

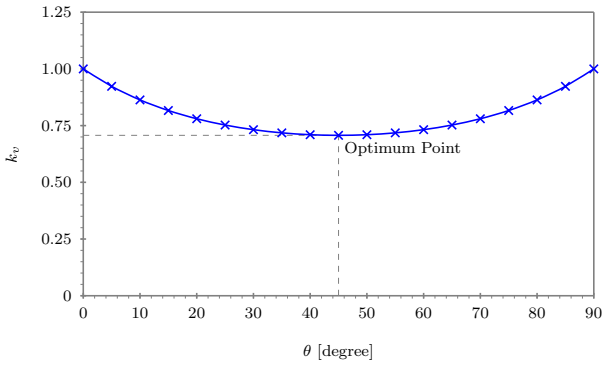

FIGURE 8.7: Relationship between the strength index k_v and the angle θ plotted at the angle of diagonal shear crack line, $\beta = 0.45°$

8.2 Finite Element Modelling Approach

As previously mentioned in Chapter 4, a finite element (FE) approach can be used instead of an experimental approach to provide reliable results and behaviour of an unfilled steel sandwich beam [37, 115]. In concrete-filled SCS sandwich beams, an FE approach can also be used to obtain reliable results compared with an experimental study [15, 71, 72].

Table 8.3 summaries the numerical studies of SCS sandwich structures and their components using the FE method. Shanmugam et al. [71] used the FE software ABAQUS to understand the ultimate load behaviour of double-skin composite (DSC) sandwich slabs. Clubley et al. [72, 73] used the FE software ANSYS to investigate the shear strength bar connectors of the Bi-Steel sandwich specimens subjected to push out load. Xie and Chapman [74] also used ANSYS to study the static and fatigue strength of the bar connectors of the Bi-Steel specimens subjected to tension load. In the Bi-Steel sandwich beams, Foundoukos and Chapman [15] also used ANSYS to understand the static behaviour of the beam. Instead of using a 3D model as used in [71–74], Foundoukos and Chapman [15] used a 2D model to reduce the complexity of the FE analysis, and it was also found to be a reliable FE method.

The FE approach is used instead of an experimental approach to investigate the transverse shear strength behaviour of the SCS sandwich beam with the proposed inclined shear connector in this research. Appropriate assumptions and criteria are provided step by step to ensure that the appropriate reliability of results can be achieved.

TABLE 8.3: Summary of the numerical study of steel-concrete-steel sandwich structures and their components using a finite element method

Reference	SCS Type	Software		Geometry		Element Type			Composite Interaction Model	Remark
		ABAQUS	ANSYS	2D	3D	Steel Face	Shear Connector	Concrete Core		
Shanmugam et al. [71]	DSC	X			X	S4R	N/A	C3D8R	Fully and partially composite	- Non-linear study of the ultimate load behaviour of slabs, validated with the experimental result in ultimate loads and load-deflection responses - The presence of shear studs was indirectly modelled by treating concrete as an anisotropic material - S4R – four-node reduced integration shell elements with five integration points and with a large strain formulation - C3D8R – eight-node solid elements with reduced integration
Clubley et al. [72, 73]	Bi-Steel		X		X	SOLID45	SOLID45	SOLID65	Partially composite	- Study of the shear strength of friction-welded bar connectors subjected to push out load, validated with the experimental result - Steel-concrete composite interaction was modelled using discrete and smeared contact element techniques - Both material and geometric non-linearity were considered
Xie and Chapman [74]	Bi-Steel	X			X	CAX4R	CAX4R	CAX4R	Partially composite	- Study of the static and fatigue strength of the friction-welded connections with the bar loaded in tension - Both the steel and concrete material properties were linear elastic - Steel and concrete contact interfaces were modelled using the contact pair approach, all the contact surfaces had a frictional surface interaction - CAX4R – four-node axisymmetric solid elements
Foundoukos and Chapman [15]	Bi-Steel	X		X		CPS4R	CPS4R	CPS4R	Partially composite	- Study of the static behaviour of beams, validated with the experimental result, parametric study of the transverse shear strength of beams - Concrete was modelled as linear stress-strain curve - For study of the transverse shear strength of beams, the friction coefficient between the steel and concrete was zero, the tensile strength of concrete was also zero, the steel was modelled as linear stress-strain curve to prevented other failure modes - CPS4R – two-dimensional, plane stress, reduced integration, solid elements

8.2.1 General Criteria

The numerical study of the strength of concrete-filled sandwich beams was also carried out using the FE software ANSYS Release 11.0 [123]. The ANSYS software was run under the software and hardware conditions as presented in Sec. 4.2.1.

The concrete-filled sandwich beam was modelled in 3D using solid elements. The unfilled sandwich beam model presented in Chapter 4 was adapted by filling the void with elements with material properties equivalent to concrete. The topologies of the shear connector varied from no shear connector to vertical shear connector to inclined shear connector. The analytical method was in nonlinear static mode with the simplified bi-linear stress-strain behaviour of the steel as already presented in Sec. 4.2.2 and the simplified nonlinear stress-strain behaviour of the concrete. In this chapter, the typical mesh size of FE model was approximately 2.0 cm.

8.2.2 Material Properties of Concrete

In addition to the steel material properties defined in Sec. 4.2.2, the material properties of the concrete need to be defined in this chapter. Concrete is a quasi-brittle material. Its compression behaviour is different from its tension behaviour [124]. Therefore, unlike steel, the concrete's compression and tension behaviour need to be considered separately.

Compressive Stress and Strain Behavior: Practically, the compressive strength of concrete, f_c, is usually obtained from short-time, moderate-speed, uni-axial compressive loading test of 28-day-old, 6-in. by 12-in. concrete cylinder specimens [87].

The compressive stress-strain relationship curve is approximately linear from zero up to about one-half the ultimate compressive strength, f'_c, [141]. Then, it begins to curve up to the ultimate compressive strength. The curve in this range depends on the strength of the concrete [142][1]. While the peak of the curve for low-strength concrete is relatively flat, the peak of the curve for high-strength concrete is relatively sharp [141]. The strain at the ultimate compressive strength, f'_c, ranges approximately from 0.002 to 0.003 for normal density concrete [86]. Beyond the ultimate compressive strength, f'_c, the curve begins to descend [86] and finally reaches the point of rupture at strain ranges approximately from 0.003 to 0.004 [87].

Although there are several different modulus of elasticity, E_c, e.g. the initial modulus, the tangent modulus, and the secant modulus, deduced from the compressive stress-strain relationship curve [87], the ACI 318 Code states that the modulus of elasticity,

[1] cited by Park and Paulay [141]

E_c, expressed as Eq. 8.11 may be used for normal-weight concrete weighting from $1,442$ to $2,483\ kg/m^3$ (from 90 to 155 lb/ft^3)[2] and for the ultimate compressive strength, f'_c, less than 41 N/mm^2 $(6,000\ psi)$[3] [87].

$$E_c = 0.043 w_c^{1.5} \sqrt{f'_c} \tag{8.11}$$

Here, the weight of concrete, w_c, is in kg/m^3, the ultimate compressive strength, f'_c, of 28-day-old cylinder specimen is in N/mm^2, and the modulus of elasticity, E_c, is the second modulus of line from the point of zero stress to the point of approximately $0.45 f'_c$ [87] and is in N/mm^2.

Tensile Stress and Strain Behavior: Technically, the tensile strength behaviour of the concrete may be obtained directly from the direct tensile loading test or from other two indirect tests: the split-cylinder test and the bending test [86, 87, 141]. These tests provide the approximate tensile strength in terms of the square root of the ultimate compressive strength f'_c [86] as presented in Table 8.4.

TABLE 8.4: Tensile strength of concrete obtained by different tests [modified from 86]

Test	Property	Notation	Value	
			N/mm^2	psi
Direct Tensile Loading Test	Direct Tensile Strength	f'_t	0.249 to $0.415\sqrt{f'_c}$	3 to $5\sqrt{f'_c}$
Split-Cylinder Test	Split-Cylinder Strength	f_{ct}	0.498 to $0.664\sqrt{f'_c}$	6 to $8\sqrt{f'_c}$
Bending Test	Modulus of Rupture	f_r	0.664 to $0.996\sqrt{f'_c}$	8 to $12\sqrt{f'_c}$

Practically, the modulus of rupture, f_r, is used to present the tensile strength of the concrete. In the ANSYS software [124], it is expressed as $f_r = k\sqrt{f'_c}$ where the value of k equals 0.623 (7.5 in psi unit) [141]. This value of k is also recommended by the ACI 318 Code [87]. Therefore, the modulus of rupture, f_r, as expressed in Eq. 8.12 was used in this research.

$$f_r = 0.623\sqrt{f'_c} \tag{8.12}$$

The tensile stress-strain relationship curve is approximately linear from zero up to the ultimate tensile strength at crack [141]. Then, the tensile stress gradually decreases to zero [143][4].

It should be noted that, unlike the compressive strength, the tensile strength of the concrete is sometimes ignored in structural strength analysis because of its low strength

[2] 1 $lb/ft^3 = 16.02\ kg/m^3$
[3] 1 $psi = 0.00689\ N/mm^2$
[4] cited by Kachlakev et al. [124]

capacity. The tensile strength of the concrete is generally less than 20% of the compressive strength.

Simplified Stress-Strain Relationship Curve: Instead of defining the stress-strain relationship of the concrete as a perfectly non-linear curve as illustrated in Fig. 8.8(a), the simplified stress-strain relationship curve may be used to model the properties of the concrete both in compression and in tension [124, 125, 141]. The simplified curve may be constructed from three connected curves in the compression zone [124, 125] and from two connected curves in the tension zone [15, 125] as illustrated in Fig. 8.8(b).

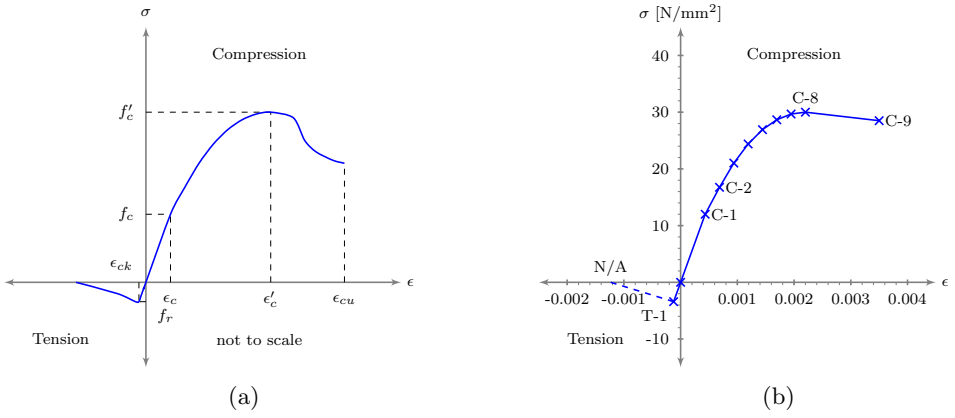

FIGURE 8.8: Stress-strain relationship curve of the concrete (a) the idealised stress-strain relationship curve [modified from 124], and (b) the simplified stress-strain relationship curve

In the compression zone, the first line is assumed to be linear. It is used to present linear elastic behaviour as expressed by Eq. 8.13a from zero up to the compressive stress, f_c, of about $0.4f'_c$ [103][5]. The second line is assumed to be a non-linear parabolic curve. It is used to present the compressive behaviour from the end of the first linear line (C-1) up to the ultimate compressive strength, f'_c, (C-8) [141]. In this research, this parabolic curve is expressed by Eq. 8.13b as recommended by Eurocode 2 [125]. The third line is also assumed to be as linear as the first line. It is used to present the descending behaviour from the ultimate compressive strength, f'_c, (C-8) down to the rupture point at the compressive stress rf'_c (C-9) [125, 141] where r is the reduction factor. In this research, Eq. 8.13c is used to express its linear behaviour.

$$f_c = E_c \epsilon_c \tag{8.13a}$$

$$f_c = \left(\frac{kn - n^2}{1 + (k-2)\, n} \right) f'_c \tag{8.13b}$$

$$f_c = \left(\frac{\epsilon_c - \epsilon'_c}{\epsilon_{cu} - \epsilon'_c} \right) (r-1)\, f'_c + f'_c \tag{8.13c}$$

[5] cited by Nguyen and Kim [125]

In Eq. 8.13b, the terms n and k are defined as follows: $n = \epsilon_c/\epsilon'_c$ and $k = 1.1E_c\epsilon'_c/f'_c$ where the strain at the ultimate compressive stress, ϵ'_c, equals 0.0022 [125]. Approximately, the same value of ϵ'_c, i.e., ϵ'_c equals 0.002, was used in the FE analysis of the DSC sandwich panels by Shanmugam et al. [71].

In Eq. 8.13c, the reduction factor r can vary from 1.0 to 0.5 for the concrete cube strength from 30 to 100 MPa [125]. Within this range, the reduction factor r may be defined as, for example, 1.0 [124] or 0.85 [125, 141]. In this research, the reduction factor r was defined as a value of 0.95 which corresponds to the ultimate compressive cube strength of 37 MPa used in this research (see Table 8.6). The strain of the concrete at failure, ϵ_{cu}, associated with rf'_c was defined according to Eurocode 2 as 0.0035 [125]. The same value of ϵ_{cu} was also used in Shanmugam et al. [71].

In the tension zone, the first line (O – T-1) is assumed to be linear. It is used to present linear elastic behaviour as expressed by Eq. 8.14a from zero down to the modulus of rupture, f_r, – the tensile strength – (T-1) at the strain at concrete crack, ϵ_{ck}, [125]. Although the second line may be also assumed to be linear as expressed by Eq. 8.14b from the modulus of rupture, f_r, (T-1) to zero tensile stress at failure strain ϵ_{cku} – approximately of ten times as ϵ_{ck} – [144][6], this may be not required to model in the ANSYS software [124]. Therefore, in this research, the property of the concrete in tension was modelled up to the modulus of rupture, f_r, where f_r is expressed as mentioned earlier as Eq. 8.12.

$$f_c = E_c\epsilon_c \tag{8.14a}$$

$$f_c = \left(\frac{\epsilon_{cku} - \epsilon_c}{\epsilon_{cku} - \epsilon_{ck}}\right) f_r \tag{8.14b}$$

Figure 8.8(b) shows the simplified stress-strain relationship of the concrete material both in the compression and in the tension used in this chapter. The simplified curve was constructed from Eq. 8.13 for the compression behaviour and Eq. 8.14a for the tension behaviour. The curve was constructed from its key points connected by straight lines. The key points and their numerical values are all presented in Table 8.5.

Poisson's Ratio: Poisson's ratio of concrete, ν_c, generally varies with the concrete compressive strength [141]. It may vary from 0.11 to 0.21 for high-strength and for low-strength concrete, respectively [87]. In this chapter, the Poisson's ratio of concrete, ν_c, was defined according to the Bi-Steel: Design & Construction Guide [50] as 0.20.

[6] cited by Nguyen and Kim [125]

TABLE 8.5: The key points and their numerical values used to simplify the stress-strain relationship curve of the concrete

Point	Value		Equation	Remark
	f_c	ϵ_c		
T-1	−3.41	−0.0001	8.12	f_r
O	0	0	-	
C-1	12.0	0.0004	8.13a	$f_c = 0.4f'_c$ [125]
C-2	16.75	0.0007	8.13b	
C-3	21.02	0.0009	8.13b	
C-4	24.39	0.0012	8.13b	
C-5	26.92	0.0014	8.13b	
C-6	28.66	0.0017	8.13b	
C-7	29.67	0.0019	8.13b	
C-8	30	0.0022	-	f'_c of concrete Class C30/37 [50] ϵ'_c as per [125]
C-9	28.5	0.0035	8.13c	$r = 0.95$ ϵ_{cu} as per [125], also used in [71]

Shear Transfer Coefficient: The shear transfer coefficient, β_t, of the concrete material needs to be defined in ANSYS [123]. This value presents the conditions of the concrete crack face. The shear transfer coefficient, β_t, varies from 0.0 for a smooth crack surface to 1.0 for a rough crack surface [123]. While the smooth crack condition cannot transfer any shear force along a crack face, the rough crack condition can completely transfer shear force from one to another crack face.

The value of β_t used in many reinforced concrete numerical studies varies between 0.05 and 0.25 [143, 145, 146][7]. In a numerical study of SCS sandwich beams by Clubley et al. [73], the shear transfer coefficients, β_t, for open and closed cracks were of 0.1 and 0.5, respectively. However, Kachlakev et al. [124] recommended β_t for open cracks in the ANSYS software as a constant of 0.2 to eliminate the divergence problem occurring at low loading conditions where β_t is less than 0.2. For closed cracks, Kachlakev et al. [124] assumed β_t as 1.0. The β_t value of 1.0 may be the idealised assumption. In this research, therefore, the shear transfer coefficient β_t were as 0.2 [124] and 0.5 [73] for open and closed cracks respectively.

Table 8.6 summaries the physical properties of the concrete material used in this research.

TABLE 8.6: Physical properties of the concrete

Property	Notation	Value	Unit	Remark
Density	w_c	2,400	kg/m^3	Normal-weight concrete [50]
Cylinder Compressive Strength	f'_c	30	N/mm^2	Concrete Class C30/37 [50]
Modulus of Rupture	f_r	3.41	N/mm^2	Eq. 8.12
Modulus of Elasticity	E_c	27,691	N/mm^2	Eq. 8.11
Poisson's Ratio	ν_c	0.20	-	[50]
Shear Transfer Coefficient	β_t	0.20	-	for an open crack [124]
		0.50	-	for a closed crack [73]

[7] cited by Kachlakev et al. [124]

To model the concrete in ANSYS, these material properties: modulus of elasticity, E_c, Poisson's ratio, ν_c, ultimate uni-axial compressive strength, f'_c, modulus of rupture, f_r and shear transfer coefficient, β_t are required. In addition, the compressive uni-axial stress-strain relationship of the concrete needs to be defined.

In ANSYS, the first two concrete properties, E_c and ν_c, are defined using the MP command [123]. The next three properties, β_t (for both open and closed cracks), f_r and f'_c, are defined after the TB command with the CONCR option using TBDATA command [123]. In the TBDATA command, eight parameters are required to input for concrete material. However, only the first four parameters were manually input. The last four parameters were automatically calculated by ANSYS [123]. Table 8.7 summaries these eight parameters and their value used in this research.

TABLE 8.7: Concrete material data for the TBDATA command

Parameter	Description	Notation	Value	Remark
1	Shear transfer coefficient for an open crack	β_t	0.20	[124]
2	Shear transfer coefficient for a closed crack	β_t	0.50	[73]
3	Ultimate uniaxial tensile strength	f_r	3.41	Eq. 8.12
4	Ultimate uniaxial compressive strength	f'_c	-1.00	[124]
5	Ultimate biaxial compressive strength	f'_{cb}	$1.2f'_c$ [a]	
6	Ambient hydrostatic stress state	σ_h^a	N/A [a]	
7	Ultimate compressive strength for a state of biaxial compression superimposed on hydrostatic stress state	f_1	$1.45f'_c$ [a]	
8	Ultimate compressive strength for a state of uniaxial compression superimposed on hydrostatic stress state	f_2	$1.725f'_c$ [a]	

[a] defaulted by ANSYS [123]

In this research, f'_c value of -1.0 was set to suppress the crushing capability of the concrete element. Kachlakev et al. [124] recommended turning off the crushing capability of the concrete element to prevent the divergence of FE solution. This is because the crushing of the concrete elements near the applied loads may develop and force a reduction in local stiffness. Consequently, the model may show a large displacement. When the crushing capability is suppressed with f'_c equals -1.0, the concrete element will crack whenever a principal stress component exceeds its modulus of rupture, f_r, [123]. Therefore, in this research, the cracking of the concrete will control the failure of the FE models.

The compressive uni-axial stress-strain relationship of the concrete is defined using the TB with MISO option. The MISO option is used to specify the concrete material model as multi-linear isotropic hardening. The concrete material behaviour is illustrated by a multi-linear stress-strain curve starting at the origin with positive stress and strain values. The initial slope of the curve is taken as the modulus of elastic, E_c, of the concrete. Beyond the stress f_c, the curve continues along the other segment lines connected to the

next key points [123]. Then, the stress-strain data at each key point is defined using the TBPT command.

8.2.3 Element Types

In addition to defining the steel material of the unfilled sandwich beam with the SOLID45 element type, the SOLID65 is additionally used in this chapter to define the concrete material in the concrete-filled sandwich beam. These element types were used by Clubley et al. [72] in their numerical study of the shear strength behaviour of the Bi-Steel panels. Figure 8.9 shows the geometry of the SOLID65 element.

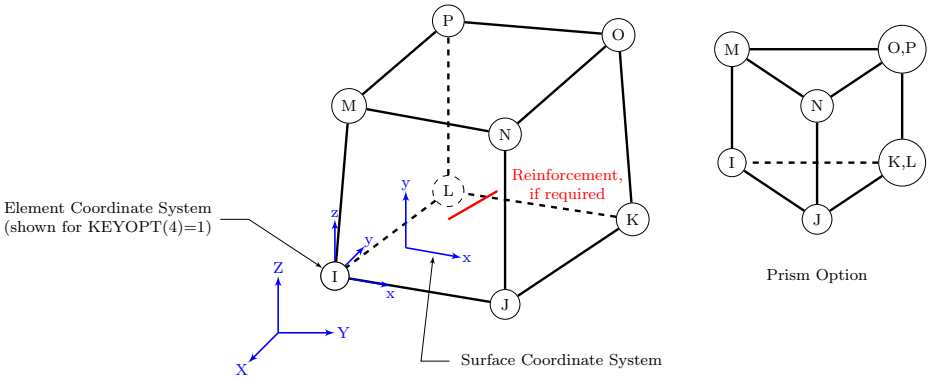

FIGURE 8.9: Geometry of the SOLID65 element [modified from 123]

The SOLID65 is a special purpose element for the 3D modelling of concrete structures with or without reinforcing bars. It was used here, however, for the plain concrete core – the concrete without reinforcing bar – only. Similar to the SOLID45, the geometry of the element is an eight-node element having three degrees of freedom, i.e., translations in the nodal x-, y-, and z-directions, at each node. The material property of the SOLID65 element is defined in the isotropic condition.

Being more advantageous than the SOLID45, the SOLID65 has special cracking in tension (in three orthogonal directions), crushing in compression, plastic deformation, and creep capabilities. The other advantage is the treatment of nonlinear material properties. The cracking and crushing capabilities provide a prediction of the failure mode of the concrete material. The failure criterion of the concrete due to a multi-axial stress state are presented in ANSYS [147][8]. In summary, the concrete material will crack or crush when the principal tensile stress in any direction or all principal compressive stress lie outside the failure surface. A small amount of stiffness of approximately 1.0E-6 is added to the concrete element when it is cracked or crushed to maintain numerical stability [123].

[8] cited by [123]

8.2.4 Modelling a Concrete-Filled Sandwich Beam

8.2.4.1 Geometry

Similar to the unfilled sandwich beam presented in Chapter 4, a 3D model of the concrete-filled SCS sandwich beam was created. A 3D FE model of a four-point loaded beam, as shown in Fig. 8.10(a), was modelled and analysed to obtain the strength behaviour of the beam and the cracking pattern of the concrete core. The concrete-filled SCS sandwich beam model consists of the steel face plates, the steel corrugated-strip-core plates, and, in addition, the concrete core. The first two parts perform as the unfilled SCS sandwich beam. The void of the unfilled sandwich beam is then filled with the concrete elements to create the concrete-filled SCS sandwich beam.

In this chapter, the length of the concrete-filled SCS sandwich beam is set so that $a/d = 3$ where the shear span, a, is the distance between the support and the applied point load, and d is the depth of the concrete core. In a study of reinforced concrete beams, Park and Paulay [141] summarised that the shear failure mechanisms of four-point loaded simply supported beams without shear reinforcement depend upon the shear span over depth, a/d, ratios. The failure mechanisms may behave in two different ways: failure of arch mechanisms when $2 < a/d < 3$, and failure of the beam mechanisms when $3 < a/d < 7$. For the arch mechanisms, the failure by crushing or splitting of the concrete may occur. In addition, the inclined crack may develop in a direction greater than 45° from the horizontal line; the crack may occasionally be in a vertical direction [87]. This phenomenon is considered as deep beam action. For the beam mechanisms, the failure of the beam occurs after the diagonal crack develops.

Due to the symmetry of the structure, only a quarter of the complete concrete-filled sandwich beam model, as shown in Fig. 8.10(b), is required for analysis. This is a sub-structure of a complete symmetrical concrete-filled sandwich beam subjected to symmetrical load, as shown in Fig. 8.10(a); it was used here to reduce computation time.

8.2.4.2 Boundary and Constraint Conditions

The conventional boundary conditions of a simply supported beam were set up at all nodes along the line 1-1'. These nodes were not free to move in the x-, y-, and z-directions, i.e., $\delta_x = \delta_y = \delta_z = 0$, to simulate the simply support at the end of the bottom face plate. To satisfy the reduced symmetrical structure condition [121, 122], the nodes on the xz-plane were free to move in the z-direction only, i.e., $\delta_x = \delta_y = 0$.

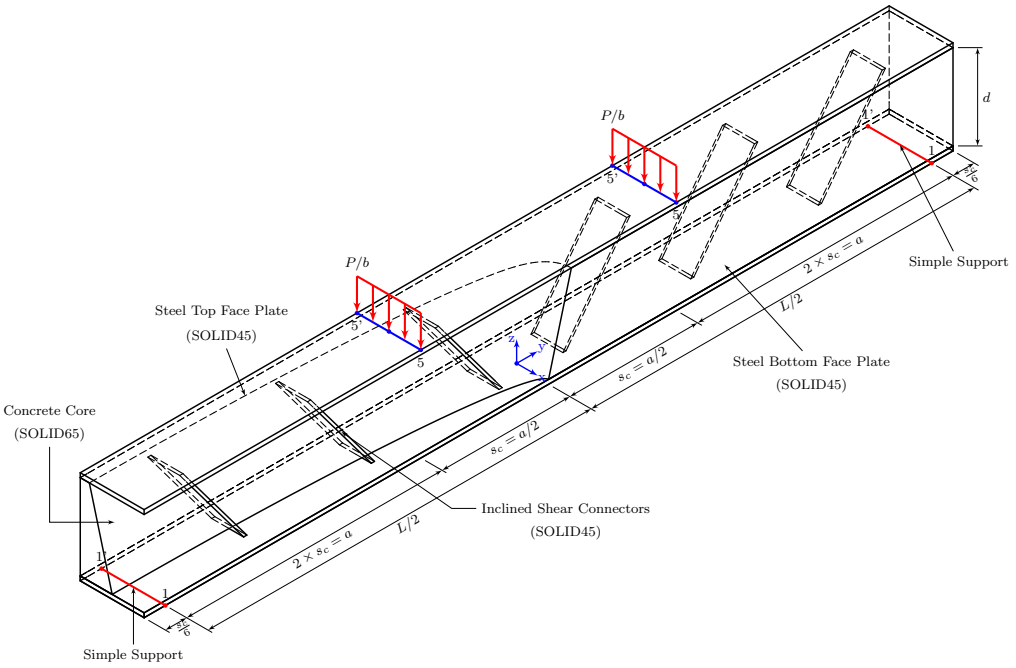

(a)

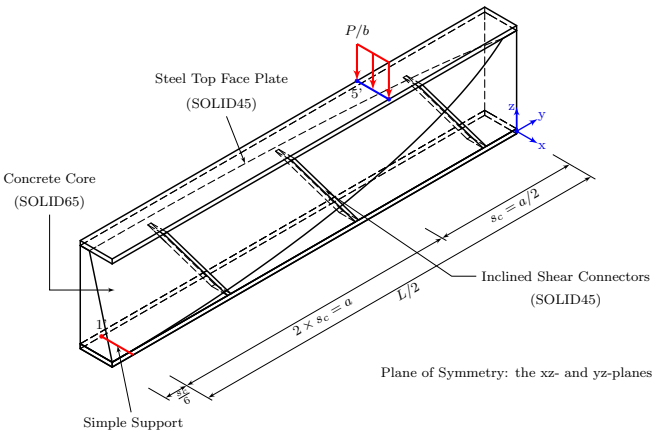

(b)

FIGURE 8.10: Geometry of (a) a four-point loaded concrete-filled steel-concrete-steel sandwich beam with inclined shear connectors, and (b) its sub-structure

8.2.4.3 Loading Condition

To simulate a four-point loaded beam, a transverse force per unit width of the sandwich beam, P/b, is imposed along the line 5-5' on the top face plate. The distributed load P/b is then proportionally distributed to element nodes on the line 5-5'.

In the non-linear analysis, the total load applied will be divided into a series of load increments. To perform an accurate non-linear analysis, the load needs to be gradually applied to the structural model. In this chapter, the total applied load was partitioned into multiple load steps. Each load step was first randomly guessed until the reliability of structural response which may depend upon the behaviour of structure [124] can be achieved. Each load step was again divided into small load increments using the NSUBST command [123]. The auto time stepping option controlled by the AUTOTS command [123] was turned off to manually control the size of the load increment.

8.2.4.4 Steel-Concrete Composite Interaction Criterion

Ideally, the precise composite interaction between the steel and concrete faces should be considered in FE modelling to provide the similar behaviour as occurred in the real structure. However, the actual steel-concrete composite interaction may not be precisely defined and modelled due to its complicated behaviour. The reliability of the numerical study may vary and depend on the steel-concrete composite interaction assumption [72] which may be assumed as one of the three possible conditions as follows: (1) no composite, (2) partially composite and (3) full composite interactions.

For the no steel-concrete composite interaction condition, the steel and concrete finite elements may be modelled as independent elements; their element nodes are not connected to each other. Although this technique is quite simple and may provide good accuracy when the steel and concrete are in separation mode, the great care should be taken when the elements are in contact mode. The steel and concrete elements, in contact mode, should not penetrate through each other [15]. In practice, the case without composite interaction may be achieved when the steel face is greased to reduce fiction [125] so that the friction coefficient between the steel and concrete faces can be ignored.

For the partial steel-concrete composite interaction condition, the interaction forces may be partially transferred from one material area to another. In addition, the relative displacement of the two areas may be different and produce significant slip displacement. This phenomenon can occur in SCS sandwich beams wherever the physical and chemical bond between the steel and concrete faces are not strong enough. An insufficient number of shear connectors in the steel-concrete composite structure may also be the cause of

this situation [71]. To provide the partial composite interaction condition in the FE model, the possible modelling techniques are as follows: (1) the thin layer technique [125], (2) the link-discrete element technique [72, 73], and (3) the smeared element technique [72, 73] as demonstrated in Fig. 8.11.

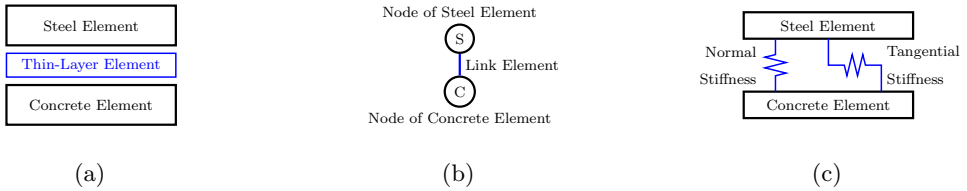

(a) (b) (c)

FIGURE 8.11: Techniques to model partial composite interaction between the steel and concrete interface (a) the thin layer technique, (b) the link-discrete element technique [72], and (c) the smeared element technique [72]

For the full steel-concrete composite interaction condition, the steel and concrete elements can be modelled independently. However, they need to share the same element nodes wherever they are in contact with each other. As a result, the interaction forces can be fully transferred from one to another and their displacements are the same. Practically, the case of full composite interaction may be achieved when the steel face is rough enough to provide a strong bond between steel and concrete faces as sometimes seen in a reinforced concrete with rebar [124, 125] or a concrete with special reinforcement sheet glued with high-strength adhesive agent [124]. The perfect bond between steel plate and concrete was also assumed in the FE study of double-skin sandwich beams by Shanmugam et al. [71].

Although the precise numerical model of steel-concrete composite interaction should be presented, the simplified technique based on the full composite interaction was decided to be used in this chapter. This simplified composite interaction model should be suitable for the present study because the main objective of this study is to understand how the shear connector topologies, especially the angle of proposed inclined shear connectors, affects the transverse shear strength capacity and the diagonal shear crack behaviour. Further investigation based on the partial composite interaction may be taken in the future to present the local behaviour in more detail. It should be done along with an experimental study of the beam so that the validation of the refined model can be carried out.

8.2.5 Analytical Method

8.2.5.1 Non-Linear Solution

Due to the material property model of the concrete being non-linear, the non-linear analysis approach is required in this chapter. This is because the non-linear stress-strain relationships of material will cause the stiffness of structure to change at different load levels [123].

In the ANSYS software, the Newton-Raphson approach is used to solve non-linear problems. This approach divides the applied load into a series of load increments. The Newton-Raphson procedure begins with evaluation of the out-of-balance load – the difference between the restoring force and the applied loads – at the beginning of each iterative solution. Then, a linear solution is performed with these out-of-balance loads. After checking the convergence criteria, the out-of-balance load vector is re-evaluated. If the criteria are unsatisfied, then the stiffness matrix is updated and a new iterative solution is obtained until the problem converges. The load increment may be reduced again if the problem is still diverging [123]. Then, the same iterative procedures are re-performed.

In ANSYS, the convergence criteria are based on forces, moments, displacements or rotations criteria, or a combination of the previously mentioned criteria. Each criterion may have its own convergence tolerance value [123]. In this chapter, the convergence criteria are based on forces and displacements. The default non-linear solution is controlled by the convergence criteria which is automatically defined by ANSYS. For typical non-linear analysis cases, the automatic solution control in ANSYS uses L2-norm of force tolerance equal to 0.5%. As optional, an L2-norm also checks on displacement with a tolerance equal to 5%. The displacement criterion is used in addition to the force criterion as a double-check on solution convergence [123].

However, Kachlakev et al. [124] recommended to increase the convergence tolerance limits in ANSYS to a maximum of five times as the default tolerance limits in order to prevent the divergence problem. Therefore, the convergence tolerance limits used in this chapter were set at 2.5% for the force criterion and at 25% for the displacement criterion. In ANSYS, this can be done using the CNVTOL command [123].

8.2.5.2 Interpretation of Concrete Crack

Generally, the cracking of concrete occurs when its principal tensile stress is greater than its own ultimate tensile strength. The crack can be usually observed from the experimental test of concrete beams and other concrete structures. Therefore, it should be predictable when using the FE method to study the behaviour of the concrete structure. To demonstrate the cracking of the concrete, there are three possible techniques to be used: (1) discrete-cracking technique [73], (2) tensile strain contour plotting technique [15], and (3) smeared-cracking technique [73, 124].

The discrete-cracking technique is a direct approach in which the formation of cracks is modelled using de-coupling element nodes [73]. Although this is the direct approach, it seems to be difficult to model due to the unknown orientation of the first concrete crack. In addition, the model needs to be changed when the load is increased; as a result, the analysis may be remarkably slow [124]. The convergence problems due to poor geometry and the poor results may be inevitable [73]. This technique is considered to be worse than the smeared-cracking technique [148][9].

The tensile strain contour plotting technique is an indirect approach in which the formation of cracks is demonstrated by plotting the maximum analysed principal tensile strain contours of concrete elements [15]. The crack is assumed to occur when the element reaches its limited capacity, and then the element is highlighted to present a virtual crack.

The smeared-cracking technique is also an indirect approach in which the formation of cracks is demonstrated by a virtual analogous distributed cracking indicator whenever an analysed principal tensile stress of the concrete element exceeds its own ultimate tensile strength [73, 124]. Having achieved this condition, the elastic modulus of the concrete in the direction parallel to the principal tensile stress direction is assumed to be zero [150][10]. This technique is considered to be easy to perform because the pre-defined first crack orientation is not required [73].

In this chapter, the smeared-cracking technique was chosen to demonstrate the concrete crack because of the simplicity of the technique. It is also available in the ANSYS software [123]. The cracking indicator in the ANSYS software appears as a circle on a plane perpendicular to the direction of the principal stress at the integration points of the solid elements.

To interpret the meaning of the cracking indicator in ANSYS, Kachlakev et al. [124] illustrated three typical cases of cracking of concrete beams as shown in Fig. 8.12(b).

[9] cited by Sigfusson [149]
[10] cited by Kachlakev et al. [124]

Region (a) shows the typical case of cracking in a flexural mode which normally appears at the bottom of the beam at midspan. The flexural crack occurs when the principal tensile stress in the y-direction of an element exceeds its ultimate tensile strength. In ANSYS, as a result, many crack indicators develop and appear as vertical lines. The typical case of cracking in a diagonal mode is shown in region (b). This crack also occurs when the concrete elements subjected to high principal tensile stress. However, the principal tensile stress of this case aligns in a diagonal direction due to the stress transformation obtained from both normal and shear stresses. In any element of the concrete beam, for example, subject to the normal stress in the y-direction and shear stress in the yz-plane, the principal tensile stress direction will be inclined from the y-direction. As a result, the crack appears as a diagonal line. Region (c) shows the typical case of cracking in a compressive mode. This crack occurs when the concrete element is subjected to high compressive stress. Due to the Poisson's effect, consequently, the tensile crack develops in the direction perpendicular to the plane of the compressive stress [151, 152][11]. In concrete beams subjected to load in the z-direction, the crack may develop in the x-direction and appears as the circle indicator.

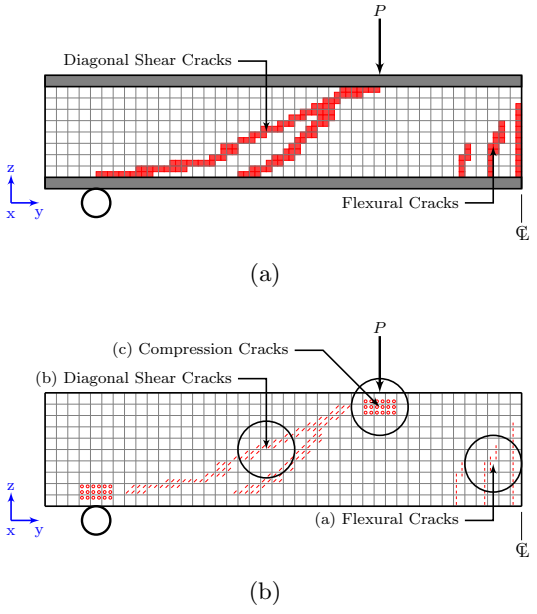

FIGURE 8.12: Virtual techniques to demonstrate the cracks of a concrete beam (a) the principal tensile strain contour plotting technique [modified from 15], and (b) the smeared cracking technique [modified from 124]

[11] cited by Kachlakev et al. [124]

8.3 Evaluation of the Performance of the Proposed Shear Connector

In this section, the performance of the SCS sandwich beam with variable patterns of inclined shear connector was evaluated. The configuration of the core with and without shear connector was as shown in Fig. 8.13. They were set to evaluate the contribution of each pattern of the shear connector to the strength behaviour and the cracking development of the concrete core of a concrete-filled SCS sandwich beam. All geometric parameters were kept constant except the ratio of s_y/d. This parameter indirectly represents the angle of the inclined part of the shear connector which can vary from 0° to 90°. Here, s_y/d varies from 0 to 1.0; therefore, the angle of shear connector varies from 45° to 90°. Table 8.8 summarises the values of geometric parameters used in this section.

Table 8.8: Configuration of the case studies

Parameter	Case Study							Unit	Note
	SCS-NSC	SCS-SYD000	SCS-SYD025	SCS-SYD050	SCS-SYD075	SCS-SYD100	SCS-SYD050-A		
	Fig. 8.13(a)	Fig. 8.13(b)	Fig. 8.13(c)				Fig. 8.13(d)		
s_y/d	N/A	0.00	0.25	0.50	0.75	1.00	−0.50		
θ	N/A	90.0°	76.0°	63.4°	53.1°	45.0°	−63.4°		
b	200	200	200				200	mm	
t_t	12	12	12				12	mm	$t_t/t_b = 1$
t_b	12	12	12				12	mm	
k_{cb}	N/A	0.50	0.50				0.50		
t_c	N/A	12	12				12	mm	$t_c/t_b = 1$
s_c	600	600	600				600	mm	
f_c	N/A	300	250	200	150	100	200	mm	
h_c	400	400	400				400	mm	$h_c/b = 2$

It should be noted that the proposed Bi-CSC is reduced to a simplified pattern of a single-leg shear connector in the y-direction only. This model is used to understand the effect of the pattern of the single-leg shear connector first. A more complicated behaviour would occur in the situation of a concrete-filled SCS beam with all parts of the proposed Bi-CSC. Further investigation to understand its behaviour should therefore be carried out in the future. The reduced Bi-CSC topology with 90° single-leg shear connector may represent an equivalent 90° Bi-Steel connector with two numbers of bar diameter 27.6 mm arranged in the x-direction and spaced at $s_x = 100\ mm$ (see Fig. 8.5(b)). These Bi-Steel connectors are also repeated in the y-direction at an interval of $s_y = 600\ mm$.

8.3.1 Load-Deflection Relationship

Figure 8.14 presents the relationship between the applied load, P, and the vertical deflection at midspan of beam, Δ. The applied load P is normalised by the load P_c

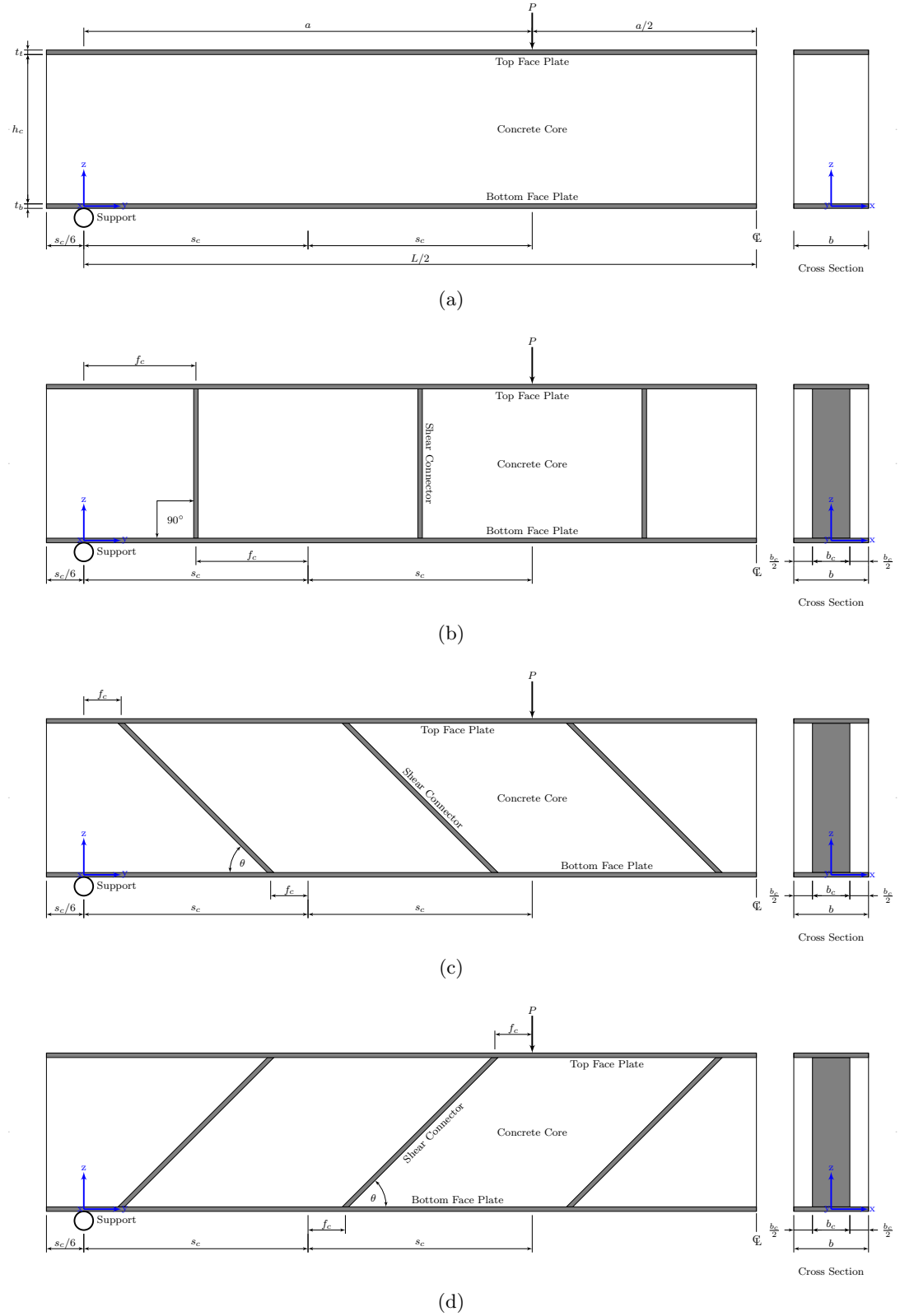

FIGURE 8.13: Configurations of concrete-filled steel-concrete-steel sandwich beam case studies (a) without shear connector, (b) with vertical shear connectors, (c) with inclined shear connectors, and (d) with inclined shear connectors (reverse direction)

and the deflection Δ is also normalised by the deflection Δ_c. Here, the load P_c is the possible maximum load which can be applied to the beam ID SCS-NSC before ANSYS stops running due to non-convergence solution. The deflection Δ_c is the response at the applied load P_c.

It can be seen from Fig. 8.14 that the response of the SCS beams are the same in the range of applied load $0 \leq P/P_c \leq 1.00$ for all cases except for the beam ID SCS-SYD050-A (a particular case of a beam with inclined shear connectors). Beyond this point, the response of the beams is still similar with approximately the same load-deflection relationship.

At the point of $P/P_c = 1.00$, the beam ID SCS-NSC (the beam without any shear connector) reaches its maximum strength. In the beam ID SCS-SYD000 (the beam with vertical shear connector), more applied load P/P_c can be obtained before reaching its maximum strength at $P/P_c = 1.03$. A remarkable increasing load can be found beyond this point for the remaining cases, i.e., the beam with inclined shear connector where $0.25 \leq s_y/d \leq 1.00$. The maximum load P/P_c applied to the beam ID SCS-SYD025 and SCS-SYD100 are 1.26 and 1.50, respectively. The maximum load P/P_c applied to the remaining cases are between 1.26 and 1.50. For the beam ID SCS-SYD050-A, the response of beam is different from those previously mentioned. The maximum load P/P_c applied to the beam equal to 1.00 – the maximum load of the beam ID SCS-NSC – with a bit more deflection Δ/Δ_c compared with the beam ID SCS-NSC.

The load-deflection response of the beam, as presented in Fig. 8.14, may imply that the beam without shear connector and the beam with shear connector in any alignment pattern perform in a similar manner up to the point that the beam with no shear connector reaches its maximum strength. In this range, there is no contribution provided by the shear connector regardless of orientation; the strength of the beam is dominated by the concrete only. After the concrete fails, the strength of the beam with shear connectors is further enhanced by the shear connector. The beam can then withstand more applied load P/P_c. Considering the SCS beam with shear connectors, it is found that the strength of the beam in terms of the applied load P/P_c varies according to the alignment pattern of shear connector.

Figure 8.15 presents the relationship between the applied load P/P_v and the angle θ of shear connector. In this figure, the applied load P is normalised by the load P_v where the load P_v is the maximum applied load of the beam with vertical shear connectors (the beam ID SCS-SYD000).

By comparison, it is found that the strength of the beam steadily increases from 0.00 to 1.38 when the angle θ reduces from 90° ($s_y/d = 0.00$) to 63.4° ($s_y/d = 0.50$). Then,

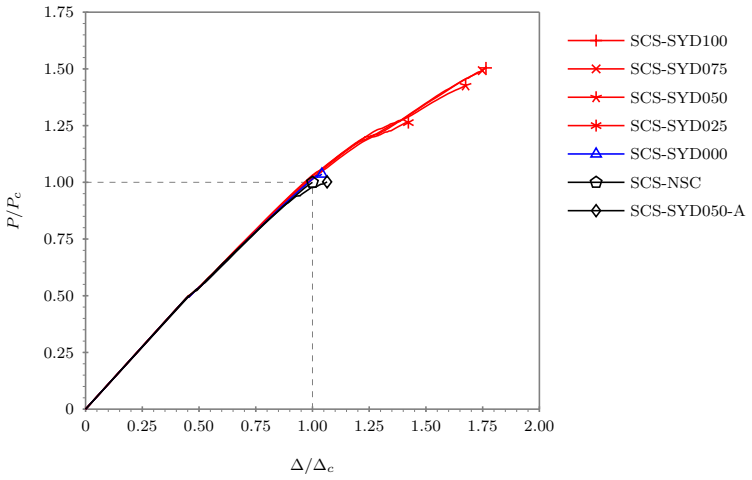

FIGURE 8.14: Relationship between the applied load P/P_c and the corresponding displacement Δ/Δ_c

the strength of beam gradually rises from 1.38 to 1.44 when the angle θ reduces from 63.4° ($s_y/d = 0.50$) to 53.1° ($s_y/d = 0.75$). Beyond this point, only the small amount of increased strength of beam is obtained before reaching the maximum value of 1.45 at the angle θ equals 45° ($s_y/d = 1.00$).

As can be seen from Fig. 8.15, the maximum strength of the SCS beam with the shear connector can be obtained if the angle θ equals 45° ($s_y/d = 1.00$). At this point, the strength of the SCS sandwich beam with 45° inclined shear connector is 145% stronger than of the SCS sandwich beam with 90° vertical shear connector. This behaviour is similar to the behaviour of the simple mechanism of concrete beam with inclined shear reinforcements as previously demonstrated in Fig. 8.7 in which the maximum strength at the diagonal crack section can be obtained if the angle θ of the transverse shear reinforcement equals 45°. At this point, the maximum strength of the beam with a 45° inclined shear reinforcement is 141% stronger than of the beam with a 90° vertical shear reinforcement. It may imply, therefore, that the concept of inclined shear reinforcement can also be introduced to the SCS sandwich beam.

As previously mentioned, the reduced Bi-CSC topology with 90° single-leg shear connector referred to here as the beam ID SCS-SYD000 may represent an equivalent 90° Bi-Steel connector with a group of bars diameter 27.6 mm spaced at $s_x = 100$ mm and $s_y = 600$ mm. This equivalent Bi-Steel topology provides the transverse shear strength, V_{BS}, obtained from the formula presented in Table 8.1 of 262 kN. Therefore, the reduced Bi-CSC topology with 45° single-leg shear connector referred to here as the beam ID SCS-SYD100 provides a transverse shear strength, V_{BS}, 1.41 times that of the Bi-Steel equivalent.

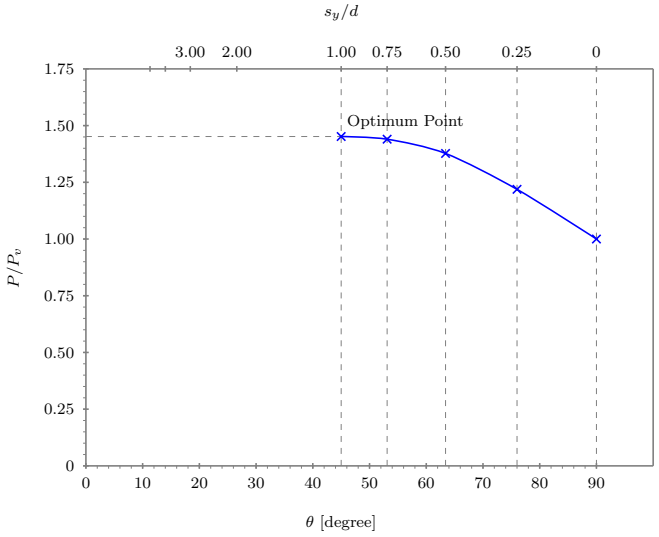

FIGURE 8.15: Relationship between the applied load P/P_v and the angle θ of the shear connectors

8.3.2 Development of Concrete Cracks

Figures 8.16 to 8.21 present the cracking development of the concrete core for each SCS sandwich beam recorded at each applied load step from the ANSYS software. Here, the cracking signs of the concrete elements (SOLID65) obtained from the ANSYS outputs are calculated at integration points of the elements and interpreted as previously mentioned in Sec. 8.2.5.2.

In general, the cracking patterns of the concrete core for all beams are similar at the initial period of applying load P/P_c from 0 to 1.0. The initial flexural cracks occur first at the midspan of the beam at an applied load $P/P_c = 0.50$. Then, the initial diagonal shear cracks occur near the support and below the point of the applied load. These cracks initially begin from the interface between the concrete core and the bottom face plate and move upward to the top face plate.

In cases of the SCS beam without shear connector (beam ID SCS-NSC) and with vertical shear connector (beam ID SCS-SYD000), the diagonal shear crack can quickly develop and then stop before passing the neutral axis of the SCS beam. At this stage, these two SCS beams are assumed to have failed at an applied load P/P_c about 1.0.

In case of the SCS beam with inclined shear connectors (beam ID SCS-SYD025 to SCS-SYD100), the diagonal shear cracks can further develop when a higher load P/P_c is applied. As can be seen from Figs. 8.18 to 8.21, a few more diagonal crack lines can occur and further develop above the neutral axis. In the extreme case of the beam with 45° angle shear connector (beam ID SCS-SYD100), the diagonal shear crack can develop upward to the top face plate near the point of applied load.

In addition to the flexural and diagonal shear cracks, numerous cracks can be found on the left side of the first two shear connectors near the support of the beam when an applied load P/P_c is higher than 1.0. This cracking pattern may demonstrate that the concrete core is confined by the shear connector plates so that the concrete can develop crushing failure in the y-direction instead of tensile cracking failure in the same direction, as can be seen from numerous cracking indicators appearing in circular shape.

8.4 Concluding Remark

The diagonal shear crack of the concrete-core of the concrete-filled SCS sandwich beams were reviewed and demonstrated using the fundamental concept of reinforced concrete beam. The transverse shear strength of the cross section of a concrete-filled Bi-Steel sandwich beam was also reviewed and demonstrated its limitations. The alternative solution to overcome the limitations of state-of-the-art Bi-Steel sandwich beam was proposed.

The numerical study of the concrete-filled SCS sandwich beams with various shear connector patterns was carried out using 3D FE models. A four-point-loaded concrete-filled SCS sandwich beam was modelled and analysed using the FE software ANSYS Release 11.0 [123]. The full composite of steel-concrete interaction was assumed. The analysis was performed in non-linear mode with non-linear stress-strain relationships for steel and concrete. The presented FE models were used to evaluate the performance of the proposed shear connector pattern. The load-deflection relationship of the beam and the crack development of the concrete core of beam were obtained from the FE model. The smeared-cracking technique was used to demonstrate the development of cracks in the concrete core.

It was found that the response of the load-deflection of the concrete-filled SCS sandwich beam with various shear connector patterns was similar when the applied load P/P_c was between 0 and 1.0. Beyond the point of $P/P_c = 1.0$, the response of the beam varied according to the angle θ of shear connector. The ultimate applied load P/P_c increased where the angle θ of shear connector decreased. It was found that the response of the relationship between ultimate applied load P/P_c and the angle θ of shear connector was similar to the fundamental concept of a reinforced concrete beam. The optimum applied load P/P_c occurred at $\theta = 45°$, i.e., at 45° inclined shear connector pattern.

It was also found that the evolution of the crack in the concrete core with various shear connector patterns was similar from the beginning of applied load until the initial flexural crack occurring at an applied load P/P_c about 0.5. Beyond the initial flexural crack,

however, the cracking pattern varied according to the pattern of the shear connector. The diagonal shear crack of the concrete-filled SCS sandwich beam with inclined shear connector was further developed than of the beam with vertical shear connector. The extreme case where the diagonal shear crack can develop through the depth of concrete core was found at 45° inclined shear connector pattern. Numerous cracks were also found on the left-side of inclined shear connectors only.

By comparison, it was found that the responses of the concrete-filled and the unfilled SCS sandwich beams, previously mentioned in Chapters 4 to 7, were similar. The responses of both the unfilled and concrete-filled SCS sandwich beams varied with the alignment pattern of the Bi-CSC – the shear connectors. The optimum advantage of the transverse shear stiffness of the unfilled SCS sandwich beam was found when the inclined parts of the proposed Bi-CSC align at an angle about 45°. The optimum advantage of the transverse shear strength of the concrete-filled SCS sandwich beam was also found when the inclined shear connectors align at an angle 45°. This may imply that creating the Bi-CSC with a 45° pattern can provide a great advantage in transverse shear stiffness and strength in both the unfilled and concrete-filled SCS sandwich beams.

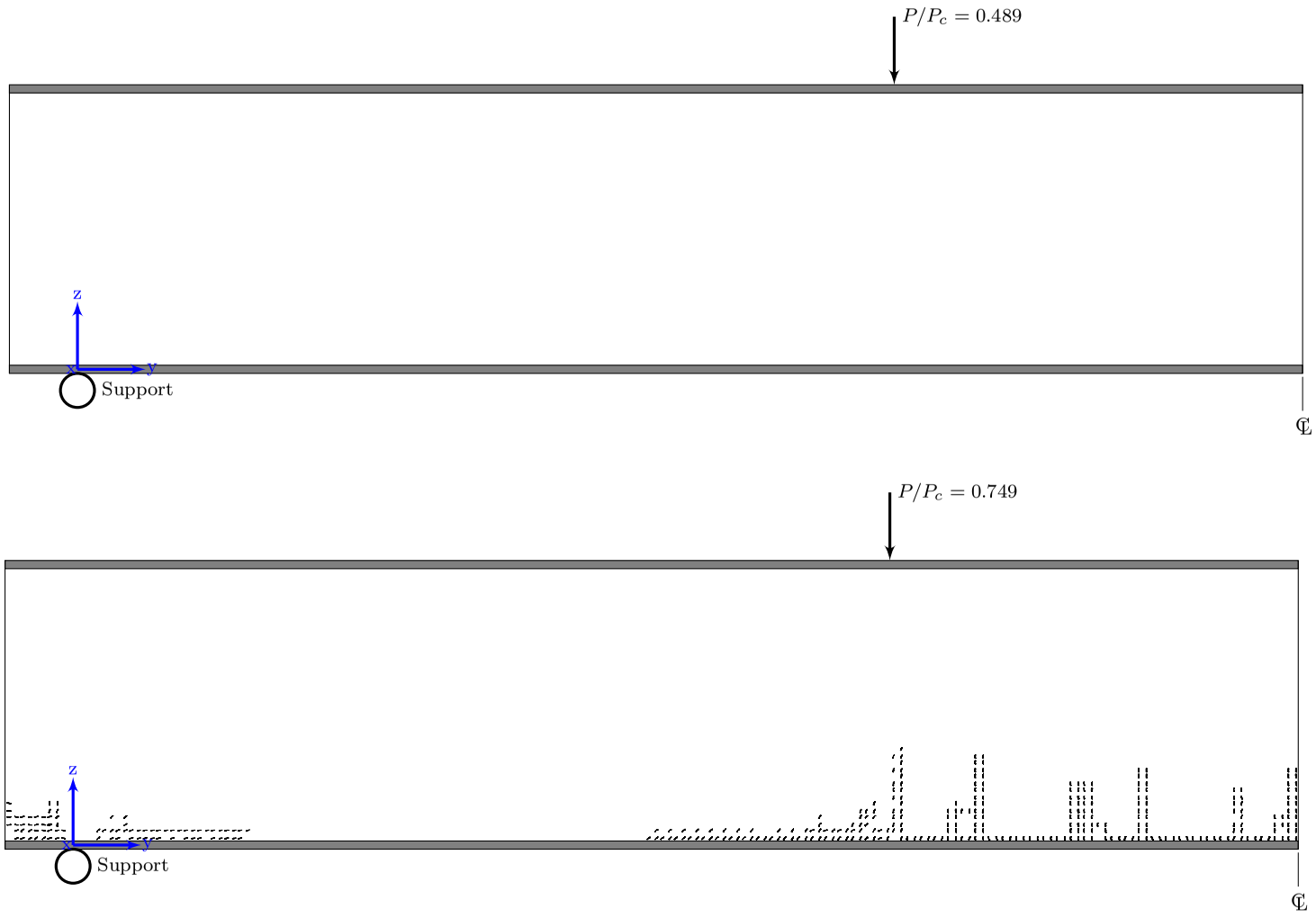

FIGURE 8.16: Crack development in the concrete core of the concrete-filled sandwich beam case study ID: SCS-FPB-NSC

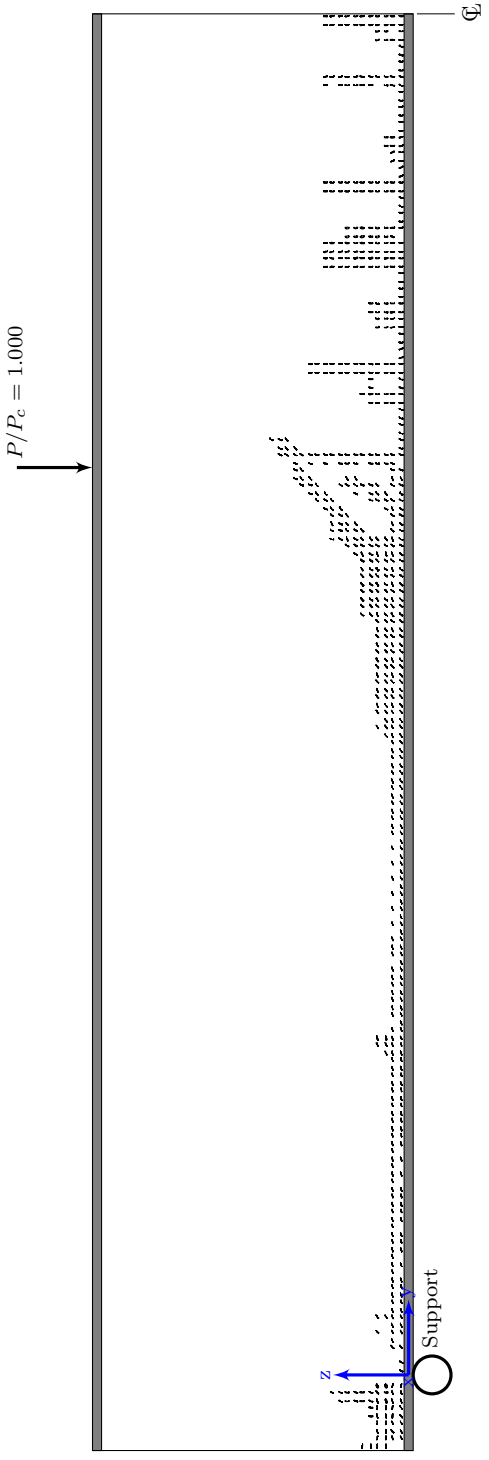

FIGURE 8.16: Crack development in the concrete core of the concrete-filled sandwich beam case study ID: SCS-FPB-NSC (cont'd)

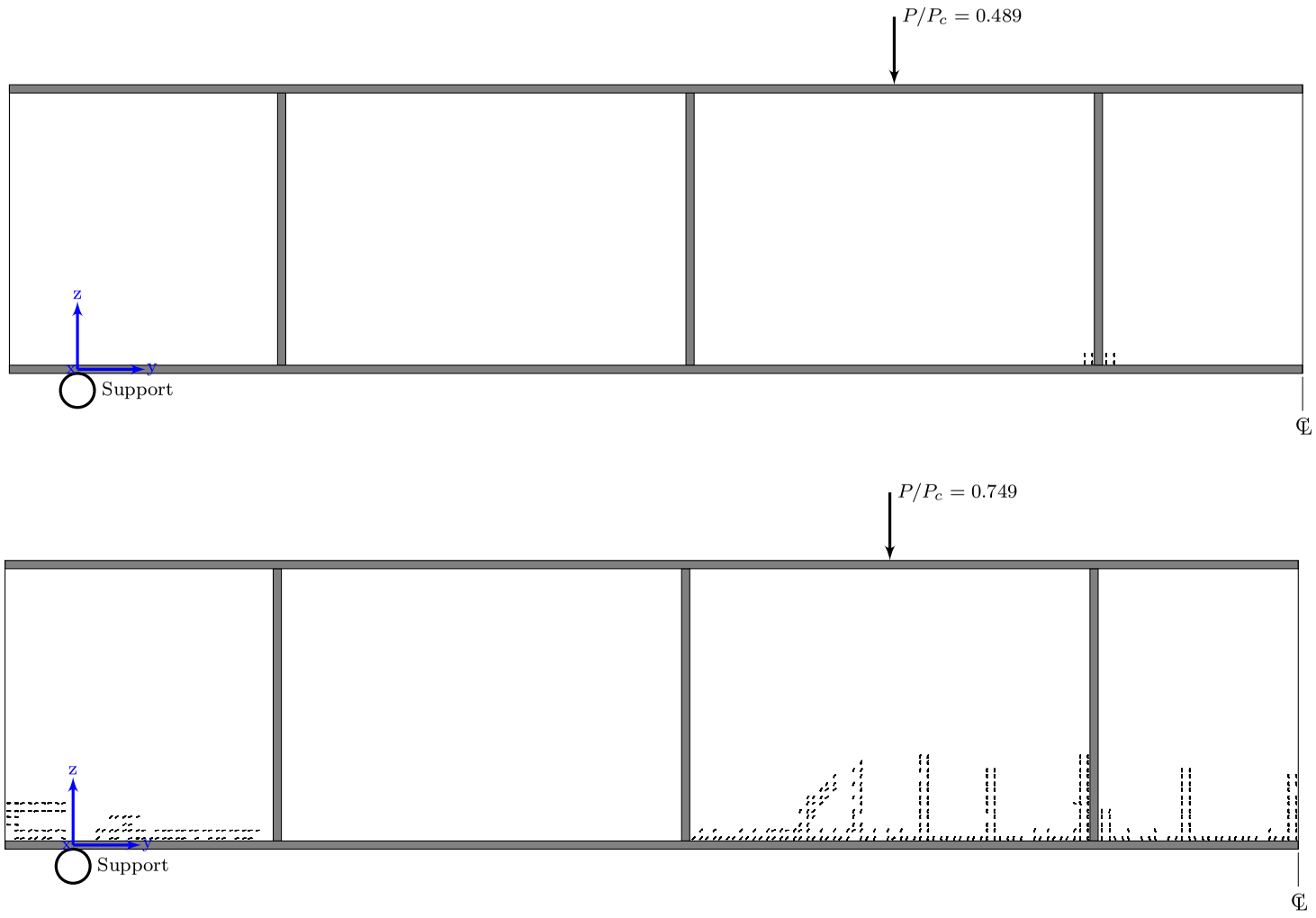

FIGURE 8.17: Crack development in the concrete core of the concrete-filled sandwich beam case study ID: SCS-FPB-SXD000

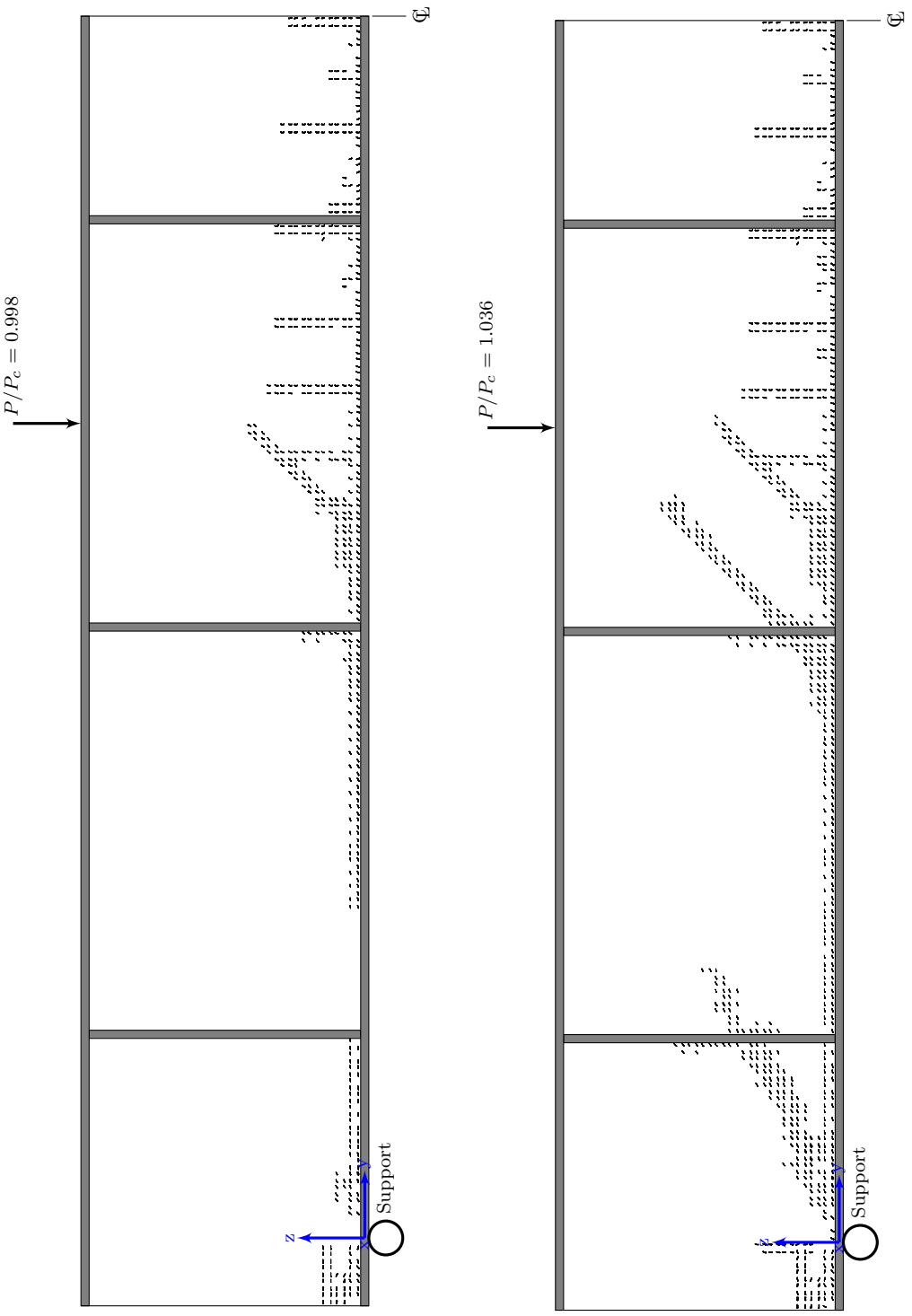

FIGURE 8.17: Crack development in the concrete core of the concrete-filled sandwich beam case study ID: SCS-FPB-SXD000 (cont'd)

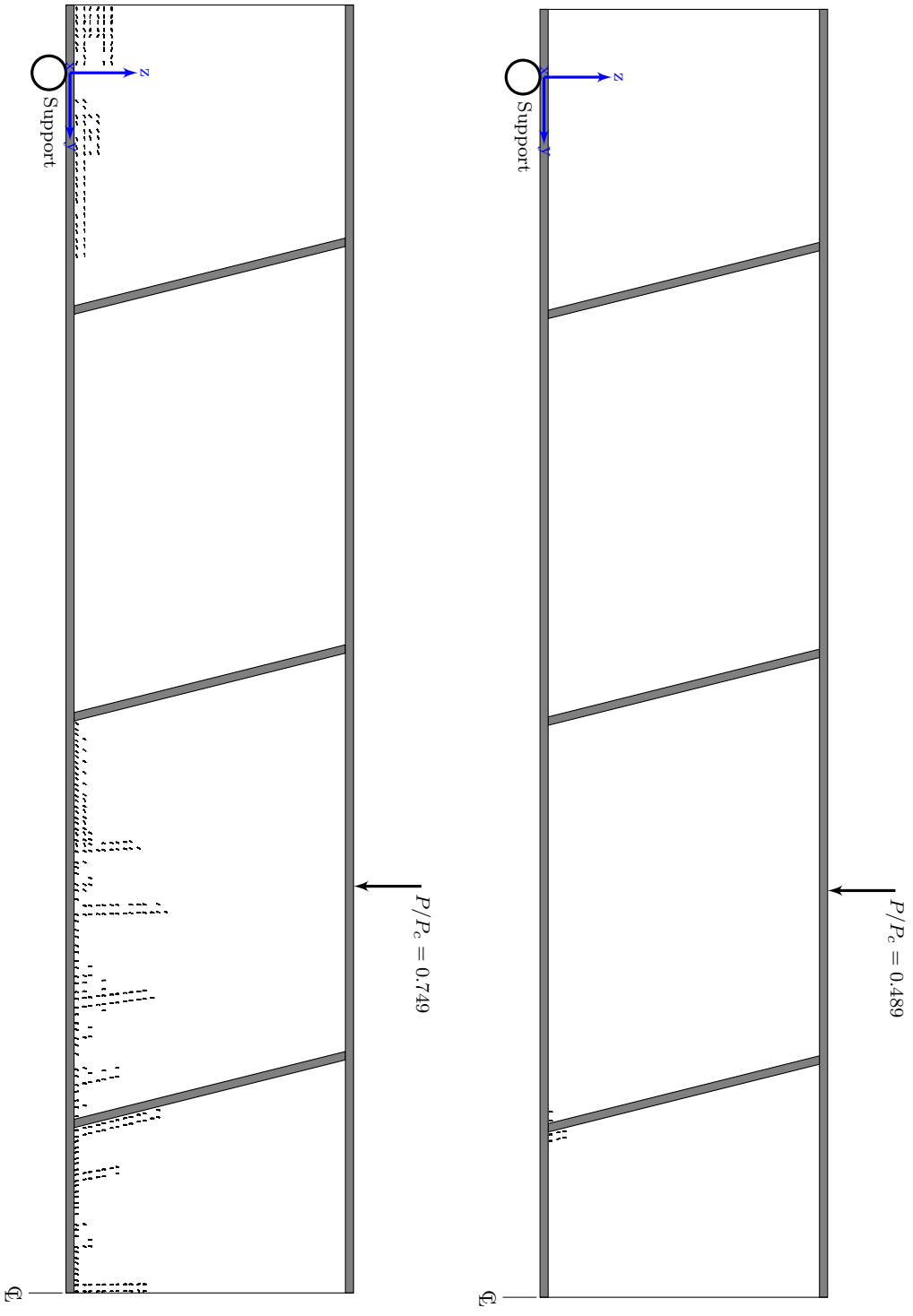

FIGURE 8.18: Crack development in the concrete core of the concrete-filled sandwich beam case study ID: SCS-FPB-SXD025

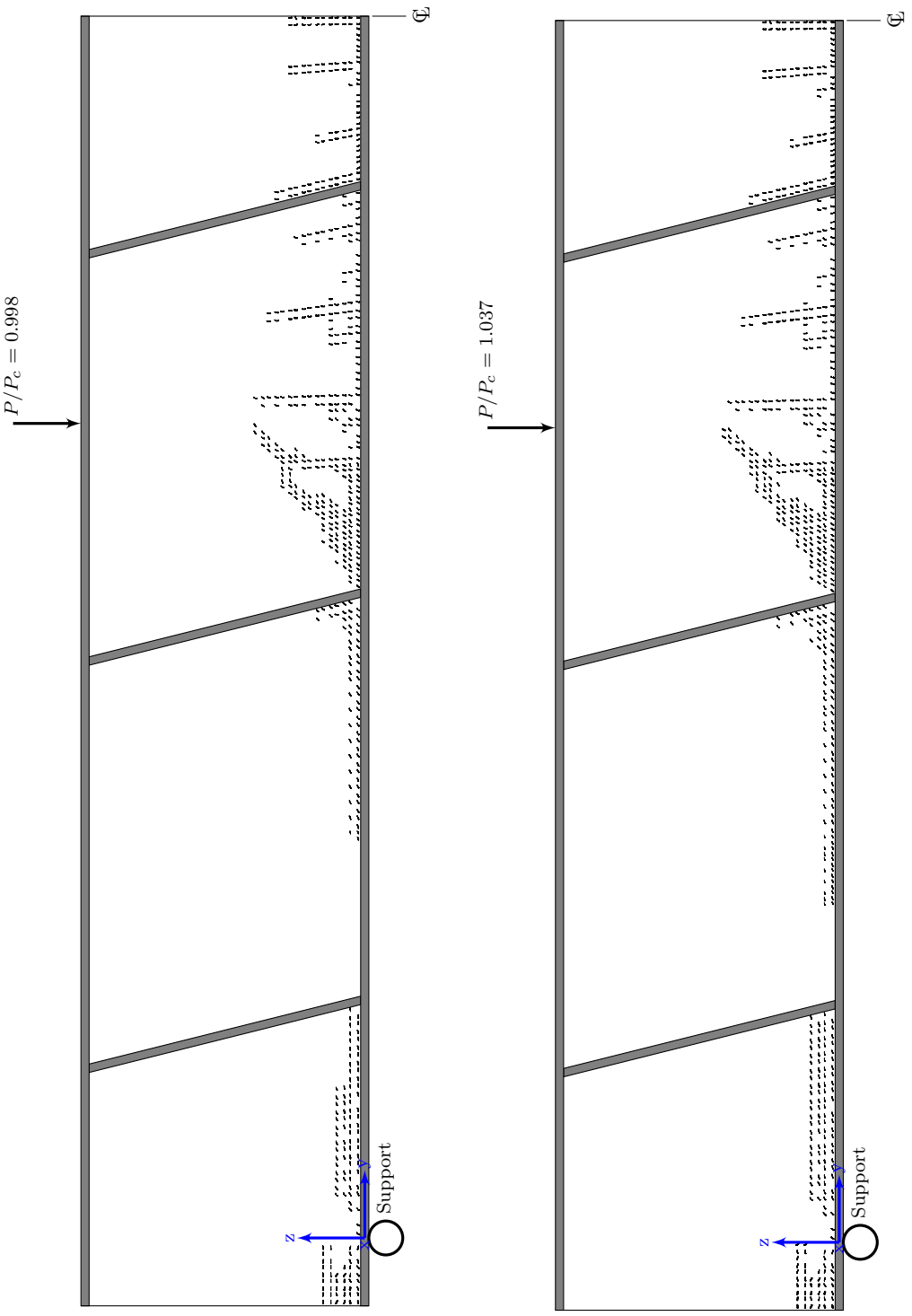

FIGURE 8.18: Crack development in the concrete core of the concrete-filled sandwich beam case study ID: SCS-FPB-SXD025 (cont'd)

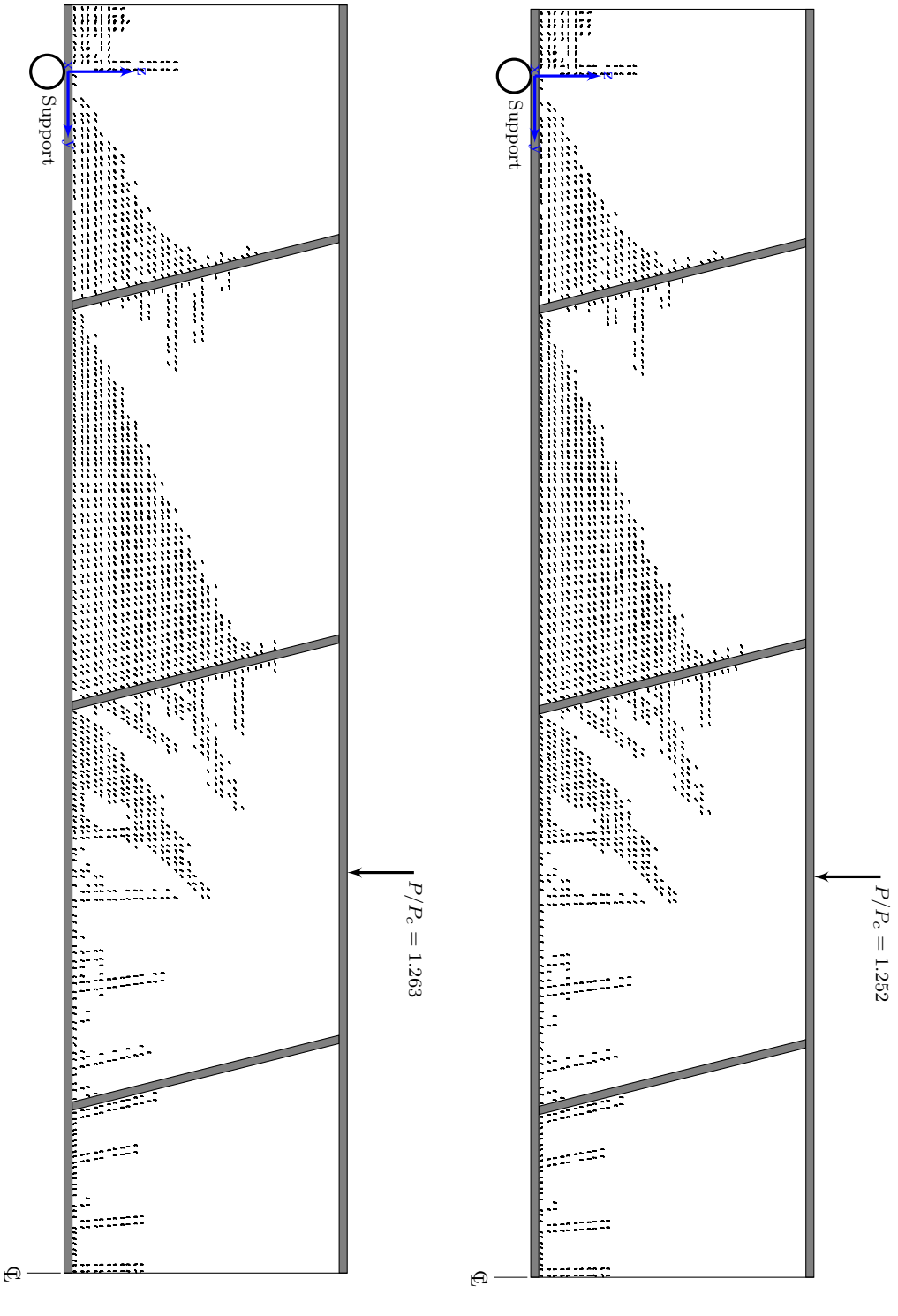

FIGURE 8.18: Crack development in the concrete core of the concrete-filled sandwich beam case study ID: SCS-FPB-SXD025 (cont'd)

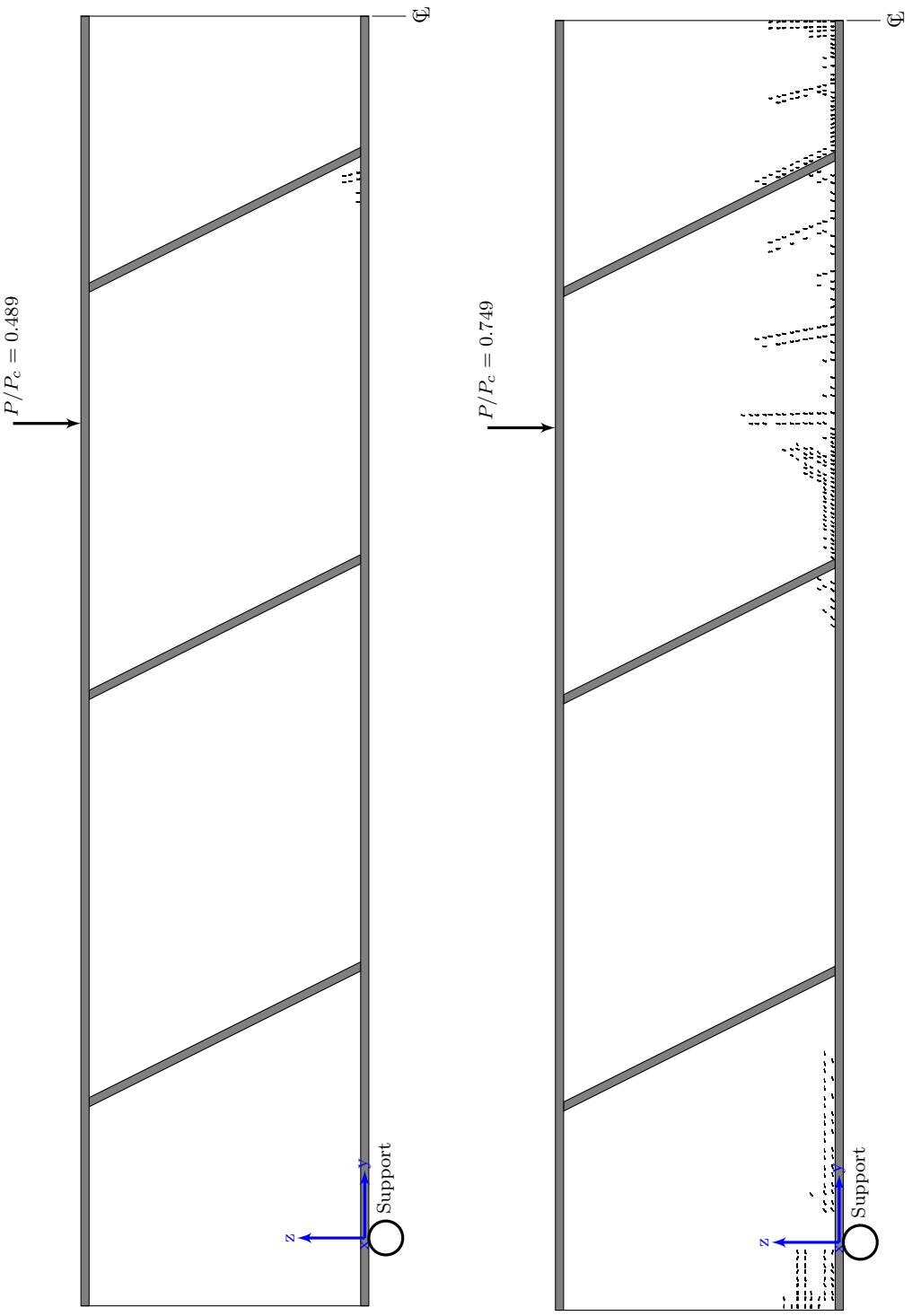

FIGURE 8.19: Crack development in the concrete core of the concrete-filled sandwich beam case study ID: SCS-FPB-SXD050

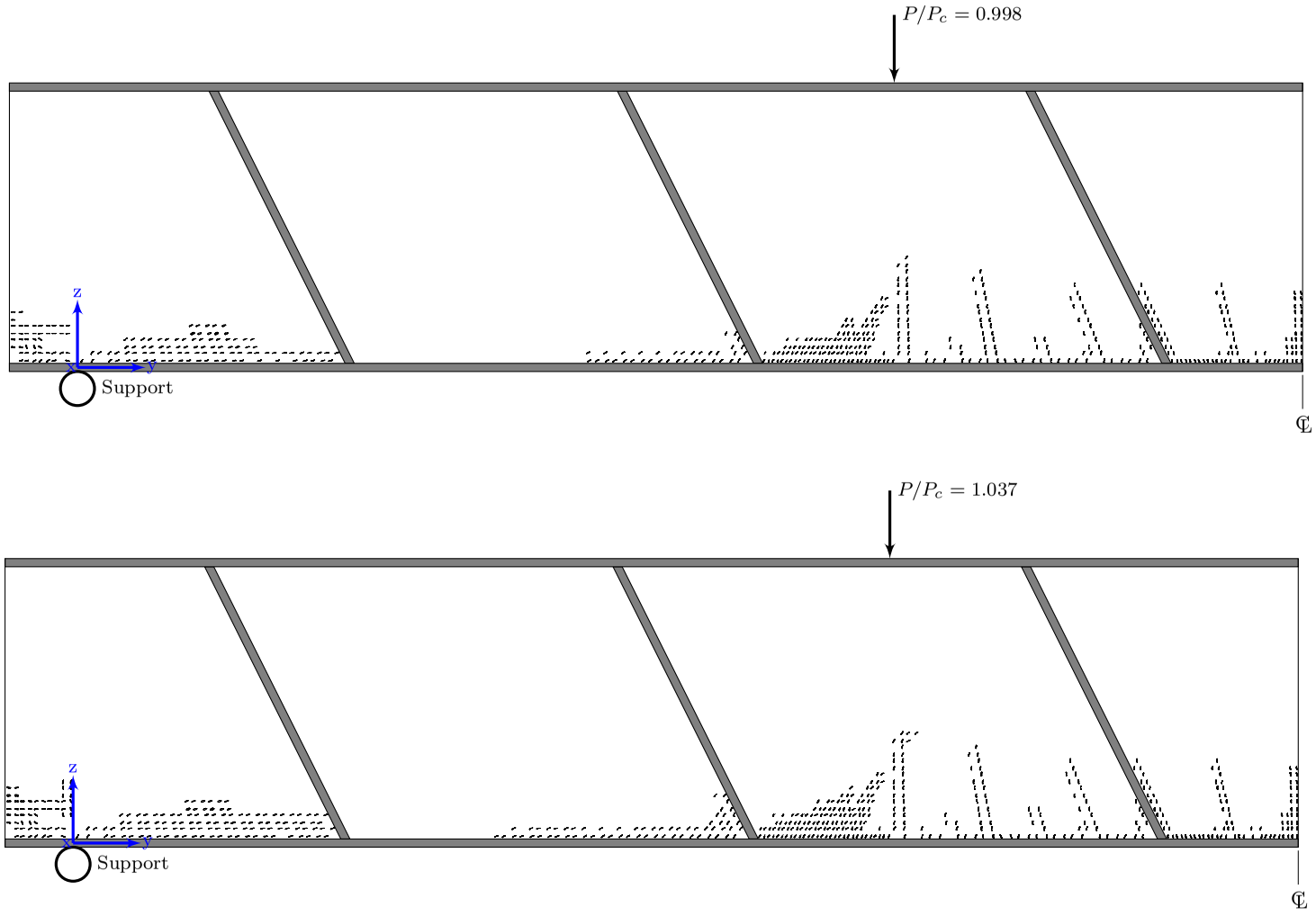

FIGURE 8.19: Crack development in the concrete core of the concrete-filled sandwich beam case study ID: SCS-FPB-SXD050 (cont'd)

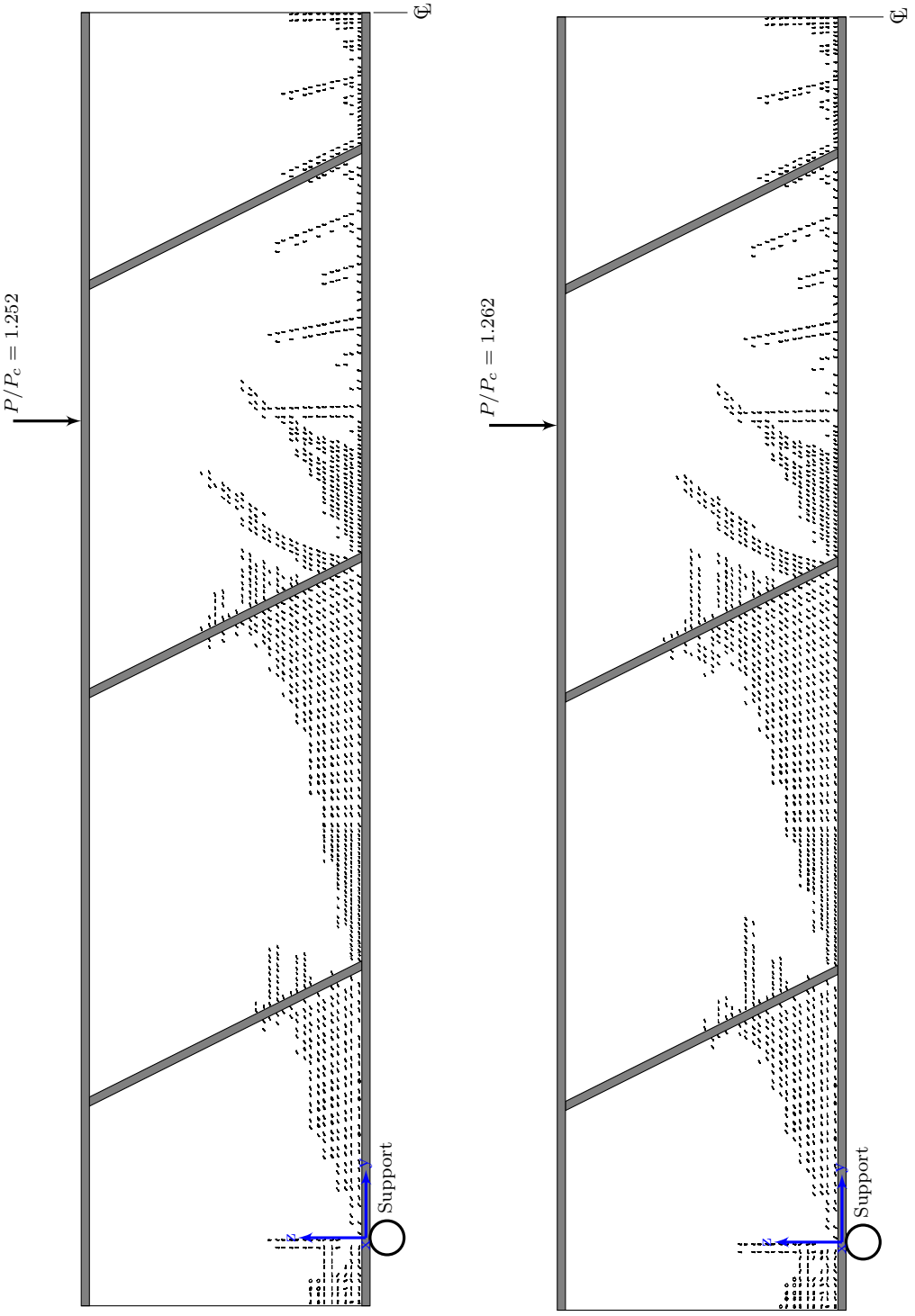

FIGURE 8.19: Crack development in the concrete core of the concrete-filled sandwich beam case study ID: SCS-FPB-SXD050 (cont'd)

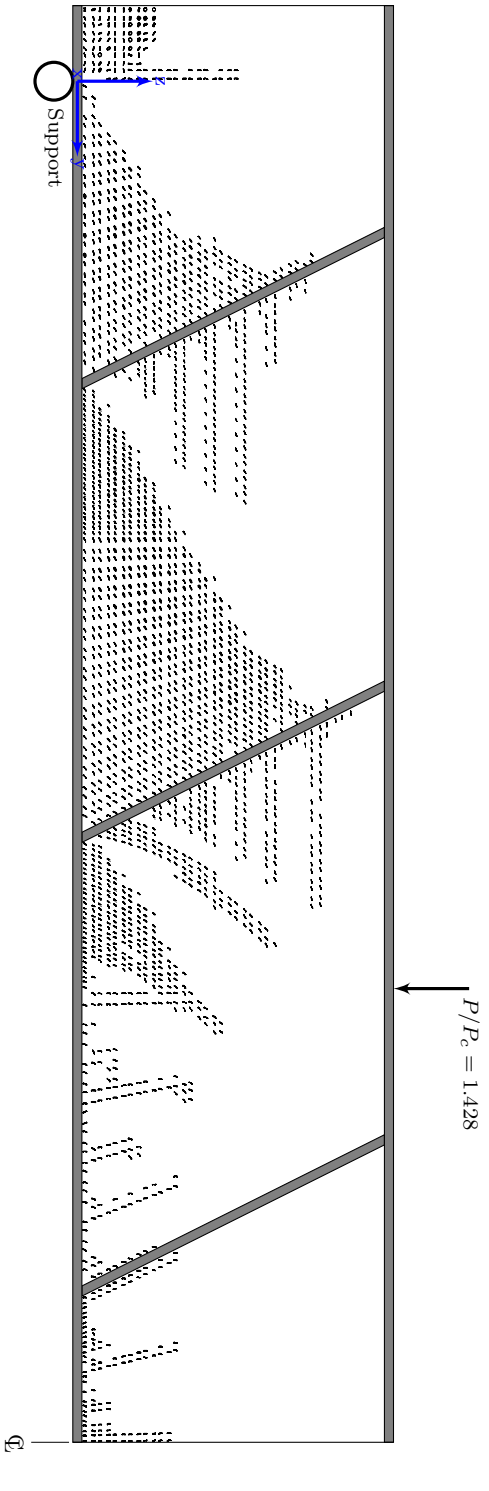

FIGURE 8.19: Crack development in the concrete core of the concrete-filled sandwich beam case study ID: SCS-FPB-SXD050 (cont'd)

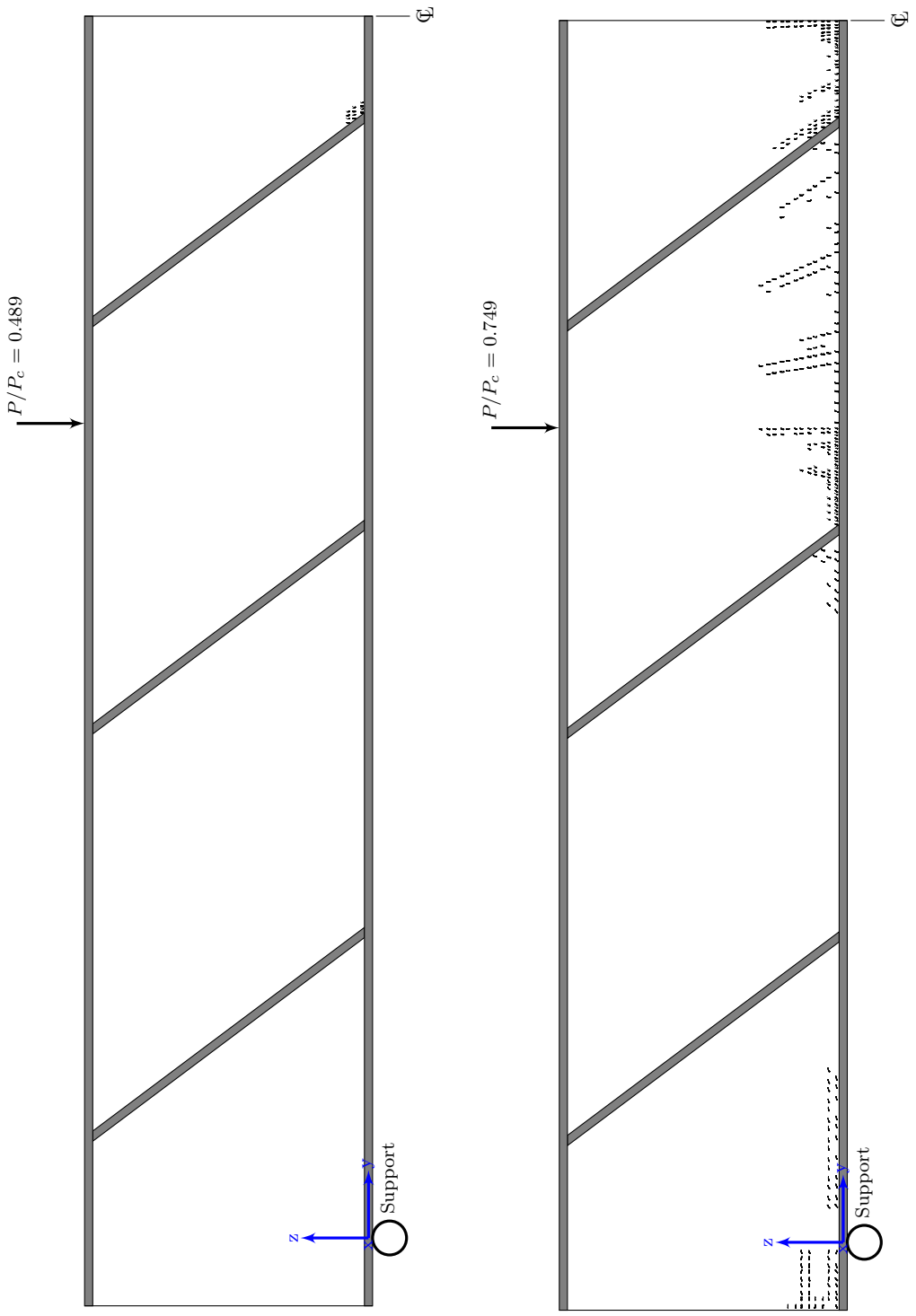

FIGURE 8.20: Crack development in the concrete core of the concrete-filled sandwich beam case study ID: SCS-FPB-SXD075

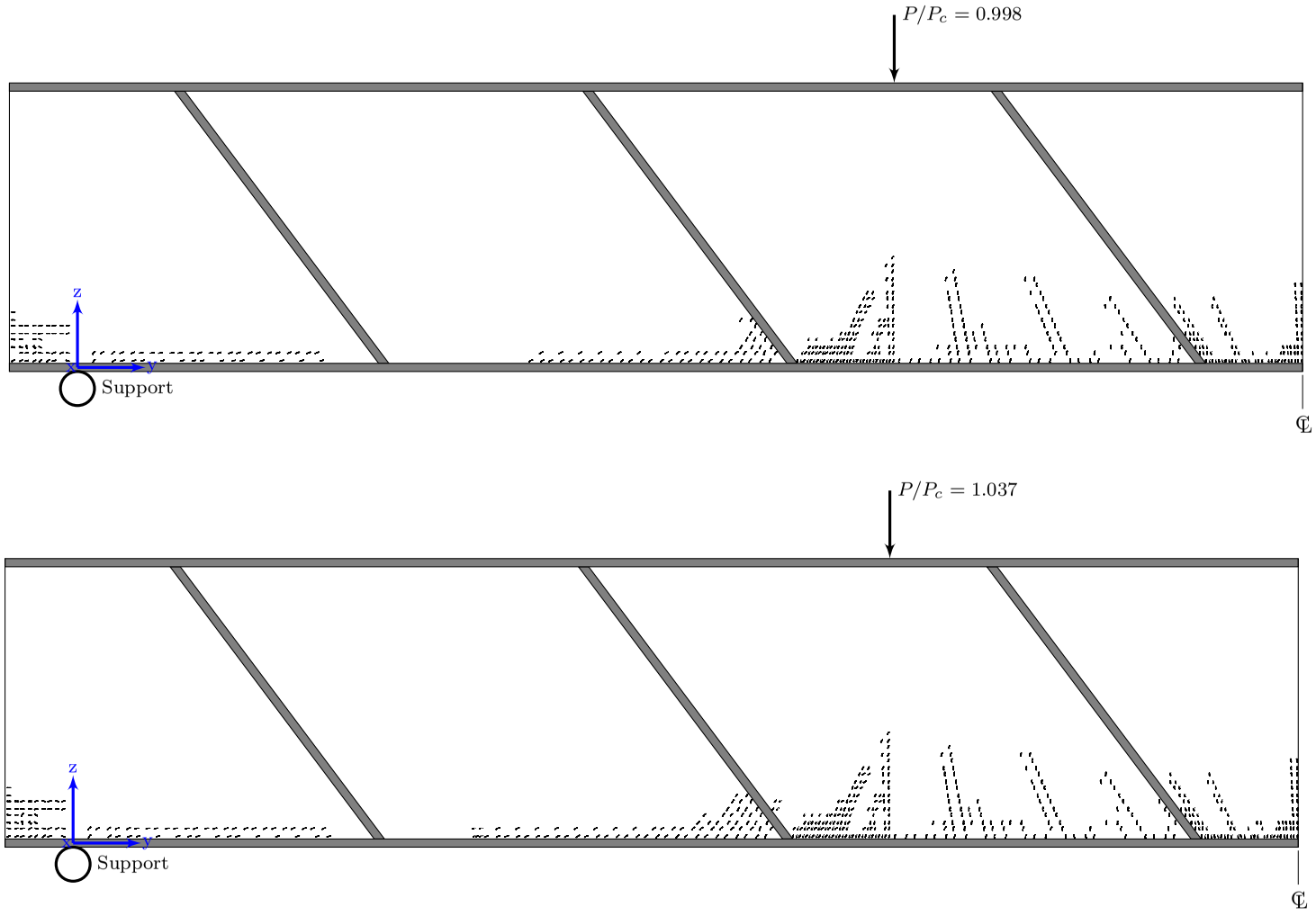

FIGURE 8.20: Crack development in the concrete core of the concrete-filled sandwich beam case study ID: SCS-FPB-SXD075 (cont'd)

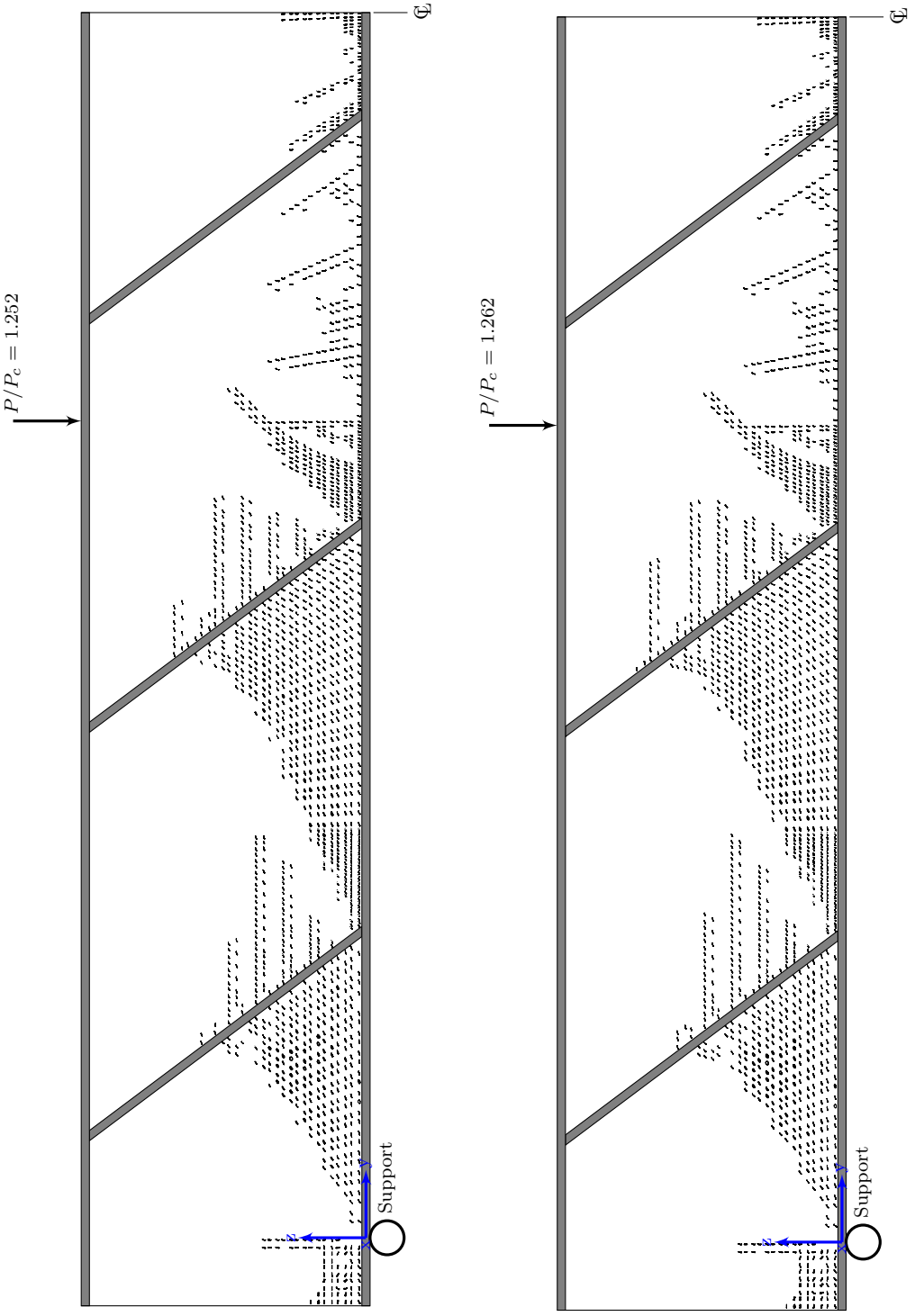

FIGURE 8.20: Crack development in the concrete core of the concrete-filled sandwich beam case study ID: SCS-FPB-SXD075 (cont'd)

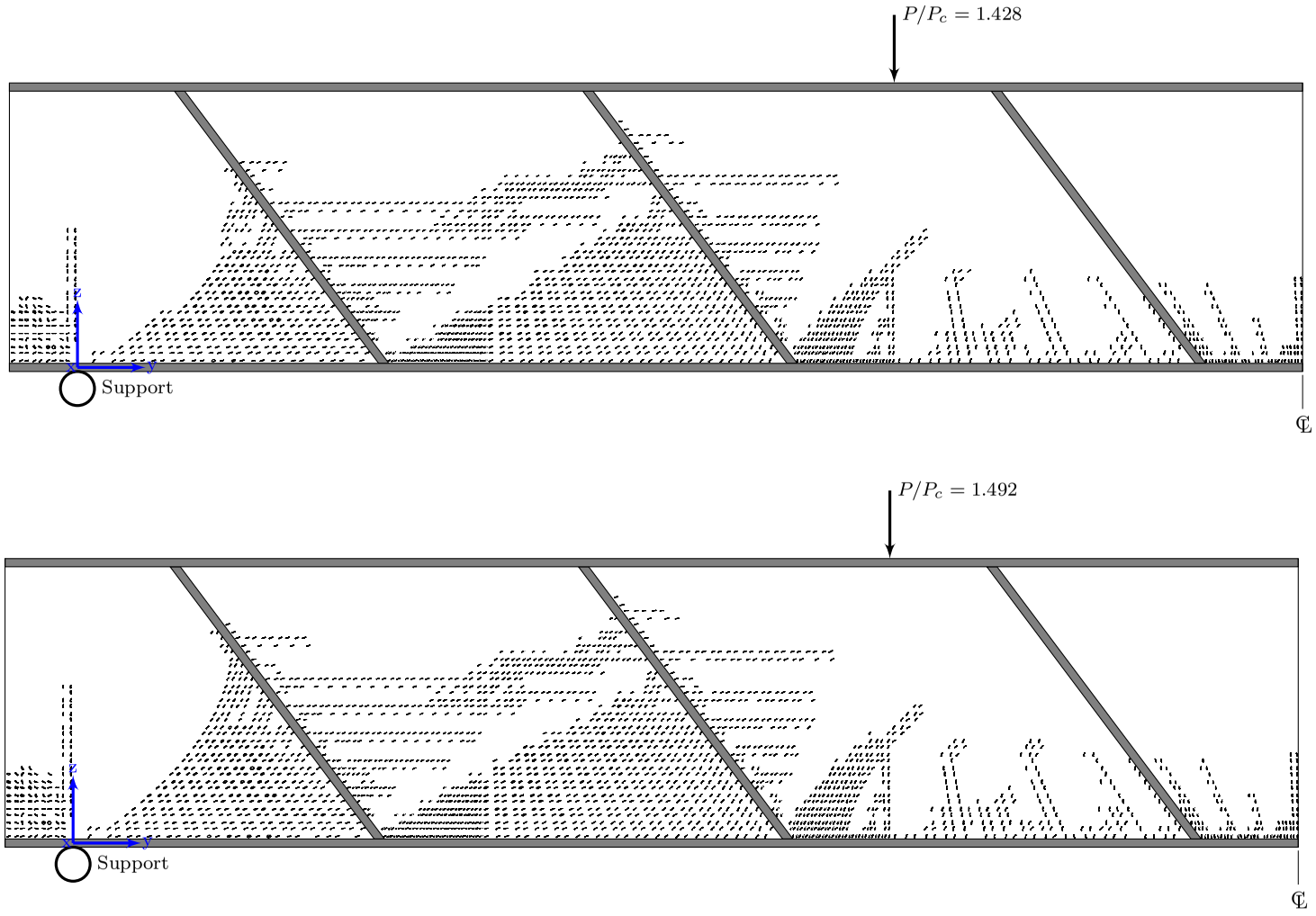

FIGURE 8.20: Crack development in the concrete core of the concrete-filled sandwich beam case study ID: SCS-FPB-SXD075 (cont'd)

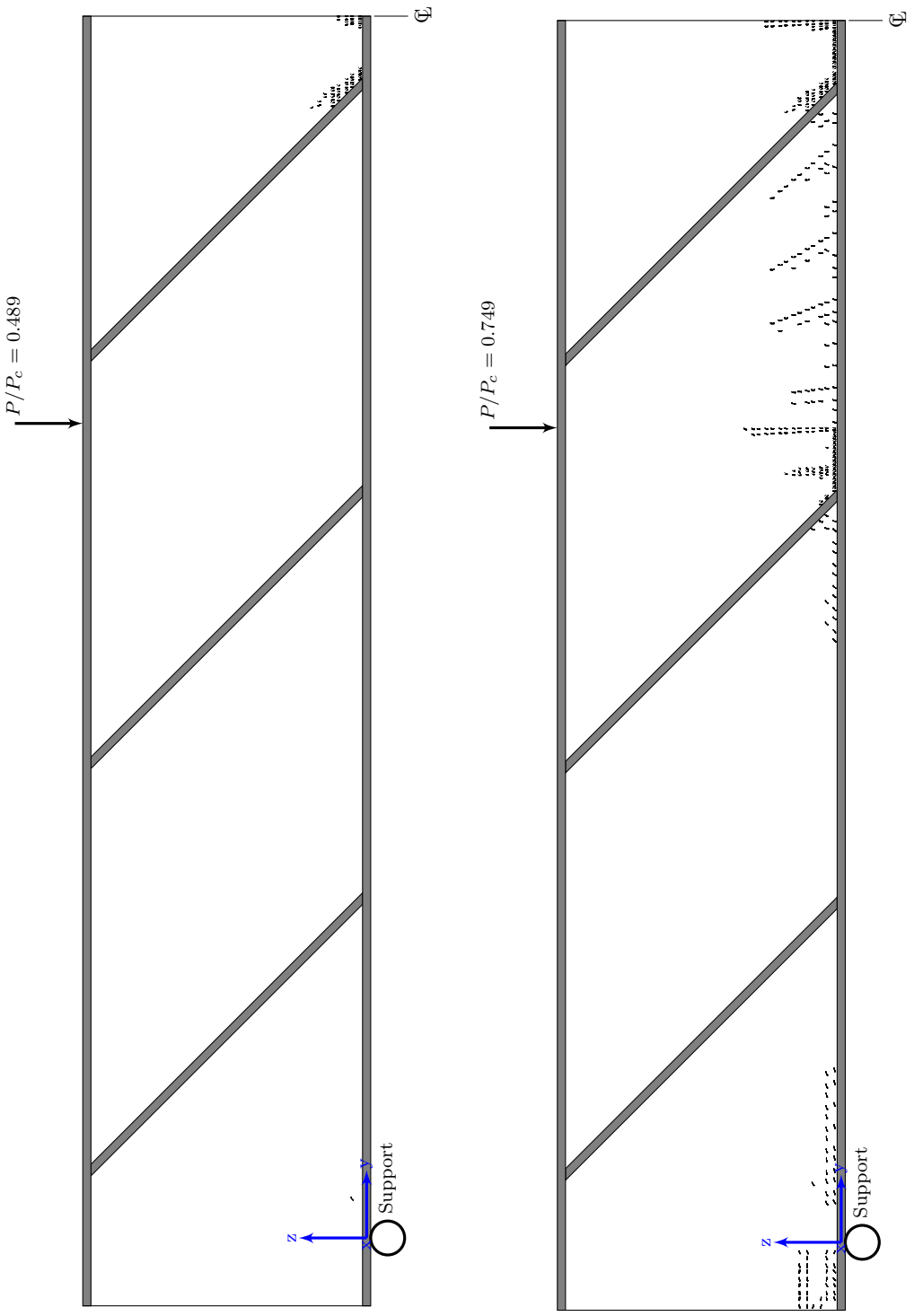

FIGURE 8.21: Crack development in the concrete core of the concrete-filled sandwich beam case study ID: SCS-FPB-SXD100

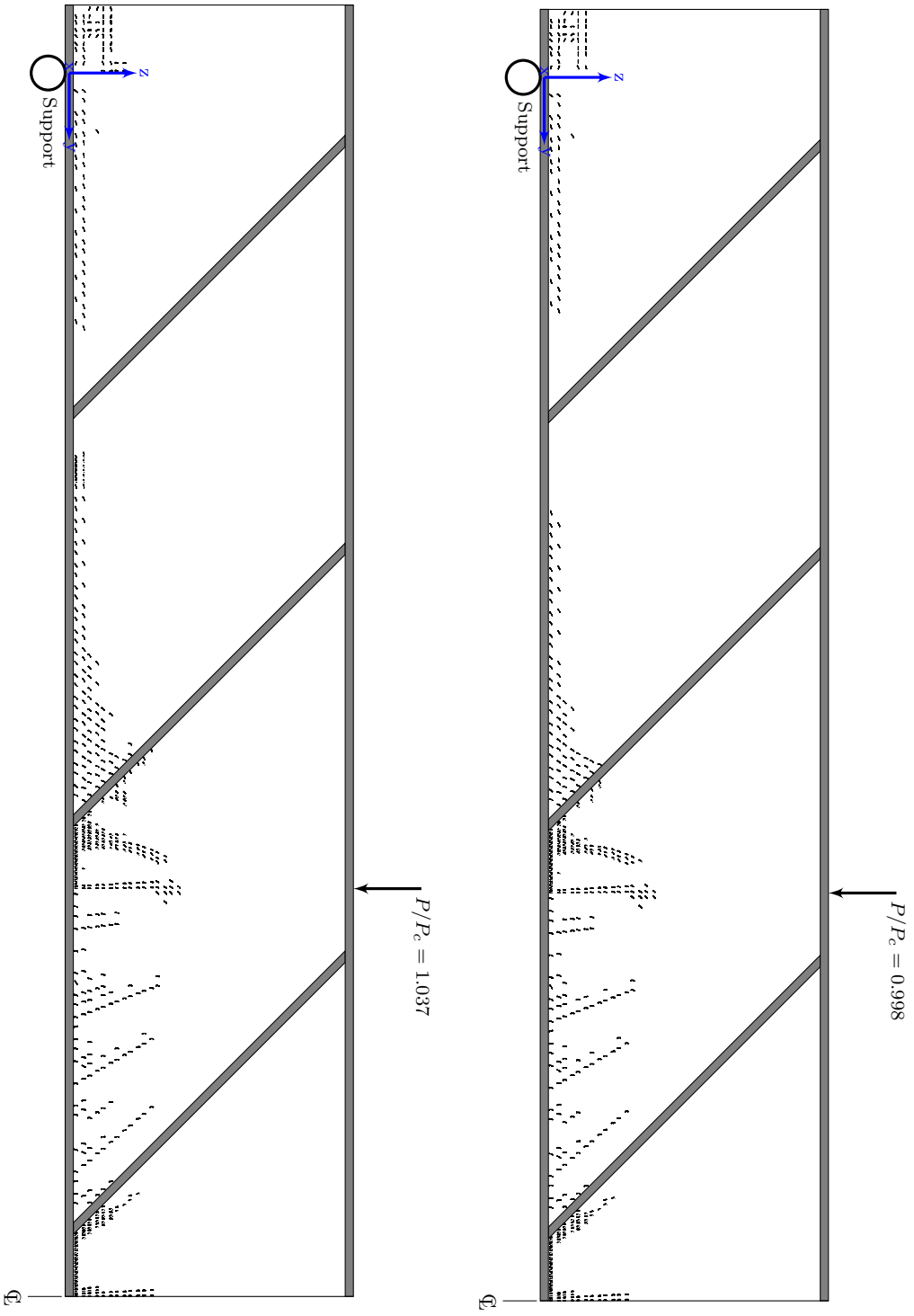

FIGURE 8.21: Crack development in the concrete core of the concrete-filled sandwich beam case study ID: SCS-FPB-SXD100 (cont'd)

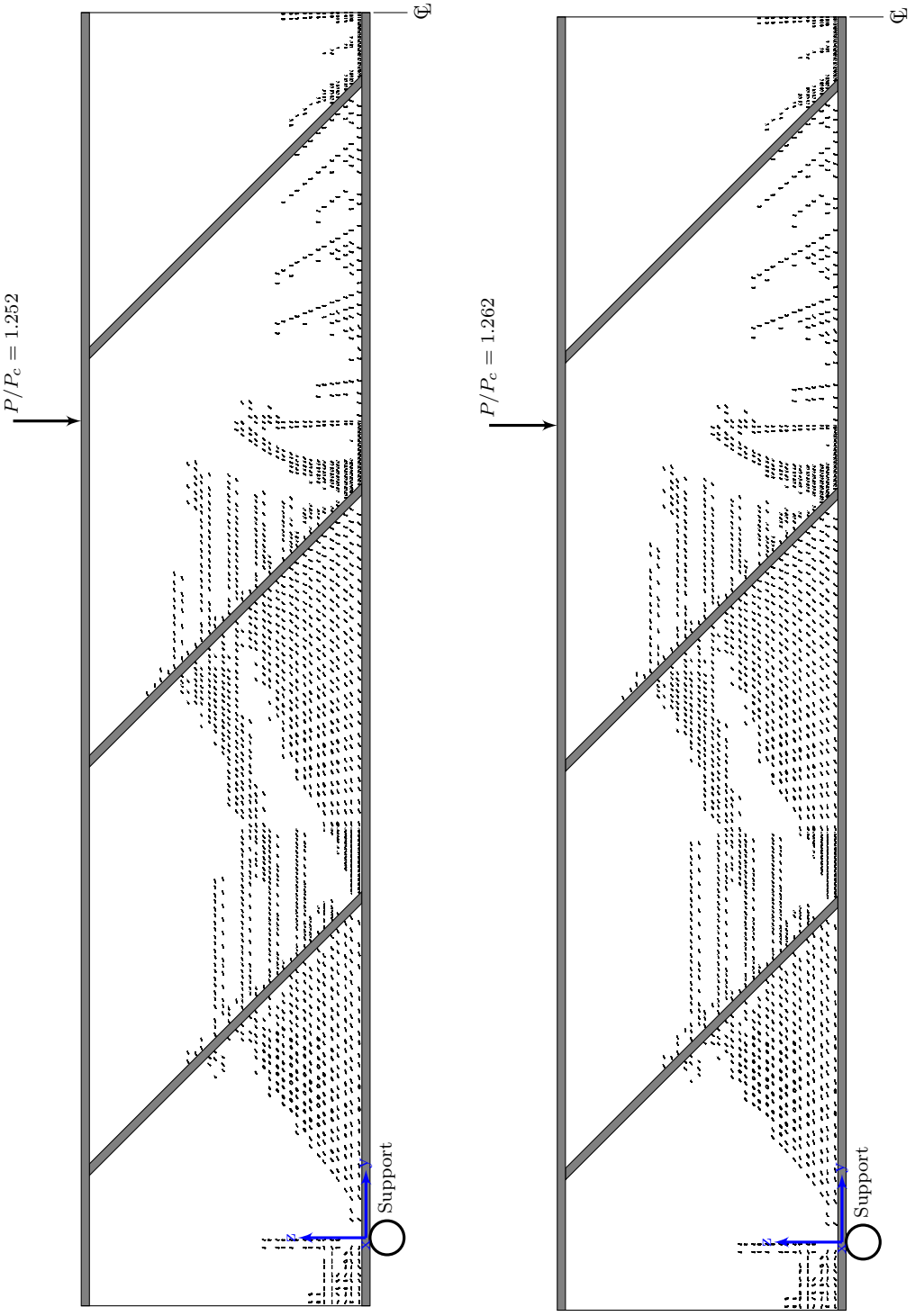

FIGURE 8.21: Crack development in the concrete core of the concrete-filled sandwich beam case study ID: SCS-FPB-SXD100 (cont'd)

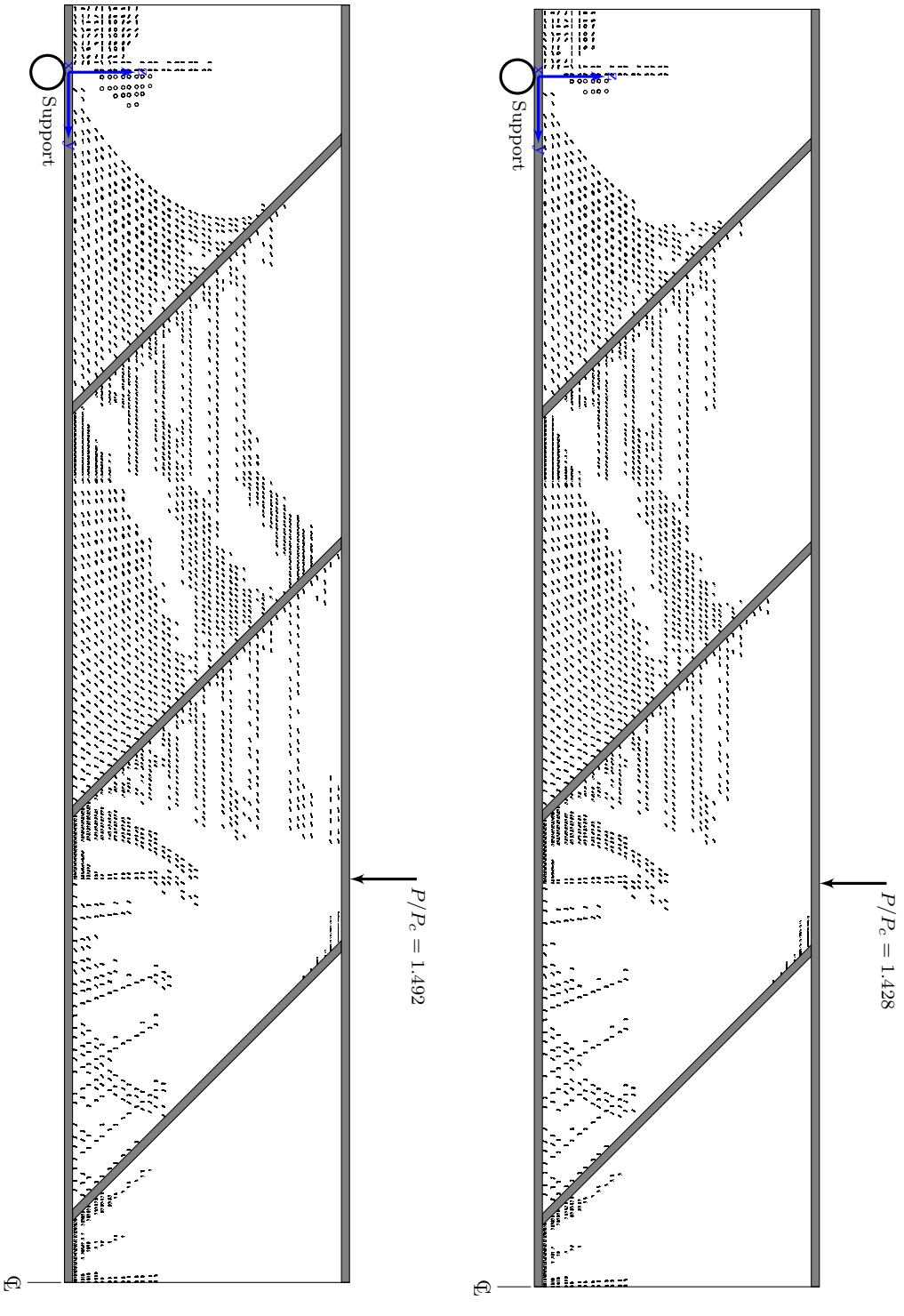

FIGURE 8.21: Crack development in the concrete core of the concrete-filled sandwich beam case study ID: SCS-FPB-SXD100 (cont'd)

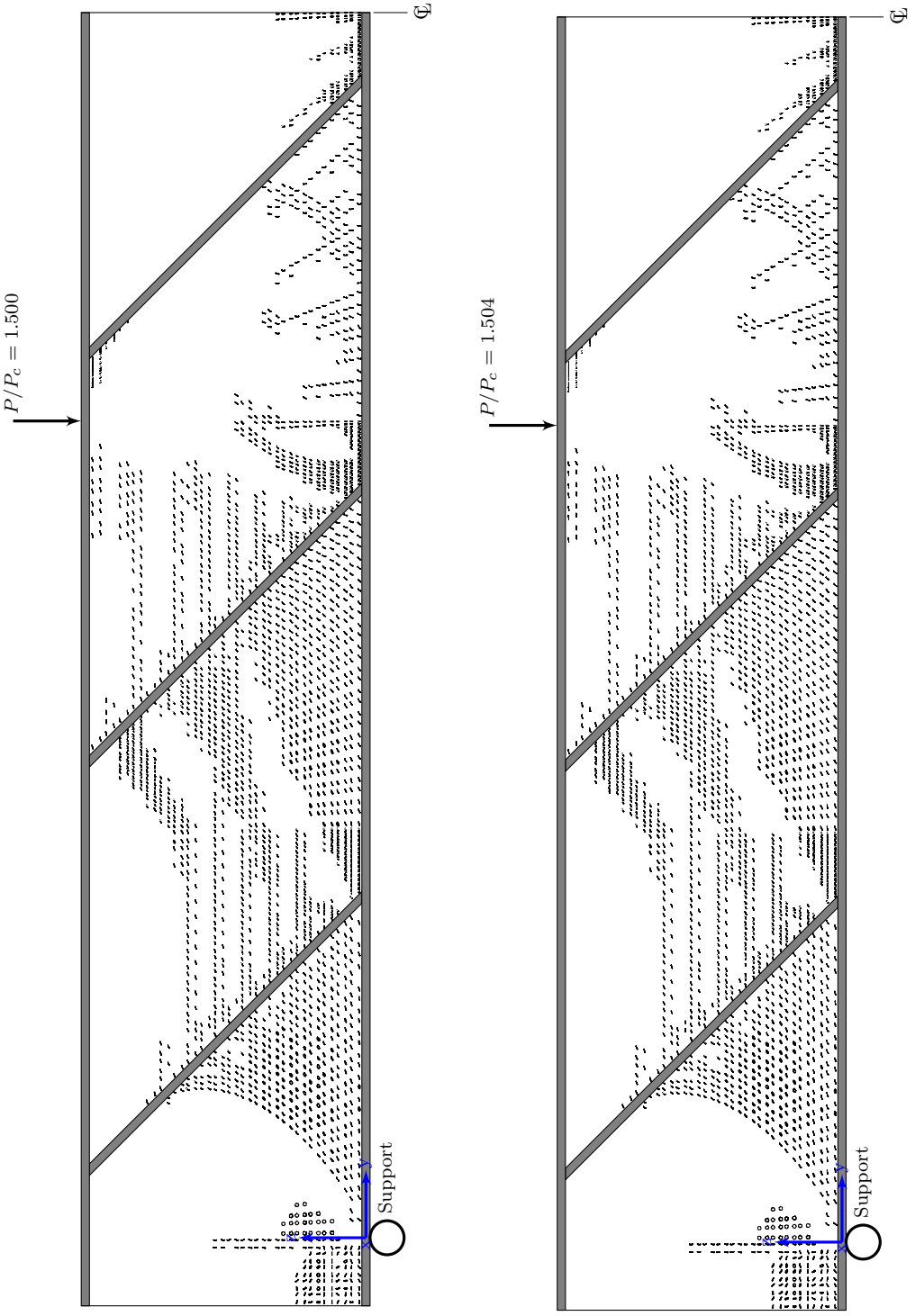

FIGURE 8.21: Crack development in the concrete core of the concrete-filled sandwich beam case study ID: SCS-FPB-SXD100 (cont'd)

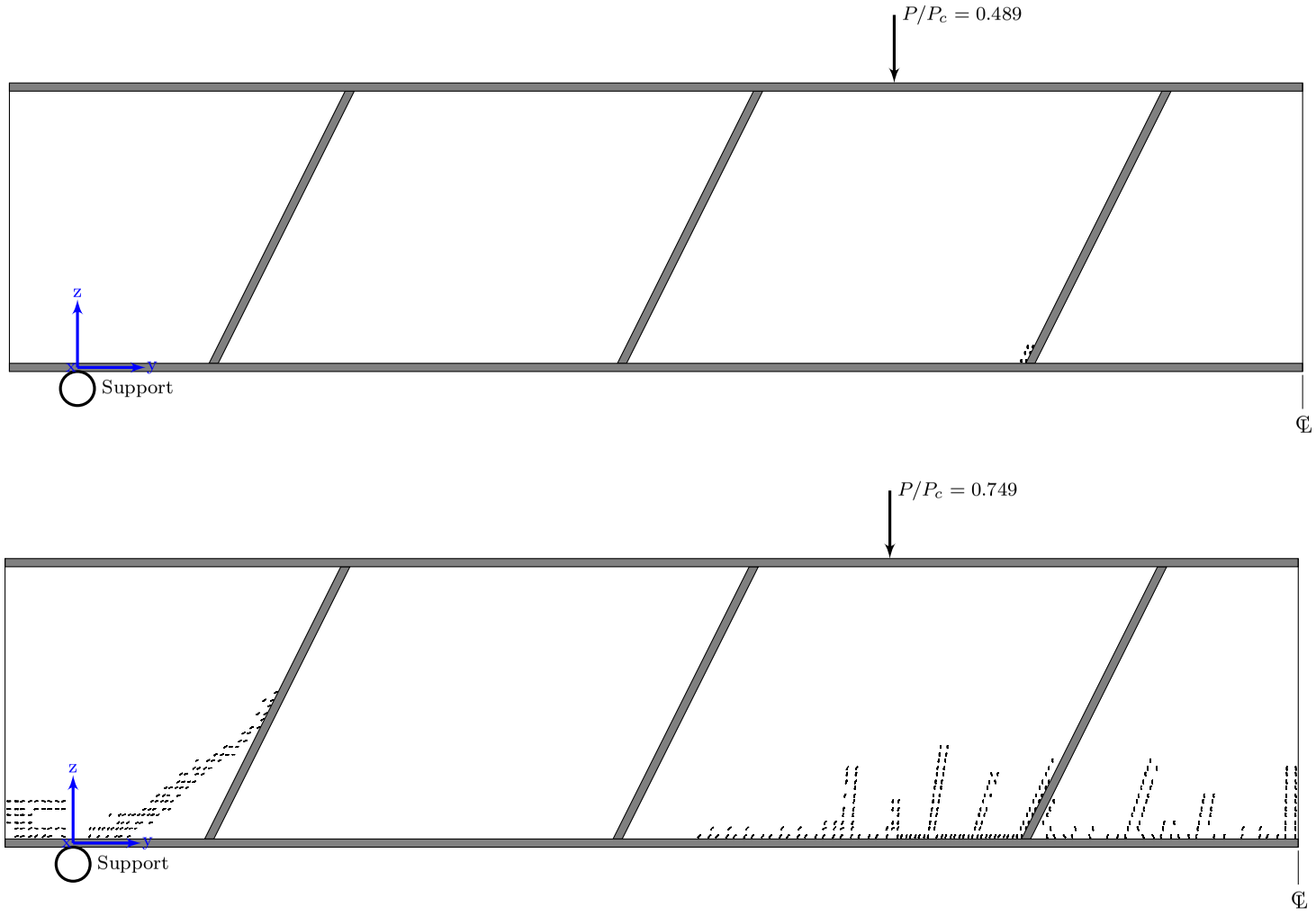

FIGURE 8.22: Crack development in the concrete core of the concrete-filled sandwich beam case study ID: SCS-FPB-SXD050-A

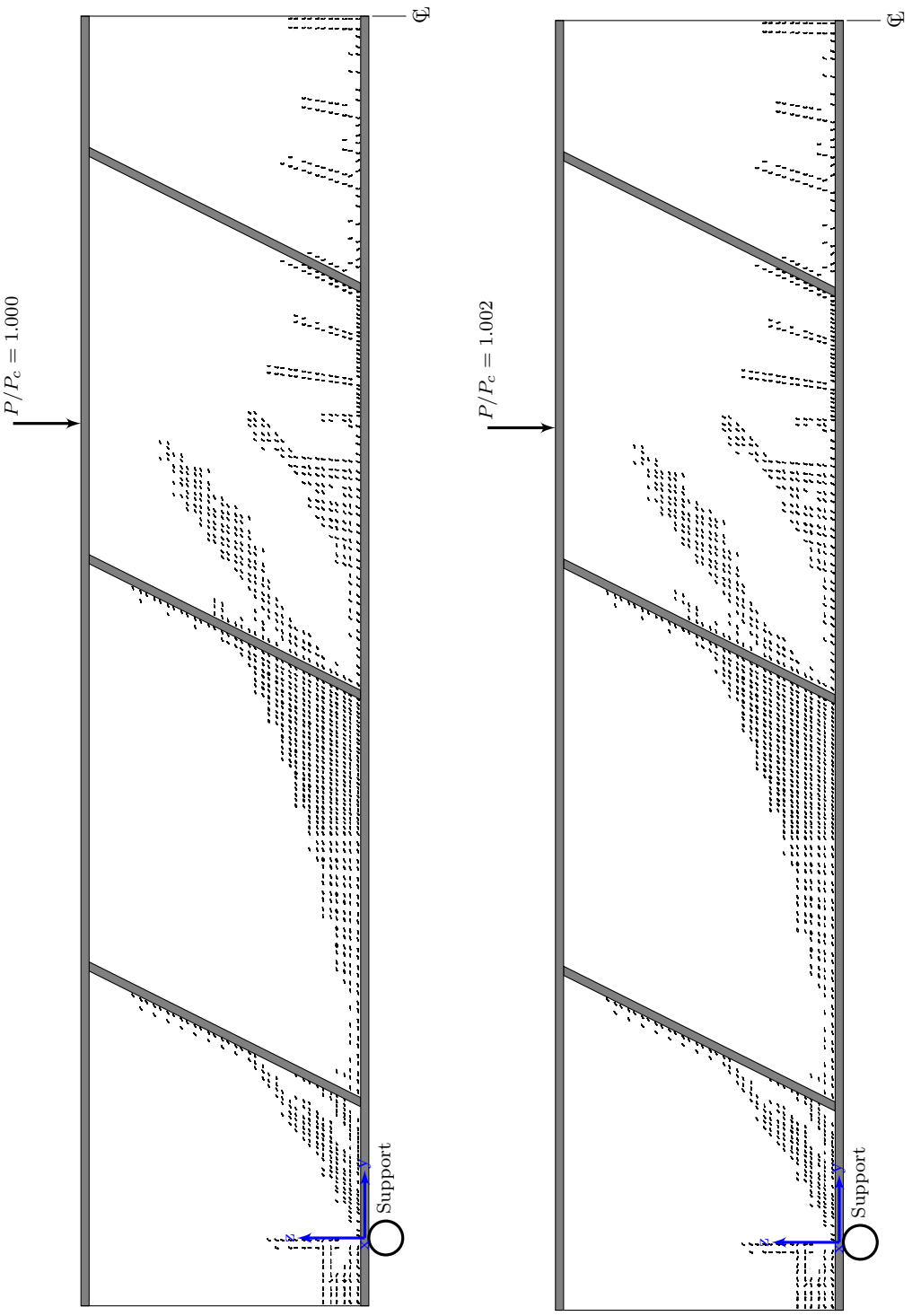

FIGURE 8.22: Crack development in the concrete core of the concrete-filled sandwich beam case study ID: SCS-FPB-SXD050-A (cont'd)

Chapter 9

Conclusion and Recommendation for Further Work

9.1 Conclusion

The research was conducted to deliver a new type of steel-concrete-steel (SCS) sandwich construction. The novel SCS sandwich structure with bi-directional corrugated-strip core (Bi-CSC) was proposed. The aims of the research were to present the possibility to implement this novel sandwich structure and to present the potential advantages in terms of structural performance. The main objective of the research was to address the advantages of the stiffness and strength of the proposed sandwich beam using numerical and analytical methods. The focus was on the effect of the angle of the inclined part of the corrugated-strip core (CSC) to the stiffness and strength of the unfilled SCS sandwich beam and to the transverse shear strength of a concrete-filled SCS sandwich beam.

The research was conducted in four stages: (1) the review of sandwich construction, (2) the feasibility study to implement the proposed SCS sandwich structure, (3) the numerical and analytical studies of the stiffness and strength of the unfilled SCS sandwich beam with Bi-CSC, and (4) the numerical study of the transverse shear strength of the concrete-filled SCS sandwich beam with corrugated-strip core. Therefore, the summary of this research may be drawn in the four following sections.

9.1.1 Literature Review of Sandwich Construction

The literature, as presented in Chapter 2, demonstrated the variety of the design and construction of the sandwich structures and presented the possibility to invent a new

type of sandwich construction. In the SCS sandwich construction, it was found that the major progression of development was to introduce a shear connector using a single-ended friction-welded shear stud through a double-ended friction-welded shear stud and an innovative J-hook connector. However, it was found that the existing forms of shear connectors recently used in the SCS sandwich construction were all aligned perpendicular to the steel face plates.

The literature showed that the concrete-filled SCS sandwich beams could suffer a diagonal shear crack of the concrete core. It was found that the existing shear connectors might not provide the optimum strength capacity to overcome this diagonal shear crack. In comparison with another similar construction such as a reinforced concrete (RC) beam, the inclined shear connectors were found to be an alternative solution to provide more transverse strength capacity. However, the literature in the SCS sandwich construction demonstrated that there was no existing SCS sandwich beam with inclined shear connectors. It was implied that the understanding of the structural behaviour due to the inclined shear connector was missing from the current knowledge of the SCS sandwich construction, both in the unfilled and concrete-filled types.

9.1.2 Implementation of Steel-Concrete-Steel Sandwich Structures with Bi-Directional Corrugated-Strip Core

The conceptual design of the SCS sandwich structure with Bi-CSC was proposed and presented in Chapter 3. The construction of the unfilled SCS sandwich structure with Bi-CSC was the major construction stage needed to implement. The feasibility study demonstrated that the production of this proposed SCS sandwich structure could be possible. The existing construction techniques of corrugated-strip core sandwich plates presented by Ray [16, 17] could be adapted to this proposed SCS sandwich structure. Two possible methods to create Bi-CSC pattern, i.e., the top-down (TD) and the slide-rotate (SR) methods, were originally presented in this research.

9.1.3 Numerical and Analytical Studies of the Stiffness and Strength of Unfilled Sandwich Beams

The stiffness and strength of the unfilled SCS sandwich beam with Bi-CSC and other similar truss-like cores were carried out using a numerical and three analytical approaches. The numerical approach was a three-dimensional (3D) finite element method (FEM) (presented in Chapter 4). The analytical approaches were the modified stiffness matrix method (MSM) (presented in Chapter 5), the braced frame analogy method (BFA) (presented in Chapter 6), and the discrete beam method (DBM) (presented in Chapter 7).

In the 3D FEM, as presented in Chapter 4, the unfilled SCS sandwich beam was modelled and analysed using the FE software ANSYS Release 11.0 [123] along with the force-distortion relationship of a three-point loaded beam. The repetitive unit cell of the unfilled SCS sandwich beam was also modelled and analysed using the same software along with the force-distortion relationship of the unit cell.

The FE models were validated with the existing FE solutions of the unfilled web core sandwich beam provided by Romanoff and Varsta [37] and of the unfilled truss core sandwich beam provided by Lok et al. [19, 20]. The validation demonstrated that the presented FE models provided good correlation with these references. In addition, both the unfilled sandwich beam and the unit cell approaches were also good correlation with each other. It was found that the unit cell could be used to deduce the transverse shear stiffness, D_{Qy}, of the unfilled SCS sandwich beam with Bi-CSC to reduce the computation time required for the analysis of the unfilled SCS sandwich beam.

The FE models were used to evaluate the performance of the unfilled SCS sandwich beam with Bi-CSC and two other similar cores, i.e., a truss core and an X-truss core. It was found that the flexural stiffness, D_y, of the unfilled SCS sandwich beam with these cores could be neglected. However, it was found that the transverse shear stiffness, D_{Qy}, of the unfilled SCS sandwich beam with these cores was significantly dominated by the configuration of the cores and could not be neglected. The transverse shear stiffness, D_{Qy}, varied with the ratio of s_y/d and reached the optimum point at s_y/d about 1.0, i.e., at the angle of the inclined part of the CSC about 45°. It was found that the stress at the face plates of the unfilled SCS sandwich beam with Bi-CSC was improved. In comparison with two other truss-like cores, the normal stress at the face plates of the unfilled SCS sandwich beam with Bi-CSC was more uniform. The peak stress at the connection point of the web was also reduced.

In the analytical approaches, the MSM was the first analytical method presented in Chapter 5. The method was based on the force-distortion relationship of the repetitive unit cell of the unfilled SCS sandwich beam and the conventional stiffness matrix method. The MSM was proposed in this research as a simplified analytical method to obtain the transverse shear stiffness, D_{Qy}, and to overcome the high degree of indeterminacy of the proposed Bi-CSC.

The unfilled SCS sandwich beam with Bi-CSC and other similar truss-like cores were simplified as two-dimensional (2D) plane-frame model (PFM) with beam elements. The connections between the sandwich face plates and the core were modelled using rigid-link elements. The local stiffness matrix of each beam element was performed using the model of the beam with linear rotational springs at both ends of the beam element.

The MSM was validated against the existing analytical solution of the truss core sandwich beam provided by Lok et al. [19, 20] and also against the FE solutions based on the 3D FE model of a three-point loaded beam presented in Chapter 4. It was found that the MSM correlated well with the references and the FE approach.

The MSM was used to evaluate the performance of the proposed unfilled SCS sandwich beam with Bi-CSC compared with the truss core and the X-truss core. It was found that the transverse shear stiffness, D_{Qy}, of these cores varied significantly as a function of s_y/d, f_c/s_c. By comparison, the unfilled SCS sandwich beam with Bi-CSC was less advantageous than the X-truss core. However, the proposed Bi-CSC was more advantageous than the truss core if s_y/d was less than 1.0 (the angle of the inclined part of a corrugation was greater than 45°) or if f_c/s_c was greater than 0.2.

The BFA, as presented in Chapter 6, was another analytical method based on the force-distortion relationship of the repetitive unit cell of the unfilled SCS sandwich beam. The BFA was also proposed in this research as another simplified analytical method to obtain the transverse shear stiffness, D_{Qy}, and to overcome the high degree of indeterminacy of the proposed Bi-CSC. In addition, the BFA was proposed as a method to separate the stiffness contribution of the core from the overall stiffness so that the stiffness contribution of the core could be studied.

The 2D PFM with beam elements previously used in the MSM was further adapted for use in the BFA. Rather than modelling the inclined part of the CSC as beam elements, the truss elements were used in the BFA. The truss element assumption was made in accordance with the solution previously obtained from the MSM.

The BFA was used to formulate the flexural stiffness, D_y, and the transverse shear stiffness, D_{Qy}, from the mechanism of a repetitive unit cell subjected to the flexural load and transverse shear load, respectively. The formulation of the stiffness equations was obtained from the equilibrium of forces and the displacement compatibility equations. The elongation of the inclined chord was approximated in advance as a function of the elongation factors k_b and k_s (as detailed in Appendix A). In the transverse shear load mechanism, the repetitive unit cell subjected to the transverse shear load was assumed to deform into two separate modes: (1) deformation in the z-direction due to the transverse shear force, Q_y, and (2) deformation in the y-direction due to a couple of horizontal force, H, where $H = Q_y s_c/d$.

The flexural and transverse shear stiffnesses obtained from the BFA were verified. It was also found that the flexural stiffness, D_y, of the unfilled SCS sandwich beam with Bi-CSC could exist if the unfilled SCS sandwich beam was unsymmetrical. In comparison with the 3D FEM, it was found that the transverse shear stiffness, D_{Qy}, was not good

correlation in magnitude with the FE solution obtained from the unfilled SCS sandwich beam model.

Although the BFA was less accurate than the MSM, it was used in this research as a method to evaluate the stiffness contribution of the proposed core. It was found that the flexural stiffness contribution of the core could be neglected. However, the transverse shear stiffness contribution of the core could not be neglected. The transverse shear stiffness, D_{Qy}, was significantly dominated by the contribution of the core. The maximum contribution of the core to the transverse shear stiffness, D_{Qy}, could be about 90% of the overall stiffness. The contribution of the core itself also varied as a function of s_y/d. The optimum point of transverse shear stiffness contributed by the core was at s_y/d about 0.75 (the angle of the inclined part of a corrugation being about 53°).

The DBM, as presented in Chapter 7, was another simplified analytical method proposed in this research. Unlike the MSM and BFAs, the DBM was based on the transformation of the local stress and strain of each part of the repetitive unit cell of the unfilled SCS sandwich beam to the global coordinate system. This method was also proposed as an alternative simplified analytical method to overcome the high degree of indeterminacy of the presented Bi-CSC. The derivation approaches to obtain the transverse shear stiffness, D_{Qy}, of the DBM was similar to those of the BFA.

The transverse shear stiffness obtained from the DBM was verified. It was found that the transverse shear stiffness, D_{Qy}, obtained from the DBM diverged from the FEM if $s_y/d < 1.00$. However, the convergence could be achieved if the stiffness contribution of the face plates was extracted. It was also found that the DBM yielded poor correlation with the FEM. Again, the trend of the results was similar but the magnitude was different.

According to the study of the unfilled SCS sandwich beam with various cores using the numerical and analytical methods, it can be concluded that only the transverse shear stiffness, D_{Qy}, of the unfilled SCS sandwich beam was significantly dominated by the configuration of the cores. The optimum configuration of the core was found at the ratio of s_y/d about 1.0, i.e., the angle of the inclined part of the corrugation was about 45°.

In comparison with the solution obtained by the FEM, it was found that the MSM was the most accurate analytical method to obtain the transverse shear stiffness, D_{Qy}. The BFA and the DBM were less accurate.

9.1.4 Numerical Study of the Transverse Shear Strength of Concrete-Filled SCS Sandwich Beams

The presence of the diagonal shear crack in the concrete-core of a concrete-filled SCS sandwich beam was first demonstrated using the concept of a reinforced concrete beam. The limitations of the transverse shear strength of the Bi-Steel cross section was reviewed and an alternative concept to improve the limitations of Bi-Steel cross section was proposed.

The numerical study of the concrete-filled SCS sandwich beam with various shear connector patterns was carried out using 3D FE model of a four-point loaded concrete-filled SCS sandwich beam. The 3D FE model was analysed in non-linear mode using the FE software ANSYS Release 11.0 [123] with the applied assumptions.

The presented FE models were used to evaluate the performance of the various shear connector patterns. The load-deflection relationship of the beam and the evolution of the concrete crack of the beam were obtained. It was found that the load-deflection relationship of the concrete-filled SCS sandwich beams with various shear connector patterns were similar before the initial diagonal crack occurred in the concrete core at the applied load P/P_c about 1.0. Beyond this point, the response of beam varied according to the angle of shear connector. The ultimate applied load, in terms of P/P_c, increased when the angle of the shear connector decreased. It was found that this response was similar to the fundamental concept of the reinforced concrete beam. The optimum applied load occurred when the shear connectors were aligned in angle about 45°.

It was also found that the evolution of the crack of concrete core with various shear connector patterns was similar from the beginning of applied load until the initial flexural crack occurred. Beyond this point, the cracking pattern varied in accordance to the pattern of shear connector. The diagonal shear crack of the concrete-filled SCS sandwich beam with an inclined shear connector was more improved than of the beam with vertical shear connector. The extreme case where the diagonal shear crack could develop through the depth of concrete core was found when the shear connectors were aligned in angle of 45°.

9.2 Recommendation for Further Work

In summary, the work conducted in this research can be listed in tabular form as presented in Table 9.1.

TABLE 9.1: Summary of the work done in this research and the gaps for further study

Subject	Mode of Study			
	Feasibility Study	Numerical Study	Analytical Study	Experimental Study
Fabrication and Construction Techniques	To present the possibility to implement the SCS sandwich beam with Bi-CSC system using the available construction techniques The main focus is on the implementation of the corrugated-strip plates in bi-direction format	–	–	Future Work
Study of Unfilled SCS Sandwich Beam with Bi-CSC System	–	To understand the static behaviour of the unfilled SCS sandwich beam with Bi-CSC using the 3D finite element model	To present the simplified analytical techniques to deliver stiffness and strength of the unfilled SCS sandwich beam with Bi-CSC To understand the static behaviour of the unfilled SCS sandwich beam with Bi-CSC using the presented analytical techniques	Future Work
		The main focus is on the transverse shear stiffness of the unfilled SCS sandwich beam with Bi-CSC affected by variable configurations of core		
Study of Concrete-filled SCS Sandwich Beam with Bi-CSC System	–	To understand the static behaviour of the concrete-filled SCS sandwich beam with Bi-CSC using the 3D finite element model The main focus is on the transverse shear strength and the diagonal shear crack behaviour of the concrete-filled SCS sandwich beam with various configurations of the proposed core	Future Work	Future Work

In the author's opinion, there are some areas of work that need to be carried out in the future. The work should be broken down into three tasks: (1) the further study of the production and construction techniques of the unfilled and concrete-filled SCS sandwich beam with Bi-CSC, (2) the further study of the unfilled SCS sandwich beam with Bi-CSC, and (3) the further study of the concrete-filled SCS sandwich beam with Bi-CSC, as further detailed in the three following sections.

9.2.1 Production and Construction Techniques

To ensure that the proposed SCS sandwich structure with Bi-CSC can be produced and constructed in both the unfilled and concrete-filled stages, further details of production and construction techniques need to be implemented and developed. In the current research, only the conceptual design, especially in the unfilled stage, has been presented (see Chapter 3). Therefore, the prototype of the proposed SCS sandwich structure should be made. Besides making the prototype, the development of the production and construction techniques should be conducted to deliver higher efficient and economical methods.

9.2.2 Further Study of Unfilled Sandwich Beams

In the study of the unfilled SCS sandwich beam with Bi-CSC, it was found that the analytical approaches seem to provide good correlation with the numerical approach with some applied assumptions and limitations. However, it should be more appropriate if an experimental study be carried out. This is to ensure that both the analytical and numerical approaches in this research are properly validated with the real response of the proposed unfilled SCS sandwich structure. The three- or four-point loaded beam of the proposed unfilled SCS sandwich beam with various cores subject to static load conditions should be tested to obtain the response of the beam as well as to obtain the local and global failure mechanisms of the beam.

Besides the experimental testing, the development of the analytical approaches, especially the BFA and the DBM, should be further conducted to improve the approaches so that a higher accuracy with minimal assumptions can be achieved. Each assumption assumed in each analytical approach should be further studied in more detail to understand its response clearly. In addition, the analytical approaches should be further developed so that both the stiffness and stress responses of the unfilled SCS sandwich beam with Bi-CSC can be achieved. The theory of an unfilled web core sandwich beam developed by Romanoff et al. [37, 115] may be adapted and used as the basis for the unfilled SCS sandwich beam with Bi-CSC.

Other responses of the unfilled sandwich beam such as the buckling strength of the corrugated-strip core, which is quite thin, may need to be investigated. The flexibility of the connection between the face plate and the core may also be investigated to assess any actual flexibility effect due to real connection, as may be seen in, for example, Fung and Tan [131].

9.2.3 Further Study of Concrete-Filled Sandwich Beams

In the study of the concrete-filled SCS sandwich beam with CSC, only the numerical study of the load-deflection response and the development of concrete crack were presented in this research (see Chapter 8). Therefore, it should be more appropriate if the experimental study will be conducted. A three- or four-point loaded beam should be carried out to understand the real response and the failure mechanism of the beam. The push-out shear test of a repetitive concrete-filled unit cell should be also conducted. A series of the tests of concrete-filled Bi-Steel sandwich beam intensively presented in [12] and concrete-filled SCS sandwich beam with J-hook connectors presented in [77] may be used as the guidance for the experimental testing of the concrete-filled SCS sandwich with CSC. Further experimental study of the concrete-filled SCS sandwich beam with Bi-CSC should also be carried out.

In comparison with the experimental results, the numerical study of the concrete-filled SCS sandwich beam with CSC should be further validated in more detail. The FE model should be further developed to include the local response of the beam which may be found in the experimental study, for example, the partial slip between the concrete core and the face plates and/or the CSC. The parametric study should be further study based on the new refined FE model.

In addition to the numerical and experimental studies, the analytical solution of the concrete-filled SCS sandwich beam with CSC and with Bi-CSC should be developed. The design equations should also be developed.

In summary, further development in any approach should be conducted to understand the response of the proposed SCS sandwich beam in both unfilled and concrete-filled types in detail. This should be done to ensure that the new proposed SCS sandwich beam is safe for the public use.

Appendix A

Supplementary Note of the Braced Frame Analogy

A.1 Location of the Neutral Axis

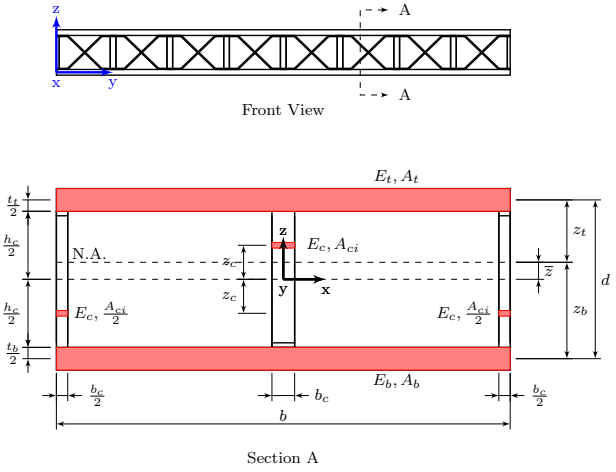

FIGURE A.1: Location of the neutral axis of the cross section of an unfilled sandwich beam with bi-directional corrugated-strip core

Considering Fig. A.1, the location of the neutral axis of the cross section of an unfilled sandwich beam with bi-directional corrugated-strip core (Bi-CSC) can be calculated as

follows:

$$\begin{aligned}\bar{z} &= \frac{E_t A_t\left(\frac{h_c}{2}+\frac{t_t}{2}\right)-E_b A_b\left(\frac{h_c}{2}+\frac{t_b}{2}\right)+E_c A_{ci} z_c-\left(\frac{E_c A_{ci}}{2}+\frac{E_c A_{ci}}{2}\right) z_c}{E_t A_t+E_b A_b+E_c A_{ci}+\left(\frac{E_c A_{ci}}{2}+\frac{E_c A_{ci}}{2}\right)} \\ &= \frac{E_t A_t\left(\frac{h_c}{2}+\frac{t_t}{2}\right)-E_b A_b\left(\frac{h_c}{2}+\frac{t_b}{2}\right)}{E_t A_t+E_b A_b+2E_c A_{ci}} \\ &= \frac{E_t t_t\left(\frac{h_c}{2}+\frac{t_t}{2}\right)-E_b t_b\left(\frac{h_c}{2}+\frac{t_b}{2}\right)}{E_t t_t+E_b t_b+2E_c k_{cb} t_{ci}}\end{aligned} \tag{A.1}$$

Consequently,

$$z_t = \frac{h_c}{2}+\frac{t_t}{2}-\bar{z} \tag{A.2a}$$

$$z_b = \frac{h_c}{2}+\frac{t_b}{2}+\bar{z} \tag{A.2b}$$

A.2 Elongation Factor k_b

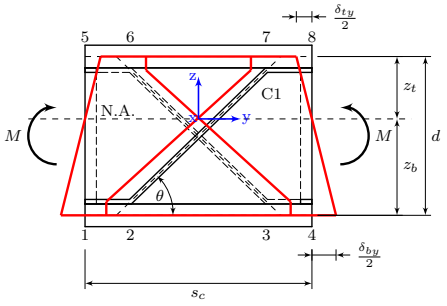

FIGURE A.2: Elongation length of the inclined member of the deformed unit cell subjected to pure bending moment

Considering Fig. A.2, the initial length of the inclined member can be expressed as follows:

$$L_c = L_z\sqrt{1+Y_c} \tag{A.3}$$

where

$$Y_c = \frac{L_y^2}{L_z^2} \tag{A.4a}$$

$$L_z = h_c - t_c \tag{A.4b}$$

$$L_y = s_c - 2f_c \tag{A.4c}$$

Similarly, the axially deformed length of the inclined member can be expressed as follows:

$$L_{cb} = L_z\sqrt{1+Y_{cb}} \tag{A.5}$$

where

$$
\begin{aligned}
Y_{cb} &= Y_c + \delta_{cb} && \text{(A.6a)}\\
\delta_{cb} &= \frac{1}{L_z^2}\left(-2L_y\delta_a + \delta_a^2\right) && \text{(A.6b)}\\
\delta_a &= \frac{1}{2}\left(1 - \frac{z_b}{z_t}\right)\delta_{ty} && \text{(A.6c)}
\end{aligned}
$$

Thus, the axial deformation of the inclined member, δ_c, can be expressed in terms of L_{cb} and L_c in which it can be further expressed in terms of the Taylor series if $|Y_{cb} < 1|$ and $|Y_c < 1|$, as follows:

$$
\begin{aligned}
\delta_c &= L_{cb} - L_c\\
&= L_z\left(\sqrt{1+Y_{cb}} - \sqrt{1+Y_c}\right)\\
&= L_z\left[\sum_{n=0}^{\infty}\frac{(-1)^n\,(2n)!}{(1-2n)\,n!^2 4^n}Y_{cb}^n - \sum_{n=0}^{\infty}\frac{(-1)^n\,(2n)!}{(1-2n)\,n!^2 4^n}Y_c^n\right]\\
&= L_z\sum_{n=0}^{\infty}\frac{(-1)^n\,(2n)!}{(1-2n)\,n!^2 4^n}\left(Y_{cb}^n - Y_c^n\right)
\end{aligned}
\qquad \text{(A.7)}
$$

Substitute Eq. A.6a into Eq. A.7 and neglect the higher-order terms of δ_{cb}, thus

$$
\delta_c = L_z\delta_{cb}\sum_{n=0}^{\infty}\frac{(-1)^n\,(2n)!}{(1-2n)\,n!^2 4^n}nY_c^{n-1} \qquad \text{(A.8)}
$$

Substitute Eq. A.6b into Eq. A.8, thus

$$
\delta_c = L_z\left(\frac{-2L_y\delta_a + \delta_a^2}{L_z^2}\right)\sum_{n=0}^{\infty}\frac{(-1)^n\,(2n)!}{(1-2n)\,n!^2 4^n}nY_c^{n-1} \qquad \text{(A.9)}
$$

Substitute Eq. A.6c into Eq. A.9 and neglect the higher-order terms of δ_{ty}, thus

$$
\begin{aligned}
\delta_c &= -\frac{L_y}{L_z}\left(1 - \frac{z_b}{z_t}\right)\delta_{ty}\sum_{n=0}^{\infty}\frac{(-1)^n\,(2n)!}{(1-2n)\,n!^2 4^n}nY_c^{n-1}\\
&= -\frac{L_y}{L_z}\left(1 - \frac{z_b}{z_t}\right)\delta_{ty}\sum_{n=0}^{\infty}\frac{(-1)^n\,(2n)!}{(1-2n)\,n!^2 4^n}n\left(\frac{L_y^2}{L_z^2}\right)^{n-1}\\
&= k_b\delta_{ty}
\end{aligned}
\qquad \text{(A.10)}
$$

where

$$
\begin{aligned}
k_b &= -\frac{L_y}{L_z}\left(1 - \frac{z_b}{z_t}\right)\sum_{n=0}^{\infty}\frac{(-1)^n\,(2n)!}{(1-2n)\,n!^2 4^n}n\left(\frac{L_y^2}{L_z^2}\right)^{n-1}\\
&= -\frac{s_y}{d}\left(1 - \frac{z_b}{z_t}\right)\sum_{n=0}^{\infty}\frac{(-1)^n\,(2n)!}{(1-2n)\,n!^2 4^n}n\left(\frac{s_y^2}{d^2}\right)^{n-1}
\end{aligned}
\qquad \text{(A.11)}
$$

It should be noted that the Taylor series could be converged only if $|Y_{cb} < 1|$ and $|Y_c < 1|$, i.e., $L_y < L_z$. In case of $L_y > L_z$, therefore, the axial deformation of the inclined member, δ_c, is slightly changed as follows:

$$\begin{aligned}\delta_c &= -\left(1-\frac{z_b}{z_t}\right)\delta_{ty}\sum_{n=0}^{\infty}\frac{(-1)^n(2n)!}{(1-2n)\,n!^2 4^n}nY_c^{n-1} \\ &= -\left(1-\frac{z_b}{z_t}\right)\delta_{ty}\sum_{n=0}^{\infty}\frac{(-1)^n(2n)!}{(1-2n)\,n!^2 4^n}n\left(\frac{L_z^2}{L_y^2}\right)^{n-1} \\ &= k_b\delta_{ty}\end{aligned} \tag{A.12}$$

where

$$\begin{aligned}k_b &= -\left(1-\frac{z_b}{z_t}\right)\sum_{n=0}^{\infty}\frac{(-1)^n(2n)!}{(1-2n)\,n!^2 4^n}n\left(\frac{L_z^2}{L_y^2}\right)^{n-1} \\ &= -\left(1-\frac{z_b}{z_t}\right)\sum_{n=0}^{\infty}\frac{(-1)^n(2n)!}{(1-2n)\,n!^2 4^n}n\left(\frac{d^2}{s_y^2}\right)^{n-1}\end{aligned} \tag{A.13}$$

In general, the elongation factor k_b can be expressed as follows:

$$k_b = \begin{cases} -\dfrac{s_y}{d}\left(1-\dfrac{z_b}{z_t}\right)\displaystyle\sum_{n=0}^{\infty}\frac{(-1)^n(2n)!}{(1-2n)\,n!^2 4^n}n\left(\frac{s_y^2}{d^2}\right)^{n-1} & \text{if } s_y \le d \\ -\left(1-\dfrac{z_b}{z_t}\right)\displaystyle\sum_{n=0}^{\infty}\frac{(-1)^n(2n)!}{(1-2n)\,n!^2 4^n}n\left(\frac{d^2}{s_y^2}\right)^{n-1} & \text{if } s_y \ge d \end{cases} \tag{A.14}$$

A.3 Elongation Factors k_{sz} and k_{sy}

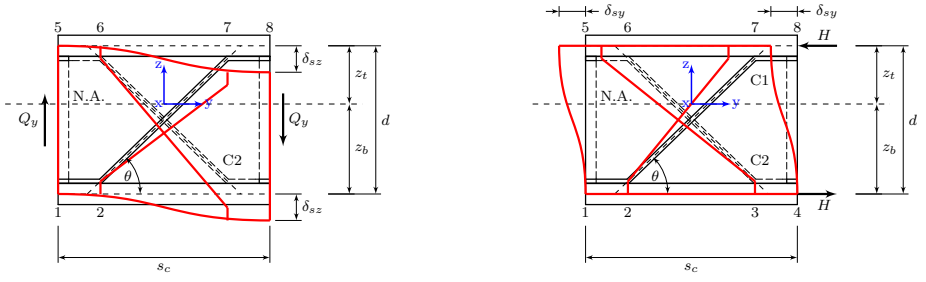

FIGURE A.3: Elongation length of the inclined member of the deformed unit cell subjected to (a) transverse shear force, Q_y, and (b) a couple of horizontal force, H

To derive the elongation factors k_{sz} and k_{sy}, the similar procedure as of the elongation factor k_b is carried out. For k_{sz}, considering Fig. A.3(a), the axially deformed length of

the inclined member C1 can be expressed as follows:

$$L_{csz1} = L_z\sqrt{1+Y_{csz1}} \tag{A.15}$$

where

$$Y_{csz1} = Y_c + \delta_{csz1} \tag{A.16a}$$

$$\delta_{csz1} = \frac{1}{L_z^2}\left[2L_z\frac{L_y}{s_c}\delta_{sz} + \left(\frac{L_y}{s_c}\delta_{sz}\right)^2\right] \tag{A.16b}$$

Thus, the axial deformation of the inclined member C1 can be expressed in terms of L_{csz1} and L_c in which it can be further expressed in terms of the Taylor series if $|Y_{csz1} < 1|$ and $|Y_c < 1|$, as follows:

$$\begin{aligned}
\delta_{c1} &= L_{csz1} - L_c \\
&= L_z\delta_{csz1}\sum_{n=0}^{\infty}\frac{(-1)^n(2n)!}{(1-2n)\,n!^2 4^n}nY_c^{n-1} \\
&= 2\frac{L_y}{s_c}\delta_{sz}\sum_{n=0}^{\infty}\frac{(-1)^n(2n)!}{(1-2n)\,n!^2 4^n}nY_c^{n-1} \\
&= 2\frac{L_y}{s_c}\delta_{sz}\sum_{n=0}^{\infty}\frac{(-1)^n(2n)!}{(1-2n)\,n!^2 4^n}n\left(\frac{L_y^2}{L_z^2}\right)^{n-1} \\
&= k_{sz1}\delta_{sz}
\end{aligned} \tag{A.17}$$

where

$$k_{sz1} = 2\frac{L_y}{s_c}\sum_{n=0}^{\infty}\frac{(-1)^n(2n)!}{(1-2n)\,n!^2 4^n}n\left(\frac{L_y^2}{L_z^2}\right)^{n-1} \tag{A.18}$$

Similarly, the axially deformed length of the inclined member C2 can be expressed as follows:

$$L_{csz2} = L_z\sqrt{1+Y_{csz2}} \tag{A.19}$$

where

$$Y_{csz2} = Y_c + \delta_{csz2} \tag{A.20a}$$

$$\delta_{csz2} = \frac{1}{L_z^2}\left[-2L_z\frac{L_y}{s_c}\delta_{sz} + \left(\frac{L_y}{s_c}\delta_{sz}\right)^2\right] \tag{A.20b}$$

Thus, the axial deformation of the inclined member C2 can be expressed in terms of L_{csz2} and L_c in which it can be further expressed in terms of the Taylor series if $|Y_{csz2} < 1|$

and $|Y_c < 1|$, as follows:

$$\begin{aligned}
\delta_{c2} &= L_{csz2} - L_c \\
&= L_z \delta_{csz2} \sum_{n=0}^{\infty} \frac{(-1)^n (2n)!}{(1-2n)\, n!^2 4^n} n Y_c^{n-1} \\
&= -2\frac{L_y}{s_c} \delta_{sz} \sum_{n=0}^{\infty} \frac{(-1)^n (2n)!}{(1-2n)\, n!^2 4^n} n Y_c^{n-1} \\
&= -2\frac{L_y}{s_c} \delta_{sz} \sum_{n=0}^{\infty} \frac{(-1)^n (2n)!}{(1-2n)\, n!^2 4^n} n \left(\frac{L_y^2}{L_z^2}\right)^{n-1} \\
&= k_{sz2} \delta_{sz}
\end{aligned} \tag{A.21}$$

where

$$k_{sz2} = -2\frac{L_y}{s_c} \sum_{n=0}^{\infty} \frac{(-1)^n (2n)!}{(1-2n)\, n!^2 4^n} n \left(\frac{L_y^2}{L_z^2}\right)^{n-1} \tag{A.22}$$

Considering Eqs. A.18 and A.22, it can be seen that the absolute values of k_{sz1} and of k_{sz2} are identical. Therefore, it can be concluded that both the inclined members C1 and C2 are axially deformed in the same elongation length, thus

$$\delta_{c1} = -\delta_{c2} = \delta_c = k_{sz} \delta_{sz} \tag{A.23}$$

where

$$\begin{aligned}
k_{sz} &= 2\frac{L_y}{s_c} \sum_{n=0}^{\infty} \frac{(-1)^n (2n)!}{(1-2n)\, n!^2 4^n} n \left(\frac{L_y^2}{L_z^2}\right)^{n-1} \\
&= 2\frac{s_c - 2f_c}{s_c} \sum_{n=0}^{\infty} \frac{(-1)^n (2n)!}{(1-2n)\, n!^2 4^n} n \left(\frac{s_y^2}{d^2}\right)^{n-1}
\end{aligned} \tag{A.24}$$

It should be noted that the Taylor series could be converged only if $|Y_{csz1} < 1|$, $|Y_{csz2} < 1|$ and $|Y_c < 1|$, i.e., $L_y < L_z$. In case of $L_y > L_z$, therefore, the axial deformation of the inclined member, δ_c, is slightly changed. As a result, the elongation factor k_{sz} is as follows:

$$\begin{aligned}
k_{sz} &= 2\frac{L_z}{s_c} \sum_{n=0}^{\infty} \frac{(-1)^n (2n)!}{(1-2n)\, n!^2 4^n} n \left(\frac{L_z^2}{L_y^2}\right)^{n-1} \\
&= 2\frac{h_c - t_c}{s_c} \sum_{n=0}^{\infty} \frac{(-1)^n (2n)!}{(1-2n)\, n!^2 4^n} n \left(\frac{d^2}{s_y^2}\right)^{n-1}
\end{aligned} \tag{A.25}$$

In general, the elongation factor k_{sz} can be expressed as follows:

$$k_{sz} = \begin{cases} 2\dfrac{s_c - 2f_c}{s_c} \displaystyle\sum_{n=0}^{\infty} \frac{(-1)^n (2n)!}{(1-2n)\, n!^2 4^n} n \left(\frac{s_y^2}{d^2}\right)^{n-1} & \text{if } s_y \le d \\ 2\dfrac{h_c - t_c}{s_c} \displaystyle\sum_{n=0}^{\infty} \frac{(-1)^n (2n)!}{(1-2n)\, n!^2 4^n} n \left(\frac{d^2}{s_y^2}\right)^{n-1} & \text{if } s_y \ge d \end{cases} \tag{A.26}$$

For k_{sy}, considering Fig. A.3(b), the axially deformed length of the inclined member C1 can be expressed as follows:

$$L_{csy1} = L_z \sqrt{1 + Y_{csy1}} \tag{A.27}$$

where

$$Y_{csy1} = Y_c + \delta_{csy1} \tag{A.28a}$$

$$\delta_{csy1} = \frac{1}{L_z^2}\left(2L_y\delta_{sy} + \delta_{sy}^2\right) \tag{A.28b}$$

Thus, the axial deformation of the inclined member C1 can be expressed in terms of L_{csy1} and L_c in which it can be further expressed in terms of the Taylor series if $|Y_{csy1} < 1|$ and $|Y_c < 1|$, as follows:

$$\begin{aligned} \delta_{c1} &= L_{csy1} - L_c \\ &= L_z\delta_{csy1} \sum_{n=0}^{\infty} \frac{(-1)^n (2n)!}{(1-2n)\, n!^2 4^n} n Y_c^{n-1} \\ &= 2\frac{L_y}{L_z}\delta_{sy} \sum_{n=0}^{\infty} \frac{(-1)^n (2n)!}{(1-2n)\, n!^2 4^n} n Y_c^{n-1} \\ &= 2\frac{L_y}{L_z}\delta_{sy} \sum_{n=0}^{\infty} \frac{(-1)^n (2n)!}{(1-2n)\, n!^2 4^n} n \left(\frac{L_y^2}{L_z^2}\right)^{n-1} \\ &= k_{sy1}\delta_{sy} \end{aligned} \tag{A.29}$$

where

$$k_{sy1} = 2\frac{L_y}{L_z} \sum_{n=0}^{\infty} \frac{(-1)^n (2n)!}{(1-2n)\, n!^2 4^n} n \left(\frac{L_y^2}{L_z^2}\right)^{n-1} \tag{A.30}$$

Similarly, the axially deformed length of the inclined member C2 can be expressed as follows:

$$L_{csy2} = L_z \sqrt{1 + Y_{csy2}} \tag{A.31}$$

where

$$Y_{csy2} = Y_c + \delta_{csy2} \tag{A.32a}$$
$$\delta_{csy2} = \frac{1}{L_z^2}\left(-2L_y\delta_{sy} + \delta_{sy}^2\right) \tag{A.32b}$$

Thus, the axial deformation of the inclined member C2 can be expressed in terms of L_{csy2} and L_c in which it can be further expressed in terms of the Taylor series if $|Y_{csy2} < 1|$ and $|Y_c < 1|$, as follows:

$$\begin{aligned}
\delta_{c2} &= L_{csy2} - L_c \\
&= L_z\delta_{csy2}\sum_{n=0}^{\infty}\frac{(-1)^n(2n)!}{(1-2n)\,n!^2 4^n}nY_c^{n-1} \\
&= -2\frac{L_y}{L_z}\delta_{sy}\sum_{n=0}^{\infty}\frac{(-1)^n(2n)!}{(1-2n)\,n!^2 4^n}nY_c^{n-1} \\
&= -2\frac{L_y}{L_z}\delta_{sy}\sum_{n=0}^{\infty}\frac{(-1)^n(2n)!}{(1-2n)\,n!^2 4^n}n\left(\frac{L_y^2}{L_z^2}\right)^{n-1} \\
&= k_{sy2}\delta_{sy}
\end{aligned} \tag{A.33}$$

where

$$k_{sy2} = -2\frac{L_y}{L_z}\sum_{n=0}^{\infty}\frac{(-1)^n(2n)!}{(1-2n)\,n!^2 4^n}n\left(\frac{L_y^2}{L_z^2}\right)^{n-1} \tag{A.34}$$

Considering Eqs. A.30 and A.34, it can be seen that the absolute values of k_{sy1} and of k_{sy2} are identical. Therefore, it can be concluded that both the inclined members C1 and C2 are axially deformed in the same elongation length, thus

$$\delta_{c1} = -\delta_{c2} = \delta_c = k_{sy}\delta_{sy} \tag{A.35}$$

where

$$\begin{aligned}
k_{sy} &= 2\frac{L_y}{L_z}\sum_{n=0}^{\infty}\frac{(-1)^n(2n)!}{(1-2n)\,n!^2 4^n}n\left(\frac{L_y^2}{L_z^2}\right)^{n-1} \\
&= 2\frac{s_y}{d}\sum_{n=0}^{\infty}\frac{(-1)^n(2n)!}{(1-2n)\,n!^2 4^n}n\left(\frac{s_y^2}{d^2}\right)^{n-1}
\end{aligned} \tag{A.36}$$

It should be noted that the Taylor series could be converged only if $|Y_{csy1} < 1|$, $|Y_{csy2} < 1|$ and $|Y_c < 1|$, i.e., $L_y < L_z$. In case of $L_y > L_z$, therefore, the axial deformation of the inclined member, δ_c, is slightly changed. As a result, the elongation factor k_{sy} is as

follows:

$$\begin{aligned} k_{sy} &= 2\sum_{n=0}^{\infty} \frac{(-1)^n (2n)!}{(1-2n)\, n!^2 4^n} n \left(\frac{L_z^2}{L_y^2}\right)^{n-1} \\ &= 2\sum_{n=0}^{\infty} \frac{(-1)^n (2n)!}{(1-2n)\, n!^2 4^n} n \left(\frac{d^2}{s_y^2}\right)^{n-1} \end{aligned} \tag{A.37}$$

In general, the elongation factor k_{sy} can be expressed as follows:

$$k_{sy} = \begin{cases} 2\dfrac{s_y}{d}\displaystyle\sum_{n=0}^{\infty} \frac{(-1)^n (2n)!}{(1-2n)\, n!^2 4^n} n \left(\frac{s_y^2}{d^2}\right)^{n-1} & \text{if } s_y \le d \\ 2\displaystyle\sum_{n=0}^{\infty} \frac{(-1)^n (2n)!}{(1-2n)\, n!^2 4^n} n \left(\frac{d^2}{s_y^2}\right)^{n-1} & \text{if } s_y \ge d \end{cases} \tag{A.38}$$

Bibliography

[1] H. Bowerman, N. Coyle, and J. C. Chapman. An innovative steel-concrete construction system. *The Structural Engineer*, 80(20):33–38, 2002.

[2] J. Y. R. Liew and T. Y. Wang. Novel sandwich composite structures. In *Pacific Structural Steel Conference 2007: Steel Structures in Natural Hazards*, Wairakei, New Zealand, 13–16 March 2007.

[3] J. Y. R. Liew, C. G. Koh, and K. M. A. Sohel. Development of composite sandwich structures for impact resistance. In *Pacific Structural Steel Conference 2007: Steel Structures in Natural Hazards*, Wairakei, New Zealand, 13–16 March 2007.

[4] J. Y. R. Liew and K. M. A. Sohel. Lightweight steel-concrete-steel sandwich system with J-hook connectors. *Engineering Structures*, 31(5):1166–1178, 2009.

[5] J. Y. R. Liew, K. M. A. Sohel, and C. G. Koh. Impact tests on steel-concrete-steel sandwich beams with lightweight concrete core. *Engineering Structures*, 31(9): 2045–2059, 2009.

[6] X. X. Dai and J. Y. R. Liew. Fatigue performance of lightweight steel-concrete-steel sandwich systems. *Journal of Constructional Steel Research*, 66(2):256–276, 2010.

[7] H. Bråthen and N. E. Rangøy. Perfect timing for concrete sandwich. *DNV Forum*, 2:24–25, 2005.

[8] Anonymous. Sandwich design concept may revolutionise shipbuilding. *DNV Classification News*, 4:5–7, 2005.

[9] X. X. Dai and J. Y. R. Liew. A novel concept to enhance fatigue performance of steel-concrete-steel sandwich panel. In *International Colloquium on Stability and Ductility of Steel Structures*, Lisbon, Portugal, 6–8 September 2006.

[10] X. X. Dai and J. Y. R. Liew. Steel-concrete-steel sandwich system for ship hull construction. In *International Colloquium on Stability and Ductility of Steel Structures*, Lisbon, Portugal, 6–8 September 2006.

[11] T. O. S. Oduyemi and H. D. Wright. An experimental investigation into the behaviour of double-skin sandwich beams. *Journal of Constructional Steel Research*, 14(3):197–220, 1989.

[12] M. Xie, N. Foundoukos, and J. C. Chapman. Static tests on steel-concrete-steel sandwich beams. *Journal of Constructional Steel Research*, 63(6):735–750, 2007.

[13] N. K. Subedi and N. R. Coyle. Improving the strength of fully composite steel-concrete-steel beam elements by increased surface roughness–an experimental study. *Engineering Structures*, 24(10):1349–1355, 2002.

[14] M. Xie and J. C. Chapman. Developments in sandwich construction. *Journal of Constructional Steel Research*, 62(11):1123–1133, 2006.

[15] N. Foundoukos and J. C. Chapman. Finite element analysis of steel-concrete-steel sandwich beams. *Journal of Constructional Steel Research*, 64(9):947–961, 2008.

[16] H. Ray. Bi-directionally corrugated sandwich construction. United States Patent, Patent Number: 5,543,204, Date of Patent: 6 August, 1996.

[17] H. Ray. Panel having cross-corrugated sandwich construction. United States Patent, Patent Number: 5,609,942, Date of Patent: 11 March, 1997.

[18] H. Ray. Investigation of advanced lightweight sandwich structural concept. Report NAWCADWAR-93064-60, Naval Air Warfare Center, Aircraft Division, Warminster, PA, 1993.

[19] T. S. Lok, Q. Cheng, and L. Heng. Equivalent stiffness parameters of truss-core sandwich panel. In *Proceedings of the Ninth (1999) Internatioanl Offshore and Polar Engineering Conference*, volume IV, pages 292–298, Brest, France, 30 May – 4 June 1999.

[20] T. S. Lok and Q. H. Cheng. Elastic stiffness properties and behavior of truss-core sandwich panel. *Journal of Structural Engineering*, 126(5):552–559, 2000.

[21] H. G. Allen. *Analysis and Design of Structural Sandwich Panels*. Pergamon Press Ltd., London, 1969.

[22] D. Zenkert. *The Handbook of Sandwich Construction*. Engineering Materials Advisory Services Ltd., UK, 1997.

[23] C. Chen, A.-M. Harte, and N. A. Fleck. The plastic collapse of sandwich beams with a metallic foam core. *International Journal of Mechanical Sciences*, 43(6): 1483–1506, 2001.

[24] A. M. Harte, N. A. Fleck, and M. F. Ashby. The fatigue strength of sandwich beams with an aluminium alloy foam core. *International Journal of Fatigue*, 23 (6):499–507, 2001.

[25] M. F. Ashby, A. G. Evans, N. A. Fleck, L. J. Gibson, J. W. Hutchinson, and H. N. G. Wadley. *Metal Foams: A Design Guide*. Butterworth-Heinemann, Boston, MA, 2000.

[26] D. J. Sypeck and H. N. G. Wadley. Multifunctional microtruss laminates: textile synthesis and properties. *Journal of Materials Research*, 16(3):890–897, 2001.

[27] J. Y. R. Liew. Innovative SCS system for marine and offshore applications. *The Structural Engineer*, 86(12):24–25, 2008.

[28] LightConcrete LLC. High-strength structural lightweight concrete. Retrieved: 15 March, 2010. URL `http://www.lightconcrete.com/images/LightConcrete.pdf`.

[29] Moxie International. Concrete answers to moisture problem since 1975. Retrieved: 15 March, 2010. URL `http://www.moxie-intl.com/glossary.htm`.

[30] Foam Concrete Limited. Foam concrete basics. Retrieved: 15 March, 2010. URL `http://www.foamconcrete.co.uk`.

[31] H. G. Allen. Sandwich construction. Prepared as Report CE/1/72 in January 1972, University of Southampton, 1971.

[32] EconCore N.V. Economic core and panel technologies. Retrieved: 03 Febuary, 2009. URL `http://www.econcore.com`.

[33] Cellular Materials International Inc. Cellular materials. Retrieved: 03 Febuary, 2009. URL `http://www.cellularmaterials.com`.

[34] H. Ray. Method of making an offset corrugated sandwich construction. United States Patent, Patent Number: 5,348,601, Date of Patent: 20 September, 1994.

[35] H. Ray. Offset corrugated sandwich construction. United States Statutory Invention Registration, Reg. Number: H1481, Published: 5 September, 1995.

[36] C. C. Porter, P. J. Jacoy, and W. P. Schmitigal. Core design for use with precision composite reflectors. United States Patent, Patent Number: 5,162,143, Date of Patent: 10 November, 1992.

[37] J. Romanoff and P. Varsta. Bending response of web-core sandwich beams. *Composite Structures*, 73(4):478–487, 2006.

[38] T. C. Fung, K. H. Tan, and T. S. Lok. Shear stiffness D_{Qy} for C-core sandwich panels. *Journal of Structural Engineering*, 122(8):958–966, 1996.

[39] Meyer Werft GmbH. I-core. Retrieved: 03 Febuary, 2009. URL `http://www.i-core.com`.

[40] H. J. Rathbun, Z. Wei, M. Y. He, F. W. Zok, A. G. Evans, D. J. Sypeck, and H. N. G. Wadley. Measurement and simulation of the performance of a lightweight metallic sandwich structure with a tetrahedral truss core. *Journal of Applied Mechanics*, 71(3):368–374, 2004.

[41] H. N. G. Wadley, N. A. Fleck, and A. G. Evans. Fabrication and structural performance of periodic cellular metal sandwich structures. *Composites Science and Technology*, 63(16):2331–2343, 2003.

[42] F. Cote, V. S. Deshpande, N. A. Fleck, and A. G. Evans. The compressive and shear responses of corrugated and diamond lattice materials. *International Journal of Solids and Structures*, 43(20):6220–6242, 2006.

[43] G. W. Kooistra, V. Deshpande, and H. N. G. Wadley. Hierarchical corrugated core sandwich panel concepts. *Journal of Applied Mechanics*, 74(2):259–268, 2007.

[44] T. Bhat, T. G. Wang, and L. J. Gibson. Micro-sandwich honeycomb. *SAMPE Journal*, 25(3):43, 1989.

[45] R. Lakes. Materials with structural hierarchy. *Nature*, 361(6412):511–515, 1993.

[46] U. K. Vaidya, A. N. Palazotto, and L. N. B. Gummadi. Low velocity impact and compression-after-impact response of Z-pin reinforced core sandwich composites. *Journal of Engineering Materials and Technology*, 122(4):434–442, 2000.

[47] U. K. Vaidya, M. V. Kamath, M. V. Hosur, H. Mahfuz, and S. Jeelani. Low-velocity impact response of cross-ply laminated sandwich composites with hollow and foam-filled Z-pin reinforced core. *Journal of Composites Technology & Research*, 21(2):84–97, 1999.

[48] H. Kolsters. Stiffness and strength of laser-welded sandwich panels. Master's thesis, Department of Aeronautics, Division of Lightweight Structures, Royal Institute of Technology, Sweden, 2002.

[49] Nida-Core Corporation. Nida-core structural honeycomb core materials. Retrieved: 03 Febuary, 2009. URL `http://www.nida-core.com`.

[50] *Bi-Steel: Design & Construction Guide*. Corus UK Ltd., 2nd edition, 2003.

[51] R. Dixon and H. G. Bowerman. Advantages of steel-concrete-steel sandwich construction in highrise buildings. In *CIB Report, Proceedings of the CIB-CTBUH International Conference on Tall Buildings*, number 290, pages 639–648, Malaysia, 20–23 October 2003.

[52] Corus Bi-Steel. Corus in construction. Retrieved: 17 March, 2010. URL `http://www.corusconstruction.com/en/about_us/bi-steel`.

[53] C. Schlaseman and J. Russell. Application of advanced construction technologies to new nuclear power plants. Prepared Report for U.S. Department of Energy, under contract for DE-AT01-02NE23476, Report MPR-2610, Revision 2, 2004.

[54] P. Kujala and P. Noury. *Theory and Applications of Sandwich Structures*, chapter 17 Design of Ship Structures from Metallic Sandwich Topology, pages 515–570. University of Southampton, UK, 2005.

[55] H. D. Wright, T. O. S. Oduyemi, and H. R. Evans. The experimental behaviour of double skin composite elements. *Journal of Constructional Steel Research*, 19 (2):97–110, 1991.

[56] H. D. Wright, T. O. S. Oduyemi, and H. R. Evans. The design of double skin composite elements. *Journal of Constructional Steel Research*, 19(2):111–132, 1991.

[57] H. D. Wright and T. O. S. Oduyemi. Partial interaction analysis of double skin composite beams. *Journal of Constructional Steel Research*, 19(4):253–283, 1991.

[58] T. M. Roberts, D. N. Edwards, and R. Narayanan. Testing and analysis of steel-concrete-steel sandwich beams. *Journal of Constructional Steel Research*, 38(3): 257–279, 1996.

[59] T. M. Roberts and O. Dogan. Fatigue of welded stud shear connectors in steel-concrete-steel sandwich beams. *Journal of Constructional Steel Research*, 45(3): 301–320, 1998.

[60] B. McKinley. *Large Deformation Structural Performance of Double Skin Composite Construction using British Steel's Bi-Steel.* PhD thesis, City University, 1999.

[61] S. K. Clubley. *Computational Structural Analysis and Testing of Bi-Steel Plate.* PhD thesis, University of Southampton, 2001.

[62] N. R. Coyle. *Development of Fully Composite Steel-Concrete-Steel Beam Elements.* PhD thesis, University of Dundee, 2001.

[63] N. Foundoukos. *Behaviour and Design of Steel-Concrete-Steel Sandwich Construction.* PhD thesis, Imperial College of Science, Technology and Medicine, University of London, 2005.

[64] B. McKinley and L. F. Boswell. Behaviour of double skin composite construction. *Journal of Constructional Steel Research*, 58(10):1347–1359, 2002.

[65] N. Foundoukos, M. Xie, and J. C. Chapman. Fatigue tests on steel-concrete-steel sandwich components and beams. *Journal of Constructional Steel Research*, 63 (7):922–940, 2007.

[66] B. A. Burgan and F. J. Naji. Steel-concrete-steel sandwich construction. *Journal of Constructional Steel Research*, 46(1-3):Paper No.125, 1998.

[67] G. C. Hoff. A major research program on steel-concrete-steel sandwich elements. *ACI Special Publications*, 174:37–88, 1998.

[68] B. J. Sun and D. Johnson. Shear resistance of steel-concrete-steel beams. *Journal of Constructional Steel Research*, 46(1-3):Paper No.311, 1998.

[69] M. Takeuchi, M. Narikawa, I. Matsuo, K. Hara, and S. Usami. Study on a concrete filled structure for nuclear power plants. *Nuclear Engineering and Design*, 179(2): 209–223, 1998.

[70] H. Bowerman and J. C. Chapman. Bi-steel steel-concrete-steel sandwich construction. In J. F. Hajjar, M. Hosain, W. S. Easterling, and B. M. Shahrooz, editors, *Composite Construction in Steel and Concrete IV, Proceedings of the Conference, May 28-June 2, 2000, Banff, Alberta, Canada*, pages 656–667. 2002.

[71] N. E. Shanmugam, G. Kumar, and V. Thevendran. Finite element modelling of double skin composite slabs. *Finite Elements in Analysis and Design*, 38(7): 579–599, 2002.

[72] S. K. Clubley, S. S. J. Moy, and R. Y. Xiao. Shear strength of steel-concrete-steel composite panels. Part I–Testing and numerical modelling. *Journal of Constructional Steel Research*, 59(6):781–794, 2003.

[73] S. K. Clubley, S. S. J. Moy, and R. Y. Xiao. Shear strength of steel-concrete-steel composite panels. Part II–Detailed numerical modelling of performance. *Journal of Constructional Steel Research*, 59(6):795–808, 2003.

[74] M. Xie and J. C. Chapman. Static and fatigue tensile strength of friction-welded bar-plate connections embedded in concrete. *Journal of Constructional Steel Research*, 61(5):651–673, 2005.

[75] M. Xie, N. Foundoukos, and J. C. Chapman. Experimental and numerical investigation on the shear behaviour of friction-welded bar-plate connections embedded in concrete. *Journal of Constructional Steel Research*, 61(5):625–649, 2005.

[76] K. M. A. Sohel. *Impact Performance of Steel-Concrete-Steel Sandwich Structures.* PhD thesis, National University of Singapore, 2008.

[77] D. Xuexin. *Fatigue Analysis and Design of Steel-Concrete-Steel Sandwich Composite Structures.* PhD thesis, National University of Singapore, 2009.

[78] D. Collings. *Steel-Concrete Composite Bridges.* Thomas Telford Publishing, Thomas Telford Ltd., London, 2005.

[79] H. R. Evans and H. D. Wright. *Steel-Concrete Composite Structures: Stability and Strength*, chapter 2 Steel-Concrete Composite Flooring Deck Structures, pages 21–52. Elsevier Applied Science Publishers Ltd., England, 1988.

[80] G. Hanswille, M. Porsch, and C. Ustundag. Resistance of headed studs subjected to fatigue loading: Part I: Experimental study. *Journal of Constructional Steel Research*, 63(4):475–484, 2007.

[81] R. P. Johnson. Resistance of stud shear connectors to fatigue. *Journal of Constructional Steel Research*, 56(2):101–116, 2000.

[82] C.-S. Shim, P.-G. Lee, and T.-Y. Yoon. Static behavior of large stud shear connectors. *Engineering Structures*, 26(12):1853–1860, 2004.

[83] P.-G. Lee, C.-S. Shim, and S.-P. Chang. Static and fatigue behavior of large stud shear connectors for steel-concrete composite bridges. *Journal of Constructional Steel Research*, 61(9):1270–1285, 2005.

[84] E. Steinberg, R. Selle, and T. Faust. Connectors for timber–lightweight concrete composite structures. *Journal of Structural Engineering*, 129(11):1538–1545, 2003.

[85] I. Valente and P. J. S. Cruz. Experimental analysis of perfobond shear connection between steel and lightweight concrete. *Journal of Constructional Steel Research*, 60(3-5):465–479, 2004.

[86] A. H. Nilson and G. Winter. *Design of Concrete Structures.* McGraw-Hill, Inc., Singapore, 11th edition, 1991.

[87] J. C. McCormac. *Design of Reinforced Concrete.* John Wiley & Sons, Inc., 5th edition, 2001.

[88] B. B. Adhikary and H. Mutsuyoshi. Shear strengthening of reinforced concrete beams using various techniques. *Construction and Building Materials*, 20(6):366–373, 2006.

[89] B. Taljsten and L. Elfgren. Strengthening concrete beams for shear using CFRP-materials: evaluation of different application methods. *Composites Part B: Engineering*, 31(2):87–96, 2000.

[90] O. Chaallal, M.-J. Nollet, and D. Perraton. Shear strengthening of RC beams by externally bonded side CFRP strips. *Journal of Composites for Construction*, 2 (2):111–113, 1998.

[91] C. Diagana, A. Li, B. Gedalia, and Y. Delmas. Shear strengthening effectiveness with CFF strips. *Engineering Structures*, 25(4):507–516, 2003.

[92] Z. Zhang, C.-T. T. Hsu, and J. Moren. Shear strengthening of reinforced concrete deep beams using carbon fiber reinforced polymer laminates. *Journal of Composites for Construction*, 8(5):403–414, 2004.

[93] Z. Zhang and C.-T. T. Hsu. Shear strengthening of reinforced concrete beams using carbon-fiber-reinforced polymer laminates. *Journal of Composites for Construction*, 9(2):158–169, 2005.

[94] B. Taljsten. Strengthening concrete beams for shear with CFRP sheets. *Construction and Building Materials*, 17(1):15–26, 2003.

[95] *ACI 318-95: Building Code Requirements for Reinforced Concrete.* American Concrete Institute, 1995.

[96] *ACI Committee 440: Guide for the Design and Construction of Externally Bonded FRP Systems for Strengthening Concrete Structures.* American Concrete Institute, Farmington Hills, MI, USA, 2002.

[97] A. L. L. Baker. *Reinforced Concrete.* Concrete Publications Limited, London, 1949.

[98] P. Bhatt, T. J. MacGinley, and B. S. Choo. *Reinforced Concrete: Design Theory and Examples.* Taylor & Francis, 3rd edition, 2006.

[99] J. N. Cernica. *Fundamentals of Reinforced Concrete.* Addison-Wesley Publishing Company, Inc., U.S.A., 1964.

[100] J. F. Chen and J. G. Teng. On the strength of RC beams shear strengthened with prestressed FRP straps. In *FRP Composites in Civil Engineering, Proceedings of the International Conference*, pages 695–704, 2001.

[101] *Concrete Society Technical Report 55: Design Guidance for Strengthening Concrete Structures Using Fibre Composite Materials*. Concrete Society, UK, 2000.

[102] C. W. Dunham. *The Theory and Practice of Reinforced Concrete*. McGraw-Hill Book Company, Inc., 2nd edition, 1944.

[103] *Eurocode 2: Design of Concrete Structures - Part 1-1: General Rules and Rules for Buildings*. European Committee for Standardization (CEN), 1992.

[104] G. Gendron, A. Picard, and M. C. Guerin. A theoretical study on shear strengthening of reinforced concrete beams using composite plates. *Composite Structures*, 45(4):303–309, 1999.

[105] P. B. Hughes. *Limit State Theory for Reinforced Concrete Design*. Pitman Publishing Ltd., London, 2nd edition, 1976.

[106] W. H. Mosley, J. H. Bungey, and R. Hulse. *Reinforced Concrete Design*. Palgrave, New York, 5th edition, 1999.

[107] C. Pellegrino and C. Modena. Fiber reinforced polymer shear strengthening of reinforced concrete beams with transverse steel reinforcement. *Journal of Composites for Construction*, 6(2):104–111, 2002.

[108] T. C. Triantafillou. Composites: a new possibility for the shear strengthening of concrete, masonry and wood. *Composites Science and Technology*, 58(8):1285–1295, 1998.

[109] Y. H. Kim, Y. S. Yoon, W. D. Cook, and D. Mitchell. Repeated loading tests of concrete walls containing headed shear reinforcement. *Journal of Structural Engineering*, 130(8):1233–1241, 2004.

[110] K. Pilakoutas and X. Li. Alternative shear reinforcement for reinforced concrete flat slabs. *Journal of Structural Engineering*, 129(9):1164–1172, 2003.

[111] S. Y. Cao, J. F. Chen, J. G. Teng, Z. Hao, and J. Chen. Debonding in RC beams shear strengthened with complete FRP wraps. *Journal of Composites for Construction*, 9(5):417–428, 2005.

[112] S. Hay, K. Thiessen, D. Svecova, and B. Bakht. Effectiveness of GFRP sheets for shear strengthening of timber. *Journal of Composites for Construction*, 10(6): 483–491, 2006.

[113] M. R. Islam, M. A. Mansur, and M. Maalej. Shear strengthening of RC deep beams using externally bonded FRP systems. *Cement and Concrete Composites*, 27(3):413–420, 2005.

[114] J. G. Teng, L. Lam, and J. F. Chen. Shear strengthening of RC beams with FRP composites. *Progress in Structural Engineering and Materials*, 6(3):173–184, 2004.

[115] J. Romanoff, P. Varsta, and A. Klanac. Stress analysis of homogenized web-core sandwich beams. *Composite Structures*, 79(3):411–422, 2007.

[116] Q. H. Cheng, H. P. Lee, and C. Lu. A numerical analysis approach for evaluating elastic constants of sandwich structures with various cores. *Composite Structures*, 74(2):226–236, 2006.

[117] D. Zangani, M. Robinson, and A. Gibson. Evaluation of stiffness terms for Z-cored sandwich panels. *Applied Composite Materials*, 14(3):159–175, 2007.

[118] K. H. Tan, P. Montague, and C. Norris. Steel sandwich panels: Finite element, closed solution, and experimental comparisons, on a 6m x 2.1m panel. *The Structural Engineer*, 67(9):159–166, 1989.

[119] T. M. Nordstrand and L. A. Carlsson. Evaluation of transverse shear stiffness of structural core sandwich plates. *Composite Structures*, 37(2):145–153, 1997.

[120] C. Libove and R. E. Hubka. Elastic constants for corrugated-core sandwich plates. Technical Note NACA-TN-2289, National Advisory Committee for Aeronautics, Langley Aeronautical Laboratory, Langley Field, VA, 1951.

[121] P. G. Glockner. Symmetry in structural mechanics. *Proceedings of the American Society of Civil Engineers, Journal of the Structural Division*, 99(ST1):71–89, 1973.

[122] W. McGuire, R. H. Gallagher, and R. D. Ziemian. *Matrix Structural Analysis*. John Wiley & Sons, Inc., New York, 2nd edition, 2000.

[123] *ANSYS Release 11.0*. Swanson Analysis Systems Inc., 2007.

[124] D. Kachlakev, T. Miller, S. Yim, K. Chansawat, and T. Potisuk. Finite element modeling of reinforced concrete structures strengthened with FRP laminates. Final Report SPR 316, Oregon Department of Transportation, 2001.

[125] H. T. Nguyen and S. E. Kim. Finite element modeling of push-out tests for large stud shear connectors. *Journal of Constructional Steel Research*, 65(10-11):1909–1920, 2009.

[126] S. P. Timoshenko and J. M. Gere. *Mechanics of Materials*. Van Nostrand Reinhold Company, New York, 1972.

[127] W. L. Ko. Elastic constants for superplastically formed/diffusion-bonded corrugated sandwich core. Technical Paper NASA-TP-1562, National Aeronautics and Space Administration, 1980.

[128] T. Nordstrand, L. A. Carlsson, and H. G. Allen. Transverse shear stiffness of structural core sandwich. *Composite Structures*, 27(3):317–329, 1994.

[129] T. C. Fung, K. H. Tan, and T. S. Lok. Analysis of C-core sandwich plate decking. In *Proceedings of the Third (1993) International Offshore and Polar Engineering Conference*, volume IV, pages 244–249, Singapore, 6–11 June 1993.

[130] T. C. Fung, K. H. Tan, and T. S. Lok. Elastic constants for Z-core sandwich panels. *Journal of Structural Engineering*, 120(10):3046–3055, 1994.

[131] T. C. Fung and K. H. Tan. Shear stiffness for Z-core sandwich panels. *Journal of Structural Engineering*, 124(7):809–816, 1998.

[132] G. R. Monforton and T. S. Wu. Matrix analysis of semi-rigidly connected frames. *Proceedings of the American Society of Civil Engineers, Journal of the Structural Division*, 89(ST6):13–42, 1963.

[133] S. P. Timoshenko and J. M. Gere. *Theory of Elastic Stability.* McGraw-Hill Book Co., Tokyo, International edition, 1981.

[134] C. K. Wang. *Intermediate Structural Analysis.* McGraw-Hill Book Co., Singapore, International edition, 1983.

[135] R. T. Fenner. *Mechanics of Solids.* Blackwell Scientific, Oxford, 1989.

[136] Z. Aboura, N. Talbi, S. Allaoui, and M. L. Benzeggagh. Elastic behavior of corrugated cardboard: experiments and modeling. *Composite Structures*, 63(1):53–62, 2004.

[137] N. Talbi, A. Batti, R. Ayad, and Y. Q. Guo. An analytical homogenization model for finite element modelling of corrugated cardboard. *Composite Structures*, 88(2): 280–289, 2009.

[138] M. W. Hyer. *Stress Analysis of Fiber-Reinforced Composite Materials.* WCB/McGraw-Hill Co.,Ltd., Singapore, International edition, 1998.

[139] M. D. Hayes. *Structural Analysis of a Pultruded Composite Beam: Shear Stiffness Determination and Strength and Fatigue Life Predictions.* PhD thesis, Faculty of the Virginia Polytechnic Institute and State University, 2003.

[140] J. R. Hutchinson. Shear coefficients for Timoshenko beam theory. *Journal of Applied Mechanics*, 68(1):87–92, 2001.

[141] R. Park and T. Paulay. *Reinforced Concrete Structures.* John Wiley & Sons, Inc., Singapore, 1975.

[142] H. Rüsch. Versuche zur festigkeit der biegedruckzone. Deutscher Ausschuss für Stahlbetonbau, Bulletin No. 120, Berlin, 1955.

[143] M. Y. H. Bangash. *Concrete and Concrete Structures: Numerical Modeling and Applications.* Elsevier Science Publishers Ltd., London, England, 1989.

[144] *ABAQUS Standard User's Manual Version 6.6.* Dassault Systèmes, USA, 2006.

[145] L. Huyse, Y. Hemmaty, and L. Vandewalle. Finite element modeling of fiber reinforced concrete beams. In *Proceedings of the ANSYS Conference*, volume 2, Pittsburgh, Pennsylvania, May 1994.

[146] Y. Hemmaty. Modelling of the shear force transferred between cracks in reinforced and fibre reinforced concrete structures. In *Proceedings of the ANSYS Conference*, volume 1, Pittsburgh, Pennsylvania, August 1998.

[147] K. J. Willam and E. D. Warnke. Constitutive model for the triaxial behavior of concrete. *Proceedings of the International Association for Bridge and Structural Engineering, ISMES*, 19:174, 1975.

[148] W. F. Chen. *Plasticity in Reinforced Concrete.* John Wiley & Sons, Inc., New York, 1982.

[149] T. Sigfusson. Nonlinear analysis of reinforced concrete shear walls in low-rise Icelandic residential buildings. Master's thesis, Department of Civil and Environmental Engineering, Faculty of Engineering, University of Iceland, 2001.

[150] M. Suidan and W. C. Schnobrich. Finite element analysis of reinforced concrete. *Proceedings of the American Society of Civil Engineers, Journal of the Structural Division*, 99(ST10):2109–2122, 1973.

[151] S. Mindess and J. F. Young. *Concrete.* Prentice-Hall, Inc., Englewood Cliffs, New Jersey, 1981.

[152] S. P. Shah, S. E. Swartz, and C. Ouyang. *Fracture Mechanics of Concrete.* John Wiley & Sons, Inc., New York, 1995.